Large-Scale Networks in the Human Brain revealed by Functional Connectivity MRI

A dissertation presented by

Fenna Marie Krienen

to

The Department of Psychology

in partial fulfillment of the requirements

for the degree of

Doctor of Philosophy

in the subject of

Psychology

Harvard University

Cambridge, Massachusetts

July 2013

Dissertation Advisor: Professor Randy L. Buckner Fenna Marie Krienen

Large-Scale Networks in the Human Brain revealed by Functional Connectivity MRI

Abstract

The human brain is composed of distributed networks that connect a disproportionately large neocortex to the brainstem, cerebellum and other subcortical structures. New methods for analyzing non-invasive imaging data have begun to reveal new insights into human brain organization. These methods permit characterization of functional interactions within and across brain networks, and allow us to appreciate points of departure between the human brain and non-human primates.

The purpose of this dissertation is to explore the properties of large-scale networks in the human brain. Functional connectivity MRI (fcMRI) is a technique that capitalizes on the slow, intrinsic activity fluctuations in the blood oxygen level dependent (BOLD) signal. Though its limitations are still being explored, fcMRI provides a powerful, if indirect, method for mapping brain circuits in humans. In the first part of this dissertation I use fcMRI to map cerebro-cerebellar networks (Paper I). These networks replicate known anatomical circuits from non-human primates. Other regions in the human cerebellum that are expanded relative to other primates appear to participate in distributed cerebral cortical association networks.

I next examine factors that affect functional connectivity profiles and the resultant topography of fcMRI networks (Paper II). While functional connectivity is constrained by anatomy, analysis considerations as well as transient contributions reflecting task or behavioral state are sufficient to change network topography. Despite this, broad features of organization are preserved across task states.

Finally, I present our best estimates of the topography of functional networks in the cerebrum using resting-state data collected from 1000 participants (Paper III). These maps indicate that human association cortex is comprised of a set of large, interdigitated functional networks that span the frontal, parietal, temporal, cingulate and limbic cortices. These can be distinguished from sensory and motor networks that are dominated by local, hierarchical coupling. I discuss the promise of fcMRI to provide new insights into human brain organization, as well as the limitations and caveats that constrain its interpretation.

Table of Contents

Acknowledgements

Many people directly contributed to this work. I thank Angela Castellanos, Brian Yang, Marisa Hollinshead, Michelle Zad and Susanna Crowell for assistance with data collection, Tanveer Talukdar for development of the fcMRI processing stream, Jeremy Schmahmann, Avram Holmes, Justin Vincent, Justin Baker, Jorge Sepulcre, Hesheng Liu and Daisy Wang for useful discussion, and the Harvard Center for Brain Science Neuroimaging Core, the Athinoula A. Martinos Center and the Harvard Neuroinformatics Research Group (Gabriele Fariello, Timothy O'Keefe, and Victor Petrov) for imaging and data support. I was supported by fellowships from the Department of Defense, an Ashford Graduate Fellowship in the Sciences, and the Sackler Scholars Program in Psychobiology. I would like to thank the Ashford family and the Harvard Horizons program in particular for supporting and promoting the work of graduate students in GSAS. I thank Amitai Shenhav for helping me survive graduate school. I am indebted to Thomas Yeo, whose friendship and collaboration I continue to benefit from greatly. I thank my advisor, Randy Buckner, for inspiring me with his incredible scientific vision, guidance and mentorship. I thank Dan Schacter for his feedback and support over the years, as well as my other committee members, Josh Buckholtz and Dost Öngür. My mother Anneke and brother Frank were instrumental in keeping me grounded during this time, as was my fellow bower, Maude Baldwin. I thank 20 School St for general enlightenment but most importantly for my wonderful fiancé Ben, who has made my world a bigger place. This thesis is dedicated to the memory of my father, Frank Krienen Sr. (1917-2008), who certainly would have been proud and who might have expressed it thusly: "Niet slecht, kind."

Introduction

"The investigation of the various areas of the brain by means of electrical stimulation is a method which is now very nearly exhausted." This line appeared in a paper entitled, "Notes on Cortical Localization," read by Gregory Jefferson before the Victoria Medical Society. Jefferson's proclamation, made in 1915, was certainly premature. Nearly 100 years later, electrical stimulation and recording of electrical impulses continue to be a mainstay of the neuroscientific toolbox. However, Jefferson's comment was not so much an objection against stimulation per se, but rather was to make the case that histology, not stimulation, would be the 'final arbiter of the exact nature' of cortical tissue (Jefferson 1916). At that time such a statement would not have been unreasonable. Much of the cerebrum, beyond the motor cortex and select sensory areas, was deemed 'inexcitable' using the stimulation techniques available at the turn of the 20th century (Ferrier 1874; Jefferson 1916). According to Jefferson, cortical localization should be left to the innovative histologists who were developing new ways of cutting and staining. These methods showed great promise in revealing new features of brain organization.

Histologists were also engaged in protracted debates about which of the observable macro- and microscopic features of cortex were functionally relevant. These ranged from the significance of folding patterns (Jefferson 1916) to the relevance of cytoarchitectonic borders (Lashley & Clark 1946). While some of these theories have since gone out of favor, many of the early efforts to map the cytoarchitectural and morphological features remain relevant today, such as the work of Brodmann, Flechsig,

Campbell, Ramon y Cajal, Betz, the Vogts and others. While he was wrong to dismiss methods for stimulating the brain, Jefferson was certainly right to give histology its due.

New techniques have given neuroscientists new entry points for addressing the question of brain organization. Brodmann area maps still greatly inform our understanding of the architectonic subdivisions of mammalian neocortex, but we now generally recognize three additional attributes as being important for areal parcellation: topography, function, and connectivity (Kass 1982; 1987). In practice, only a few areas have been interrogated in enough detail to satisfy the four-pronged definition, such as primary visual area V1.

Standardizing the definition of a cortical area has been helpful in determining homologies across extant species in order to infer what the brains of the earliest mammals might have looked like. The present understanding is that the basic eutherian (placental) mammalian plan probably involved a small number of primary sensory fields and motor strip (Krubitzer & Kahn 2003), and comparative work in primates has suggested that the early primates probably had a relatively larger number of distinct cortical fields, including premotor areas (Kaas 2006; 2011). However, because the classical methods for interrogating cortical organization cannot be used in humans, making the jump from the general primate plan to the organization of the human brain and its early hominin antecedents remains an area of speculation (Kaas 2005).

With the ever-increasing popularity of functional neuroimaging as a tool to understand the organization of the human brain, the need for accurate means of determining structure-function relationships in the brain remains paramount. In an article entitled, “In Praise of Tedious Anatomy,” Devlin and Poldrack eloquently argue that the

primary goal of cognitive neuroscience – functional localization – is hampered by a lack of adequate means and standards for determining the relevant structural features underlying functional responses (Devlin & Poldrack 2007). A fundamental complication is that the typical structural MRI scan only provides information about macroscopic features of an individual's brain. Despite earlier assumptions (e.g. Jefferson 1916; Sanides 1969), folding patterns and gyral/sulcal landmarks do not correspond uniformly to underlying cytoarchitectural areas (Van Essen & Dierker 2007; Amunts, Schleicher & Zilles 2007). Boundaries between cortical areas are more consistent in the central sulcus (Geyer et al. 1999) than in parietal and lateral prefrontal cortex (Amunts et al. 1999).

Properties of organization that can inform functional organization are therefore sought, and the work in this dissertation describes our efforts to use functional imaging to infer connectivity patterns in the human brain. That is, while Devlin and Poldrack focus on the need for better ways to identify structural features of discrete cortical areas, here we are interested in determining which discrete regions couple together to form functional networks, what the properties of those networks are, and how they might have evolved or become differentiated in the modern human. Without denying that localization and specialization occurs in discrete regions of the brain, this work seeks to shift emphasis away from characterizing the properties of isolated regions, and towards a better understanding of how interacting networks process information and support human cognition.

Because characterization of connectivity and other intrinsic, functionally important properties of the brain have historically required invasive methods, studies of non-human primates (typically macaques) have been the best source for detailed

information about anatomy and connectivity. However there are numerous issues with assuming homology or correspondence between our brain and that of a single monkey species. For one, the expansion of the cerebral cortex in humans is not uniform relative to macaque brains (Hill et al. 2010). Humans diverged from a common ancestor with macaques over 25 million years ago, making differences and even similarities between the species difficult to model. When the goal is determining what kinds of specializations are 'uniquely human' in the brain or what is conserved in a particular clade versus part of a 'general mammalian plan,' comparison to a single out-group is insufficient (Preuss et al. 2004). Though the data are scarce, researchers working with chimpanzee brain tissue continue to make valuable insights into how much our brains differ from our closest living relatives (e.g. Sherwood et al. 2011). For example, quantitative assessment of myelination across development indicates that chimps achieve adult-like myelination density around sexual maturity. In comparison, humans experience prolonged myelination in infancy and adolescence that continues into early adulthood (Miller et al. 2012). This observation contributes to a growing body of evidence that, from a comparative perspective, adolescence and young adulthood is a unique period in the development of human connectional architecture.

This dissertation describes three studies we have undertaken to examine the macroscopic topography and dynamic properties of functional brain networks in humans. We have relied on a neuroimaging technique – functional connectivity MRI (fcMRI) – that measures the temporal correlation of slow, intrinsic fluctuations in the BOLD fMRI signal. This technique has proven a useful, if indirect, indicator of functional interaction between distant brain regions, and the results in many instances conform to broad

properties of underlying anatomic connectivity (Biswal et al. 1995; Beckmann et al. 2005; Fox & Raichle 2007; Vincent et al. 2007; Petrides et al. 2009; Smith et al. 2011; Yeo et al. 2011).

fcMRI reflects more than direct, monosynaptic connectivity. Temporal correlations are observed between regions that are indirectly connected or driven by common input (Vincent et al. 2007). Variability in the fcMRI signal across subjects is non-uniform across the cortical mantle and correlates with individual variability in aspects of cortical structure such as folding patterns (Mueller et al. 2013). The source of the slow, intrinsic fluctuations in neurovascular coupling captured by fcMRI, as well as their functional significance, remain an area of active inquiry (Lu et al. 2007; Nir et al. 2008).

Despite these limitations and ambiguities, fcMRI has provided new insights into functional coupling in the human brain. Our perspective is that fcMRI is a valuable, if indirect, means of inferring connectivity patterns in the human brain. The three papers in this dissertation describe our efforts to examine these patterns in the context of cerebro-cerebellar coupling, as well as coupling across the cortical surface. A major theme (and the focus of the second paper) is exploring the extent to which we can use fcMRI to validate and extend our understanding of organizational features derived from the anatomical record – that is, what is known from non-human primate studies. In some cases the agreement is promising, for instance in the pattern of connectivity between the cerebrum and contralateral cerebellum (Kelley & Strick 2003) or in the connectivity between regions in the canonical visuomotor hierarchy (Felleman & Van Essen 1991). Other applications of fcMRI seem less fruitful. For example, our results do not support

the use of fcMRI to recover the boundaries between functional areas in the neocortex (Paper II).

A more minor theme addresses the dynamic contributions to the fcMRI signal. The fact is that we do not really know how much the functional connectivity measures we use change across task states. For instance, we do not know whether, as a general rule, coactivation of different regions during a task is sufficient to induce an increase in the fcMRI correlation between them. If a task involves pressing a key in response to an auditory stimulus, will we observe an increased correlation between motor cortex and auditory cortex? Are there regions whose connectivity patterns remain stable regardless of behavioral state? These are questions we are still actively exploring. The answers have implications for how we conceptualize fcMRI measured in the resting state, which is currently the most prevalent way to measure functional coupling in the human brain. In each case, our understanding of the anatomy should constrain our predictions as much as possible.

New methods are continually being developed for mapping gene expression patterns (http://www.brain-map.org), transmitter receptor types (Zilles et al. 2002), structural connectivity imaging, and even visualizing intact, anatomic connectivity of human brain tissue (Chung et al. 2013). We anticipate that the predictions generated by noninvasive imaging techniques such as fcMRI, both about the topography and the functional relevance of connectivity networks, will be revised and greatly refined. More generally, the development of tissue staining, genetic labeling, anatomical tracing and noninvasive imaging techniques allow the field of human neuroscience to progress towards multimodal atlases of brain organization (Toga et al. 2006).

Overview of the Dissertation

Paper I. In 2001, Middleton & Strick identified multiple, segregated fronto-cerebellar circuits using viral tracing techniques in the cebus monkey. These techniques allowed them to trace the thalamic projections to prefrontal cortex, as well as the projections from the prefrontal cortex that terminated in the dentate nucleus. The dentate is the obligate step for projections from the cortex to enter the cerebellar cortex, and prefrontal channels were spatially distinct from motor cortex channels. This approach was later extended to map the precise locations in cerebellar cortex that received prefrontal input (Kelley & Strick 2003). The discovery of reciprocal loops between prefrontal cortex and the posterior cerebellar hemispheres challenged the traditional view that motor control comprises the complete repertoire of the cerebellum (Middleton & Strick 2001; Kelley & Strick 2003; see also Leiner et al. 1986).

Little is known about the topography of human cerebro-cerebellar networks. Providing evidence for such circuits would provide a substrate for cerebellar contributions to cognition, as well as provide an initial map of human cerebellar network topography that serves as a foundation for further analysis. Motivated from nonhuman primate anatomy, Paper I (Krienen & Buckner 2009) mapped the topography of functional connectivity between frontal cortex and the cerebellum in humans using functional connectivity MRI.

Of particular interest were the posterior lobes of the cerebellum that are expanded in apes and humans relative to other mammals (Macleod et al. 2003). The posterior lobes,

which include the major extent of the lateral hemispheres, were predicted to project to association areas of cortex and largely spare regions directly involved in motor function. We mapped human cerebellar topography using functional connectivity and demonstrated the presence of four separate frontal-cerebellar circuits, including three distinct posterior cerebellar circuits that associate with prefrontal cortex (Krienen & Buckner 2009).

Paper II. Sharp, reproducible spatial transitions in resting state functional connectivity suggest its ability to reveal meaningful differences in functional coupling between adjacent regions in the brain. However, a growing literature shows that functional coupling is sensitive to behavioral state as well as choices made in analysis. Here, we explored factors that affect functional connectivity profiles and the resultant network topography (Krienen, Yeo & Buckner *in prep*). We sought to determine how the spatial properties of networks change when factors such as the task performed and the weighting criteria used during analysis are manipulated.

First, we demonstrated that rs-fcMRI computed in small (N=16) independent samples of passive rest scans produce highly replicable network boundaries. This corroborates earlier observations that suggest rs-fcMRI likely reflects stable properties of functional networks. Next, we showed that the particular choice of cost function when using a clustering algorithm changes network topography. Finally, we observed changes when comparing fcMRI derived from passive rest scans to fcMRI measured while participants were engaged in different behavioral states. We measured fcMRI patterns in several continuous task paradigm datasets, including a battery of passive behavioral tasks

that were perceptually identical to the often-used passive fixation paradigm. In some sense observing connectivity changes as a function of state is not unexpected, as the assumption that connectivity is dynamic and context-dependent follows from classic theories of information processing in the brain, particularly throughout association cortex (Mesulam 1998). Dynamic network structure also constitutes a basic premise for methods exploring effective connectivity such as dynamic causal modeling (Friston 1994, 2011; Friston et al. 2003).

Task-related increases and decreases in coupling strength were observed both within and across networks defined from resting state data. Moreover, task-defined network borders better explained task activation patterns than did resting-state borders. Despite this, we show that several broad features of organization are preserved across task states. For example, multiple homotopic maps reflecting cerebral cortical network organization are preserved in the cerebellum, though the exact locations and topography of networks follows the task-induced changes in cerebral networks. Another broad principle that is maintained across task states is the general tendency for there to be multiple, interdigitated networks that span distributed portions of association cortex.

Taken together, the analyses in Paper II suggest that while rs-fcMRI is constrained by underlying anatomical connectivity, it should not be expected to identify areal boundaries as traditionally defined (Kaas 1987). However, the replication of many general features of organization independent of task suggests the utility of fcMRI techniques for understanding properties of human neocortical organization. Moreover, the results from the task analyses highlight opportunities for discovery. Comparing measures computed from different task states rather than considering organization

derived from passive rest alone affords the opportunity to characterize the dynamic range of functional networks in the human brain.

Paper III. Paper III uses a graph theoretic clustering approach to identify networks across the human cerebrum in a dataset of 1,000 passively resting subjects (Yeo, Krienen et al. 2011). With the caveats and complexities observed in Paper II in mind, we capitalized on the large data sample to explore the stable properties of resting state connectivity and their ability to inform current understanding of human brain organization. We found evidence for multiple parallel circuits that are interdigitated throughout association cortex, such that each cortical lobe contains components of multiple association networks. These networks were largely distinct from sensory and motor networks, which formed local clusters of connectivity and did not have a distributed topographic profile.

In addition to the parcellations, we employed a series of seed-based analyses to quantify the relationships between regions that lie along a well-characterized sensorimotor processing hierarchy. These results demonstrate the utility of fcMRI as a tool for identifying functionally pathways in the cerebral cortex. We discuss the organization of these large-scale cerebral networks in relation to monkey anatomy, note consistencies and departures, and discuss their potential evolutionary expansion in humans to support cognition.

Paper I

Fronto-Cerebellar Circuits Revealed by Intrinsic Functional Connectivity

Krienen, FM & Buckner, RL. *Cerebral Cortex,* 2009

Abstract

Multiple, segregated fronto-cerebellar circuits have been characterized in nonhuman primates using transneuronal tracing techniques including those that target prefrontal areas. Here we used functional connectivity MRI (fcMRI) in humans (n=40) to identify four topographically distinct fronto-cerebellar circuits that target (1) motor cortex, (2) dorsolateral prefrontal cortex, (3) medial prefrontal cortex and (4) anterior prefrontal cortex. All four circuits were replicated and dissociated in an independent data set (n=40). Direct comparison of right- and left-seeded frontal regions revealed contralateral lateralization in the cerebellum for each of the segregated circuits. The presence of circuits that involve prefrontal regions confirms that the cerebellum participates in networks important to cognition including a specific fronto-cerebellar circuit that interacts with the default network. Overall, the extent of the cerebellum associated with prefrontal cortex included a large portion of the posterior hemispheres consistent with a prominent role of the cerebellum in non-motor functions. We conclude by providing a provisional map of the topography of the cerebellum based on functional correlations with the frontal cortex as well as a discussion of the strengths and limitations of fcMRI for making inferences about brain circuits.

Introduction

The identification of multiple, segregated fronto-cerebellar circuits using viral tracing techniques in nonhuman primates has challenged the traditional view that motor control comprises the complete repertoire of the cerebellum (Middleton & Strick 1994, 2001; Kelly & Strick 2003; see also Leiner et al. 1986; Schmahmann,1991). The presentation of cerebellar patients with cognitive deficits in the absence of motor deficits similarly suggests cerebellar involvement in non-motor functions (Schmahmann 2004; Schmahmann et al. 2007a). Neuroimaging studies finding cerebellar activation in response to non-motor components of cognitive tasks have complemented this view (Petersen et al. 1998; Allen et al. 1997; Desmond & Fiez 1998; O'Reilly, Mesulam, & Nobre 2008; Stoodley & Schmahmann 2009).

However, there has been no adequate technique to explore the existence of segregated cerebro-cerebellar circuits in humans. Characterizing such circuits would provide strong evidence of the anatomical substrate of cerebellar contributions to cognition as well as provide a mapping of cerebellar regions as a foundation for further analysis. Of particular interest are the posterior lobes of the cerebellum that are markedly expanded in apes and humans relative to other mammals (Macleod et al. 2003). The posterior lobes, which include the major extent of the lateral hemispheres, are predicted to project to association areas of cortex and largely spare regions directly involved in motor function.

Functional connectivity based on intrinsic activity fluctuations provides a potentially powerful method for mapping fronto-cerebellar circuits (Biswal et al. 1995;

see Fox & Raichle, 2007 for a review). Intrinsic fluctuations detected by fMRI are constrained by anatomic pathways such that connected brain regions show correlated fluctuations (Vincent et al. 2007; Johnston et al. 2008). Analysis of functional correlations, often referred to as functional connectivity MRI (fcMRI) analysis, has been used to map multiple brain systems linked to sensory, motor, and cognitive functions (e.g., Biswal et al. 1995; Greicius et al. 2003; De Luca et al. 2006; Fox et al. 2006; Vincent et al. 2006, 2008; Dosenbach et al. 2007; Margulies et al. 2007; Kahn et al. 2008; Zhang et al. 2008). There are strengths and limitations of the technique.

Emerging evidence suggests that fcMRI reflects both monosynaptic and polysynaptic connections (Greicius et al. 2009; Honey et al. 2009). Sensitivity to indirect connectivity presents an opportunity for mapping fronto-cerebellar circuits because the cerebral cortex is anatomically connected to the cerebellum only through polysynaptic projections via the pons or thalamus (Schmahmann 1996; Middleton & Strick, 2001; Kelly & Strick 2003). However, sensitivity to indirect connections and the fact that fcMRI reflects coherence rather than direct anatomic projections also limits the specificity of the method (see Buckner et al., 2009 for discussion). For example, fcMRI does not permit recovery of information about the directionality of connections. Also, fcMRI results can lead to ambiguous interpretations of the specific structure of connectivity. When three regions show coherent fluctuations it is not possible to know whether they are all connected or whether two regions show correlation mediated by their common connections to the third region. Despite these limitations, the method is particularly useful for identifying segregated pathways even if the directionally of connectivity cannot be determined. Work on the cingulate (Margulies et al. 2007) and the

medial temporal lobe memory system (Kahn et al. 2008) provide examples where segregated brain pathways have been successfully characterized.

Here we use fcMRI to provide a detailed analysis of fronto-cerebellar circuits, taking advantage of the method's ability to identify segregated pathways. Several prior studies have noted fluctuations in the cerebellum that correlate with the cerebral cortex (e.g., Allen et al. 2005; Fransson et al. 2005; Vincent et al. 2008). Allen et al. (2005) demonstrated the feasibility of using fcMRI to study the functional connectivity between the cerebral cortex and the cerebellar cortex (including the dentate nucleus) in humans, and provided evidence that fcMRI is sensitive to the anatomical constraints governing cerebro-cerebellar connectivity.

The present work expands upon these observations. The full extent of the cerebellum and cerebral cortex was imaged across two independent data sets (each n= 40) to systematically map connectivity by seeding multiple frontal regions and exploring correlations in the cerebellum. We sought to determine whether correlations between the frontal cortex and cerebellum could be detected using fcMRI and whether the detected correlations would be consistent with circuit properties previously observed in nonhuman primates. Studies in the monkey demonstrate that cortical areas project to the contralateral cerebellum via efferents that cross hemispheres between the pons and the cerebellar cortex and afferents between the deep cerebellar nuclei and the thalamus. Furthermore, certain fronto-cerebellar connections are organized as closed, independent circuits, wherein neocortical areas receive input from the very same cerebellar regions that they project to (Middleton & Strick 2000). This connectional architecture, unlike projections between neocortical areas that show convergence and divergence, is ideally

structured to test the specificity of fcMRI. Thus, the monkey anatomy suggests there should exist multiple, parallel polysynaptic circuits between frontal cortex and the cerebellum and also that these circuits should exhibit crossed-laterality.

Methods

Participants.

80 young adults participated for payment (ages 18 to 28, mean age = 21.5 yrs, 35 male). All had normal or corrected-to-normal vision and were right-handed, native speakers of English with no reported history of a neurologic or psychiatric condition. Participants provided written informed consent in accordance with guidelines set by institutional review board of Partners Healthcare.

Data acquisition.

Scanning was conducted on a 3T TimTrio scanner (Siemens, Erlangen, Germany) using a 12-channel phased-array head coil. The functional imaging data were acquired using a gradient-echo echo-planar sequence sensitive to blood oxygen-level dependent (BOLD) contrast (TR = 3000 ms; TE = 30 ms; flip angle = 90º; 3 x 3 x 3 mm voxels; 0.5 mm gap between slices; FOV = 256; interleaved acquisition). Whole-brain coverage including the entire cerebellum was achieved with 43 slices aligned to the anterior-posterior commissure plane. Structural data included a high-resolution T1-weighted magnetization-prepared gradient-echo (MP-RAGE) image (TR = 2530 ms, TE = 3.44 ms,

FA = 7º, 1.0 mm isotropic voxels; FOV 256 x 256). Head motion was minimized by using a pillow and padded clamps, and earplugs were used to attenuate noise.

Two separate datasets were collected (*Data Set 1: n = 40; Data Set 2: n = 40*). *Data Set 1* was used to identify, in an exploratory manner, the regions of frontal cortex that correlate with regions in the cerebellum. *Data Set 2* was used to formally test for dissociation among fronto-cerebeller circuits generated from the findings in *Data Set 1*. During all runs of *Data Set 1*, participants engaged in a passive task state that was either (1) eyes closed rest, (2) eyes open fixating a visual crosshair, or (3) eyes open without fixating. These rest-state variants show minimal differences in functional connectivity (van Dijk et al., 2008) so, in order to optimize signal-to-noise, all variants were used when available. Between 2 (n=11) and 6 (n=29) runs of 104 timepoints were collected from each participant. For participants with 6 runs, two of each passive task variant were acquired. For participants with 2 runs, only visual fixation was acquired. One participant completed 4 runs of eyes closed rest. Participants completed various tasks unrelated to the present study before the rest runs analyzed here. The visual crosshair was generated on an Apple MacBook Pro (Apple Computer Inc., Cupertino, CA) using Matlab software (The Mathworks, Inc., Natick, MA) and the Psychophysics Toolbox extension (Brainard, 1997) and projected onto a screen positioned at the head of the magnet bore. Participants viewed the screen though a mirror attached to the head coil. In *Data Set 2*, two runs were collected from each participant. During both runs of *Data Set 2*, participants engaged in eyes open without fixating.

Data preprocessing.

Procedures previously optimized for fcMRI analysis were employed (Fox et al. 2005; Vincent et al. 2006, Van Dijk et al. 2008) based on the method of Biswal et al. (1995). Preprocessing included: (1) removing the first four volumes to allow for T1-equilibration effects, (2) compensation of systematic, slice-dependent time shifts, and (3) motion correction. Functional data were normalized to the Montreal Neurological Institute (MNI) atlas space using a T2-weighted EPI BOLD-contrast atlas (SPM2, Wellcome Department of Cognitive Neurology, London, UK) yielding a time series resampled to 2-mm cubic voxels. A low-pass temporal filter then removed constant offsets and linear trends over each run while retaining frequencies below 0.08 *Hz*. A 6-mm full-width half-maximum Gaussian blur was used to spatially smooth the images. Sources of spurious variance, along with their temporal derivatives, were removed through linear regression including: (1) six parameters obtained by correction for rigid body head motion, (2) the signal averaged over the whole brain, (3) the signal averaged over the lateral ventricles, and (4) the signal averaged over a region centered in deep cerebral white matter. This regression procedure minimized signal contributions of non-neuronal origin including respiration-induced signal fluctuations (Wise et al. 2004; Birn et al. 2006).

Mapping cerebro-cerebellar circuitry using functional connectivity.

To identify regions that are intrinsically correlated with distinct frontal regions, two sites of interest were selected: motor cortex (MOT) and dorsolateral prefrontal cortex (DLPFC). To identify whether the circuits exhibited crossed-laterality, separate right and left frontal regions were constructed for each site. Specifically, 8-mm radius spherical

seed regions were constructed separately for the right and left hemispheres (i.e. mirrored about the x-axis for each site; MOT coordinates: +/- 42, -24, 60; DLPFC coordinates: +/- 42, 16, 36; coordinates reflect the centers of the regions, see Table 1). The particular regions were selected by visual inspection of the anatomical template (for instance, the MOT coordinates were selected so that they fell within the precentral gyrus). Correlation maps were computed for all four seed regions for each participant in *Data Set 1*, and a group-averaged, Fisher's *r-to-z* transformed correlation map was generated for each seed. These were whole-brain maps, however here we focus only on the connectivity patterns in the cerebellum. In order to test for crossed-laterality, direct comparisons of the left and right MOT and DLPFC seed regions were computed by means of arithmetic subtraction of the *z* score correlation maps. In this manner, connectivity patterns were generated for each of the separate frontal sites that could reveal the lateralization of the cerebellar connectivity.

Table 1.1: Locations of Frontal Seed Regions. Notes: Atlas coordinates (x,y,z) represent the Montreal Neurological Institute (MNI) coordinate system (Evans et al., 1993) based on the MNI152/ACBM-152 target. MOT = motor cortex, DLPFC = dorsolateral prefrontal cortex, MPFC = medial prefrontal cortex, APFC = anterior prefrontal cortex.

Frontal Seed		x	y	z
MOT				
	L	-42	-24	60
	R	42	-24	60
DLPFC				
	L	-42	16	36
	R	42	16	36
MPFC				
	L	-12	48	20
	R	12	48	20
APFC				
	L	-32	40	28
	R	32	40	28

Random effect analyses were then conducted to test for statistical significance. Specifically, paired t-tests on the generated *r(z)* maps were conducted for the left and right seeds of MOT and DLPFC. Only significant results were interpreted. We display the correlation maps (after *r-to-z* transform) and map differences because they represent the best estimates of the topography. Hypothesis-testing statistics slightly distort the maps due to differential variance across the image (e.g., the center of mass of an object tends to shift away from brain edges in t-maps because of increased variance). For completeness, we also display the full maps based on random-effects analysis in the Supplemental Materials.

We next investigated whether the connectivity between a given frontal site and a cerebellar region is reciprocal and selective, that is, whether maps produced by cerebellar seed regions exhibit "closed-loop circuitry" by showing preferential correlations with those frontal sites that originally produced the cerebellar correlations. Note that this is not an obligatory property. It is possible that cerebellar seeds could correlate with widespread regions of the cerebral cortex. To test for closed-loop circuitry, we identified the peaks of functional connectivity in the cerebellum in the MOT map (CBM_{MOT}) and in the DLPFC map (CBM_{DLPFC}). Spherical regions of 2 mm radius were defined around these cerebellar peaks (CBM_{MOT} coordinates, Right: 22, -52, -22, Left: -20, -50, -24; CBM_{DLPFC} coordinates, Right: 10, -82, -26, Left: -12, -82, -28; see Table 2) and the corresponding correlation maps were computed for the cortex. The circuit properties were then tested by exploring to what degree the cerebellar regions projected to separate or overlapping regions of the cerebral cortex. Specifically, we predicted that the CBM_{MOT} seed would result in selective correlations with motor cortex and would not correlate with prefrontal

regions, and that the CBM_{DLPFC} correlated regions would project to prefrontal cortex and would spare the motor strip.

It is important to emphasize again that fcMRI does not permit recovery of information about the *directionality* of connections (Allen et al. 2005). That is, seeding a region in the cerebellum will likely result in correlations with both the efferent and the afferent connections to it; functional connectivity analysis only assesses the degree of coherence between spontaneous activity in different regions, not the direction of influence. Nonetheless, fcMRI remains a valuable method for investigating the topography of connectivity between brain regions, especially when the circuits under consideration exhibit separable correlation profiles.

Cerebellar topography.

As the results of the preceding analysis will show, functional connectivity reveals distinct fronto-cerebellar circuits when comparing a dorsolateral prefrontal region to a motor cortex region. Based on this result, we next extended the approach to explore fronto-cerebellar topography more extensively. Tracing studies in the monkey suggest that there are multiple prefrontal zones that project to the pontine nucleus, as well as other zones that markedly lack pontine projections (Schmahmann & Pandya 1997; Middleton & Strick 2001). Importantly, previous diffusion imaging work has presented initial evidence that human prefrontal cortex may contribute relatively more projections to the pontine nucleus than does monkey prefrontal cortex (Ramnani et al. 2006), but the topography of fronto-cerebellar connectivity has not yet been characterized. Two additional frontal regions (for a total of four) were targeted: medial prefrontal cortex

(MPFC) and anterior prefrontal cortex (APFC), and again bilateral 8-mm radius, spherical regions were drawn (MPFC: +/- 12, 48, 20; APFC: +/- 32, 40, 28) (Table 1). The corresponding correlational maps were computed for each participant and a *z* transformed, group-averaged map was generated. The subtraction method was again employed to assess the differential correlation patterns found in the cerebellum from each of the MOT, DLPFC, MPFC and APFC seed regions. Random effects analyses formally quantified the statistical significance of the correlation maps for selective pairs of the seed regions. Effects were interpreted only if they were significant (corresponding to $p < .05$ correcting for multiple comparisons using the False Discovery Rate method).

Using the same approach that was applied to the MOT and DLPFC maps above, peak search was employed on the MPFC and APFC maps to obtain local maxima in the cerebellum (CBM_MPFC coordinates: 34, -80, -36 and -32, -76, -34; CBM_APFC coordinates: +/- 36, -52, -34) (Table 2). Spherical 2-mm radius seed regions were created around them to compute correlation maps for the cerebral cortex. The previous analysis compared cortical networks resulting from seeding anterior and posterior cerebellar regions. This test enabled us to assess the extent to which different locations in the posterior cerebellum are functionally coupled with the similar or distinct cortical networks.

Table 1.2: Locations of Cerebellar Projections from Frontal Cortex. Atlas coordinates and abbreviations for cortical regions are similar to Table 1. R= right, L = left. Coordinates in **bold** correspond to the centers of seed regions that were drawn in cerebellar cortex in order to compute correlation maps for the cerebral cortex (see Figure 2 and Figure 7). Labels represent approximate lobule locations based on the MRI atlas of the human cerebellum (Schmahmann et al. 1999; 2000).

Frontal Seed	Label	Peak Cerebellar Coordinate			z(r)
L MOT					
	Lobule V	**22,**	**-52,**	**-22**	0.26
	Lobule VIIIB	20,	-58,	-54	0.23
R MOT					
	Lobule V	**-20,**	**-50,**	**-24**	0.28
	Lobule VIIIB	-19,	-57,	-53	0.21
L DLPFC					
	Crus I	**10,**	**-82,**	**-26**	0.35
	Crus II	36,	-68,	-44	0.32
	Crus I	-36,	-66,	-40	0.17
R DLPFC					
	Crus I	**-12,**	**-82,**	**-28**	0.36
	VIIB	-36,	-70,	-46	0.32
	Crus I	12,	-82,	-28	0.19
L MPFC					
	Crus I	**34,**	**-80,**	**-36**	0.29
	Crus I	-30,	-78,	-34	0.26
R MPFC					
	Crus I	**-32,**	**-76,**	**-34**	0.29
	Crus I	24,	-80,	-32	0.20
L APFC					
	Lobule VI/Crus I	**36,**	**-52,**	**-34**	0.21
	Lobule VI	-36,	-52,	-34	0.22
R APFC					
	Lobule VI	**-36,**	**-52,**	**-34**	0.29
	Lobule VIIB/Crus II	38	-46,	-48	0.23

Control analyses.

An important internal control for our investigation is to show that seeding regions in cerebral cortex known to lack anatomic connections with the cerebellum will similarly fail to produce fcMRI correlations in the cerebellum. Research in the rhesus monkey

suggests that striate cortex does not have any projections to the pons—an obligatory step to the cerebellar cortex—although other regions in the occipital cortex do (Schmahmann & Pandya 1993). Accordingly, we placed bilateral 8-mm radius seeds in or near primary auditory and visual cortices (AUD: +/- 46, -18, 8; VIS: +/- 4, -88, 2).

As an additional control, we investigated the sensitivity of the overall pattern of cerebellar topography to our choice of particular seed locations in frontal cortex. Accordingly, we created new pairs of frontal seeds several millimeters away from the coordinates of the original seeds, taking care that the seed remained in the same general frontal zone (for instance, the new MOT seeds were moved approximately 8mm medially, while remaining in the precentral gyrus). Because we were interested in the overall cerebellar topography resulting from each region, the correlation maps from the left and right seed regions were averaged together to increase statistical power.

Replication and dissociation of fronto-cerebellar circuits.

As the results will reveal, multiple distinct fronto-cerebellar circuits are observed. To formally test whether these circuits can be dissociated we extracted their corresponding seed regions in the cerebellum and frontal cortex and formally tested, in an independent dataset, whether differential correlation could be replicated. For this analysis, we asked whether each circuit demonstrated selective coherence that was greater between its cerebellar seed and frontal target than any of the other frontal targets. Specifically, the cerebellar topography generated by the different frontal seed regions (MOT, DLPFC, MPFC and APFC) in *Data Set 1* was used to define cerebellar regions that were used as *a priori* seeds in *Data Set 2* (Vincent et al. 2006; 2008; Kahn et al.

2008). Bilateral 2-mm radius spherical seeds were constructed around local maxima in the cerebellum maps generated from each bilateral frontal seed pair in *Data Set 1.* These regions were then used as seeds in *Data Set 2* to test the prediction that four distinct fronto-cerebellar circuits exist. Two-way *t*-tests directly compared correlation strengths between each site in the cerebellum and each frontal region of interest, yielding 12 comparisons in total.

Results

Seed-based fcMRI was used to map fronto-cerebellar circuits in the human. We first provide evidence that the governing principles of these same pathways in nonhuman primates, for instance, the crossed laterality of the cerebro-cerebellar connections, are present in humans and can be detected using fcMRI. We next show that the human cerebellum contains at least four distinct fronto-cerebellar circuits, including three associated with distinct prefrontal regions. Importantly, control seeds placed in or near primary auditory and visual cortices do not produce correlations in the cerebellar hemispheres. In a final analysis, we directly demonstrate that the four dissociated fronto-cerebellar circuits replicate in an independent data sample.

Figures show connectivity maps overlaid onto an anatomical template generated by averaging the T1 structural scans of all of the participants in the present study. To assist visualization, the volumetric results are also projected onto the inflated cortical surface of the PALS (population-average landmark- and surface- based) atlases of the cerebrum (Figure 1.2) and of the cerebellum (Figure 1.8) using Caret software (Van

Essen 2005). Anatomic description of the cerebellum is based on Schmahmann et al. (2000).

fcMRI reveals contralateral lateralization of fronto-cerebellar connectivity.

Cerebellar connectivity generated by subtracting the MOT and DLPFC maps from their contralateral counterparts is shown in Figure 1.1. Anatomically selective regions of the cerebellum reveal robust correlations with the two sets of frontal seeds. Cerebellar connectivity shows crossed-lateralization in relation to the cortex.

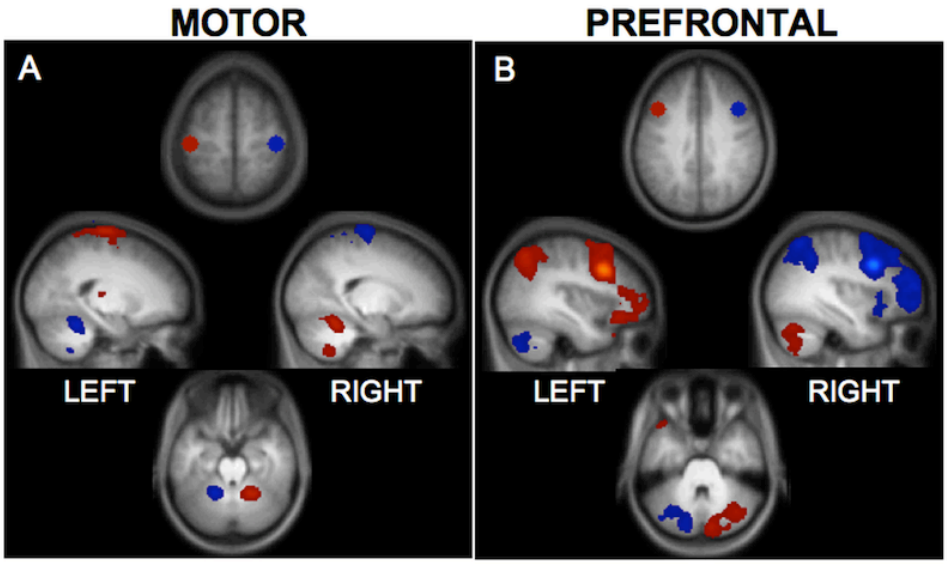

Figure 1.1. Motor and prefrontal cortex project to distinct, preferentially contralateral regions of the cerebellum. Correlation maps for motor and prefrontal seed regions are displayed overlaid on the participants' averaged T1 structural scan. (A) Bilateral spherical seed regions in motor cortex (MOT coordinates: +/- 42, -24, 60) correlate with regions in lobules IV-VI in the anterior cerebellum and with VIIIB in ventral aspects. (B) Bilateral seed regions in dorsolateral prefrontal cortex (DLPFC coordinates: +/- 42, 16, 36) correlate with distinct regions in Crus I and Crus II in the posterior cerebellum. In each map, red corresponds to preferentially greater correlations with seed regions in the left hemisphere and blue corresponds to preferentially greater correlations with seed regions in the right hemisphere. Maps are at a threshold of $z(r) > 0.1$. All image sections and atlas coordinates are referenced to the Montreal Neurological Institute (MNI) coordinate system (Evans et al. 1993). Numbers refer to z coordinate of axial slices. Left is displayed on the left.

From a technical perspective, these results provide further evidence that spontaneous BOLD fluctuations are constrained by anatomical projections (Biswal et al. 1995; Fox & Raichle 2007; Vincent et al. 2007; Johnston et al. 2008). It is especially compelling in the present case as the contralateral connectivity pattern observed cannot be attributed to artifacts such as shared vasculature—the cerebellum is supplied by its own major arteries (Schmahmann 2007b)—or to head motion. Moreover, there are no direct anatomic projections between the cerebral cortex and cerebellum. Thus, the results reinforce that fcMRI correlations can reflect polysynaptic connectivity.

Motor and prefrontal cortex form independent circuits with the cerebellum.

Cerebellar correlations with MOT versus DLPFC seed regions reveal clear anatomic dissociation (Figure 1.1). MOT correlations recover the dual motor representations in the anterior/superior cerebellum and in the inferior cerebellum (Figure 1.1A), consistent with the expected topography of primary and secondary representations (Snider & Eldred 1951; Grodd et al. 2001), while DLPFC correlations are found in the posterior hemispheres (Crus I/II, Figure 1.1B). The cerebellar regions associated with MOT correspond to lobules IV-VI and VIIIB (lobule locations estimated based on Schmahmann et al. 1999, 2000). Importantly, these lobules contain a preponderance of labeled neurons from viral injections to M1 in the cebus monkey (Kelly & Strick 2003). The DLPFC correlations (Figure 1.1B) appear in regions that correspond to Crus I and Crus II of the cerebellum (Schmahmann et al. 1999, 2000), which contain the majority of labeled neurons from viral injections in monkey prefrontal area 46 (Kelly & Strick 2003).

Random effects analyses comparing left and right MOT and DLPFC maps are displayed in Supplementary Figure S1.1.

Further analysis revealed that seeding the peaks of the cerebellar regions recovered from the preceding analysis results in correlations with distinct cerebral networks. Figure 1.2A displays the two networks that are correlated with cerebellar seeds CBM_{MOT} and CBM_{DLPFC} (locations of seeds displayed in Figure 1.2B and listed in Table 1.2,), projected onto the inflated cortical surface (peak frontal coordinates and z(r) values listed in Supplementary Table S1.1). Importantly, cortical regions correlated with these two cerebellar sites were non-overlapping, supporting the characterization of cerebral-cerebellar circuits as closed, segregated loops (Kelly & Strick 2003).

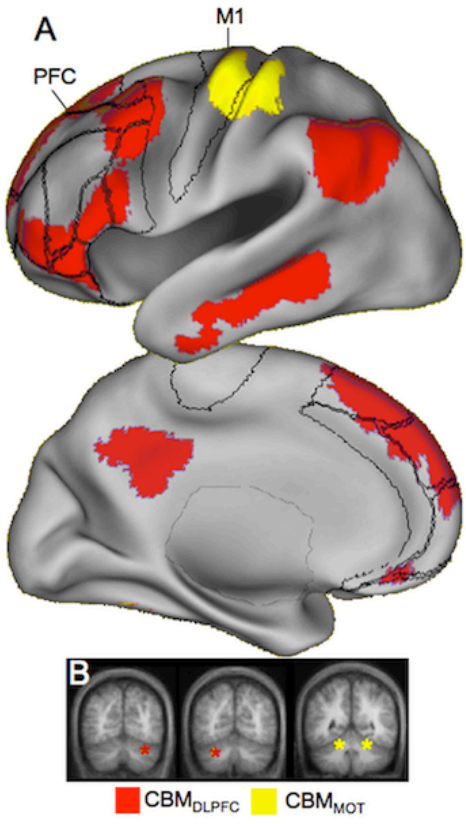

Figure 1.2. Projections from the cerebellum form closed-loop circuits. Regions in the anterior and posterior cerebellar hemispheres correlate with distinct, non-overlapping cerebral networks. (A) Regions correlated with CBM_{MOT} (lobule V) are almost entirely restricted to motor cortex in the frontal lobe, while regions correlated with CBM_{DLPFC} (Crus I) include lateral dorsal, ventral as well as medial prefrontal cortex. Note that the CBM_{MOT}-correlated region at the base of the temporal lobe on the medial view is most likely actually correlated activation in the cerebellum that has "spilled over" into the cerebral cortex because of the cortical inflation and does not actually reflect correlations in the temporal lobe. Maps are at a threshold of $z(r) > 0.1$. The volumes are projected onto the left hemisphere cortical surface of the PALS atlas (Van Essen 2005). The right hemisphere produces indistinguishable results. Borders reflect approximate borders of relevant Brodmann areas encompassing the prefrontal cortex and motor cortex (see Fig 1.7). M1 = Primary motor cortex, PFC = Prefrontal cortex. (B) Locations of the seed regions are shown schematically (colored asterisks) on slices of the cerebellum.

The cerebellum contains (at least) four distinct projection zones from the frontal cortex.

Having established that fcMRI can map distinct fronto-cerebellar circuits, we next extended the approach to map the cerebellar targets of four separate frontal regions: MOT, DLPFC, MPFC and APFC. For these analyses, because between-circuit contrasts were the target and not evidence for lateralization, bilateral seeds were used to increase statistical power. Figure 1.3 displays subtractions between two given maps, effectively revealing the relative differences in connectivity patterns for different fronto-cerebellar connections.

All comparisons show dissociations in the topography of the cerebellar correlations based on connectivity with the different frontal regions. Figure 1.3A exhibits the dissociation of cerebellar connectivity with MOT and DLPFC seeds, respectively, as discussed above. Figure 1.3B shows further fractionation of posterior cerebellum by comparing DLPFC to MPFC. Specifically, MPFC-correlated regions of the cerebellum localize to lobule Crus I, while DLPFC-correlated regions span Crus I as well as Crus II in its lateral and ventral extent (Schmahmann et al. 1999, 2000). APFC correlations, relative to MPFC correlations, appear largely in lobule VI (Figure 1.3C), and more ventrally in VIIIA. MOT and APFC correlations dissociate between lobules VIIIB and VIIIA/VIIB in ventral cerebellum (Figure 1.3D) and between lobules V and VI in dorsal cerebellum (not shown). The results from the random effects analyses comparing cerebellar connections with different frontal sites are shown in Supplementary Figure S1.2 (peak coordinates and t-scores summarized in Table S1.3).

Table 1.3: Peak Cerebellar Coordinates from Frontal Seeds. Atlas coordinates and abbreviations for cortical regions are similar to Table 1.1. R= right, L = left. Labels represent approximate lobule locations based on the MRI atlas of the human cerebellum (Schmahmann et al. 1999; 2000).

Contrast	Label		Coordinate			z(r)
MOT-DLPFC						
	L	Lobule VIIIB	-24	-54	-56	0.33
	L	Lobule V	-20	-52	-22	0.32
	R	Lobule VIIIB	20	-60	-56	0.28
	R	Lobule V	24	-54	-20	0.27
DLPFC-MPFC						
	L	VIIB	-34	-68	-50	0.32
	L	Crus II	-10	-76	-28	0.31
	R	Crus II	10	-78	-25	0.28
	R	Crus II	34	-70	-50	0.25
MPFC-APFC						
	R	IX	6	-54	-48	0.41
	R	Crus I	26	-82	-34	0.39
	L	Crus I	-26	-82	-34	0.38
APFC-MOT						
	L	VI/Crus I border	-34	-54	-34	0.43
	L	VI	-30	-66	-28	0.41
	R	VI/Crus I border	36	-56	-32	0.32
	L	VIIB/VIIA border	-38	-46	-46	0.31
	L	VI	-34	-66	-26	0.31
	L	Crus I	-46	-54	-36	0.29
	R	VIIB/VIIA border	38	-48	-48	0.26

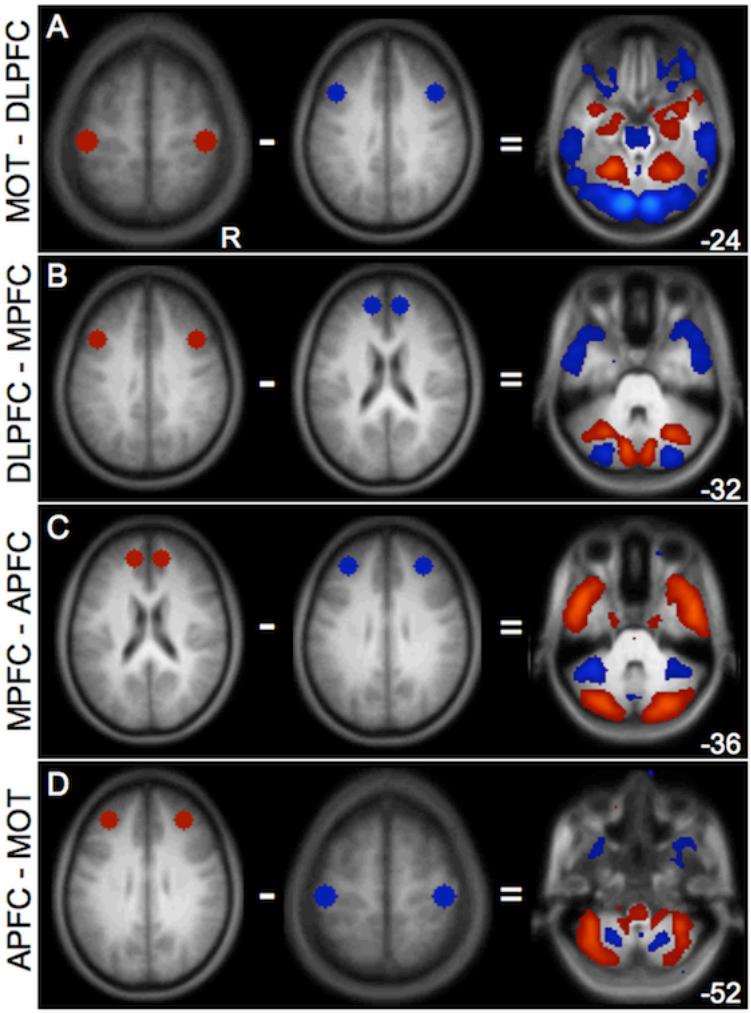

Figure 1.3. The cerebellum contains at least four distinct zones associated with frontal cortex. To illustrate the presence of multiple cerebro-cerebellar circuits, maps from distinct frontal seeds are directly compared. Each panel shows the regions being subtracted (left) and the resulting correlation map (right). Maps are at a threshold of $z(r) > 0.1$. (A) MOT – DLPFC results in preferential correlations with MOT in lobule V in the anterior hemisphere as well as in lobule VIIIB. Preferentially DLPFC correlated regions include Crus I, Crus II, VIIB and IX. (B) DLPFC – MPFC further divides the posterior cerebellum: MPFC has greater correlations with Crus I, while DLPFC has relatively greater with Crus II (C) MPFC – APFC dissociates in anterior cerebellum betweeen Crus I and lobule VI, respectively. In ventral cerebellum MPFC preferentially correlates with IX while APFC correlates with VIIIA. (D) APFC – MOT: APFC preferentially correlates with VI while MOT correlates with lobule V in the anterior lobe. APFC continues to correlate with the extent of VI moving ventrally and also appears to correlate with VIIB-VIIIA and Crus II at the ansoparamedian fissure, while MOT retains correlations in VIIIB. Numbers refer to z coordinate plane of the cerebellar slice.

We are cautious about claiming precise anatomical localization of our findings due to the smoothing and averaging of our functional data. However, in addition to the group-averaged maps we also inspected the maps of individual subjects to determine whether the same general patterns also holds at the single-subject level. Figure 1.4 shows the results of the above comparisons carried out in three subjects projected onto their respective anatomical volumes. The dissociations in the cerebellum are evident even at the individual-subject level.

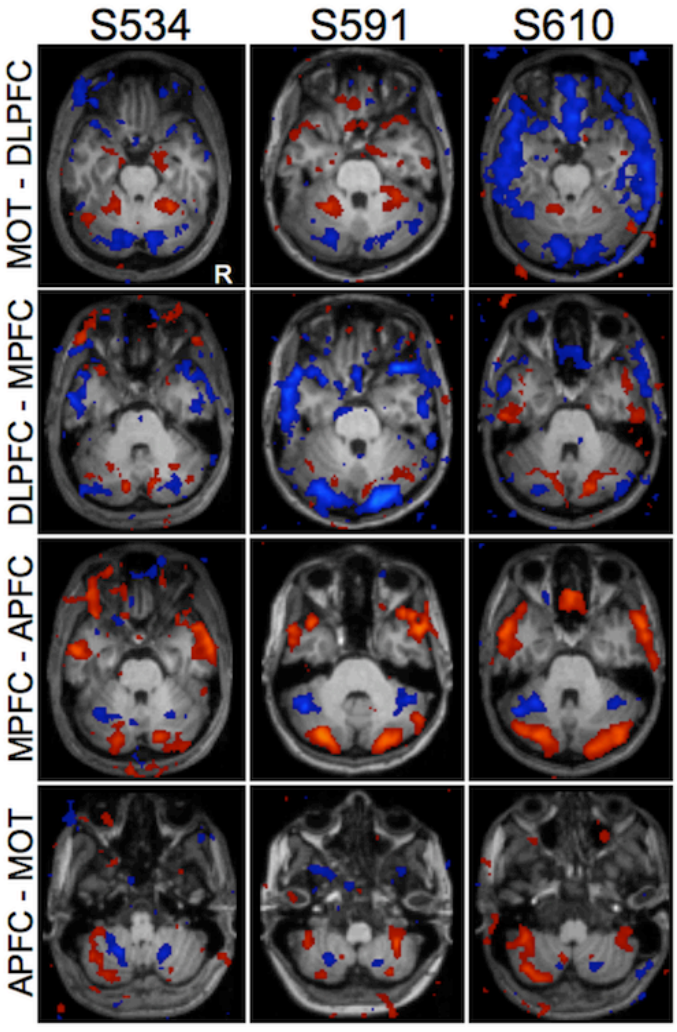

Figure 1.4. Gross topographical pattern is seen on the individual subject level. The same comparisons in Figure 1.3 are computed individually for three representative subjects. Results are overlaid on each subject's own anatomical volume. While the locations of the peak correlations vary somewhat, the overall pattern of connectivity is very similar to that seen at the group level.

Note also that the specificity of the cerebellar effect is particularly prominent when the background correlations that are common between the left and right seeded maps are removed via the subtraction method. As shown in Figure 1.5, raw correlation maps of the cerebellum without subtraction reveal bilateral functional connectivity (peak correlation coordinates in Table 1.2); the contralateral cerebellum shows relatively stronger connectivity that becomes prominent when the right and left hemisphere seeded maps are directly contrasted (as in Figure 1.1). These observations are consistent with the known contralateral, polysnaptic connections between cerebral cortex and the cerebellum (Schmahmann 1996; Middleton & Strick 2001; Kelly & Strick 2003). It should also be noted that in all of our analyses we saw robust connectivity with the thalamus, which is the obligatory anatomical step in projections from the cerebellum to the cerebral cortex (see also Zhang et al. 2008). We could also detect correlations in the pons but not in all instances (Figure 1.3).

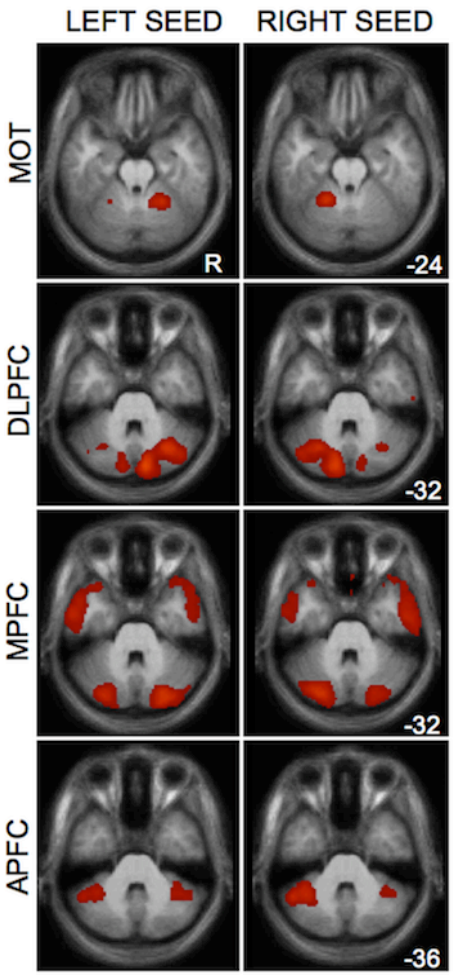

Figure 1.5. Raw correlation maps show some bilateral cerebellar connectivity from unilateral cortical seeds. While subtraction of left and right seeds in a given cortical region highlights the contralateral organization of cerebellar connectivity (see Figure 1.1), the raw left and right seeds show present, but weaker, ipsilateral connectivity with the cerebellum. This observation is consistent with the smaller percentage of cerebellar projections that cross back to the ipsilateral hemisphere (see text). Maps are at a threshold of $z(r) > 0.1$.

Cerebro-cerebellar circuits are not detected for primary auditory and visual cortices.

All of the frontal sites we tested resulted in robust functional correlation with different parts of the cerebellum. However, in order to interpret these differences it is equally important to demonstrate that cerebellar correlations are also selective. To this end we seeded regions in or near primary auditory (Heschl's gyrus) and primary visual cortex, both of which do not appear to project to the cerebellar hemispheres (Schmahmann & Pandya 1993). The results of these analyses are displayed in Figure 1.6, which also includes correlation maps produced from MOT and DLPFC for comparison purposes. In keeping with expectations, although the auditory and visual seeds produced robust cortical correlations they failed to correlate with activity in the cerebellar hemispheres.

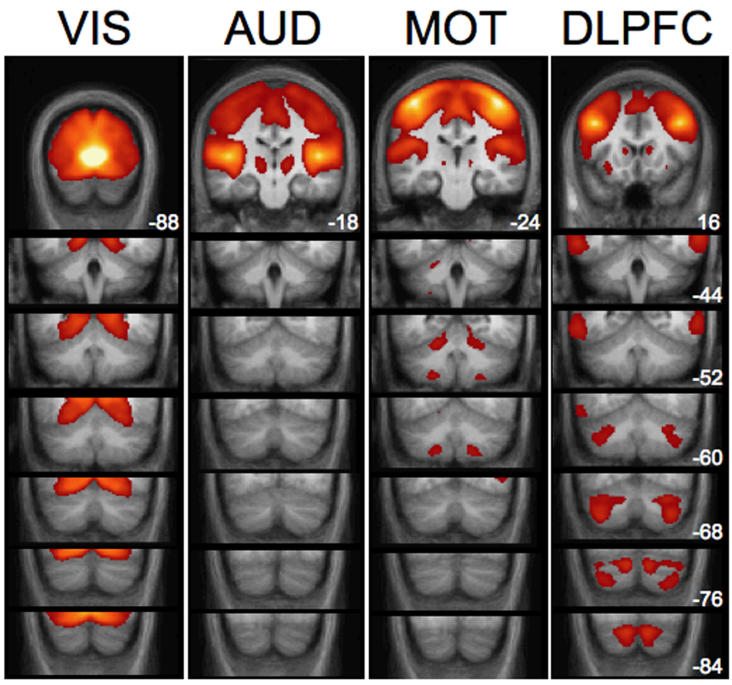

Figure 1.6. Cerebellar hemispheres are not correlated with primary visual and auditory cortices. While seeding striate cortex (VIS) and Heschl's gyrus (AUD) produces robust correlations in the cerebral cortex, no connectivity appears to be present in the cerebellum. Correlations with each of the four cerebral regions are displayed in successive coronal slices of the cerebellum. Maps are thresholded at $z(r) > 0.1$. MOT and DLPFC correlations are shown for comparison purposes. The location of the seed regions corresponds to the highest intensity values (white/yellow patches) in the first panel of each column. Numbers correspond to the y coordinate of each coronal slice.

A map of projection cortical zones from the cerebellum.

Our final inquiry assessed the distribution of cortical connectivity resulting from seeding the dissociated regions in the cerebellum that were each linked to distinct prefrontal regions. We have already demonstrated that regions in lobule V and Crus I of the cerebellum are correlated with non-overlapping cortical networks (Figure 1.2). Figure 1.7 displays the result of seeding different regions within the posterior lobe of the cerebellum (cerebellar seed coordinates in Table 1.2). While largely different cortical networks are obtained, there is also a good deal of overlap in the networks for the two most posterior seeds (located in Crus I and the Crus I/Crus II border of the cerebellum, see Figure 1.7B). Thus, cerebellar regions associated with prefrontal cortex are embedded within distinct cortical circuits but these circuits are not entirely independent at the resolution explored here.

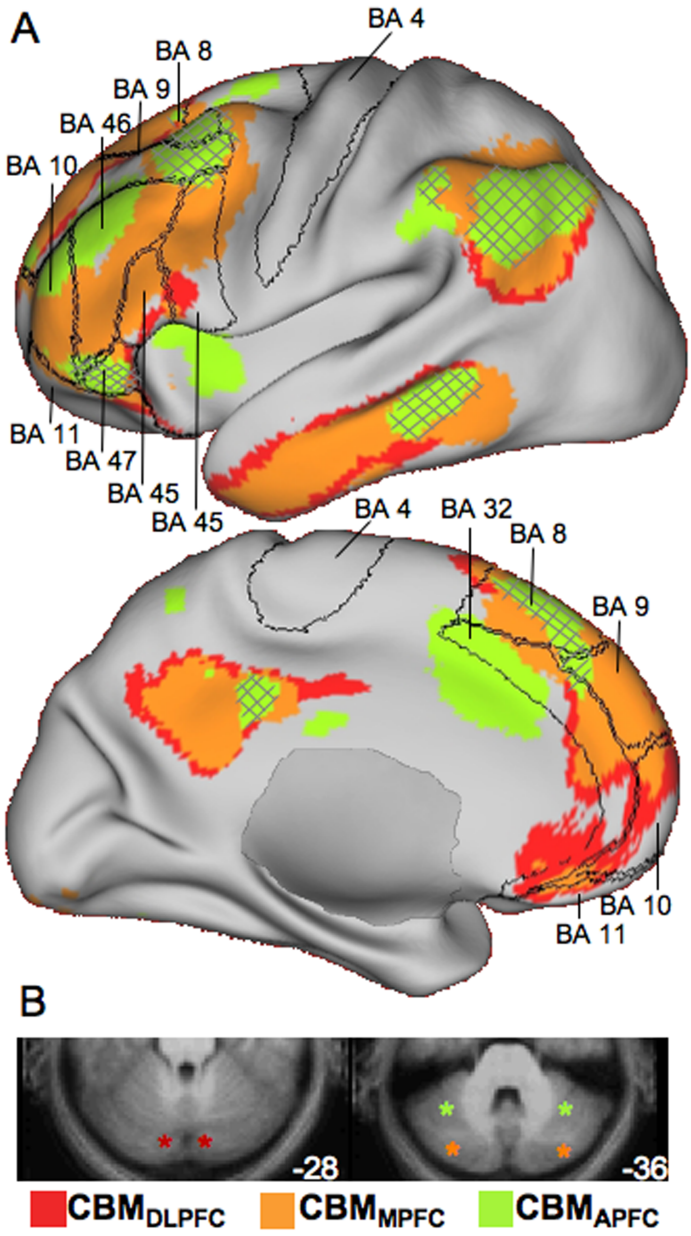

Figure 1.7. Neighboring regions of the cerebellum participate in distinct, yet partially overlapping, cerebral networks. (A) Cortical connectivity with bilateral CBM_{DLPFC}, CBM_{MPFC} and CBM_{APFC} seeds did not show the same strict segregation that was seen in the comparison between CBM_{DLPFC} and CBM_{MOT} (Figure 1.2). These regions, especially CBM_{DLPFC} and CBM_{MPFC} appear to participate in distributed cortical networks which converge in dorso-, ventro- and medial prefrontal cortex, at the posterior midline, and in regions of the lateral parietal and temporal lobes. The CBM_{APFC} network appears to be segregated from the other two networks shown in the prefrontal cortex, though some convergence was also seen, for example in BA 47. Borders reflect approximate borders of relevant Brodmann areas encompassing the prefrontal cortex and motor cortex. Hatched regions represent overlap of the CBM_{APFC} correlation map with the two other networks. BA = Brodmann area. (B) Schematic representation of the seed locations (asterisks) on cerebellar slices. CBM_{DLPFC} coordinates: +/- 12, -82, -28; CBM_{MPFC} coordinates: 34, -80, -36 and -32, -52, -34; CBM_{APFC} coordinates: +/- 36, -52, -34.

A map of cerebellar topography.

As a summary of our findings, a comprehensive map of the cerebellar correlations with the four frontal regions is shown in slice view as well as projected onto the cortical

surface of the cerebellum in Figure 1.8. While some overlap of correlated regions does occur—between DLPFC and MPFC and between DLPFC and APFC—the segregated topography of cerebellum is nonetheless impressive. Each of the four frontal regions correlates with distinct cerebellar regions.

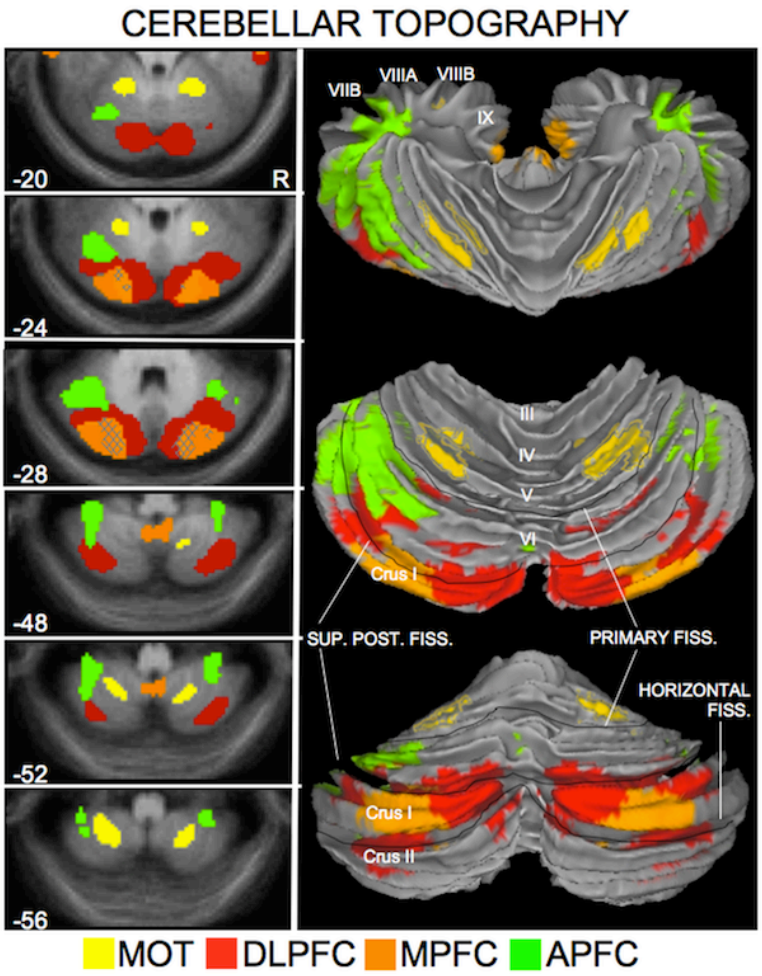

Figure 1.8. A provisional map of human cerebellar topography. All of the data in the present study were combined to provide an estimate of cerebellar topography based on the four dissociated regions illustrated in Figure 1.3. Correlations with the four frontal regions are illustrated for descending transverse sections of the cerebellum in the left panel. Each map is based on the averaged (N=40) $z(r)$ correlation map (threshold = $z(r) > 0.1$). Hatched regions represent overlap of two correlation maps. The $z(r)$ correlation maps are projected onto the cortical surface of the cerebellum in the right panel to illustrate the topographical organization of the fronto-cerebellar connectivity. This map provides a provisional (and certainly incomplete) characterization of the human cerebellum based on connectivity to the frontal cortex. The top projection is a superior view looking down on the rostral and dorsal faces of the cerebellum; the bottom projection shows the view from behind. The middle projection is a rotation between the other two (showing the entire dorsal face) to emphasize the relationships among all four dissociated cerebellar zones. Note that the majority of the mapped portion of the posterior cerebellum is associated with prefrontal (cognitive) regions of the neocortex. Anatomical labels and major divisions based on the MRI atlas of the human cerebellum (Schmahmann et al. 1999; 2000).

The results of displacing each seed while remaining within the four frontal zones is displayed in Supplementary Figure S1.3. Note that despite moving the seeds at least 8 mm from the original locations, the cerebellar topography remains remarkably similar to that shown in Figure 1.8. This implies that the overall topography of fronto-cerebellar connectivity we show here is not merely a product of the idiosyncratic choice of coordinates within the four frontal zones we investigated. On the other hand, it also implies that the resolution applied here may not be able to investigate fine-grained differences in connectivity with the cerebellum for proximal locations in cortex.

The presence of segregated circuits that involve three distinct prefrontal regions confirms that the cerebellum participates in multiple different networks subserving cognition. Relevant to recent interest in the 'default network,' which includes MPFC (Gusnard et al. 2001; Raichle et al. 2001; Buckner et al. 2008), the cerebellar region correlated with MPFC (Figure 1.8) is a prominent component of the default network. In fact, seeding this region results in correlations in the cerebral cortex that nearly fully encompass the cortical regions that comprise the default network (Figure 1.7). Taken as a group, the regions of the cerebellum linked to prefrontal cortex occupy a significant portion of the posterior hemisphere suggesting that, in humans, a large portion of the cerebellum may be dedicated to supporting cognitive functions.

Fronto-cerebellar circuits replicate and dissociate in an independent data sample.

The analyses above map four distinct fronto-cerebellar circuits. To formally explore whether the circuits dissociate we extracted seed regions in frontal cortex and the

cerebellum from *Data Set 1* and tested for segregation in the independent *Data Set 2*. Specifically, we predicted a quadruple dissociation between cerebellar regions that preferentially correlate with four different zones in the frontal cortex. This is a stringent and conservative prediction: the correlation between each cerebellar region and its prefrontal target was predicted to be significantly stronger than any of the other three prefrontal targets. Results confirmed this prediction each of the four cerebellar regions (Figure 1.9): two-tailed *t*-tests between each frontal region and each cerebellar zone revealed that correlations between lobule V and MOT, between Crus I and DLPFC, between Crus II and MPFC, and between lobule VIIIA and APFC were significantly stronger than any other pairing of these cerebellar and frontal sites (all p's $< .001$). These results demonstrate that the cerebellar regions under consideration reliably and preferentially correlate with different frontal regions within the cerebellum.

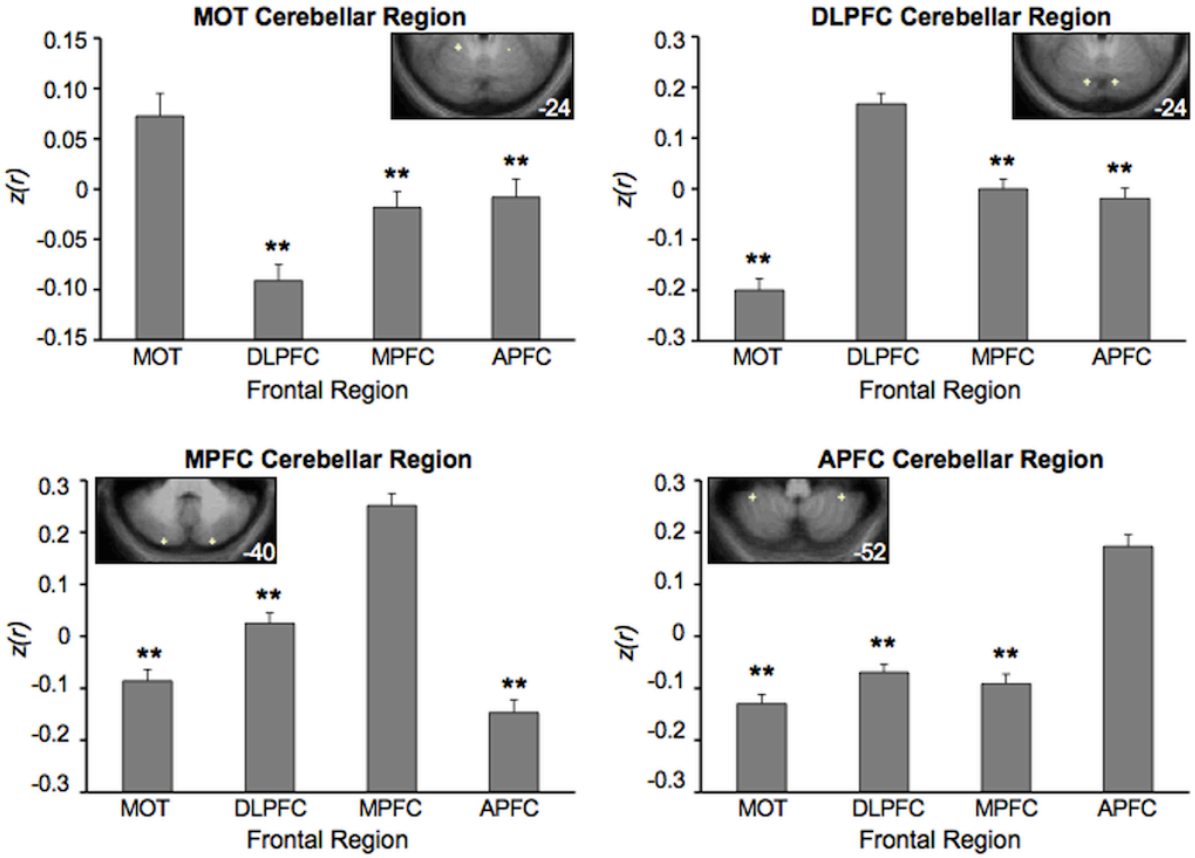

Figure 1.9. Frontal-cerebellar circuits dissociate in an independent data set. Spherical seed regions of 2-mm radius were drawn around local maxima in the cerebellar maps generated from *Data Set 1*. These regions were then carried forward and tested in the independent *Data Set 2* to formally quantify the dissociation between the four fronto-cerebellar circuits. Each graph depicts the mean *z(r)* between a given (bilateral) cerebellar region and each of the four bilateral frontal target regions. The cerebellar seed regions are depicted in the insets on each graph (coordinates: MOT cerebellar region: +/- 20, -50, -24; DLPFC cerebellar region: +/- 12, -80, -24; MPFC cerebellar region: +/- 22, -86, -40; APFC cerebellar region: +/- 36, -46, -52). ** $p < .001$.

Discussion

Leiner et al. (1986) proposed that the cerebellum exerts influence over non-motor functions. Viral tracing and neurophysiological techniques in nonhuman primates (Middleton & Strick 1994, 2001; Schmahmann & Pandya 1997; Dum & Strick 2003; Kelly & Strick 2003) and neuroimaging and neuropsychological techniques in humans

(Fiez et al. 1992; Desmond & Fiez 1998; Schmahmann 2004; Ravizza et al. 2006; Schmahmann 2007a; O'Reilly et al. 2008; Schmahmann & Pandya 2008) all point compellingly to a role for the cerebellum in cognition. However, little is known about the topography of the human cerebellum in relation to frontal-cerebellar circuits. Here we map human cerebellar topography using functional connectivity and demonstrate the presence of four separate frontal-cerebellar circuits including three distinct circuits that associate with prefrontal cortex (Figure 1.6).

As a group, the regions of the cerebellum functionally coupled with prefrontal cortex occupy a significant extent of the posterior hemisphere. Interestingly, the prefrontal-coupled regions of cerebellum in particular appear to have undergone significant expansion in recent hominid evolution. We also note that the network of cortical regions correlated with a particular lobule in posterior cerebellum, Crus I, is similar to the default network (Raichle et al. 2001; Buckner et al. 2008). Thus, the human cerebellum contains multiple regions that are correlated with distinct areas of prefrontal cortex. Functional understanding of the cerebellum should consider these distinctions.

Early anatomical work demonstrated that the dentate nucleus projects to regions of the thalamus with known connections to association areas of cerebral cortex (for a review see Leiner et al. 1986), providing an initial hint of the neural architecture that could support cerebellar influence on these areas. However, the application of both antereograde and retrograde viral tracers in the monkey provided the most compelling evidence for this hypothesis by showing that different areas of cortex participate in closed circuits with different regions of the cerebellum (Middleton & Strick 1999, 2001; Kelly

& Strick 2003). Our use of fcMRI produces results consistent with the known anatomy of cerebro-cerebellar connections.

On the basis of the tracing work, we expected to find predominately crossed-laterality in our fronto-cerebellar correlation maps. Though all cortical regions were preferentially correlated with contralateral cerebellum (i.e. MOT and DLPFC), bilateral connectivity was present for all regions tested to varying degrees (i.e. Figure 1.5). While the connectional architecture is mostly crossed, a moderate number of projections from neocortex (20-30%) terminate—via the pons—on ipsilateral cerebellum. Similarly, the pathway from cerebellum to the thalamus is predominantly, but not wholly, crossed (Schmahmann 1996).

Inspection of the raw correlation maps (Figure 1.5) suggests that the motor cortex seeds produce relatively few ipsilateral correlations compared to the more robust bilateral pattern seen for the 3 prefrontal seed regions. Future work on this topic can determine whether this is a meaningful functional or anatomic difference. It is also possible that the ipsilateral cerebellar correlations reflect correlations with the *frontal* site contralateral to the original neocortical seed. A neocortical seed in one hemisphere often produces robust correlations with the same region in the opposite hemisphere (Biswal et al. 1995), presumably reflecting strong interconnectivity of these regions via the corpus callosum (Johnston et al. 2008). Therefore ipsilateral cerebellar correlations could arise indirectly via the correlated ipsilateral neocortex.

As predicted, we observed intrinsic, correlated activity between motor cortex and the anterior cerebellar hemispheres and lobule VIIIB and between DLPFC and the posterior cerebellar hemispheres. Examining our results in more detail reveals a

fractionation of the posterior cerebellum into regions that preferentially correlated with MPFC relative to DLPFC (such as Crus I) and vice versa (Crus II). Additionally, we found that placing a seed region in APFC resulted in correlated activity in dorsal lobule VI and ventral VIIB-VIIIA, defining a fourth zone (which can also be distinguished from MOT representations). The cerebellar topography resulting from motor and dorsolateral prefrontal cortex seeds is well in keeping with established anatomical connectivity in the monkey. We additionally provide strong evidence that there are at least two other circuits connecting the cerebellum to medial and anterior prefrontal cortices in humans. Studies in nonhuman primates suggest that there are some projections to the pons from dorsomedial prefrontal convexities but not from ventrolateral or orbitofrontal cortices (for a summary see Schmahmann & Pandya 1997). Our map of cortical correlations with the posterior cerebellar hemispheres (Figure 1.7) suggests the possibility that there exist cerebro-cerebellar circuits in human prefrontal cortex that may not find a homologue in nonhuman primates. Placing seeds in primary auditory and visual cortices did not produce correlations in the cerebellum, providing an internal control for our results.

The observation that extensive portions of the posterior cerebellum are associated with putatively 'cognitive' networks is especially interesting in light of the suggestion that phylogenetic expansion of certain lateral and ventral aspects of the cerebellum and cerebellar nuclei has paralleled the expansion of the frontal cortex (Rilling & Insel 1998; MacLeod et al. 2003; Whiting & Barton 2003). The ventral half of the dentate nucleus, which comprises the fiber connections to frontal cortex, is more developed in humans than in great apes (Middleton & Strick 1994, 2001; Matano & Hirasaki 1997; Matano 2001; Dum & Strick 2003; Akkal et al. 2007). Further, relative to cerebellar midline

(vermis), the lateral hemispheres of the cerebellum have undergone significant expansion in hominoids relative to monkeys (MacLeod et al. 2003). The thalamus and pons, relay stations between the cerebellum and the neocortex, have also displayed correlated evolutionary development (Whiting & Barton 2003). The preferential expansion of these particular cerebellar regions may contribute to cognitive functions particularly well developed in humans, such as language and reasoning (Leiner et al. 1991, 1993).

Interestingly, seeding a region in Crus I resulted in a pattern of correlated cortical activity including MPFC that resembles the default network (Figure 1.5) – a network of cortical regions linked to social cognition, remembering, and planning the future (Gusnard & Raichle 2001; Svoboda et al. 2006; Buckner & Carroll 2007; Buckner et al. 2008; Spreng et al. 2009).

Caveats.

Several caveats and open questions must be considered when interpreting fcMRI connectivity results. A pertinent issue to the present study is to what degree functional connectivity reflects underlying structural connectivity. The observation that DLPFC and MOT seed regions produced correlated regions in the cerebellum that are predicted by the monkey tracing work suggests that fcMRI respects anatomical constraints. Additionally, our control seeds in striate and auditory cortex did not produce correlations in the cerebellum, consistent with known anatomy. However, fcMRI connectivity is inherently a more pervasive measure than anatomical connectivity because two regions can be correlated with one another just by virtue of the fact that they participate in a common functional network.

One implication of the possibility of indirect correlations for the present study is that other regions outside of the frontal cortex may drive the coherence patterns observed between the neocortex and the cerebellum. For example, seeding the posterior cerebellum (Crus I) produced a distributed network of correlations similar to the default network, including medial prefrontal cortex, the inferior parietal lobule and the posterior cingulate (Figure 1.7). Although medial prefrontal cortex was identified as the neocortical region exhibiting the strongest correlations with Crus I, we cannot rule out the possibility that another region within that network, for example the posterior cingulate, could mediate the relationship between MPFC and the cerebellum or contribute to the correlations in the cerebellum. For instance, parietal cortex has known anatomical connections with the cerebellum (Clower et al. 2001). This may also explain why regions in inferior temporal cortex exhibit correlations with regions in the cerebellum (i.e. Figure 1.7) despite evidence from tracing work that few, if any, projections exist between the pons and inferior temporal cortex (Glickstein et al. 1985; Schmahmann & Pandya 1991). Similarly, neocortical regions contralateral to a seed region may be responsible for driving the ipsilateral cerebellar response (Figure 1.5). Functional connectivity in other animals for which anatomical pathways are well characterized may help to resolve these questions. However, it is important to note that while the issue of pervasiveness makes the overlap of two correlation maps difficult to interpret, it does not undermine the interpretation of correlated networks that are clearly segregated; fcMRI remains a powerful technique for detecting divergent networks and for characterizing the topography of regions participating in them.

Conclusions.

Our main objectives in this study were to explore fronto-cerebellar connectivity using fcMRI and to provide a preliminary map of the resulting topography. The results identify patterns of correlated activity consistent with the principles derived from the foundational tract-tracing work on this subject (Kelly & Strick 2003). The results suggest that fcMRI is constrained by anatomy and that it detects polysynaptic connectivity between regions. Moreover, while we present functional topography from four distinct regions in frontal cortex, viral tracing techniques have also identified widespread cerebellar projections to other association cortices including parietal cortex (Clower et al. 2001); clearly a great deal of cerebro-cerebellar connectivity remains to be explored. Direct comparisons with other primates may also be useful; for instance, in *Cebus* monkeys, ventral area 46 and lateral area 12 in prefrontal cortex do not appear to be anatomically connected with the cerebellum (Middleton & Strick 2001). Whether homologous areas in humans would also lack functional connectivity with the cerebellum is an open empirical question. Our provisional results suggest the intriguing possibility that the prefrontal cortex in humans is functionally coupled with a considerable extent of the cerebellum.

References

Akkal D, Dum RP, Strick PL. Supplementary motor area and presupplementary motor area: Targets of basal ganglia and cerebellar output. *J Neurosci* 27: 10659-10673, 2007.

Allen G, Buxton RB, Wong EC, Courchesne E. Attentional activation of the cerebellum independent of motor involvement. *Science* 275: 1940-1943, 1997.

Allen G, McColl R, Barnard H, Ringe WK, Fleckenstein J, Cullum CM. Magnetic resonance imaging of cerebellar-prefrontal and cerebellar-parietal functional connectivity. *Neuroimage* 28: 39-48, 2005.

Birn RM, Diamond JB, Smith MA, Bandettini PA. Separating respiratory-variation-related neuronal-activity-related fluctuations in fluctuations from fMRI. *Neuroimage,* 31: 1536-1548, 2006.

Biswal B, Yetkin FZ, Haughton VM, Hyde JS. Functional connectivity in the motor cortex of resting human brain using echo-planar MRI. *Magn Reson Med* 34: 537-541, 1995.

Brainard DH. The psychophysics toolbox. *Spatial Vision* 10: 433-436, 1997.

Buckner RL, Carroll DC. Self-projection and the brain. *Trends Cogn Sci* 11: 49-57, 2007.

Buckner RL, Andrews-Hanna JR, Schacter DL. The brain's default network - anatomy, function, and relevance to disease. *Year in Cognitive Neuroscience 2008,* 1124: 1-38, 2008.

Buckner RL, Sepulcre, J, Talukdar T, Krienen, FM, Liu H, Hedden T, Andrews-Hanna JR, Sperling R, Johnson KA. Cortical hubs revealed by intrinsic functional connectivity: mapping, assessment of stability, and relation to Alzheimer's disease. *J Neurosci* 29: 1860-73, 2009.

Clower DM, West RA, Lynch JC, Strick PL. The inferior parietal lobule is the target of output from the superior colliculus, hippocampus, and cerebellum. *J Neurosci* 21: 6283-6291, 2001.

De Luca M, Beckmann CF, De Stefano N, Matthews PM, Smith SM. fMRI resting state networks define distinct modes of long-distance interactions in the human brain. *Neuroimage* 29: 1359-1367, 2006.

Desmond JE, Fiez JA. Neuroimaging studies of the cerebellum: Language, learning and memory. *Trends Cogn Sci* 2: 355-362, 1998.

Dosenbach NUF, Fair DA, Miezin FM, Cohen AL, Wenger KK, Dosenbach RAT, Fox MD, Snyder AZ, Vincent JL, Raichle ME, Schlaggar BL, Petersen SE. Distinct brain networks for adaptive and stable task control in humans. *Proc Natl Acad Sci USA* 104: 11073-11078, 2007.

Dum RP, Strick PL. An unfolded map of the cerebellar dentate nucleus and its projections to the cerebral cortex. *J Neurophysiol* 89: 634-639, 2003.

Evans AC, Collins DL, Mills SR, Brown ED, Kelly RL, Peters TE. 3D statistical neuroanatomical models from 305 MRI volumes. Paper presented at the Proc. IEEE-Nuclear Science Symposium and Medical Imaging Conference, 1993.

Fiez JA, Petersen SE, Cheney MK, Raichle ME. Impaired nonmotor learning and error-detection associated with cerebellar damage - a single case-study. *Brain* 115: 155-178, 1992.

Fox MD, Snyder AZ, Vincent JL, Corbetta M, Van Essen DC, Raichle ME. The human brain is intrinsically organized into dynamic, anticorrelated functional networks. *Proc Natl Acad Sci USA* 102: 9673-9678, 2005.

Fox MD, Corbetta M, Snyder AZ, Vincent JL, Raichle ME. Spontaneous neuronal activity distinguishes human dorsal and ventral attention systems. *Proc Natl Acad Sci USA* 103: 10046-10051, 2006.

Fox MD, Raichle ME. Spontaneous fluctuations in brain activity observed with functional magnetic resonance imaging. *Nat Rev Neurosci* 8: 700-711, 2007.

Fransson P. Spontaneous low-frequency bold signal fluctuations: An fMRI investigation of the resting-state default mode of brain function hypothesis. *Hum Brain Mapp* 26: 15-29, 2005.

Greicius MD, Krasnow B, Reiss AL, Menon V. Functional connectivity in the resting brain: A network analysis of the default mode hypothesis. *Proc Natl Acad Sci USA* 100: 253-258, 2003.

Greicius MD, Supekar K, Menon V, Dougherty RF. Resting-state functional connectivity reflects structural connectivity in the default mode network. *Cereb Cortex* 19: 72-78, 2009.

Grodd W, Hülsmann ML, Wildgruber D, Erb, M. Sensorimotor mapping of the human cerebellum: fMRI evidence of somatotopic organization. *Hum Brain Mapp* 13: 55-73, 2001.

Gusnard DA, Akbudak E, Shulman GL, Raichle ME. Medial prefrontal cortex and self-referential mental activity: Relation to a default mode of brain function. *Proc Natl Acad Sci USA* 98: 4259-4264, 2001.

Gusnard DA, Raichle ME. Searching for a baseline: Functional imaging and the resting human brain. *Nat Rev Neurosci* 2: 685-694, 2001.

Honey CJ, Sporns O, Cammoun L, Gigandet X, Meuli R, Hagmann P. Predicting human resting state functional connectivity from structural connectivity. *Proc Natl Acad Sci USA* 106: 2035-40, 2009.

Huffman RF, Henson, OW. The descending auditory pathway and acousticomotor systems: connections with the inferior colliculus. *Brain Res Rev* 15: 295-323, 1990.

Johnston JM, Vaishnavi SN, Smyth MD, Zhang DY, He BJ, Zempel JM, Shimony JS, Snyder AZ, Raichle ME. Loss of resting interhemispheric functional connectivity after complete section of the corpus callosum. *J Neurosci* 28: 6453-6458, 2008.

Kahn I, Andrews-Hanna JR, Vincent JL, Snyder AZ, Buckner RL. Distinct cortical anatomy linked to subregions of the medial temporal lobe revealed by intrinsic functional connectivity. *J Neurophys* 100: 129-139, 2008.

Kelly RM, Strick PL. Cerebellar loops with motor cortex and prefrontal cortex of a nonhuman primate. *J Neurosci* 23: 8432-8444, 2003.

Leiner HC, Leiner AL, Dow RS. Does the cerebellum contribute to mental skills. *Behav Neurosci* 100: 443-454, 1986.

Leiner HC, Leiner AL, Dow RS. The human cerebrocerebellar system - its computing, cognitive, and language-skills. *Behav Brain Res* 44: 113-128, 1991.

Leiner HC, Leiner AL, Dow RS. Cognitive and language functions of the human cerebellum. *Trends Cogn Sci* 16: 444-447, 1993.

MacLeod CE, Zilles K, Schleicher A, Rilling JK, Gibson KR. Expansion of the neocerebellum in hominoidea. *J Hum Evol* 44: 401-429, 2003.

Margulies DS, Kelly AMC, Uddin LQ, Biswal BB, Castellanos FX, Milham MP. Mapping the functional connectivity of anterior cingulate cortex. *Neuroimage* 37: 579-588, 2007.

Matano S, Hirasaki E. Volumetric comparisons in the cerebellar complex of anthropoids, with special reference to locomotor types. *Am J Phys Anthropol* 103: 173-183, 1997.

Matano S. Brief communication: Proportions of the ventral half of the cerebellar dentate nucleus in humans and great apes. *Am J Phys Anthropol* 114: 163-165, 2001.

Mesulam MM, Nobre AC. The cerebellum predicts the timing of perceptual events. *J Neurosci* 28: 2252-2260, 2008.

Middleton FA, Strick PL. Anatomical evidence for cerebellar and basal ganglia involvement in higher cognitive function. *Science* 266: 458-461, 1994.

Middleton FA, Strick PL. Basal ganglia and cerebellar loops: Motor and cognitive circuits. *Brain Res Rev* 31: 236-250, 2000.

Middleton FA, Strick PL. Cerebellar projections to the prefrontal cortex of the primate. *J Neurosci* 21: 700-712, 2001.

O'Reilly JX, Mesulam MM, Nobre AC. The cerebellum predicts the timing of perceptual events. *J Neurosci* 28: 2252-2260, 2008.

Petersen SE, van Mier H, Fiez JA, Raichle ME. The effects of practice on the functional anatomy of task performance. *Proc Natl Acad Sci USA* 95: 853-860, 1998.

Raichle ME, MacLeod AM, Snyder AZ, Powers WJ, Gusnard DA, Shulman GL. A default mode of brain function. *Proc Natl Acad Sci USA* 98: 676-682, 2001.

Ravizza SM, McCormick CA, Schlerf JE, Justus T, Ivry RB, Fiez JA. Cerebellar damage produces selective deficits in verbal working memory. *Brain* 129: 306-320, 2006.

Rilling JK, Insel TR. Evolution of the cerebellum in primates: Differences in relative volume among monkeys, apes and humans. *Brain Behav Evol* 52: 308-314, 1998.

Ramnani N, Behrens TEJ, Johansen-Berg H, Richter MC, Pinsk MA, Andersson JLR, Rudebeck P, Ciccarelli O, Richter W, Thompson AJ, Gross CG, Robson

MD, Kastner S, Matthews PM. The evolution of prefrontal inputs to the cortico-pontine system: Diffusion imaging evidence from macaque and humans. *Cereb Cortex* 16: 811-818, 2006.

Schmahmann JD. An emerging concept - the cerebellar contribution to higher function. *Arch Neurol* 48: 1178-1187, 1991.

Schmahmann JD, Pandya DN. Projections to the basis pontis from the superior temporal sulcus and superior temporal region in the rhesus monkey. *J Comp Neurol* 308: 224-48, 1991.

Schmahmann JD, Pandya DN. Prelunate, occipitotemporal, and parahippocampal projections to the basis pontis in rhesus monkey. *J Comp Neuro* 337: 94-112, 1993.

Schmahmann JD. From movement to thought: Anatomic substrates of the cerebellar contribution to cognitive processing. *Hum Brain Mapp* 4: 174-198, 1996.

Schmahmann JD. Disorders of the cerebellum: Ataxia, dysmetria of thought, and the cerebellar cognitive affective syndrome. *J Neuropsychiatry Clin Neurosci* 16: 367-378, 2004.

Schmahmann JD. The primary motor cerebellum is in the anterior lobe but not the posterior lobe. Evidence from stroke patients. *Neurology, 68*(12), A357-A357, 2007a.

Schmahmann JD. Cerebellum and spinal cord – principles of development, anatomical organization, and functional relevance In A. Brice andS. Pulst (Eds.), *Spinocerebellar degenerations: The ataxias and spastic paraplegias.* (pp. 1-60). New York: Elsevier, 2007b.

Schmahmann JD, Pandya DN. Anatomic organization of the basilar pontine projections from prefrontal cortices in rhesus monkey. *J Neurosci* 17: 438-458, 1997.

Schmahmann JD, Pandya DN. Disconnection syndromes of basal ganglia, thalamus, and cerebrocerebellar systems. *Cortex* 44: 1037-1066, 2008.

Schmahmann JD, Doyon J, McDonald D, Holmes C, Lavoie K, Hurwitz AS, Kabani N, Toga A, Evans A, Petrides M. Three-dimensional MRI atlas of the human cerebellum in proportional stereotaxic space. *NeuroImage* 10: 233-260, 1999.

Schmahmann JD, Doyon J, Toga A, Evans A, Petrides M. *MRI atlas of the human cerebellum*. San Diego: Academic Press, 2000.

Schmahmann JD, Weilburg JB, Sherman JC. The neuropsychiatry of the cerebellum - insights from the clinic. *Cerebellum* 6: 254-267, 2007.

Snider RS, Eldred E. Cerebro-cerebellar relationships in the monkey. *J Neurophysiol* 15: 27-40, 1951.

Snider RS, Stowell, A. Receiving areas of the tactile, auditory and visual systems in the cerebellum. *J Neurophysiol* 7: 331-357, 1944.

Spreng RN, Mar R, Kim ASN. The common neural basis of autobiographical memory, prospection, navigation, theory of mind and the default mode: A quantitative meta-analysis. *J Cogn Neurosci* 21: 489-510, 2008.

Stoodley CJ, Schmahmann JD. Functional topography in the human cerebellum: A meta-analysis of neuroimaging studies. *NeuroImage* 44: 489-501, 2009.

Svoboda E, McKinnon MC, Levine B. The functional neuroanatomy of autobiographical memory: A meta-analysis. *Neuropsychologia* 44: 2189-2208, 2006.

Van Dijk KRA, Hedden T, Tu PT, Laviolette P, Sperling RA, Buckner RL. Optimal acquisition parameters for resting state functional connecitivty MRI. *Society for Neuroscience 885.24,* 2008.

Van Essen DC. A population-average, landmark-and surface-based (PALS) atlas of human cerebral cortex. *Neuroimage* 28: 635-662, 2005.

Vincent JL, Snyder AZ, Fox MD, Shannon BJ, Andrews JR, Raichle ME, Buckner RL. Coherent spontaneous activity identifies a hippocampal-parietal memory network. *J Neurophysiol* 96: 3517-3531, 2006.

Vincent JL, Patel GH, Fox MD, Snyder AZ, Baker JT, Van Essen DC, Zempel JM, Snyder LH, Corbetta M, Raichle ME. Intrinsic functional architecture in the anaesthetized monkey brain. *Nature* 447: 83-86, 2007.

Vincent JL, Kahn I, Snyder AZ, Raichle ME, Buckner RL. Evidence for a frontoparietal control system revealed by intrinsic functional connectivity. *J Neurophysiol* 100: 3328-3342, 2008.

Whiting BA, Barton RA. The evolution of the cortico-cerebellar complex in primates: Anatomical connections predict patterns of correlated evolution. *J Hum Evol* 44: 3-10, 2003.

Wise RG, Ide K, Poulin MJ, Tracey I. Resting fluctuations in arterial carbon dioxide induce significant low frequency variations in bold signal. *Neuroimage* 21: 1652-1664, 2004.

Zhang D, Snyder AZ, Fox MD, Sansbury MW, Shimony JS, Raichle ME. Intrinsic functional relations between human cerebral cortex and thalamus. *J Neurophysiol* 100: 1740-1748, 2008.

Paper II

Stability and Instability of Functional Connectivity Networks

Krienen FM, Yeo BTT & Buckner RL. *In Prep*

Abstract

Sharp spatial transitions in resting state functional connectivity suggest its possible utility in delineating the borders of functional areas. Here, we explored factors that affect functional connectivity profiles and the resultant derived boundaries. We observed that, for a fixed clustering algorithm, borders obtained from resting scans are highly consistent even across small samples. Some borders shift when coarser or finer topographic solutions are estimated, suggesting that the exact border locations reflect both the weighting of the functional connectivity gradients and the intrinsic data properties. While functional connectivity is constrained by anatomy, we found that transient contributions reflecting task state are sufficient to shift measured borders. Task-defined network borders better explain task activation patterns than do resting-state borders. However, some broad features of organization are preserved across task state. This resilience of certain features of network topography, despite substantial changes in the exact locations of borders, underscores the inherently graded nature of fcMRI connectivity patterns. We discuss the implications of these findings for making inferences about areal organization from functional connectivity. Our results underscore the importance of surveying functional connectivity across a broader range of behavioral states than is presently the norm.

Introduction

In his classic work Korbinian Brodmann (1909/1999) described architectonic properties across the human cerebral cortex that displayed sharp boundaries in some instances and smooth transitions of features in others. These microscopic features were sufficient to delineate the boundaries of certain areas. Definitive areal characterization eluded these early anatomic studies because architectonic analysis by itself, especially with limited staining techniques, is insufficient to unambiguously define areas (Kaas 1982; Maunsell & Van Essen 1987). Chemoarchitectural stains that show regional distribution of transmitter receptor types (Zilles et al. 2002) and gene expression patterns (http://www.brain-map.org/) are becoming incorporated into multimodal brain atlases. Such sources diversify the type of information that can be used for areal mapping and refine current understanding of which cytoarchitectural features are most relevant (Toga et al. 2006). Still, direct anatomic information about brain connectivity is nearly entirely absent for humans except for limited cases in the fetus where tracing techniques have some utility (Burkhalter, Bernardo & Charles 1993) and in post-mortem examination of axonal degeneration following brain lesions (Di Virgilio & Clarke 1997; Wiesendanger et al. 2004). For these reasons, indirect neuroimaging approaches for identifying connectivity patterns are needed to study cortical organization.

Resting state functional connectivity MRI (rs-fcMRI) has emerged as a widely used, non-invasive approach for estimating connectivity. The technique relies on slow (< 1 Hz), intrinsic fluctuations in the BOLD (Blood Oxygen Level Dependent) signal. Biswal and colleagues first used the correlation structure inherent in these fluctuations to map a network of correlated regions across somatomotor cortex (Biswal et al. 1995). Other brain networks known to posses direct or indirect anatomic connectivity have similarly been explored using similar fcMRI techniques (e.g. Xiong et al. 1999; Krienen & Buckner, 2009). Brain lesions disrupt functional coupling in a pattern consistent with known anatomy (Lu et al. 2011; Johnston et al. 2008; but see also Tyszka et al. 2011).

Given that functional connectivity is constrained by anatomic connectivity, mapping connectivity transitions has the potential to provide information about the functional organization of the human brain. Adjacent regions of cortex can show

markedly distinct connectivity profiles, suggesting the possible existence of meaningful boundaries (e.g., Cohen et al., 2008; Nelson et al. 2010; Yeo et al. 2011, see http://www.youtube.com/yeokrienen). Several recent reports have noted correspondence between network topography obtained from rs-fcMRI and task-induced activations measured across a range of cognitive domains (Smith et al. 2009; Nelson et al. 2010; but see Mennes et al. 2012). Some have proposed that rs-fcMRI techniques can be used to estimate areal topography in the living brain, thereby addressing a critical gap in human neuroscience (Cohen et al. 2008; Power et al. 2011; Wig et al. 2011; Hirose et al. 2012). However, there are sufficient caveats and complexities to indicate that rs-fcMRI (by itself) in most cases will not be suitable for detecting the exact locations of areal boundaries.

For instance, functional coupling can change as a function of the current task or of recent experience (McIntosh et al. 2003; Hampson et al. 2004; Rissman et al. 2004; Hampson et al. 2006; Summerfield et al. 2006; Albert et al. 2009; Lewis et al. 2009; Hasson et al. 2009; Pyka et al. 2009; Sepulcre et al. 2010; Stevens et al. 2009; Tambini et al. 2010; Shirer et al. 2011; Vahdat et al. 2011; Mennes et al. 2012; Norman-Haignere et al. 2012). Intrinsic fluctuations of activity within as well as outside task-relevant brain regions affect subsequent behavior (e.g., Fox et al. 2006b; Hesselman et al. 2008; Baldassarre et al. 2011). These observations indicate that intrinsic fluctuations and changes in connectivity are functionally meaningful. However, they also complicate efforts to use fcMRI to map underlying areal topography.

Specifically, state dynamics in the signal measured by fcMRI complicate areal mapping because estimated boundaries can shift locations. For example, using a pattern classification approach Shirer et al. (2011) distinguished functional connectivity patterns obtained from four covert cognitive task states that could even be reliably identified in an independent cohort of subjects. These stable changes in functional coupling patterns raise the question of which cognitive state(s) produces connectivity patterns most representative of underlying structural connectivity. One possibility is that networks derived from resting state data reflect a particularly unbiased estimate of functional anatomy (Cohen et al. 2008; Wig et al. 2011). An alternative is that passive rest is no more or less well suited for discerning border locations than are other active task states.

Under this view, we should not expect the borders extracted from resting state data to align with task activations or provide a privileged estimate of areal borders.

Several issues regarding comparison of task data and resting-state network topography have been raised already, for example whether a given task contrast cleanly isolates a cognitive process or constitutes a 'robust functional localizer' (Cohen et al. 2008) and whether group-averaged data are appropriate given underlying variability of individual brains (Uncapher et al. 2010; Fedorenko et al. 2010). However, rs-fcMRI may produce biased estimates of the underlying topography for more fundamental reasons. This is not incompatible with the qualitatively good correspondence between the topography of resting-state networks and meta-analysis of task-induced activations across cognitive domains broadly (e.g. Smith et al. 2009). We ourselves rely on descriptions of general functional response properties when referring to resting state networks (e.g. the "Dorsal Attention Network"; Yeo et al. 2011). In our view, the question is rather to what extent resting state connectivity can be used to delineate exact borders of functional areas, and how rigidly borders from rs-fcMRI can be used as functional localizers. While resting-state functional borders align reasonably well with many aspects of task-based functional responses, the issue at hand is exploring the implications of the unaccounted variance.

An additional issue to consider when interpreting fcMRI is whether different results are observed when different analytic techniques are employed. While sharp transitions in connectivity profiles do exist for adjacent regions of cortex (Nelson et al. 2010; Yeo et al. 2011, see http://www.youtube.com/yeokrienen), often the pattern of connectivity varies in a manner more akin to smooth transitions of gradients (e.g. see Figure 18 of Yeo et al. 2011). The identification of boundaries between networks when the transition of connectivity patterns is inherently smooth is uncertain and therefore susceptible to change due to the particular parameters employed for the estimation. More generally, network identification algorithms always require some estimation of the relevant parameters of "exemplar" networks from existing estimated members of the networks. This means that borders or subdivisions can change depending on how parameters are weighted or specified.

Here we explored these issues by changing either the technical criteria used for analysis or the type of task that participants performed during data acquisition. Foreshadowing the main results, we found that network boundary locations remain relatively stable across small samples when holding analysis and behavioral state constant. However, changing either the technical criteria for analysis or the task performed is sufficient to induce changes in the resulting correlation maps. We discuss the implications of these results for how rigidly fcMRI boundaries should be viewed, as well as the hypothesis (or common assumption) that the resting state is the most appropriate behavioral paradigm for interrogating functional coupling between regions.

Methods

Datasets

Analyses were performed on a core dataset of 480 healthy, young adults (ages 18-35, mean age = 21.0, 38.5% male) from the Genomics Superstruct Project (GSP). Participants performed two runs of eyes open rest. Analyses of these data have been published previously (e.g., Yeo et al. 2011). In order to assess behavioral state influences on network organization, two additional datasets (Semantic Classification dataset and Passive Tasks dataset) were used.

The Semantic Classification dataset consisted of 16 subjects (mean age 21.1 yr, 25.0% male) who completed two runs of a semantic classification task in addition to several passive rest scans. Briefly, the semantic task was a continuous, self-paced paradigm that required participants to classify centrally presented words as either semantically “abstract” or “concrete” by pressing one of two buttons with their right hand. The task protocol was continuous and self-paced. A new trial was initiated as soon as the participants made their response to the previous trial. A brief (250 msec) inter-trial interval consisting of a central fixation cross was inserted between each trial to make the transition from one word to the next apparent. Analyses of these data have been published previously (e.g., Buckner et al. 2009; Sepulcre et al. 2010).

The Passive Tasks dataset consisted of 54 subjects (mean age 21.1, 48% male) who completed one run each of four different passive tasks. Each run consisted of 79 time points (3.95 min). Runs always began with a passive fixation period, which lasted

30 seconds. Then the word START appeared, indicating that participants should begin performing the task. Task blocks lasted 180 seconds. Participants were instructed to perform the task continually until the word STOP appeared, after which they returned to passively fixating until the end of the run. A central fixation cross was present throughout all task portions.

In one task, participants silently counted backwards from 1000 by threes (Count Backwards). At the end of the run they were asked to verbally report the number they reached. In a second task, participants were told to imagine living out the next day, starting from the time they woke up the following morning (Imagine Tomorrow). They were to continue imagining going through the day, in as much detail as possible and in the first person perspective, until the end of the task period. At the end of the run they were asked to report what time of day they had reached. A third task consisted of passively fixating the central crosshair for the duration of the run (Fixation Only). A final task required participants to continue to fixate the center cross, but to additionally broaden their attention covertly in order to monitor the whole screen (Monitor Screen). They were told to attend to the screen for the possible appearance of rare, brief (200 ms) small dots, and to mentally note if they did notice one. It was emphasized that there was no need to count, remember the location, or otherwise keep track of any dots they perceived. Before the run commenced they were shown a short (30 s) training presentation in which sample dots were flashed at several different locations on the screen at random intervals. At the end of the task run they were asked to report whether they had noticed any dots. In no case were dots actually presented during the run, rendering this task perceptually identical to the other tasks.

Passive tasks were counterbalanced across participants. The Passive Task dataset was part of a battery of 14 tasks acquired in a single scan session. The order of the Passive Task set was also counterbalanced with the order of the other 10 tasks, which were grouped into two different sets (a set of 6 tasks using audiovisual stimuli, and a set of 4 tasks using word stimuli). Results from these other task sets will be reported elsewhere.

MRI Data Acquisition and Preprocessing

Data were acquired on 3T Tim Trio scanners (Siemens, Erlangen, Germany) using a 12-channel phased-array head coil. Functional data consisted of gradient-echo echo-planar images (EPI) sensitive to blood oxygenation level-dependent (BOLD) contrast. Parameters for the resting data were: repetition time (TR) 3,000 ms, echo time (TE) 30 ms, flip angle (FA) 85°, 3 x 3 x 3 mm voxels, field of view (FOV) 216, and 47 axial slices collected with interleaved acquisition. Slices were oriented along the anterior commissure-posterior commissure plane. Functional runs lasted 6.2 min (124 time points). Structural data included a multiecho T1-weighted magnetization-prepared gradient-echo image (van der Kouwe et al. 2008). Parameters for the Semantic Classification dataset were: TR 3,000 ms; TE 30 ms; FA 90°; 3 x 3 x 3 mm voxels; FOV 288, and 43 axial slices. Functional runs lasted 5.2 min (104 time points). Parameters for the Passive Tasks were the same as for the Semantic Classification dataset, with the exception that functional runs lasted 3.95 min (79 time points).

fMRI processing steps included 1) discarding the first four frames of each run, 2) correcting for slice acquisition-dependent time shifts in each volume with SPM2 (Wellcome Department of Cognitive Neurology, London, UK), and 3) correcting for head motion using rigid body translation and rotation parameters (FSL; Jenkinson et al. 2002; Smith et al. 2004). Linear trends over each run were removed and a low-pass temporal filter retained frequencies below 0.08 Hz. Spurious variance was removed using linear regression with terms for head motion, whole brain signal, ventricle signal, white matter signal and their derivatives.

Individual participants' T1 scans were reconstructed into surface representations using FreeSurfer (http://surfer.nmr.mgh.harvard.edu). Functional data were registered to structural images using FreeSurfer's FsFast package (Greve & Fischl 2009; http://surfer.nmr.mgh.harvard.edu/fswiki/FsFast). The structural preprocessing and structural-functional data alignment steps are detailed in Yeo et al. (2011). Functional data were smoothed on the surface using a 6-mm full-width half-maximum kernel and were downsampled to a 4-mm mesh.

Clustering

Clustering of cerebral cortical data was performed as in Yeo et al. (2011). For each subject, the Pearson's product moment correlation was computed between each surface vertex (N = 18,715) and 1,175 ROIs spread evenly over the cortical surface. The ROIs consisted of single vertices spaced approximately 16 mm apart. The "connectivity profile" of each surface vertex is its functional coupling to these ROIs. Each participant's 18,715 x 1,175 matrix of correlations was binarized to retain the top 10% of correlations before averaging for the group estimates. The connectivity profiles were clustered using a mixture of von Mises-Fisher distributions (Lashkari et al. 2010; Yeo et al. 2011). For more details, we refer the readers to Yeo et al. (2011). Using this approach the number of clusters must be specified *a priori*. Because our previous analyses (Yeo et al. 2011) identified solutions with 7 and 17 network clusters to be particularly stable, we adopted these for the present study.

Reliability of Network Boundaries in Small Data Samples

To assess the stability of resting-state fcMRI border locations, the 480 participants were divided into 30 groups of 16 subjects. Clustering was performed on each independent sample. Clustering over all 480 participants served as the reference against which the smaller samples could be compared (Figure 2.1A). Overlap between the reference and each of the 30 samples was quantified as the percentage of vertices with the same network assignment as the reference solution. The worst, median and best scores are shown in Figure 2.1B.

Sensitivity of Estimated Network Boundaries to Analysis Effects

The boundaries of the 7 and 17 network solutions were overlaid on the same surface in order to appreciate the sensitivity of boundary locations to the particular decisions made in the analysis, for instance whether seeking a 7-network or a 17-network solution (Figure 2.2).

Sensitivity of Estimated Network Boundaries to Task State

To assess the extent to which border locations shift as a function of task state, we contrasted clustering performed on passive rest scans with semantic task scans collected

in the same participants (Semantic Dataset; Figure 2.3). We computed the correlation between each vertex's whole-cortex fcMRI maps derived from the two conditions, averaged across all subjects (Figure 2.4A). A seed-based approach was used to quantify salient aspects of the clustering results. Seed regions were either taken from our previous work (e.g., Figure 9 of Yeo et al. 2011) or selected post hoc to illustrate similarities and differences between connectivity profiles derived from the different task states (Figure 2.4B-E). Each seed region was a single ~4mm vertex. Correlation maps were obtained for each individual seed as the Pearson's product moment correlation between each seed region's time course and the time courses of all other vertices on the cortical surface. Maps were transformed to *z*-maps using Fisher's *r*-to-*z* transformation and group-averaged. An inverse Fisher's *r*-to-*z* transformation was applied to obtain group-averaged correlation maps. Borders derived from the passive rest scans and from the semantic task scans were then overlaid separately on a map of beta estimates for the semantic task to show how the functional connectivity borders conform to the task activity map (Figure 2.6).

We then compared the connectivity profiles of the four tasks comprising the Passive Task dataset (Figure 2.7B) to connectivity profiles from a dataset of 1000 subjects performing eyes open rest (Yeo et al. 2011). Using seed-based analyses, we identified specific changes in whole-cortex connectivity as a function of task (Figures 2.8-9). We selected seeds based on their network assignment "confidence." This was quantified by comparing the degree of fit for the best-fit network of a given vertex to the fit of its next-best network by clustering each task independently into 7 networks (see Figure 8 in Yeo et al. 2011). In this way, we choose seed regions whose correlation map expected to conform reasonably well to their assigned networks. We only chose seeds for which their confidence values were high for at least 3 of the 4 tasks. Regions selected in this way also tended to avoid border regions, where any observed connectivity differences might be difficult to interpret. We then plotted the correlation maps for those tasks that fit our criterion (Figures 2.8-9).

Visualization

Parcellation and seed-based correlation maps were transformed from FreeSurfer surface space to the inflated PALS cortical surface using Caret (Van Essen 2005; Van Essen & Dierker 2007). Network colors match Yeo et al. (2011). Boundary lines were smoothed to remove high spatial frequency jaggedness resulting from mapping the data to PALS space.

Results

Estimates of Network Boundaries Are Reliable Across Small Samples of Subjects

Figure 2.1A displays the overlap of the borders obtained from the 7-network solution for the 30 samples of 16 participants. The worst, median and best overlap between the reference boundaries (computed from the full dataset of 480 participants) and the 30 samples are depicted in Figure 2.1B. Overlap is defined as the percentage of vertices that share the same network assignment in the reference and sampled solution. The scores were 74%, 92% and 93% overlap for the worst, median and best overlap, respectively, indicating good agreement of border locations.

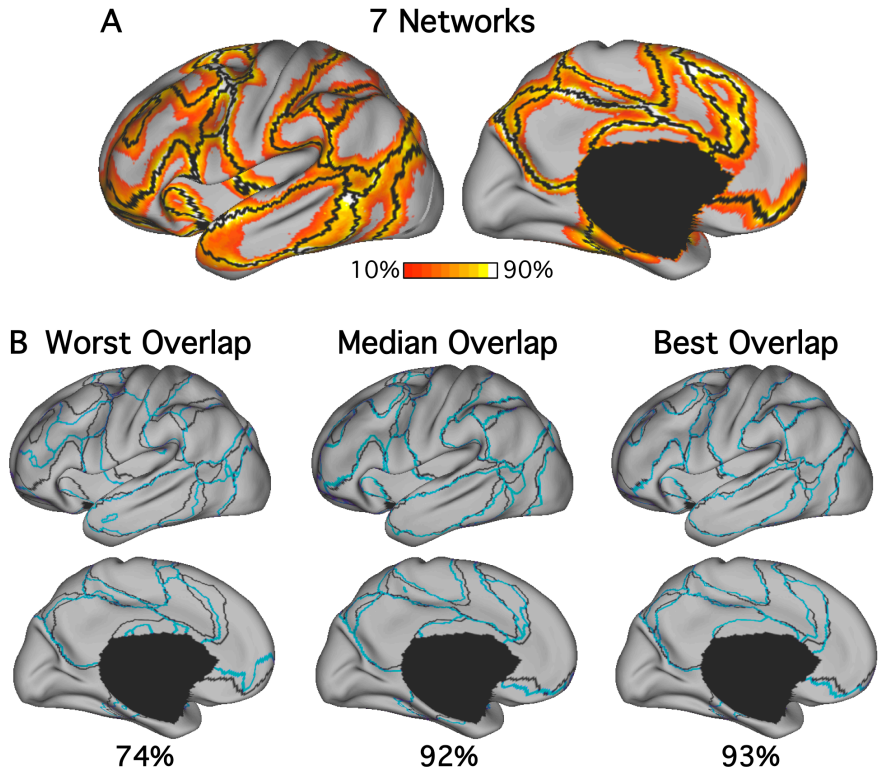

Figure 2.1. Network topography is reliable across small samples. The core dataset was divided into 30 independent samples of 16 subjects each. Borders were computed separately for each sample and plotted as a probability heat map in (A). Probability refers to the proportion of samples for which a border falls at each point across the surface. Black lines depict reference boundaries computed from the entire sample (N = 480). (B) Percent overlap between each sample and the reference networks were computed by counting the number of vertices that received the same network label. The worst, median and best-ranked percentages are shown below surface visualizations of the reference (black) and respective sample (teal) borders.

Sensitivity of Network Boundaries to Analysis Criteria

The above analyses establish a high level of reliability in the estimation of boundary locations from resting data. However, are the boundaries valid representations of meaningful functional borders? While the ground truth is difficult to estimate, one can gain insight into the question of validity by comparing multiple reasonable solutions to boundary estimation. Figure 2.2 shows the 7-network and 17-network solutions derived from the core dataset. If the 17-network solution represents a purely (spatially) hierarchical decomposition of the coarser 7-network, then the 17-network map should

cleanly subdivide the 7 networks into finer parcellations such that the 7-network boundaries are also boundaries in the 17-network estimate. Such a hierarchical split was not observed. The exact positions of boundaries reflect features of the analysis procedure in addition to intrinsic properties of the data.

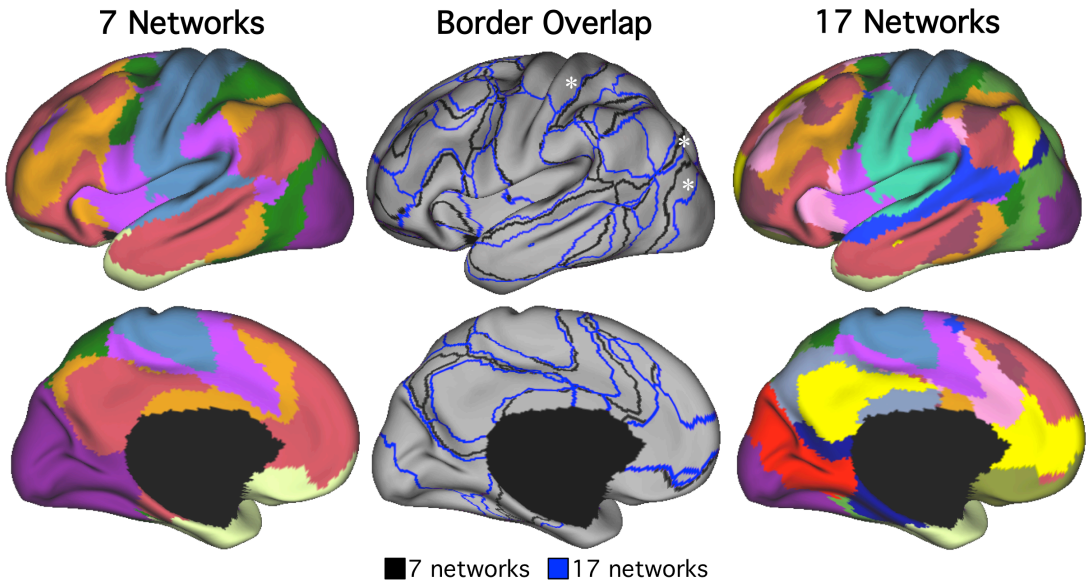

Figure 2.2. **Precise location of borders between networks can shift as a consequence of analysis procedure.** The core dataset was clustered into 7 and 17 networks and borders are overlaid in the middle column. Asterisks identify examples of good spatial correspondence (along the post-central gyrus) as well as poor correspondence (occipital and posterior parietal cortex) between two solutions. See also Figure S2.1.

While many borders do exhibit positional stability, for instance the post-central sulcus boundary between the Somatomotor and Dorsal Attention networks (asterisk in Figure 2.2), in other cases the 17-network solution produced shifted borders relative to the 7-network solution. For example, the border along parieto-occipital cortex dividing the Visual Network (purple) from the Dorsal Attention Network (green) shifts posteriorly in the 17-network solution (asterisk in Figure 2.2). The border also shifts in the posterior inferior parietal lobule (IPL) (asterisk in Figure 2.2). The emergence of the dark blue

network in the 17-network estimate, which includes posterior IPL, retrosplenial cortex and parahippocampal cortex, shifts the boundaries relative to the 7-network estimate.

Such inconsistencies arise because network estimation algorithms invariably require the (explicit or implicit) estimation of the parameters of "exemplar" networks from existing estimated members of the networks, such as the "average" connectivity profiles of the networks in our clustering algorithm (Yeo et al. 2011), the time courses of the spatially independent components in Independent Component Analysis (ICA; Beckmann et al. 2004), or the gradients in coupling strength to specified target regions (Cohen et al. 2008). A toy example (Figure S2.1) illustrates how these shifts might occur.

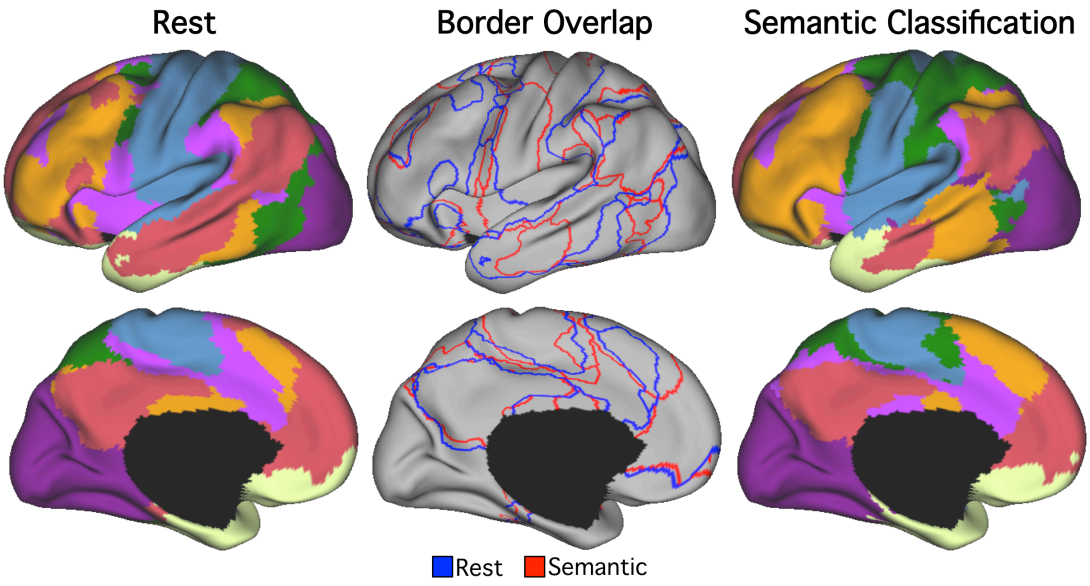

Figure 2.3. Network boundaries are sensitive to task. 7-network solutions for Rest and for the Semantic Classification task were computed in the same subjects and are shown in the first and third column. The borders for each are overlaid in the central column.

Network Boundaries are Sensitive to Task State

The above results complicate the use of intrinsic functional connectivity for estimating areal boundaries. However, the analyses above are consistent with the possibility that functional coupling properties are always stable. To assess the extent to

which the locations of borders shift dynamically as a function of the state of the subject, we compared the resulting network topography from clustering performed on passive rest scans versus semantic classification scans (Figure 2.3). Visual inspection reveals that the 7-network solutions are globally similar for the two conditions. Nonetheless, the precise locations of the boundaries vary across the two conditions (overlap = 71.8%). For comparison, the overlap between the eyes-open-rest and a passive fixation condition collected in the same participants in the same session was 91.9%.

To quantify these differences, we computed the correlation between each vertex's whole cortex fcMRI maps in the two task conditions. Average correlation values for the left hemisphere are plotted along with the reference network borders from the core dataset (Figure 2.4A). There is general agreement between the two conditions (average correlations are 0.76 and 0.77 for left and right hemispheres)[1]. Nonetheless, clear spatial variation exists that changes boundary estimates. Figure 2.4B-E depicts seed-based functional connectivity maps from 4 seeds computed separately for the semantic task and passive rest. Figure 2.4D and Figure 2.4C show regions of high and low correspondence, respectively, where correspondence is measured as the correlation between the task and rest fcMRI maps for each seed. Differences across these seed regions are further quantified in Figure 2.5, which shows the correlation strengths of each seed to a set of specified cortical target regions.

[1] For comparison, we also computed the average correlation between the passive rest condition and fcMRI maps derived from two scans of resting fixation acquired in the same participants and session as the Semantic Classification dataset. We found the correlation to be 0.87.

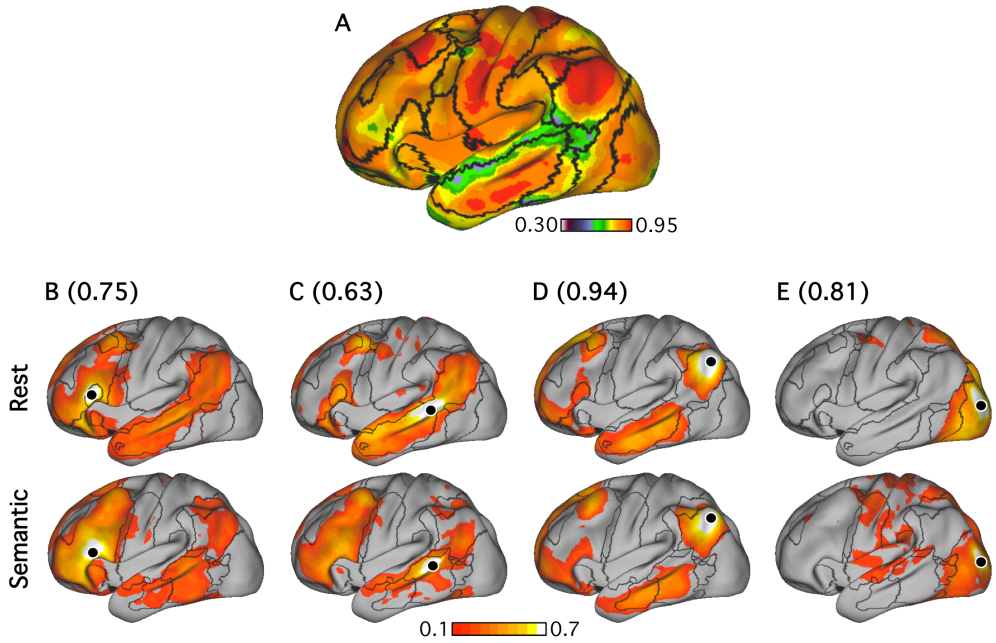

Figure 2.4. **Spatial distribution of task-dependent changes in connectivity profiles.** (A) Correlation between each vertex's whole cortex fcMRI maps derived from the passive rest and semantic task conditions, averaged across all subjects. (B-E) Seed-based correlation maps for four seed regions (black circles) plotted on a lateral view of the left hemisphere. Seed regions were single surface vertices. Black borders show the 7-network boundaries computed in each dataset. Numbers reflect correlation between the connectivity profiles of each seed region across the two conditions.

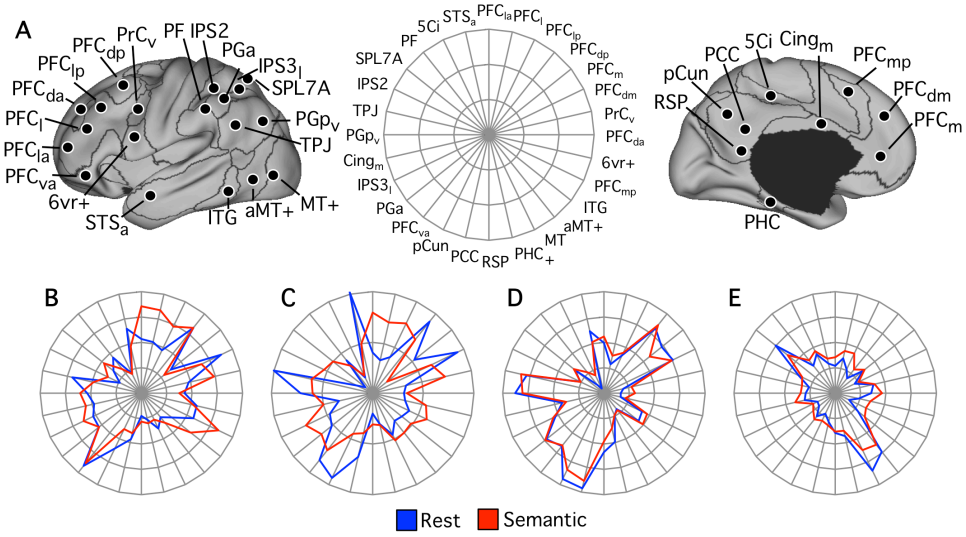

Figure 2.5 Functional connectivity fingerprints are altered in different task states. (A) Target regions. (B-E) Polar plots depict pairwise correlations between target regions in (A) and the four seed regions depicted in Figure 2.4. The scale for (B, D, E) is -0.4 to 0.6. The scale for (C) is -0.2 to 0.3.

Figure 2.6 shows that fcMRI borders computed from task data show better correspondence to the beta estimates of an event-related version of the same task than do borders computed from resting-state data. For illustration, we computed the average of beta estimates for vertices that fell in each of the 7 networks estimated from the semantic task and the passive rest task. We found that the high beta values fell primarily within one network (orange network) when using the task fcMRI borders (average beta estimate = 0.49). The average beta estimate for the same network estimated from passive rest fcMRI was 0.32. This lower average primarily occurred because more of the task responsive regions fell within an additional network (red network; average beta estimate = 0.15) relative to the task fcMRI borders (average beta estimate for the homologous network in semantic task data was -0.07).

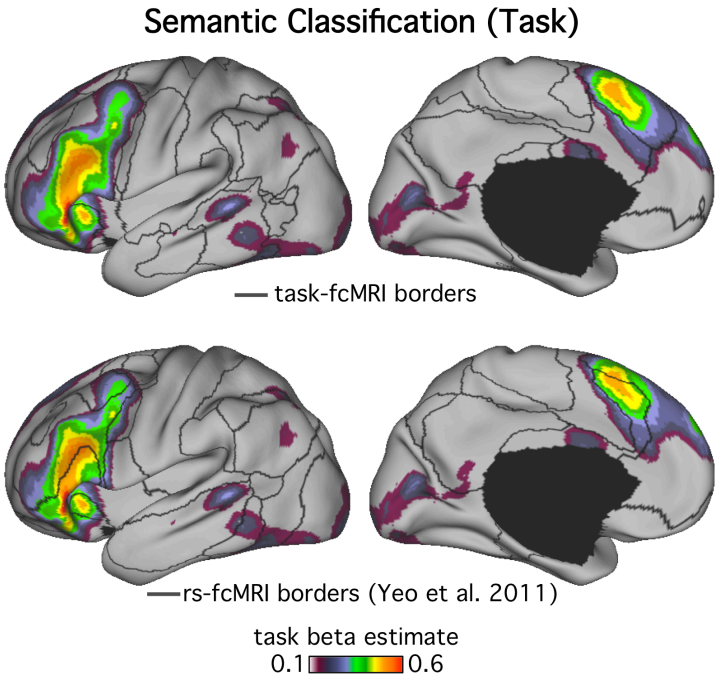

Mean Task Beta Estimate Per Network

task networks	0.09	-0.23	-0.25	-0.04	0.03	**0.49**	-0.07
rs networks	0.11	-0.22	-0.08	-0.12	0.02	**0.32**	**0.15**

Figure 2.6. Resting state networks do not conform to activations from a canonical language task. Networks defined from performing functional connectivity analysis on semantic task dataset correspond well to the task activation pattern. Borders between resting-state networks are derived from a dataset of 1000 participants (black lines; data from Yeo et al. 2011). Plotted as a heat map are beta estimates from different dataset of the same semantic classification task (data from Liu et al. 2009). The table lists the average beta estimates for each network, estimated separately for the semantic task fcMRI 7-network solution and for the passive rest fcMRI 7-network solution (colors as in Figure 2.3).

Figure 2.7A shows, for reference, the clustering solutions obtained from the 1000 subjects eyes open passive rest dataset in Yeo et al. (2011) (GSP). The maps in Figure 2.7B plot the correlation between each vertex's whole cortex task-derived fcMRI map and that same vertex's whole cortex map computed from the GSP dataset. Each

correspondence map is plotted with the GSP network borders for reference. Correspondence to the GSP dataset was on average 0.80 or greater for all four tasks, indicating that broad details of the connectivity maps were similar across passive task variants. The high correspondence also confirms that reasonably stable fcMRI results can be obtained with relatively short data acquisition periods (see also Shirer et al. 2011). Connectivity profile correspondence to the GSP results was highest for the Fixation Only task (0.89). This is reasonable given that passive fixation is the most similar to the passive eyes open rest paradigm employed in the GSP protocol. Low correspondence in certain regions, such as the anterior temporal lobes and orbital frontal cortices, are most likely due to low signal-to-noise or susceptibility artifacts. Some of the regions of lowest profile correspondence values consistently cluster around the (GSP-derived) network borders in all four tasks. However, other portions of cortex distant from border locations also show relatively low correspondence. The Count Backwards task in particular shows low correspondence to the GSP solution across distributed portions of the cortical mantel (Figure 2.7B).

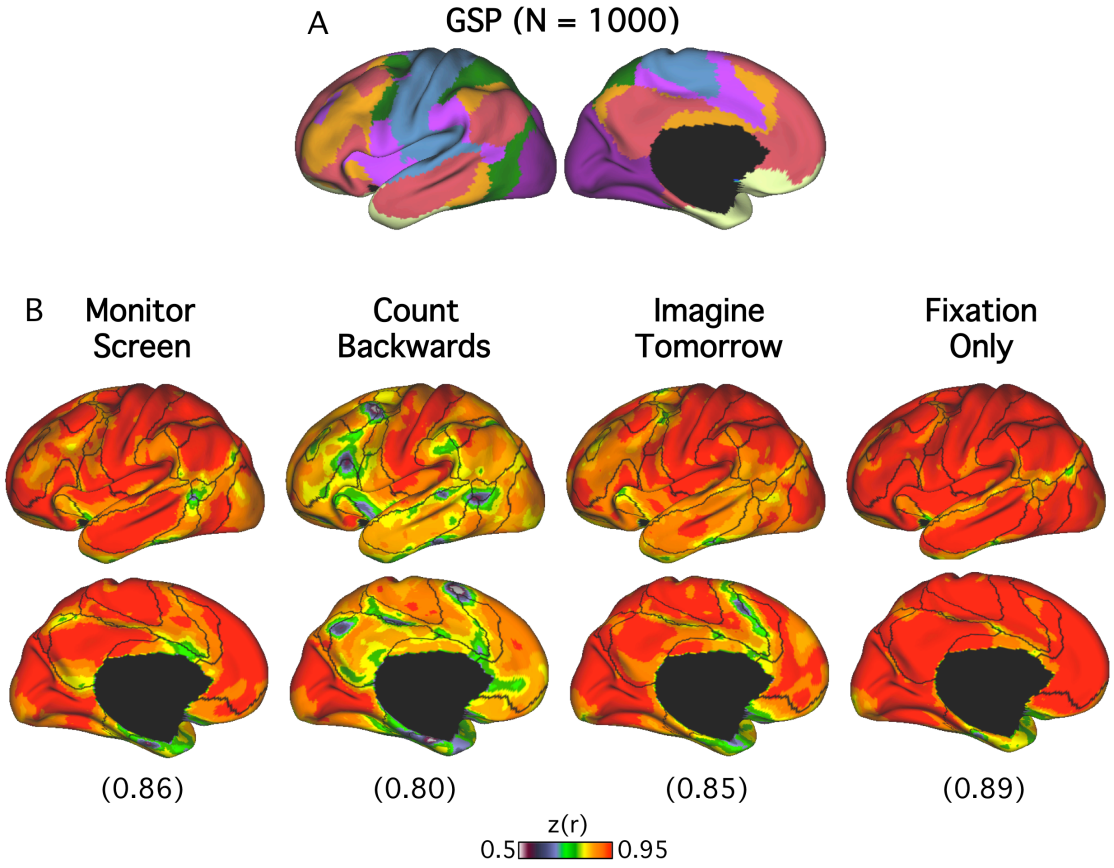

Figure 2.7. Passive task variants are sufficient to change network topography. (A) Plotted for reference are clustering results from a dataset of 1000 participants (GSP; Yeo et al. 2011). (B) Correspondence map of the correlation between each vertex's whole-brain correlation map in each of the four tasks from the Passive Task dataset to its whole-brain correlation map in the GSP data. Numbers in parenthesis refer to the average correlation across the cerebral cortex to the GSP data for each task.

Figure 2.8A shows the effect of task on the connectivity of a seed region placed on the dorsal bank of the superior parietal lobule, while Figure 2.8B shows the effect of task on a region in dorsomedial prefrontal cortex. Additional examples of regions that have different connectivity across tasks are depicted in Figure 2.9.

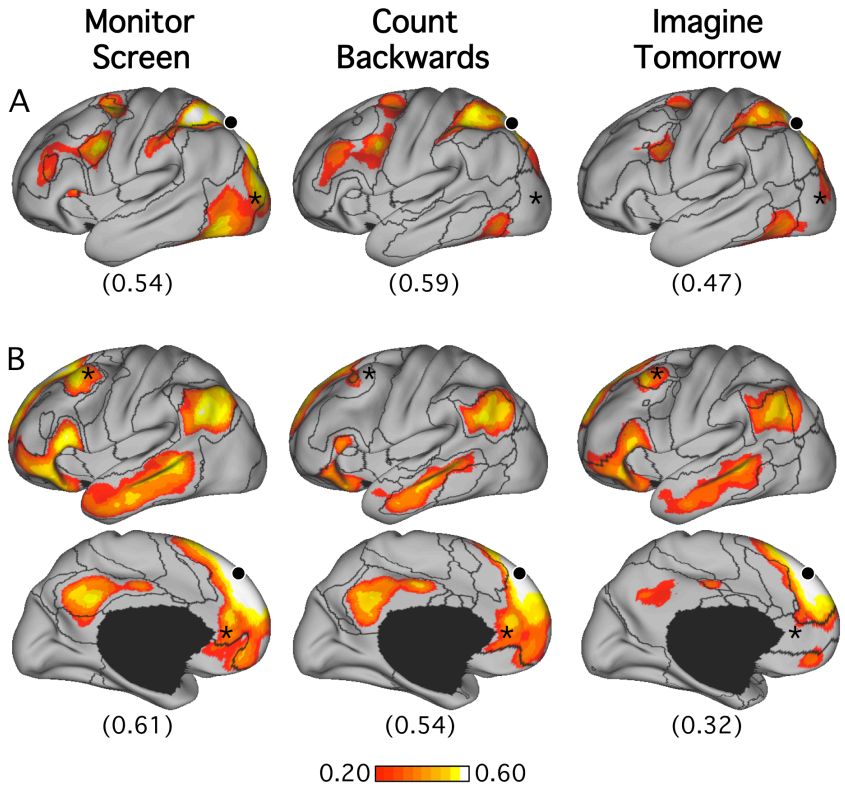

Figure 2.8. Functional connectivity maps are altered across different passive task states. (A) Seed region on the dorsal bank of the intraparietal sulcus shows different connectivity profile across tasks. A prominent difference in this seed region's connectivity between tasks is highlighted with the asterisk in lateral occipital cortex. (B) Seed region in the dorsomedial prefrontal cortex showing differential connectivity to medial prefrontal and posterior cingulate cortices as a function of task. Numbers in parentheses indicate the confidence with which regions are assigned to their networks.

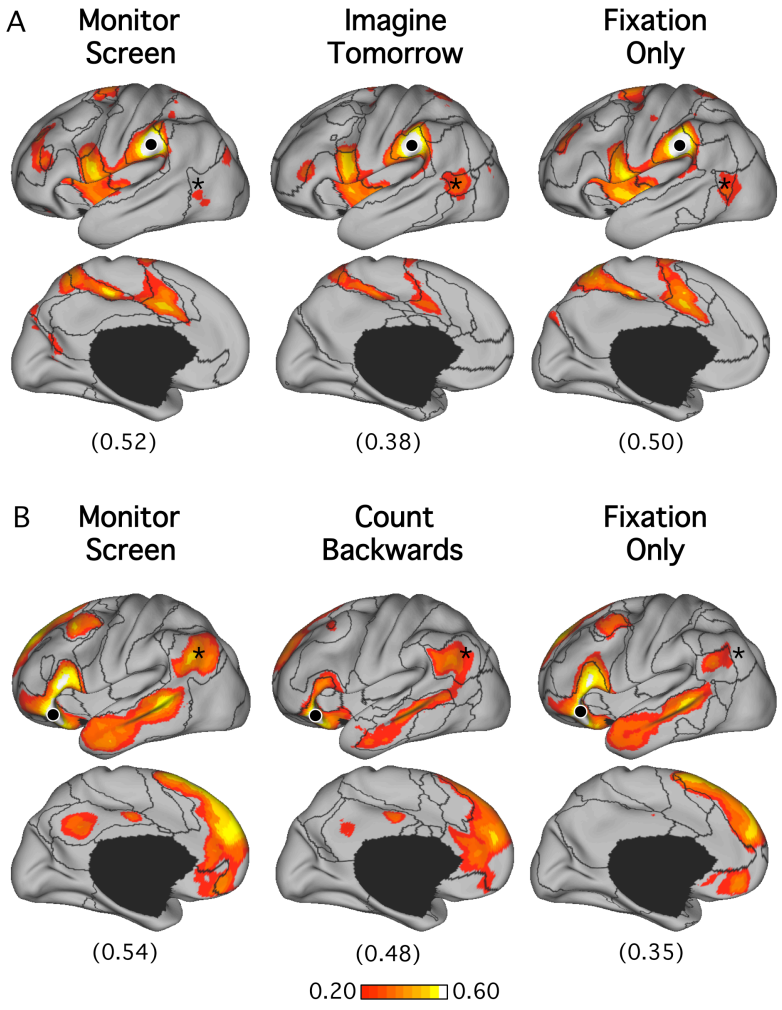

Figure 2.9. Functional connectivity maps are altered across different passive task states. (A) Seed region in parietal operculum changes connectivity to regions, including lateral temporal cortex, as a function of task. Numbers in parentheses indicate the confidence with which this region is assigned to its best-fit network for each task. (B) Seed region in ventrolateral prefrontal cortex has different connectivity to other cortical locations, including the inferior parietal lobule, as a function of task. Numbers in parentheses indicate the confidence with which regions are assigned to their networks. Higher numbers indicate better fit (relative to the next-best network).

Discussion

rs-fcMRI is a tricky method to interpret because multiple sources contribute to observed correlations between fluctuations in the BOLD signal measured across different regions of the brain. Strong evidence suggests that coupling patterns are constrained by anatomic connectivity (Lu et al. 2011). Another major contribution is the dynamic functional state of the participant, as illustrated by the results in Figures 2.3-9. Given the broad interest of the field to use functional connectivity methods to understand stable features of cortical organization, including areal boundaries, these distinct signal contributions as well as technical features of the method need to be considered carefully. Several questions motivate our discussion: Can functional connectivity measures be used to infer borders of cortical areas? If not borders of cortical areas, can functional connectivity reveal any level of meaningful functional subdivision that reflects stable organizational features of cortex?

Can functional connectivity measures be used to estimate areal boundaries?

Sharp transitions in coupling patterns of rs-fcMRI can be observed and are largely consistent across different subjects and data samples (e.g., Cohen et al. 2008). These sharp transitions raise the possibility that rs-fcMRI can be used to locate the borders between brain areas (Cohen et al. 2008). However, a complex set of factors contributes to functional coupling measured by fcMRI. The present results and review of prior literature identify four separate reasons why functional connectivity in general cannot be expected to reliably estimate areal boundaries. The first two reasons relate to the use of functional connectivity as a specific method to identify areal borders; the second two focus on details of anatomic connectivity that limit the potential of local connectivity gradients, in isolation, to define areal boundaries.

Technical limitations of boundary assignment algorithms. Gradients across a region of cortex depend on which reference regions outside of the mapped region are used to delineate the gradients (and how the reference regions are weighted). This is particularly apparent when different criteria are applied to the same data. For instance when comparing a coarse 7-network parcellation with a finer 17-network parcellation

estimated from the same data, the locations of some of the borders shifted (Figure 2.2). Different correlation thresholds also shift boundaries (see Figure 1 in Power et al. 2011). As the underlying anatomical connectivity is fixed, shifts in the exact boundary locations due to weighting criteria raises the concern that the problem of specifying precise borders is underdetermined.

The encroachment of the IPL-RSP-PHC network boundary into the Dorsal Attention Network (Figure 2.2) is likely a consequence of this kind of phenomenon. Specifically, the regions in question assigned to the Dorsal Attention Network in the 7-network solution in truth have a more similar connectivity profile with the IPL-RSP-PHC subnetwork of the Default Network, which leads to the reassignment of those regions and subsequent shift of the Dorsal Attention border in the 17-network solution. This intrusion into the Dorsal Attention Network is particularly inconsonant since the IPL-RSC-PHC network is typically regarded as a component of the Default Network (Vincent et al. 2006; Andrews-Hanna et al. 2010; Yeo et al. 2011), and the Default and Dorsal Attention Networks are often negatively correlated (Fox et al. 2005). Consequently, there exist cortical regions assigned to the Dorsal Attention Network in the 7-network solution that become assigned to a component of the Default Network in the 17-network solution.

This kind of problem is not unique to particular algorithms or neuroimaging data; it is an issue any time the outcomes from different methods (e.g., different histological stains, different cost functions) are incommensurate, or when heuristics used are ambiguous (Kaas 1987; see also Figure 32 in Rosa & Tweedale, 2005; Liang et al. 2012 and Figure S2.1). Inconsistencies between solutions containing different numbers of networks exist in other network estimation models, such as graph theory (e.g., Figure 1 of Power et al. 2011) and ICA (e.g., compare Figures 1 and 3 of Smith et al. 2009). We do not view this as an insurmountable problem as the underlying data exhibit regular and often stark transitions in functional gradients, but this issue needs to be explicitly handled in models that make use of coupling transitions, as well as in cases where sharp transitions are not readily observed.

Dynamic functional connectivity changes influence border estimates. While many aspects of global topography were preserved, we found appreciable shifts in border location when comparing a passive task to an active semantic processing task (Figures

2.3-6). Several of the differences in network topography are consistent with network changes, likely reflecting processing in task-relevant regions. For example, the left inferior prefrontal cortex and lateral temporal cortex are both active in this task when analyzed with a conventional blocked task activation approach. These regions become more correlated in the semantic classification task and cluster in the same functionally coupled network (Figure 2.6) -- what might be thought of as a form of task co-activation. In some ways, this result might seem obvious, but it underscores the point that functional connectivity is not solely constrained by anatomical connectivity and will dynamically shift to reflect the task or behavioral state.

The comparison of passive rest to an active task requiring an overt motor response may raise the concern that these task conditions are too dissimilar to be meaningfully compared. However, we also observed shifts in connectivity profiles when comparing variants of passive task conditions that were perceptually identical and did not require an overt response (Figures 2.7-9). While a given seed region produced connectivity patterns that bore general resemblance across tasks, connectivity changes were sufficient to change topographic details in the observed gradients. This underscores an important point to which we will later return: just as with active task states, different passive mental operations are sufficient to change fcMRI connectivity profiles. As others have argued, passive tasks additionally suffer from a lack of experimenter control (Morcom & Fletcher 2007). Little can be measured behaviorally to indicate what participants were actually doing. Given these ambiguities, it cannot be assumed that a passive rest state such as visual fixation is the most accurate state with which to estimate the topography of functional networks (Buckner, Krienen, & Yeo 2013).

Can functional connectivity reveal meaningful functional subdivisions that reflect stable organizational features of cortex?

We do not believe rs-fcMRI methods can generally reveal the locations of areal borders. However, the functional networks that arise may still reflect stable properties of brain organization. The tricky feature for interpreting rs-fcMRI is that it is constrained by anatomical connectivity but also sensitive to reconfigurations from dynamic processes. We suspect that selecting a constant low-level task demand (e.g., eyes closed rest or

passive fixation) does not mitigate this issue. All task states presumably encourage functional reconfigurations particular to their demands. Given these complexities, can we learn anything about stable properties of functional organization from rs-fcMRI?

While dynamical reconfigurations adjust details, certain broad properties of functional connectivity networks generalize across many contexts and analysis strategies (Buckner, Krienen & Yeo 2013). Regions at and near primary sensory and motor cortices tend to show local functional coupling, likely reflecting a fundamental organizational feature of these regions. By contrast, association regions tend to couple in large distributed networks with a prefrontal, parietal association, frontal midline, and temporal component (Figure 2.3). While the details of their exact borders change with different acquisition tasks, the general organization tends to remain. Certain networks also appear relatively robust to state changes – in particular the core regions of what has come to be known as the Default Network (e.g., Figure 2.4D, though see Figure 2.8C and Figure 2.9B for examples of changes that affect certain components of the Default Network). Stable features of anatomy may provide sufficiently strong constraints such that across many tasks, and over enough sampling time, stable network configurations emerge. Typical analysis strategies for rs-fcMRI data likely emphasize these stable components.

Another point is that rs-fcMRI should not be interpreted in isolation (Buckner, Krienen & Yeo 2013). The rich indirect data about functional organization accumulated in the human benefits from comparison to anatomical work in non-human primates – what Mesulam (2012) refers to as 'hard data'. For example, the human rs-fcMRI data highlight that the inferior parietal lobule region contains subregions that are functionally coupled to limbic association regions including the parahippocampal cortex (e.g., Vincent et al. 2006). The parietal association regions involved in the Default Network are not functionally coupled to sensory or motor systems and thus distinguish themselves from extensively studied parietal areas in the monkey including LIP.

Guided by the human data, one predicts that parietal association cortex will contain a heterogeneous cluster of areas with markedly different connectivity 'fingerprints'. That prediction is confirmed in the monkey anatomic literature. Specifically, the most caudal portion of macaque area 7a, labeled Opt by Pandya and Seltzer (1982), has a distributed connectivity pattern convergent with the human rs-

fcMRI data. In the macaque, parietal association cortex is predominantly dedicated to vision and sensory-motor integration (but has protoforms of the distributed networks seen in the human). In the modern human, parietal association cortex is largely occupied by regions that do not obviously embed themselves within distributed sensory-motor systems. Thus, the 'inferred connectivity' based on rs-fcMRI makes a valuable contribution when taken in the context of direct anatomical data (e.g., Vincent et al. 2007; Margulies et al. 2009; Mantini et al. 2011; Mars et al. 2011; Hutchison et al. 2012a,b; Choi et al. 2012). Estimated homologies between the monkey and human builds confidence in which aspects of the networks are likely constrained by anatomy and help us to understand how the networks may be uniquely organized in the human.

Finally, functional connectivity estimates are sensitive to task state. Therefore, differences could arise from how individuals engage the passive states. A growing number of studies compare functional connectivity patterns between individuals, age groups, or control and patient populations. An implicit (and sometimes explicit) assumption across many of these studies is that resting state data are not sensitive to the performance confounds that challenge task-based neuroimaging studies of individual differences. Our present results do not support this assumption. We ourselves have noted subtle differences in functional coupling with the medial temporal lobe in relation to self-report of passive thought content (Andrews-Hanna et al. 2010), but also that younger and older adults also tend to engage passive fixation differently: older adults are more likely to report focusing on the visual cross-hair than engaging in internal mentation (J. Andrews-Hanna & R.L. Buckner, unpublished observations). Levels of vigilance, eye movements, and internal thought processes could affect connectivity patterns. Though performance is not measured by traditional key press responses or verbal reports, relevant individual differences in behavior may nonetheless contribute to rs-fcMRI differences. Depending on the goal of the study, such differences may be of interest or, alternatively, act as a confound.

What can be drawn from the dynamic contributions to the coupling patterns observed in fcMRI?

The assumption that cortical regions or neuronal subpopulations shift network affiliation in the service of task goals has been thoughtfully articulated in theoretical papers by Mesulam (1998), Dehaene (1998), Fries (2005), Friston (2011) and Bullmore & Sporns (2012), among others. It is an underlying assumption for techniques such as dynamic causal modeling (Friston 2003). A common thread that emerges from these works is that functional interactions (which are constrained by anatomical connections but not fully determined by them) are critically relevant when characterizing a network's functional properties (Price & Friston 2005).

Intuitively, when regions are not anatomically connected with one another, changes in their synchronization are likely either facilitated by regions lying on a common path between them or else are jointly driven by a common (upstream) input. In the former scenario, association cortex is thought to be particularly well situated for facilitating neuronal coherence due to its ability to dynamically interface with unimodal sensory and motor processing cascades (Bullmore & Sporns, 2012). Our results and others indicate substantial variability across the cortex, including in association regions, in the stability of correlation profiles as a function of changing task demands (Figure 2.4A and Figures 2.7-9; Mennes et al. 2012; Hasson et al. 2009). A recent study further showed that intersubject variability of fcMRI patterns measured at rest is highest in heteromodal association cortex and correlates with variability in cortical folding patterns (Mueller at al. 2013).

Relevant to this point, it is often noted (including in our papers) that functional connectivity largely remains topographically stable across levels of consciousness including wakefulness, sedation (Greicius et al. 2008), sleep (Horovitz et al. 2009; Larson-Prior et al. 2009) and vegetative state (Cauda et al. 2009). However, stability across states is often only assessed for a limited number of regions, or focuses on broad qualitative correspondence between only one or two well-established large networks. Similarly, the debate surrounding the functional relevance of fcMRI networks – whether they are sequalae of active cognitive processing such as introspection or merely reflect anatomy or physiological factors – is often framed around the Default Network. Whether the observed stability of the Default Network is the exception or the rule remains to be seen. In our view, functional interpretation of any network identified by fcMRI, including

the Default Network, remains incomplete without assessment of its behavior during a broader range of behavioral states (Figure 2.9B).

An early hypothesis proposed that correlations between nodes in a functionally defined (i.e. task-evoked) network should increase during a task that recruits those nodes compared to a task that does not activate the network (Lowe et al. 2000). However, we observed a more complex relationship between task-evoked activity and fcMRI patterns. For example, while lateral prefrontal cortex and occipital regions are modulated by the semantic task (Figure 2.6), they do not increase coupling to each other during task epochs (e.g., Figure 2.4B and 2.4E). Changes in functional coupling do not always reflect task-evoked activity. Further, 'task-evoked' coupling must always be interpreted as a relative difference between the tasks or states contrasted. This complicates assumptions of direct correspondence between task (and rest) evoked patterns and fcMRI; knowing which regions are modulated by a task does not always lead to a clear prediction about changes to their functional coupling. However, it also indicates that the information conveyed by each method is not redundant.

Functional coupling is often assessed by defining networks in resting state data and then exploring their dynamics in different tasks (e.g., Hampson et al. 2002; Greicius & Menon, 2004; Eckert et al. 2008; Kelly et al. 2008; Spreng et al. 2010; Gordon et al. 2011; Huijbers et al. 2011; Leech et al. 2011). The emergent picture from this approach is one in which transient coupling occurs between networks whose "true" boundaries are measured from resting data (Deco & Corbetta 2011). That is, defining networks from resting scans and probing activity patterns within these networks during task assumes that rs-fcMRI networks are the most appropriate templates of network organization. Our data again challenge this assumption. Though broad organizational features were preserved, details of functional organization differed when they were estimated from different tasks (Figure 2.4, 2.7-9), and task fcMRI borders better captured task-evoked activation patterns relative to resting-state borders (Figure 2.6). Moving forward, comparing functional connectivity across task states without assuming that rs-fcMRI networks necessarily represent the ground truth promises to reveal novel aspects of brain organization.

References

Albert NB, Robertson EM, Miall RC. The resting human brain and motor learning. *Curr Biol* 19: 1023-1027, 2009.

Amunts K, Malikovic A, Mohlberg H, Schormann T, Zilles K. Brodmann's areas 17 and 18 brought into stereotaxic space - where and how variable? Neuroimage 11: 66-84, 2000.

Andrews-Hanna JR, Reidler JS, Sepulcre J, Poulin R, Buckner RL. Functional-anatomic fractionation of the brain's default network. *Neuron* 65: 550-562, 2010.

Andreasen NC, O'Leary DS, Cizadlo T, Arndt S, Rezai K, Watkins GL, Boles Ponto LL, Hichwa RD. Remembering the past: two facets of episodic memory explored with positron emission tomography. *Am J Psychiatry* 152: 1576-1585, 1995.

Baldassarre A, Lewis CM, Committeri G, Snyder AZ, Romani GL, Corbetta M. Individual variability in functional connectivity predicts performance of a perceptual task. *Proc Natl Acad Sci USA* 109: 3516-3521, 2001.

Barnes A, Bullmore ET, Suckling J. Endogenous human brain dynamics recover slowly following cognitive effort. *PLoS ONE* 4: e6626, 2009.

Beckmann CF, Smith SM. Probabilistic independent component analysis for functional magnetic resonance imaging. *IEEE Trans Med Imaging* 23: 137-152, 2004.

Binder JR, Desai RH, Graves WW, Conant LL. Where is the semantic system? A critical review and meta-analysis of 120 functional neuroimaging studies. *Cereb Cortex* 19: 2767-2796, 2009.

Biswal B, Yetkin FZ, Haughton VM, Hyde JS. Functional connectivity in the motor cortex of resting human brain using echo-planar MRI. *Magn Reson Med* 34: 537-541, 1995.

Brodmann K. *Localization in the Cerebral Cortex.* Translated by Garey LJ. New York: Springer 1909/2006.

Buckner RL, Krienen FM, Castellanos A, Diaz JC, Yeo BTT. The organization of the human cerebellum estimated by functional connectivity. *J Neurophysiol* 106: 2322-2345, 2011.

Buckner RL, Krienen FM, Yeo BTT. Opportunities and limitations of intrinsic functional connectivity MRI. *Nat Neurosci* in press.

Buckner RL, Sepulcre J, Talukdar T, Krienen FM, Liu H, Hedden T, Andrews-Hanna JR, Sperling RA, Johnson KA. Cortical hubs revealed by intrinsic functional connectivity: Mapping, assessment of stability, and relation to Alzheimer's disease. *J Neurosci* 29: 1860-1873, 2009.

Bullmore E, Sporns O. Complex brain networks: Graph theoretical analysis of structural and functional systems. *Nat Rev Neurosci* 10:186-198, 2009.

Burkhalter A, Bernardo KL, Charles V. Development of local circuits in human visual cortex. *J Neurosci* 13: 1916-1931, 1993.

Cauda F, Micon BM, Sacco K, Duca S, D'Agata F, Geminiani G, Canavero S. Disrupted intrinsic functional connectivity in the vegetative state. *J Neurol Neurosurg Psychiatry* 80: 429-431, 2009.

Choi EY, Yeo BTT, Buckner RL. The organization of the human striatum estimated by intrinsic functional connectivity. *J Neurophysiol* 108: 2242-2263, 2012.

Cohen AL, Fair DA, Dosenbach NUF, Miezin FM, Dierker D, Van Essen DC, Schlaggar BL, Petersen SE. Defining functional areas in individual human brains using resting functional connectivity MRI. *Neuroimage* 41: 45-57, 2008.

Deco G, Jirsa VK, & McIntosh AR. Emerging concepts for the dynamical organization of resting-state activity in the brain. *Nat Rev Neurosci* 12: 43-56, 2011.

Dehaene S, Kerszberg M, & Changeux JP. A neuronal model of a global workspace in effortful cognitive tasks. *Proc Natl Acad Sci USA* 95: 14529-14535, 1998.

Demb JB, Desmond JE, Wagner AD, Vaidya CJ, Glover GH, Gabrieli JDE. Semantic encoding and retreival in the left inferior prefrontal cortex: A functional MRI study of task difficulty and process specificity. *J Neurosci* 15: 5870-5878, 1995.

Di Virgilio G, Clarke S. Direct interhemispheric visual input to human speech areas. *Hum Brain Mapp* 5: 347-354, 1997.

Eckert MA, Kamdar NV, Chang CE, Beckmann CF, Greicius MD, Menon V. A cross-modal system linking primary auditory and visual cortices: evidence from intrinsic fMRI connectivity analysis. *Hum Brain Mapp* 29: 848-857, 2008.

Eickhoff SB, Stephan KE, Mohlberg H, Grefkes C, Fink GR, Amunts K, Zilles K. A new SPM toolbox for combining probabilistic cytoarchitectonic maps and functional imaging data. *Neuroimage* 25: 1325-1335, 2005.

Fedorenko E, Hsieh P, Nieto-Castanon A, Whitfield-Gabrieli S, Kanwisher N. New method for fMRI investigations of language: defining ROIs functionally in individual subjects. *J Neurophysiol* 104: 1177-1194, 2010.

Felleman DJ, & Van Essen DC. Distributed hierarchical processing in the primate cerebral cortex. *Cereb Cortex* 1: 1-47, 1991.

Fischl B, Rajendran N, Busa E, Augustinack J, Hinds O, Yeo BTT, Mohlberg H, Amunts K, Zilles K. Cortical folding patterns and predicting cytoarchitecture. *Cereb Cortex* 18: 1973-1980, 2008.

Fox MD, Snyder AZ, Vincent JL, Corbetta M, Van Essen DC, Raichle ME. The human brain is intrinsically organized into dynamic, anticorrelated functional networks. *Proc Natl Acad Sci USA* 102: 9673-9678, 2005.

Fox MD, Corbetta M, Snyder A, Vincent J, Raichle ME. Spontaneous neuronal activity distinguishes human dorsal and ventral attention systems. *Proc Natl Acad Sci USA* 103: 10046, 2006a.

Fox MD, Snyder AZ, Zacks JM, Raichle ME. Coherent spontaneous activity accounts for trial-to-trial variability in human evoked brain responses. *Nat Neurosci* 9: 23-25, 2006b.

Fox MD, Raichle ME. Spontaneous fluctuations in brain activity observed with functional magnetic resonance imaging. *Nat Rev Neurosci* 8: 700-711, 2007.

Fransson P. Spontaneous low-frequency bold signal fluctuations: an fMRI investigation of the resting-state default mode of brain function hypothesis. *Hum Brain Mapp* 26: 15-29, 2005.

Fries P. A mechanism for cognitive dynamics: neuronal communication through neuronal coherence. *TiCS* 9: 474-480. 2005.

Friston KJ. Functional and effective connectivity in neuroimaging: A synthesis. *Hum Brain Mapp* 2: 56-78, 1994.

Friston KJ. Functional and effective connectivity: a review. *Brain Connect* 1: 13-36, 2011.

Friston KJ, Harrison L, Penny W. Dynamic causal modelling. *Neuroimage* 19: 1273-1302, 2003.

Gabrieli JDE, Desmond JE, Demb JB, Wagner AD, Stone MV, Vaidya CJ, Glover GH. Functional magnetic resonance imaging of semantic memory processes in the frontal lobes. *Psychol Sci* 7: 278-283, 1996.

Goldman-Rakic PS. Topography of cognition: Parallel distributed networks in primate association cortex. *Annu Rev Neurosci* 11: 137-156, 1988.

Gordon E, Stollstorff M, Vaidya CJ. Using spatial multiple regression to identify intrinsic connectivity networks involved in working memory performance. *Hum Brain Mapp* 33: 1536-1552, 2011.

Greicius MD, Kiviniemi V, Tervonen O, Vainionpää V, Alahuhta S, Reiss AL, Menon V. Persistent default-mode network connectivity during light sedation. *Hum Brain Mapp* 29: 839-847, 2008.

Greicius MD, Krasnow B, Reiss AL, Menon V. Functional connectivity in the resting brain: A network analysis of the default mode hypothesis. *Proc Natl Acad Sci USA* 100: 253-258, 2003.

Greicius MD, Menon V. Default-mode activity during a passive sensory task: uncoupled from deactivation but impacting activation. *J Cog Neuro* 16: 1484-1492, 2004.

Greicius MD, Supekar K, Menon V, Dougherty RF. Resting-state functional connectivity reflects structural connectivity in the default mode network. *Cereb Cortex* 19: 72-78, 2009.

Greve DN, Fischl B. Accurate and robust brain image alignment using boundary-based registration. *Neuroimage* 48: 63-72, 2009.

Gusnard DA, Raichle ME. Searching for a baseline: functional imaging and the resting human brain. *Nat Rev Neurosci* 2: 685-694, 2001.

Hagmann P, Cammoun L, Gigandet X, Meuli R, Honey CJ, Wedeen VJ, Sporns O. Mapping the structural core of human cerebral cortex. *PLoS Biol* 6: e159, 2008.

Hampson M, Olson IR, Leung H-C, Skudlarski P, Gore JC. Changes in functional connectivity of human MT/V5 with visual motion input. *Neuroreport* 15: 1315-1319, 2004.

Hampson M, Driesen NR, Skudlarski P, Gore JC, Constable RT. Brain connectivity related to working memory performance. *J Neurosci* 26: 13338-13343, 2006.

Hasson U, Nusbaum HC, Small SL. Task-dependent organization of brain regions active during rest. *Proc Natl Acad Sci USA* 106: 10841-10846, 2009.

Hesselmann G, Kell CA, Eger E, Kleinschmidt A. Spontaneous local variations in ongoing neural activity bias perceptual decisions. *Proc Natl Acad Sci USA* 105: 10984-10989, 2008.

Hinds O, Polimeni JR, Rajendran N, Balasubramanian M, Amunts K, Zilles K, Schwartz EL, Fischl B, Triantafyllou C. Locating the functional and anatomical boundaries of human primary visual cortex. *Neuroimage* 46: 915-922, 2009.

Hirose S, Watanabe T, Jimura K, Katsura M, Kunimatsu A, Abe O, Ohtomo K, Miyashita Y, Konishi S. Local signal time-series during rest used for areal boundary mapping in individual human brains. *PLOS One* 7: e36496.

Honey CJ, Sporns O, Cammoun L, Gigandet X, Thiran JP, Meuli R, Hagmann P. Predicting human resting-state functional connectivity from structural connectivity. *Proc Natl Acad Sci USA* 106: 2035-2040, 2009.

Horovitz SG, Braun AR, Carr WS, Picchioni D, Balkin TJ, Fukunaga M, Duyn JH. Decoupling of the brain's default mode network during deep sleep. *Proc Natl Acad Sci USA* 106: 11376-11381, 2009.

Huijbers W, Pennartz CMA, Cabeza R, Daselaar SM. The hippocampus is coupled with the default network during memory retrieval but not during memory encoding. *PLoS ONE* 6: e17463, 2011.

Hutchison RM, Gallivan JP, Culham JC, Gati JS, Menon RS, Everling S. Functional connectivity of the frontal eye fields in humans and macaque monkeys investigated with resting-state fMRI. *J Neurophysiol* 107, 2463-2474, 2012a.

Hutchison RM, Womelsdorf T, Gati JS, Leung LS, Menon RS, Everling S. Resting-state connectivity identifies distinct functional networks in macaque cingulate cortex. *Cereb Cortex* 22: 1294-1308, 2012b.

Jenkinson M, Bannister P, Brady M, Smith S. Improved optimization for the robust and accurate linear registration and motion correction of brain images. *Neuroimage* 17: 825-841, 2002.

Johnston JM, Vaishnavi SN, Smyth MD, Zhang D, He BJ, Zempel JM, Shimony JS, Snyder AZ, Raichle ME. Loss of resting interhemispheric functional connectivity after complete section of the corpus callosum. *J Neurosci* 28: 6453-6458, 2008.

Kaas JH. The segregation of function in the nervous system: why do sensory systems have so many subdivisions? In: Contributions to Sensory Physiology (ed. W.P. Neff), vol. 7, 201-240, Academic Press, 1982.

Kaas JH. The organization of neocortex in mammals: Implications for theories of brain function. *Annu Rev Psychol* 38: 129-151, 1987.

Kelly AM, Uddin LQ, Biswal BB, Castellanos FX, Milham MP. Competition between functional brain networks mediates behavioral variability. *Neuroimage* 39: 527-537, 2009.

Krienen FM, Buckner RL. Segregated fronto-cerebellar circuits revealed by intrinsic functional connectivity. *Cereb Cortex* 19: 2485-2497, 2009.

Larson-Prior LJ, Zempel JM, Nolan TS, Prior FW, Snyder AZ, Raichle ME. Cortical network functional connectivity in the descent to sleep. *Proc Natl Acad Sci USA* 106: 4489-4494, 2009.

Lashkari D, Vul E, Kanwisher N, Golland P. Discovering structure in the space of fMRI selectivity profiles. *Neuroimage* 50: 1085-1098, 2010.

Leech R, Kamourieh S, Beckmann CF, Sharp DJ. Fractionating the default mode network: distinct contributions of the ventral and dorsal posterior cingulate cortex to cognitive control. *J Neurosci* 31: 3217-3224, 2011.

Lewis CM, Baldassarre A, Committeri G, Romani GL, Corbetta M. Learning sculpts the spontaneous activity of the resting human brain. *Proc Natl Acad Sci USA* 106: 17558-17563, 2009.

Liang X, Wang J, Yan C, Shu N, Xu K, Gong G, He Y. Effects of different correlation metrics and preprocessing factors on small-world brain functional networks: a resting-state functional MRI study. *PLoS ONE* 7: e32766, 2012.

Liu H, Stufflebeam SM, Sepulcre J, Hedden T, Buckner RL. Evidence from intrinsic activity that asymmetry of the human brain is controlled by multiple factors. *Proc Natl Acad Sci USA* 106: 20499-20503, 2009.

Livingstone MS, Hubel DH. Specificity of intrinsic connections in primate primary visual cortex. *J Neurosci* 4: 2830-2835, 1984.

Lowe MJ, Mock B, Sorenson JA. Functional connectivity in single and multislice echo-planar imaging using resting state fluctuations. *Neuroimage* 7: 119–132, 1998.

Lu J, Liu H, Zhang M, Wang D, Cao Y, Ma Q, Rong D, Wang X, Buckner RL, Li K. Focal pontine lesions provide evidence that intrinsic functional connectivity reflects polysynaptic anatomical pathways. *J Neurosci* 31: 15065-15071, 2011.

Mantini D, Gerits A, Nelissen K, Durand J, Joly O, Simone L, Sawamura H, Wardak C, Orban GA, Buckner RL, Vanduffel W. Default mode of brain function in monkeys. *J Neurosci* 31: 12954-12962, 2011.

Margulies DS, Vincent JL, Kelly C, Lohmann G, Uddin LQ, Biswal BB, Villringer A, Castellanos FX, Milham MP, Petrides M. Precuneus shares intrinsic functional architecture in humans and monkeys. *Proc Natl Acad Sci USA* 106: 20069–20074, 2009.

Mars RB, Jbabdi S, Sallet J, O'Reilly JX, Croxson PL, Olivier E, Noonan MP, Bergmann C, Mitchell AS, Baxter MG, Behrens TE, Johansen-Berg H, Tomassini V, Miller KL, Rushworth MFS. Diffusion-weighted imaging tractography-based parcellation of the human parietal cortex and comparison with human and macaque resting-state functional connectivity. *J Neurosci* 31: 4087-4100, 2011.

Maunsell JHR, Van Essen DC. The connections of the middle temporal visual area (MT) and their relationship to a cortical hierarchy in the macaque monkey. *J Neurosci* 3: 2563, 1983.

Maunsell JHR, Van Essen DC. Topographic organization of the middle temporal visual area in the macaque monkey: Representational biases and the relationship to callosal connections and myeloarchitectonic boundaries. *J Comp Neurol* 266: 535-555, 1987.

McIntosh AR, Rajah MN, Lobaugh NJ. Functional connectivity of the medial temporal lobe relates to learning and awareness. *J Neurosci* 23: 6520-6528, 2003.

Mennes M, Kelly C, Colcombe S, Castellanos FX, Milham MP. The extrinsic and intrinsic functional architectures of the human brain are not equivalent. *Cereb Cortex*, 2012.

Mesulam MM. From sensation to cognition. *Brain* 121 (6): 1013-1052, 1998.

Mesulam MM. The evolving landscape of human cortical connectivity: facts and inferences. *Neuroimage* 62: 2182-2189, 2012.

Mueller S, Wang D, Fox MD, Yeo BTT, Sepulcre J, Sabuncu MR, Shafee R, Lu J, Liu H. Individual varibility in functional connectivity architecture of the human brain. *Neuron* 77: 586-595, 2013.

Nelson SM, Cohen AL, Power JD, Wig GS, Miezin FM, Wheeler ME, Velanova K, Donaldson DI, Phillips JS, Schlaggar BL, Petersen SE. A parcellation scheme for human left lateral parietal cortex. *Neuron* 67: 156-170, 2010.

Norman-Haignere SV, McCarthy G, Chun MM, Turk-Browne NB. Category-selective background connectivity in ventral visual cortex. *Cereb Cortex* 22: 391-402, 2012.

Pandya DN, Seltzer B. Intrinsic connections and architectonics of posterior parietal cortex in the rhesus monkey. *J Comp Neurol* 204: 196-210, 1982.

Passingham RE, Stephan KE, Kötter R. The anatomical basis of functional localization in the cortex. *Nat Rev Neurosci* 3: 606-616, 2002.

Poldrack RA, Wagner AD, Prull MW, Desmond JE, Glover GH, Gabrieli JDE. Functional specialization for semantic and phonological processing in the left inferior prefrontal cortex. *Neuroimage* 10: 15-35, 1999.

Power JD, Cohen AL, Nelson SM, Wig GS, Barnes KA, Church JA, Vogel AC, Laumann TO, Miezin FN, Schlaggar BL, Petersen SE. Functional network organization of the human brain. *Neuron* 72: 665-678, 2011.

Power JD, Fair DA, Schlaggar BL, Petersen SE. The development of human functional brain networks. *Neuron* 67: 735-748, 2010.

Price CJ, Friston KJ. Functional ontologies for cognition: the systematic definition of structure and function. *Cogn Neuropsychol* 22: 262-275, 2005.

Pyka M, Beckmann CF, Schoning S, Hauke S, Heider D, Kugel H, Arolt V, Konrad C. Impact of working memory load on fMRI resting state pattern in subsequent resting phases. *PLoS ONE* 4: e7198, 2009.

Rakic P. Specification of cerebral cortical areas. *Science* 241: 170-176, 1988.

Rissman J, Gazzaley A, D'Esposito M. Measuring functional connectivity during distinct stages of a cognitive task. *Neuroimage* 23: 752-763, 2004.

Rosa MGP, Tweedale R. Brain maps, great and small: lessons from comparative studies of primate visual cortex organization. *Phil Trans R Soc B* 360: 665-691, 2005.

Sepulcre J, Liu H, Talukdar T, Martincorena I, Yeo BTT, Buckner RL. The organization of local and distant functional connectivity in the human brain. *PLoS Comput Biol* 6: e1000808, 2010.

Shirer WR, Ryali S, Rykhlevskaia E, Menon V, Greicius MD. Decoding subject-driven cognitive states with whole-brain connectivity patterns. *Cereb Cortex* 22: 158-165, 2011.

Shulman GL, Fiez JA, Corbetta M, Buckner RL, Meizin FM, Raichle ME, Petersen SE. Common blood flow changes across visual tasks: II. Decreases in cerebral cortex. *J Cogn Neurosci* 9: 648-663, 1997.

Smith SM, Fox PT, Miller KL, Glahn DC, Fox PM, Mackay CE, Filippini N, Watkins KE, Toro R, Laird AR, Beckmann CF. Correspondence of the brain's functional architecture during activation and rest. *Proc Natl Acad Sci USA* 106: 13040-13045, 2009.

Smith SM, Jenkinson M, Woolrich MW, Beckmann CF, Behrens TEJ, Johansen-Berg H, Bannister PR, De Luca M, Drobnjak I, Flitney D, Niazy RK, Saunders J, Vickers J, Zhang Y, De Stefano N, Brady JM, Matthews PM. Advances in functional and structural MR image analysis and implementation as FSL. *Neuroimage* 23: S208-S219, 2004.

Spreng RN, Stevens WD, Chamberlain JP, Gilmore AW, Schacter DL. Default network activity, coupled with the frontoparietal control network, supports goal-directed cognition. *Neuroimage* 53: 303-317, 2010.

Stevens WD, Buckner RL, Schacter DL. Correlated low-frequency BOLD fluctuations in the resting human brain are modulated by recent experience in category-preferential visual regions. *Cereb Cortex* 20: 1997-2006, 2009.

Summerfield C, Greene M, Wager T, Egner T, Hirsch J, Mangels J. Neocortical connectivity during episodic memory formation. *PLOS Biol* 4: 0856-0864, 2006.

Tambini A, Ketz N, Davachi L. Enhanced brain correlations during rest are related to memory for recent experiences. *Neuron* 65: 280-290, 2010.

Toga AW, Thompson PM, Mori S, Amunts K, Zilles K. Towards multimodal atlases of the human brain. *Nat Rev Neuro* 7: 952-966, 2006.

Tyszka JM, Kennedy DP, Adolphs R, Paul LK. Intact bilateral resting-state networks in the absence of the corpus callosum. *J Neurosci* 31: 15154-15162, 2011.

Uncapher MR, Hutchinson JB, Wagner AD. A roadmap to brain mapping: toward a functional map of human parietal corex. *Neuron* 67: 5-8, 2010.

Ungerleider LG, Desimone R. Cortical connections of visual area MT in the macaque. *J Comp Neurol* 248: 190-222, 1986.

Vahdat S, Darainy M, Milner TE, Ostry DJ. Functionally specific changes in resting-state sensorimotor networks after motor learning. *J Neurosci* 31: 16907-16915, 2011.

van der Kouwe AJW, Benner T, Salat DH, Fischl B. Brain morphometry with multiecho MPRAGE. *Neuroimage* 40: 559-569, 2008.

Van Dijk, KRA, Sabuncu MR, Buckner RL. The influence of head motion on intrinsic functional connectivity MRI. *Neuroimage* 59: 431-438, 2012.

Van Dijk KRA, Hedden T, Venkataraman A, Evans KC, Lazar SW, Buckner RL. Intrinsic functional connectivity as a tool for human connectomics: Theory, properties, and optimization. *J Neurophysiol* 103: 297-321, 2010.

Van Essen DC. A population-average, landmark-and surface-based (PALS) atlas of human cerebral cortex. *Neuroimage* 28: 635-662, 2005.

Van Essen DC, Dierker DL. Surface-based and probabilistic atlases of primate cerebral cortex. *Neuron* 56: 209-225, 2007.

Van Essen DC, Zeki SM. The topographic organization of rhesus monkey prestriate cortex. *J Physiol* 277: 193-226, 1978.

Vincent JL, Patel GH, Fox MD, Snyder AZ, Baker JT, Van Essen DC, Zempel JM, Snyder LH, Corbetta M, Raichle ME. Intrinsic functional architecture in the anaesthetized monkey brain. *Nature* 447:83-86, 2007.

Vincent JL, Snyder AZ, Fox MD, Shannon BJ, Andrews JR, Raichle ME, Buckner RL. Coherent spontaneous activity identifies a hippocampal-parietal memory network. *J Neurophysiol* 96: 3517-3531, 2006.

von Bonin G, Bailey P. The neocortex of Macaca mulatta. Urbana, IL: University of Illinois Press, 1947.

Wagner AD, Desmond JE, Glover GH, Gabrieli JDE. Prefrontal cortex and recognition memory: functional-MRI evidence for context-dependent retrieval processes. *Brain* 121: 1985-2002, 1998.

Wiesendanger E, Clarke S, Kraftsik R, Tardif E. Topography of cortico-striatal connections in man: anatomical evidence for parallel organization. *Eur J Neurosci* 20: 1915-1922, 2004.

Wig GS, Schlaggar BL, Petersen SE. Concepts and principles in the analysis of brain networks. *Ann NY Acad Sci* 1224: 126-146, 2011.

Xiong J, Parsons LM, Gao JH, Fox PT. Interregional connectivity to primary motor cortex revealed using MRI resting state images. *Hum Brain Mapp* 8: 151-156, 1999.

Yeo BTT, Krienen FM, Sepulcre J, Sabuncu MR, Lashkari D, Hollinshead M, Roffman JL, Smoller JW, Zollei L, Polimeni J, Fischl B, Liu H, Buckner RL. The organization of human cerebral cortex estimated by intrinsic functional connectivity. *J Neurophysiol* 106: 1125-1165, 2011.

Zilles K, Palomero-Gallagher N, Grefkes C, Scheperjans F, Boy C, Amunts K, Schleicher A. Architectonics of the human cerebral cortex and transmitter receptor fingerprints: reconciling functional neuroanatomy and neurochemistry. *Eur Neuropsychopharmacol* 12: 587-599, 2002.

Paper III

The Organization of the Human Cerebral Cortex Estimated by Intrinsic Functional Connectivity

Yeo BTT*, Krienen, FM*, et al. *2011, J Neurophysiology*

*Denotes equal author contribution

Abstract

Information processing in the cerebral cortex involves interactions among distributed areas. Anatomical connectivity suggests that certain areas form local hierarchical relations such as within the visual system. Other connectivity patterns, particularly among association areas, suggest the presence of large-scale circuits without clear hierarchical relations. Here the organization of networks in the human cerebrum was explored using resting-state functional connectivity MRI (fcMRI). Data from 1000 subjects were registered using surface-based alignment. A clustering approach was employed to identify and replicate networks of functionally coupled regions across the cerebral cortex. The results revealed local networks confined to sensory and motor cortices as well as distributed networks of association regions. Within the sensory and motor cortices, functional connectivity followed topographic representations across adjacent areas. In association cortex, the connectivity patterns often showed abrupt transitions between network boundaries. Focused analyses were performed to better understand properties of network connectivity. A canonical sensory-motor pathway involving V1, putative MT+, LIP and FEF was analyzed to explore how interactions might arise within and between networks. Results showed that adjacent regions of the MT+ complex demonstrate differential connectivity consistent with a hierarchical pathway that spans networks. The functional connectivity of parietal and prefrontal association cortices was next explored. Distinct connectivity profiles of neighboring regions suggest they participate in distributed networks that, while showing evidence for interactions, are embedded within largely parallel, interdigitated circuits. We conclude by

discussing the organization of these large-scale cerebral networks in relation to monkey anatomy and their potential evolutionary expansion in humans to support cognition.

Introduction

Complex behaviors are subserved by distributed systems of brain areas (Felleman and Van Essen 1991; Goldman-Rakic 1988; Mesulam 1990). The organization of these systems can be studied in non-human animals using invasive techniques including histology, anatomic tract tracing, electrophysiology, and lesion methods. The organization of brain systems in the human has been inferred by comparing cytoarchitectonically-defined homologies between species, and by noting similarities in neuropsychological deficits following accidental brain injury to deficits present in animal ablation studies. General agreement has emerged from these comparisons that the basic organization of brain systems is similar across mammalian species. However, there is also evidence that the human cerebral cortex, particularly association cortex, is not simply a scaled version of other species.

The German anatomist Korbinian Brodmann (1909) first emphasized that areas comprising the human inferior parietal lobule do not have clear homologues in the monkey -- an observation that continues to motivate contemporary debates (Orban et al. 2004). Gross differences are also observed in the human brain when it is compared to our evolutionarily closest relatives. For example, the human brain is triple the size of modern great apes but motor and visual cortices are about the same absolute size (Blinkov and Glezer 1968; Frahm et al. 1984). This observation suggests that expansion of the human cerebrum disproportionately involves areas beyond those subserving basic sensory and motor functions. In a recent analysis of cortical expansion based on 23 homologous areas between the macaque and human, Van Essen and colleagues noted that the greatest

growth occurs in regions distributed across frontal, parietal, and temporal association cortices (Van Essen and Dierker 2007; Hill et al. 2010). Preuss (2004) came to a similar conclusion in a detailed review of comparative anatomy. Thus, in addition to expecting the human brain to show broadly similar organizational properties with other well-studied species, expansion and perhaps elaboration of association networks is also expected.

In this paper we report results of a comprehensive analysis of networks within the human cerebral cortex using intrinsic functional connectivity MRI (fcMRI). The analysis was based on 1000 young adults who contributed uniformly collected MRI data. The data were brought into a common surface coordinate system to help preserve the surface topology of the cortical mantle. Analyses were motivated by two goals. First, we sought to provide reference maps that are a current best estimate of the organization of the human cerebral cortex as measured by functional connectivity. Second, we wanted to better understand how patterns of functional connectivity might give rise to the organizational properties that underlie distributed brain systems. Particular focus was placed on parietal and frontal association cortices. The foundations for the present work come from traditional anatomical studies of cortical organization.

Organizational properties of the cerebral cortex in the non-human primate

Distributed brain systems are organized to facilitate *both* serial and parallel processing (Felleman and Van Essen 1991; Mesulam 1998). The concept of serial hierarchies is embedded within early ideas about brain organization. For example, William James (1890) proposed that principles governing the reflex arc extend to the cerebral hemispheres. He hypothesized that excitement of sensory systems propagates

upwards from lower to higher cerebral centers governing “ideas”, then to centers producing (or inhibiting) movements. Hubel and Wiesel (1962) formally proposed the concept of serial processing across a hierarchy in cat visual cortex based on their observations of increasingly complex receptive field properties from the lateral geniculate nucleus (LGN) to the simple and complex cells of V1. Based on studies of corticocortical connections in the macaque, Pandya and Kuypers (1969) and Jones and Powell (1970) suggested that hierarchical processing across sensory systems converges on transmodal association areas.

The discovery of widespread connections among multiple cortical areas, as well as extensive feedback projections from higher to lower sensory areas, suggested strictly serial processing is not the only organizational scheme in the cerebral cortex. Instead, it was proposed that hierarchical processing exists in a distributed fashion that can be inferred from the laminar distribution of anatomical connectivity (Friedman 1983; Maunsell and Van Essen 1983; Rockland and Pandya 1979). The comprehensive meta-analysis of corticocortical connections in the macaque monkey by Felleman and Van Essen (1991) provided strong evidence that unimodal and heteromodal areas in both the visual and somatomotor systems are organized into separate distributed hierarchies (also see Ungerleider and Desimone 1986; Van Essen et al. 1992). Some projections between areas are organized as feedforward (ascending) projections, others as feedback (descending) projections, and still others as lateral projections. For example, consistent with serial processing, the primary visual area (V1) sends forward connections to and receives feedback connections from V2 in a topographic fashion that connects the corresponding receptive field representation in each area. In contrast to strictly serial

processing, these unimodal sensory cortical areas (V1 and V2) both project to higher sensory areas. Lateral projections between areas are also common (e.g., CIT and STPp).

It becomes considerably more difficult to make inferences about the organization of circuits involving association cortex. Historically, of the four criteria – function, cytoarchitecture, connectivity and topography – used to define cortical areas and thereby constrain models of organization, topography (e.g., retinotopy) and function are difficult to discern in heteromodal association areas. Cytoarchitecture and connectivity thus become especially valuable for inferring brain circuit organization beyond the sensory and motor systems. However, as noted by Felleman and Van Essen (1991), the number of violated constraints to hierarchical connectivity increases in the progression from early sensory cortex up to association cortex (red lines near the top of the visual hierarchy in Fig. 4 of Felleman and Van Essen 1991).

This raises the interesting possibility that the association areas may not follow as rigid a hierarchical organization as canonical sensory and motor areas. Violations of strict hierarchical arrangements are apparent in the visual system as noted above, but violations and alternative connectivity patterns become common in association areas. For example, paired tracer injections in association areas 7a and 46 lead to interdigitating columnar patterns of terminations in some areas and complementary (feedforward and feedback) patterns in other areas (Selemon and Goldman-Rakic 1988).

While recognizing that convergence and integration of pathways occurs in the association cortex, Goldman-Rakic (1988) emphasized that primate association cortex is organized into parallel distributed networks (see also Mesulam 1981). There are two key features to her proposed organization that depart from hierarchical organizational models.

First, each distributed network consists of association areas spanning frontal, parietal, temporal and cingulate cortices. Networks are densely interconnected, such that two areas in the parietal and frontal cortices belonging to the same network are not just anatomically connected to each other, but they are also both connected with other components of the same network (Selemon and Goldman-Rakic 1988). Second, multiple distributed networks exist adjacent to each other: adjacent areas in the parietal cortex belonging to separate networks are differentially connected to adjacent areas of corresponding networks in the frontal, temporal and cingulate cortices (Cavada and Goldman-Rakic 1989a; 1989b).

The possibility of parallel distributed circuits will be an important consideration in our analysis of fcMRI networks in the human, particularly within association cortices. An intriguing possibility is that the majority of the human cerebral cortex involves multiple parallel circuits that are interdigitated throughout association cortex, such that each cortical lobe contains components of multiple association networks. That is, the expansion of the cerebral association cortex in humans relative to the macaque may preferentially involve networks organized in the form outlined by Goldman-Rakic (1988) and anticipated by others (e.g., Mesulam 1981). To explore this possibility, analyses will focus both on evidence for hierarchical relations across regions as well as evidence for distributed networks that are interdigitated throughout association cortex.

Insights into the organization of the cerebral cortex revealed through neuroimaging

Noninvasive neuroimaging methods including positron emission tomography (PET; Raichle 1987) and functional MRI (fMRI; Kwong et al. 1992; Ogawa et al. 1992)

allow functional response properties to be measured in the human cerebral cortex. The measures are indirect, reflecting blood flow and oxygenation changes that are coupled to neural activity through incompletely understood mechanisms (Logothetis 2008), and the methods are presently limited to a spatial resolution of a few mm (e.g., Engel et al. 1997). Neuroimaging approaches have nonetheless been extremely valuable for providing insights into cortical organization. In some cases it has been possible to directly map the topography within (and borders between) cortical areas (Engel et al. 1994; Sereno et al. 1995). More generally, differential response properties between regions are the source of information about cortical mapping. For example, the increase in the complexity of receptive field properties measured from primary to secondary sensory areas in visual (Wandell et al. 2007), somatosensory (Iwamura 1998), and auditory (Wessinger et al. 2001) cortices suggest that serial hierarchical processing exists in human sensory cortex.

Neuroimaging studies of a wide range of cognitive tasks reveal simultaneous activation in multiple regions in the parietal, frontal, temporal and cingulate cortices, suggesting distributed systems of brain areas are involved in cognition. However, it is difficult to assess the organization of these distributed systems based solely on task activity because these cognitive tasks likely tap into multiple, overlapping processes, some of which reflect the operation of distributed systems and others which reflect distinct processing demands of the tasks (see Mesulam 1990 and Posner et al. 1988 for relevant discussion). For these reasons, methods that can measure connectivity may provide novel insights into the organization of distributed brain systems.

Functional connectivity and diffusion MRI provide tools to explore cortical organization

Diffusion MRI (dMRI) and fcMRI have recently emerged as promising tools for mapping the connectivity of the human brain, each with distinct strengths and weaknesses. dMRI measures the diffusion of water thus allowing direct non-invasive mapping of white matter pathways (Basser et al. 1994). However, dMRI is presently limited to resolving major fiber tracts. By contrast, fcMRI measures intrinsic functional correlations between brain regions (Biswal et al. 1995) and is sensitive to coupling between distributed as well as adjacent brain areas (e.g., see Sepulcre et al. 2010 for discussion). While not a direct measure of anatomical connectivity, the functional couplings detected by fcMRI are sufficiently constrained by anatomy to provide insights into properties of circuit organization (for reviews, see Fox and Raichle 2007; Van Dijk et al. 2010). When describing these correlations, we use the term functional connectivity as coined by Karl Friston (1994) to denote "temporal correlations between remote neurophysiological events" for which the causal relation is undetermined.

There are important limitations of fcMRI including sensitivity to indirect anatomical connectivity and functional coupling that changes in response to recent experience and the current task being engaged (Buckner 2010). For these reasons, some discussions of fcMRI have emphasized that intrinsic activity measured by fcMRI reflects the prior history of activity through brain systems and not simply static anatomic connectivity (Power et al. 2010). fcMRI also does not presently provide information about whether connections are feedforward (ascending) or feedback (descending). These limitations constrain how analyses are conducted and results can be interpreted.

Directly relevant to the present study, prior investigations using fcMRI provide estimates of large-scale cortical networks that have generally (but not in all details)

converged across a variety of analytic approaches, including seed-based fcMRI (Biswal et al. 1995), independent component analysis (Beckmann and Smith 2004; Smith et al. 2009), clustering (Bellec et al. 2010; Golland et al. 2007) and graph theory (Dosenbach et al. 2007). Because of uncertainties regarding their relation to underlying anatomic brain systems, networks identified using fcMRI have often been labeled based on their relations to task-based functional networks. Some of these networks, such as the default network (Greicius et al. 2003) and dorsal attention system (Fox et al. 2006), have been proposed to be related to anatomical tracing and task-based fMRI in the macaque (Buckner et al. 2008; Saleem et al. 2008; Vincent et al. 2007).

Motivated by the usefulness of connectivity in establishing the organization of the cerebral cortex in non-human primates, this study analyzed fcMRI data from 1000 subjects with two main goals. First, the analyses sought to provide reference maps that are a current best estimate of the organization of human cortical networks as measured by functional connectivity. Second, by using the power of a large data sample to quantitatively measure functional connectivity strength among many regions, the study explored the patterns of corticocortical functional coupling that give rise to these networks.

Methods

Overview

The present study explored the organization of large-scale distributed networks in the human cerebral cortex using resting-state fcMRI. The main analyses were based on a

core dataset of 1000 healthy, young adults whose fMRI data were acquired using the same MRI sequence on the same hardware (3 Tesla field strength, 12-channel receive coil array). For several analyses the data were divided into Discovery (n = 500) and Replication (n = 500) data samples to test for reliability and for unbiased quantification of functional connectivity patterns. Additional supplementary datasets were used to address specific questions that arose during analysis. A first supplementary fMRI dataset (n = 16) contrasted different passive tasks engaged during resting-state functional data acquisition. A second supplementary fMRI dataset (n = 4) consisted of data acquired during visual stimulation optimized to define retinotopic boundaries of early visual areas (Hinds et al. 2009; Polimeni et al. 2005). A final supplementary dataset used human histological data to define a range of cytoarchitectonic areas including human V1 (Amunts et al. 2000, Fischl et al. 2008) and the putative homologue to macaque MT+ (Malikovic et al. 2007, Yeo et al. 2010b). All data (fMRI and histological) were brought into a common surface coordinate system based on the cortical surface as reconstructed from each participant's structural anatomy. Data analyses began by examining broad properties of cortical network organization and progressed to quantify the detailed patterns of functional connectivity within and between networks.

In the first set of analyses, a clustering algorithm was used to parcellate the cerebral cortex into networks of functionally coupled regions. Parcellations were examined for a coarse solution that organized the cortex into 7 networks as well as a finer solution that identified 17 networks. As the results will reveal, the estimated networks were consistent across the Discovery and Replication data samples and confirmed by

region-based fcMRI analyses. The full dataset was used to construct a best-estimate parcellation of the human cerebral cortex to serve as a reference for future studies.

The second set of analyses explored the coupling of regions that fell within sensory and motor pathways. Since these areas are relatively well understood in both humans and macaques, they provide the opportunity to evaluate the utility and limitations of functional connectivity methods. Analyses examined quantitative coupling properties between individual regions that were within the same network as well as coupling properties between networks focusing on a sensory-motor pathway that is the putative homologue of the well-studied system in the monkey involving MT+, parietal regions at or near LIP, and premotor regions at or near FEF.

The final set of analyses characterized the organization of distributed networks in higher-order association cortex. The connectivity patterns of regions within frontal and parietal association cortices were quantified. These analyses involved constructing a series of small seed regions across frontal and parietal cortices and examining functional connectivity strength to multiple regions distributed throughout the cerebral cortex, allowing the 'fingerprint' of functional coupling to be identified for each region. For these analyses, regions were always defined in the Discovery data sample or some other source, such as histology, and functional connectivity quantified in the independent Replication data sample.

Participants

Paid participants were clinically healthy, native English speaking young adults with normal or corrected-to-normal vision (ages 18 to 35). Subjects were excluded if their

fMRI signal-to-noise ratio (SNR) was low (< 100; see below), artifacts were detected in the MR data, their self-reported health information indicated the presence of any prior neurological or psychiatric condition, or they were taking any psychoactive medications. The core dataset consisted of 1000 individuals imaged during eyes open rest (EOR) and was divided into two independent samples (each n = 500; labeled the *Discovery* and *Replication* samples). Age and gender were matched for the Discovery (mean age = 21.3 yr, 42.6% male) and Replication (mean age = 21.3 yr, 42.8% male) datasets. These data are new data presented for the first time in this study and were acquired as part of a collaborative effort across multiple local laboratories all acquiring data on matched MRI scanners (at Harvard and at the Massachusetts General Hospital). Participants provided written informed consent in accordance with guidelines set by institutional review boards of Harvard University or Partners Healthcare.

Two smaller supplementary datasets were also analyzed. The *Task Effect* dataset (n = 16, mean age = 21.1 yr, 25.0% male) consisted of fMRI data collected under different passive conditions (eyes closed rest, ECR; EOR; and fixation, FIX) and was analyzed previously (Van Dijk et al. 2010). The *Visuotopic* dataset (n = 4; mean age = 34.5 yr, 100% male) consisted of previously published visuotopic data (Hinds et al. 2009; Polimeni et al. 2005).

MRI data acquisition

All data were collected on matched 3T Tim Trio scanners (Siemens, Erlangen, Germany) using a 12-channel phased-array head coil except for the Visuotopic dataset, which was acquired on a custom-built four-channel phased-array surface coil. A software

upgrade (VB15 to VB17) occurred on all scanners during the study. Validation studies that acquired structural and functional data on the same individuals before and after the upgrade could not detect an effect of the upgrade. The functional imaging data were acquired using a gradient-echo echo-planar imaging (EPI) sequence sensitive to blood oxygenation level-dependent (BOLD) contrast. Whole-brain coverage including the entire cerebellum was achieved with slices aligned to the anterior-commissure posterior-commissure (AC-PC) plane using an automated alignment procedure ensuring consistency between subjects (van der Kouwe et al. 2005). Structural data included a high-resolution multi-echo T1-weighted magnetization-prepared gradient-echo image (multi-echo MP-RAGE; van der Kouwe et al. 2008).

For the core dataset, subjects were instructed to remain still, stay awake and to keep their eyes open. EPI parameters were as follows: TR = 3000 ms, TE = 30 ms, FA = 85º, 3 x 3 x 3 mm voxels, FOV = 216 and 47 axial slices collected with interleaved acquisition and no gap between slices. Each functional run lasted 6.2 min (124 time points). One or two runs were acquired per subject (average of 1.7 runs). Parameters for the structural scan (multi-echo MP-RAGE; van der Kouwe et al. 2008) were as follows: TR = 2200 ms, TI = 1100 ms, TE=1.54 ms for image 1 to 7.01 ms for image 4, FA = 7º, 1.2 x 1.2 x 1.2 mm voxels and FOV = 230. The multi-echo MP-RAGE allows increased contrast through weighted-averaging of the four derived images.

For the Task Effect dataset, subjects were instructed to remain still with their eyes open (EOR; two runs), eyes closed (ECR; two runs) or to passively fixate a centrally presented crosshair (FIX; two runs). For details see Van Dijk et al (2010). The order of rest conditions was counterbalanced across subjects. EPI parameters were as follows: TR

= 3000 ms; TE = 30 ms; FA = 90º; 3 x 3 x 3 mm voxels; FOV = 288 and 43 slices collected with interleaved acquisition and no gap between slices. Each functional run lasted 7.15 min (143 time points). Parameters for structural scans (MP-RAGE) were as follows: TR = 2530 ms, TI = 1100 ms, TE = 3.44 ms, FA = 7º, 1 x 1 x 1 mm voxels and FOV = 256.

The Visuotopic dataset was collected using a custom-built four-channel phased-array surface coil placed at the back of the head. During each functional run, subjects were presented with one of four visual stimuli: a clockwise rotating wedge, a counterclockwise rotating wedge, an expanding ring, or a contracting ring (DeYoe et al. 1996; Engel et al. 1994; Sereno et al. 1995). Because the four-channel surface coil provided only partial brain coverage, structural data for these four subjects were collected separately on a 1.5T Allegra scanner (Siemens, Erlangen, Germany). Further details of the acquisition and data processing protocol can be found elsewhere (Hinds et al. 2009; Polimeni et al. 2005).

Except where noted, the description of data processing and analysis below applies to the whole-brain data (the core dataset of 1000 subjects and the Task Effect dataset) and not the Visuotopic data.

Functional MRI data preprocessing

The fMRI data were preprocessed with a series of steps common to fMRI analyses. Preprocessing involved (1) discarding the first four volumes of each run to allow for T1-equilibration effects, (2) compensating for slice-acquisition-dependent time shifts per volume with SPM2 (Wellcome Department of Cognitive Neurology, London,

UK), and (3) correcting for head motion using rigid body translation and rotation with the FSL package (Jenkinson et al. 2002; Smith et al. 2004).

The data underwent further processing using procedures adapted from Biswal et al. (1995) and optimized for fcMRI analysis (Fox et al. 2005; Van Dijk et al. 2010; Vincent et al. 2006). Briefly, constant offset and linear trend over each run was removed and a temporal filter was applied to retain frequencies below 0.08 *Hz*. Sources of spurious variance, along with their temporal derivatives, were removed through linear regression including: (1) six parameters obtained by correction for rigid body head motion, (2) the signal averaged over the whole brain, (3) the signal averaged over the ventricles, and (4) the signal averaged over the deep cerebral white matter. This regression procedure minimized signal contributions of non-neuronal origin including respiration-induced signal fluctuations (Van Dijk et al. 2010). Unlike previously established fcMRI preprocessing procedures, no spatial smoothing of the resting-state data occurred up to this point of the preprocessing stream.

Structural MRI data preprocessing and functional-structural data alignment

The structural data were processed using the FreeSurfer (http://surfer.nmr.mgh.harvard.edu) version 4.5.0 software package. The FreeSurfer software package constitutes a suite of automated algorithms for reconstructing accurate surface mesh representations of the cortex from individual subjects' T1 images (Fig. 3.1B-C) and the overlay of fMRI on the surfaces for group analysis (Fig. 3.1D-E). Briefly, the cortical surface extraction process (Fig. 3.1B-C) involved (1) correcting for intensity variations due to MR inhomogeneities (Dale et al. 1999), (2) removing extra-

cerebral voxels through “skull-stripping” (Ségonne et al. 2004), (3) segmenting cortical gray and white matter voxels based on the intensity difference and geometric structure of the gray-white interface (Dale et al. 1999), (4) computing cutting planes to disconnect the two hemispheres and subcortical structures (Dale et al. 1999), (5) filling the interior holes of the segmentation using a connected-component analysis (Dale et al. 1999), (6) tessellating a triangular mesh over the gray-white boundary of each hemispheric volume and deforming the mesh to produce a smooth representation of the gray/white interface and pial surface (Dale et al. 1999), and (7) correcting topological defects in the surface so that the mesh achieves a spherical topology (Fischl et al. 2001; Ségonne et al. 2007).

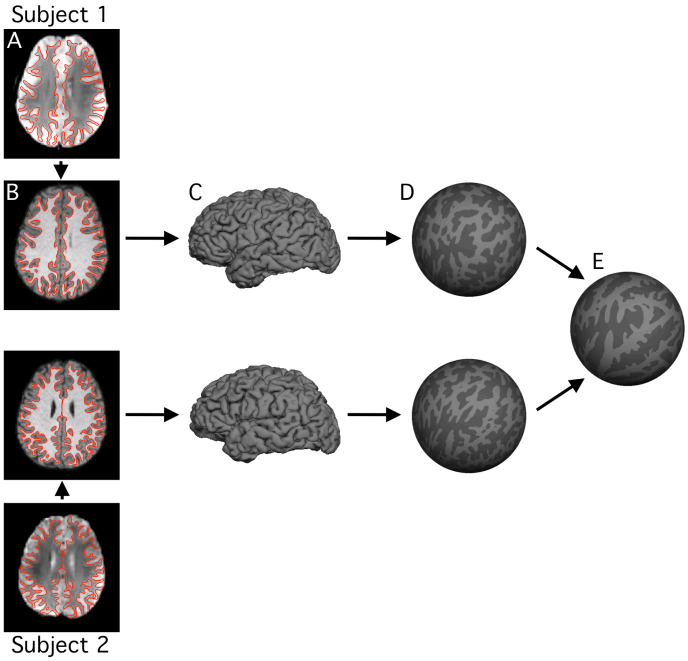

Figure 3.1. Surface coordinate system for fMRI analysis. For each subject, the T2* images yielding BOLD-contrast fMRI data (A) were registered to the T1-weighted structural data (B). The cortical gray-white and pial surfaces were estimated from the structural data. The red lines show the estimated gray-white surface (A, B). Pial surface is shown in C. The gray-white surface was inflated into a sphere (D). The inflated spheres were then aligned across subjects using surface-based registration of the cortical folding pattern, resulting in a common spherical coordinate system (E). BOLD data of individual subjects (A) can then be projected onto the spherical coordinate system (E) in a single transformation step to reduce artifacts due to multiple interpolations.

After segmentation of the cortical surface, spatial correspondences among the subjects' cortical folding patterns were established via the use of a spherical coordinate system (Fig. 3.1D-E). Briefly, the process involved (1) inflating each subject's surface mesh into a sphere while minimizing geometric distortion of the original cortical surface as measured by geodesic distances among surface vertices and ensuring the inflation constituted a one-to-one mapping, and (2) computing a smooth, invertible deformation of the resulting spherical mesh to a common spherical coordinate system that aligned the cortical folding patterns across subjects (Fischl et al. 1999a; Fischl et al. 1999b).

Once the common spherical coordinate system was established, the structural and functional images were aligned (Fig. 3.1A-B) using boundary-based registration (Greve and Fischl 2009) that is provided as part of FreeSurfer's companion package, FsFast (http://surfer.nmr.mgh.harvard.edu/fswiki/FsFast). The preprocessed resting state fMRI data were then propagated to the common spherical coordinate system via sampling from the middle of the cortical ribbon in a single interpolation step (Fig. 3.1A-E). The choice of sampling fMRI data from the middle of the cortical ribbon was motivated by the desire to reduce the blurring of fMRI signal across sulci or gyri and also by a recent study on the point-spread function of fMRI (Polimeni et al. 2010). The study showed that large draining vessels on the pial surface increased BOLD signal close to the pial surface but reduced spatial specificity of the hemodynamic response. Sampling fMRI data from the middle of the cortical ribbon therefore represented a trade-off between spatial specificity and signal sensitivity. Since our fMRI voxels were relatively large (3mm), we were not as concerned about laminar bias in the functional connectivity analysis.

The cerebral cortex is a thin sheet, with common organizational features along its radial axis. Along the dimensions parallel to this sheet is a mosaic of cortical areas that differ in function, cytoarchitecture, connectivity, and topography (Felleman and Van Essen 1991; Kaas 1987). The spherical representation of the cortex therefore affords a more accurate alignment of the cortical folding pattern and has the consequence of improving cytoarchitectonic (Fischl et al. 2008; Hinds et al. 2008; Yeo et al. 2010a) and functional (Fischl et al. 1999b; Van Essen 2005) correspondences across subjects compared with 3D volumetric registration even though cortical folds do not completely predict cytoarchitecture or function (Rajkowska and Goldman-Rakic 1995; Thirion et al. 2007; Yeo et al. 2010b). The acquisition resolution and inherent limitations of the BOLD signal also provided restrictions on achievable resolution.

A 6mm FWHM (full width at half maximum) smoothing kernel was applied to the fMRI data in the surface space and the data were downsampled to a 4mm mesh[2]. Smoothing after the fMRI data were projected onto the surface helped to minimize the blurring of fMRI signal across sulci or gyri. Since our algorithms are not perfectly accurate, any registration or segmentation errors will likely cause blurring of fMRI signal across sulci or gyri. Consequently, we did not expect to eliminate the blurring issues completely, which is important to keep in mind when interpreting the results. The steps taken could only minimize the problem.

---

[2] It is not possible to generate a high resolution uniform mesh on the sphere. However, one can work with approximately uniform spherical meshes at different spatial resolutions by starting with a regular icosahedron mesh consisting of 20 equal faces and 12 vertices and iteratively subdividing each mesh triangle into four smaller triangles. Here each cortical hemisphere is represented by a subdivided icosahedron mesh with 20480 faces and 10242 vertices, where neighboring pairs of vertices are on average 3.8 mm apart (max = 4.1 mm, min = 3.4 mm).

The processing of the Visuotopic dataset was broadly similar except that older versions of FreeSurfer and FsFast were used for the processing and so manual interventions were required to correct the T2* to T1 registration. Details of the processing can be found elsewhere (Hinds et al. 2009; Polimeni et al. 2005).

Quality control

Visual inspection of the registered data suggested that accurate representation of the cortical surface was extracted for each subject and that structural and functional image registration was successful. Figure 3.2 shows the results of cortical surface extraction from the T1 images and T2* to T1 registration of 3 randomly chosen subjects. These examples represent typical subjects. Note that functional data distortion remains in areas prone to susceptibility artifacts including anterior prefrontal regions, regions near lateral temporal cortex, and orbital frontal cortex.

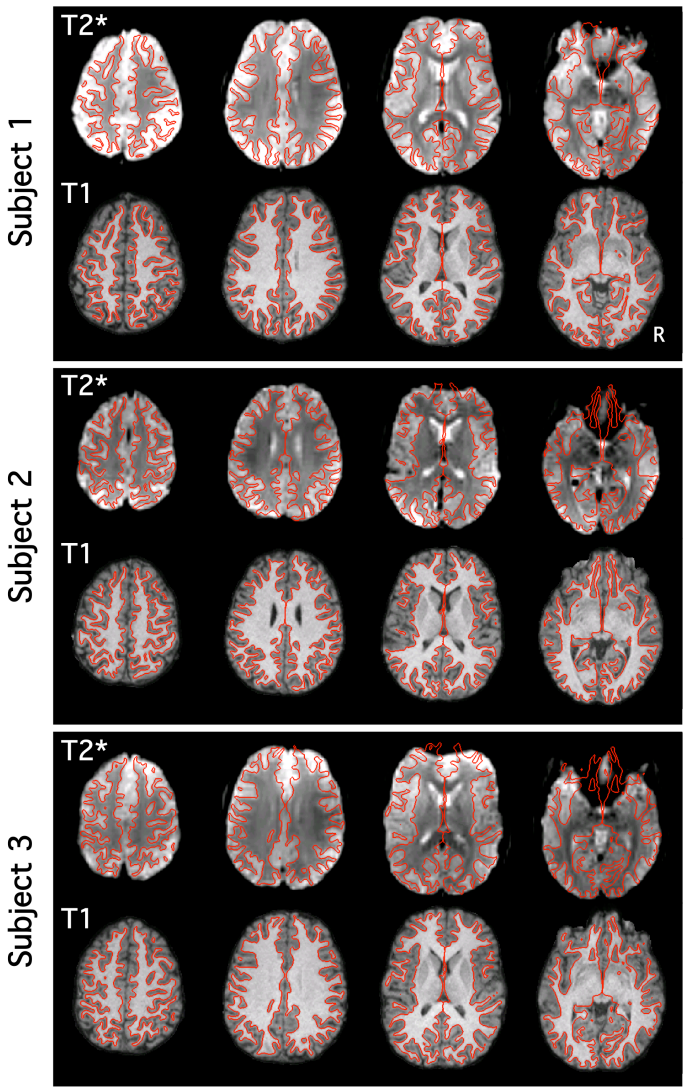

Figure 3.2. Examples of intrasubject surface extraction and registration of structural-functional images. Examples of extracted cortical gray-white surfaces (red lines) are overlaid on T2* and T1 images of three random subjects in their native T1 space. Imperfections are apparent in BOLD data especially in regions of susceptibility artifact (e.g., orbital frontal cortex).

Visualization

While all subsequent analyses were performed in FreeSurfer surface space, for the purpose of visualization, all maps were transformed and displayed on the inflated PALS cortical surfaces using Caret software (Van Essen 2004; 2005; Van Essen and Dierker 2007). In addition, this study also transformed and visualized the estimated networks in FMRIB Software Library (FSL) MNI152 space (Smith et al. 2004). The mapping between FSL MNI152 volumetric space and FreeSurfer surface space is detailed in our companion study (Buckner et al. submitted).

Signal-to-noise ratio (SNR) maps

Signal loss and distortion (susceptibility artifacts) occur as a result of magnetic field inhomogeneities. Field inhomogeneities are particularly pronounced in regions where the brain is adjacent to air, causing signal loss and distortion in T2*-dependent (BOLD) images (Ojemann et al. 1997). To estimate the effects of susceptibility artifacts in the present data, the signal-to-noise ratio (SNR) of the motion corrected fMRI time series was computed for each voxel in subjects' native volumetric space by averaging the signal intensity across the whole run and dividing it by the standard deviation over time. SNR was also used as exclusionary criteria. If the SNR for the whole brain (mean SNR over all voxels within the brain mask) was <100 for an fMRI run, the subject was excluded. Thus, all 1000 subjects contributed data with SNR > 100 for each fMRI run. For subjects with two runs, the SNR was averaged across the runs. The SNR was then projected to FreeSurfer surface space, averaged across the 1000 subjects from the core dataset, and displayed in Caret PALS space (Fig. 3.3). As expected, low SNR is present

in the anterior portion of the inferior and medial temporal lobe, as well as in the orbital frontal cortex. There is also clear spatial variation in the SNR across the cortical mantle, which is important to keep in mind when interpreting the results, such as the absence of a cortical region of low SNR from a network.

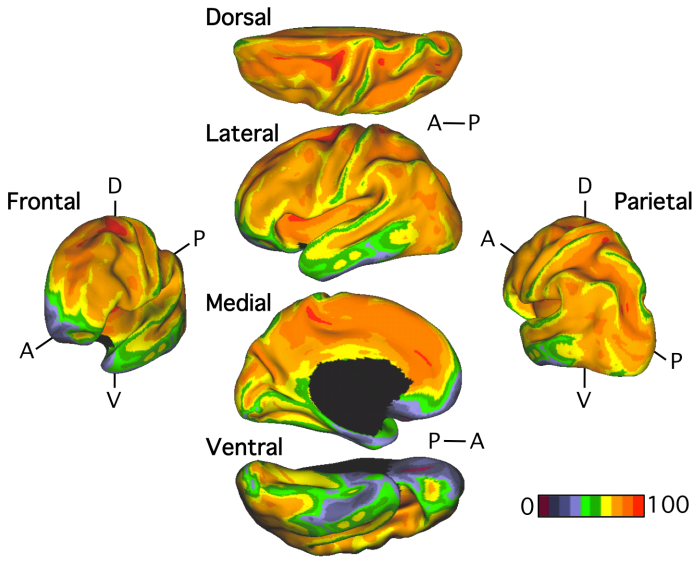

Figure 3.3 Signal-to-noise ratio (SNR) maps of the functional data from the full sample (N = 1000). The mean estimate of the BOLD fMRI data SNR is illustrated for multiple views of the left hemisphere in Caret PALS space. A = anterior, P = posterior, D = dorsal and V = ventral.

Clustering

We applied a clustering approach to define the boundaries of functionally distinct cortical regions and their relations to regions distributed throughout the cerebral cortex (forming networks). Distinguishing neighboring cortical regions by their pattern of connectivity has a long history in both non-human primate (e.g., Cavada and Goldman-Rakic 1989a; Goldman-Rakic 1988; Passingham et al. 2002) and human (e.g., Cohen et al. 2008; Johansen-Berg et al. 2004; Nelson et al. 2010) research. Here we began our analyses by defining cortical networks to be sets of cortical regions with similar profiles

of corticocortical functional connectivity. The idea follows the empirical finding that in primates, regions of association cortex that are anatomically connected tend to have similar patterns of anatomical connectivity to other cortical and subcortical regions, thus forming a densely connected distributed network (Goldman-Rakic 1988). Note that this assumption about the organizational properties of corticocortical connectivity is probably neither a characteristic of all cortical regions nor a full characterization of the connectivity pattern of any cortical region. As will be shown, the procedure identified functionally coupled networks that could be verified with seed-based regional analyses that made no assumptions about the connectivity patterns.

For this initial analysis, we defined the connectivity profile of a cortical region to be its functional coupling to 1175 region of interest (ROI) vertices. The 1175 ROI vertices were uniformly sampled in FreeSurfer surface space (shown in Caret PALS space in Fig. 3.4) and consisted of single vertices spaced about 16mm apart. For each subject, we computed the Pearson's product moment correlation between the fMRI time series at each spatial location (18715 vertices) and the 1175 ROI vertices. Each spatial location is therefore characterized by its functional coupling to the 1175 ROI vertices. We binarized the 18715 x 1175 matrix of correlations for each subject by keeping the top 10% of the correlations and averaged the binarized matrices independently across each group of 500 subjects in the Discovery and Replication samples. If a subject had two runs, we averaged the correlation matrices across the two runs before binarization. As will be shown in the results, binarization of the correlation matrix leads to significantly better clustering results, although the algorithm appears robust to the particular choice of threshold. Visual inspection of the connectivity profiles (not shown) suggested that the

1175 ROI vertices were sufficiently dense to capture spatial variation in corticocortical connectivity given the limits of our acquisition procedures.

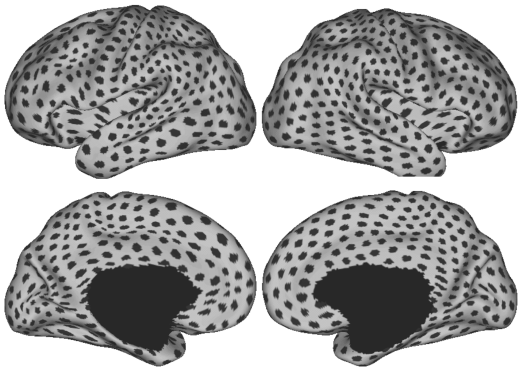

Figure 3.4. Cortical regions utilized in constructing functional connectivity profiles. A total of 1175 regions are sampled uniformly on the surface-based representations of the left and right hemispheres within the FreeSurfer surface coordinate system and shown here in Caret PALS space, where each dark patch represents the location of a single regional vertex. Each vertex in the surface coordinate system is characterized by its profile of functional connectivity to the 1175 regions. The visually non-uniform distribution of the regions in Caret PALS space is due to the non-linear deformation from FreeSurfer space to Caret PALS space. This image thus also serves to illustrate the subtle differences between the two surface space coordinate systems.

A clustering algorithm was then applied separately to the Discovery and Replication samples to estimate networks of cortical regions with similar connectivity profiles. The two independent datasets thus allowed exploration of the reliability of estimated networks. The idea behind clustering can be illustrated with a toy example. Figure 3.5A shows hypothetical points scattered in a structured fashion on a two-dimensional canvas. Clustering aims to recover this structure by dividing the points into different groups so that points within a group are physically close, such as shown in Figure 3.5B.

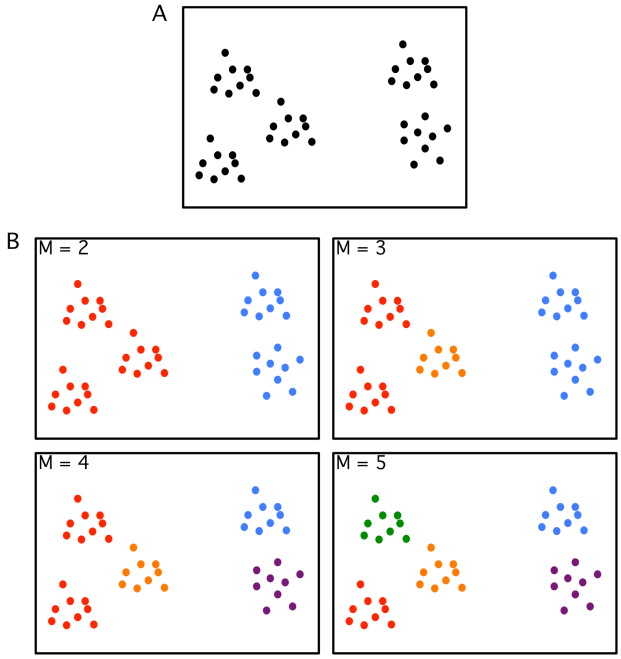

Figure 3.5. Toy example illustrating clustering. (A) Hypothetical points are scattered in a structured fashion on a two-dimensional canvas. Clustering aims to recover the underlying structure. (B) Example solutions for M = 2, 3, 4 or 5 clusters are shown. The solutions for M = 2 or 5 clusters agree with visual assessment of the underlying structure and are therefore useful representations. On the other hand, seeking 3 or 4 clusters does not lead to satisfying solutions because solutions are ambiguous. For example, the M = 3 solution is not unique in the sense that an "equally good" alternate solution is for one group of points in the red cluster to be grouped with the orange cluster. Seeking M = 3 or 4 clusters is therefore unstable in the sense that different random initializations of the clustering algorithm lead to different "equally good" solutions. In the present study we employed a stability analysis to estimate the numbers of clusters and also examined both a relatively coarse solution (7-network) and fine-resolution solution (17-network) so as to survey the solution space broadly (see Fig. 3.6).

The clustering algorithm employed in this study modeled the data with a von Mises-Fisher distribution (Lashkari et al. 2010). More specifically, the data were modeled as 18715 points on an 1174-dimensional unit hypersphere embedded in an 1175-dimensional Euclidean space, where distances between points were measured by their

geodesic distance on the hypersphere. Like the toy example, clustering aims to group vertices that are close together in this non-Euclidean canvas (i.e., have similar connectivity profiles) into the same cluster or network. Measuring distances between points by their geodesic distance is equivalent to defining the similarity between two correlation profiles to be the correlation between the correlation profiles. By using correlation as a measure of similarity, differences in correlation strength were normalized among points so that regions are clustered together based on their connectivity profiles (rather than their strengths of connectivity). In theory, this should mitigate the effects of spatial variation in SNR (Fig. 3.3).

The algorithm operated by randomly assigning the 18715 points to different groups and then iteratively reassigning the group memberships of points to maximize the agreement of connectivity profiles among points of the same group. More details of the clustering algorithm can be found elsewhere (Lashkari et al. 2010).

Stability analysis

A drawback of most clustering approaches is that one must choose the number of clusters *a priori*. In this instance, the question is how many clusters – cerebral networks – are needed to correctly parcellate the cortex? We do not have an answer to this question or know if there is a single correct answer given that the cerebral cortex possesses complex patterns of diverging and converging connections among areas. As such, none of our conclusions will depend on a strong assumption that there is a single correct solution to parcellating the cortex. Nonetheless, we sought a principled approach

to identify parcellation solutions that captured significant portions of the correlation structure among cortical regions.

One popular method for estimating the number of clusters is by analyzing the stability of the clustering algorithm (Ben-Hur et al. 2002; Lange et al. 2004; also see Fig. 3.5). We employed two variations of the stability analysis on the full set of 1000 subjects. Both variations estimated the same numbers of clusters. The first variation involved (repeatedly and randomly) dividing the ROIs into two groups and measuring the reproducibility of the clustering algorithm's results when applied separately to the two groups of ROIs. The second variation involved (repeatedly and randomly) dividing the 18715 vertices into two groups and applying the clustering algorithm separately to the two groups of vertices. The model parameters learned from clustering one group of vertices was then used to predict the clustering results of the second group of vertices. The agreement between the prediction and clustering results of the second group measured the generalization power of the clustering results (Fig. 3.6). Further details of the stability analysis can be found elsewhere (Lange et al. 2004).

The stability analyses (Fig. 3.6) suggested 7 and 17 networks were appropriate starting points for parcellating the cortex. As the results will reveal, these parcellation solutions were excellent for capturing significant components of the regional variation that could be replicated across datasets and independently revealed by seed-based analyses. However, the focus on 7- and 17-network solutions should not be taken to imply that meaningful properties are absent in alternative parcellation schemes. By focusing on both a relatively coarse solution (7-network) and fine-resolution solution (17-network), we were able to survey the solution space broadly.

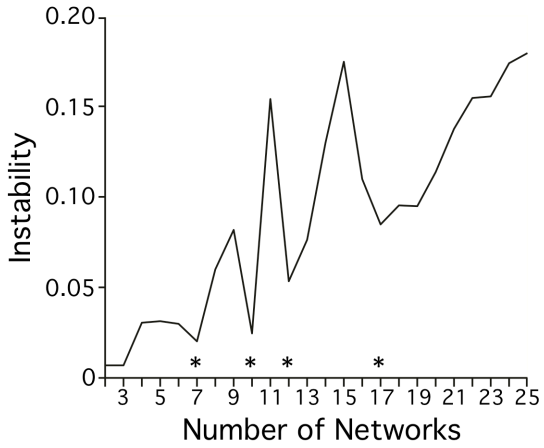

Figure 3.6. 7 and 17 networks can be stably estimated. Instability of the clustering algorithm is plotted as a function of the number of estimated networks for the vertex-resampling variant of the stability analysis applied to 1000 subjects. The clustering algorithm is less stable with increasing number of estimated networks, which is an expected property since the number of estimated networks enlarges the solution space (and thus complexity) of the clustering problem. The local minima of the graphs (marked with asterisks) indicate the number of networks that can be stably estimated by the clustering algorithm. The stability analysis suggests that 7, 10, 12 or 17 networks can be stably estimated. Resampling the ROIs yields almost identical results and is not shown. Here we focus on the 7- and 17-network estimates to provide a broad survey of the solution space.

Parcellation maps

Parcellation maps of the cerebral cortex were generated for both 7-network and 17-network solutions for the Discovery sample and replicated in the Replication sample. The reliability analysis was conducted to illustrate the stability of the topographic boundaries that the solutions converged upon. In this regard, a powerful feature of analyzing large data samples is that the analyses are able to detect the presence of stable cerebral networks and also to establish the boundaries of regions with a high degree of confidence, including contiguous regions that may be part of distinct networks. As a final

step the full sample (N = 1000) was used to compute parcellations that represent our best estimates of the networks (Figs. 3.11 and 3.13).

Confidence maps

A useful visualization of the cortical parcellation is to look at the confidence of each spatial location belonging to its assigned network. We used the silhouette measure (Rousseeuw 1987) from the clustering literature for this purpose (Figs. 3.8 and 3.10). The silhouette of a data point (spatial location in our case) measures the similarity (correlation in our case) of the data point to other data points of the same cluster (network in our case) compared with data points belonging to the next closest cluster. The resulting silhouette at each spatial location lies between -1 and 1, so that a larger value indicates higher confidence of the spatial location in belonging to its assigned network. A negative value indicates that the connectivity profile at the spatial location is on average closer to the next closest cluster than to its assigned cluster. A negative value is therefore unlikely, but is still possible because the clustering cost function is not equivalent to the silhouette measure.

Correlation maps and correlations between regions

Large-scale cortical networks can be reliably estimated. To better understand the meaning of the networks resolved by the clustering technique, all salient results were followed up with focused analyses using seed-based regional analysis. The coordinates for all seed regions used in these analyses can be found in Tables 3.1-5. For these analyses, group-averaged functional connectivity maps were used to inspect the validity

of clustering results and to visualize differences in connectivity patterns of regions in sensory and association cortices.

Each region consisted of single surface vertex (~4 mm x 4 mm) but should be considered spatially more extensive because of the spatial smoothing and intersubject averaging. Correlation maps were obtained by computing the Pearson's product moment correlation between the region's preprocessed resting fMRI time course and the time courses of all other vertices across the cortical mantle. To obtain a group-averaged correlation *z*-map, the correlation map of each subject in the group was converted to individual subject *z*-map using Fisher's *r*-to-*z* transformation and then averaged across all subjects in the group. The Fisher's *r*-to-*z* transformation increases normality of the distribution of correlations in the sample. For subjects with multiple runs, the individual subject *z*-maps were first averaged across the runs before submitting to the group average. An inverse Fisher's *r*-to-*z* transformation was then applied to the group-averaged correlation *z*-map yielding a group-averaged correlation map.

To quantify functional connectivity among regions, Fisher's *r*-to-*z* transformed correlations were computed among the regions for each subject within a group. For several targeted, *a priori* analyses, classical statistical tests, including t-tests (e.g., see Figs. 3.20 and 3.21) and ANOVA (e.g., see Figs. 3.22 and 3.27), were performed on the *z*-transformed correlations using Matlab 7.4 (Mathworks, Natick, USA) or SPSS 18.0 (IBM, Armonk, USA). All tests survive Bonferroni correction for multiple comparisons.

Selecting regions for functional connectivity analysis

Throughout the analyses, seed regions for functional connectivity were selected using different criteria depending on the purpose of the analysis. In all cases, if a particular dataset was used for selecting the region (e.g., Discovery sample), functional connectivity was always computed with a different dataset (e.g., Replication sample), thus providing an unbiased measurement of correlation strength. We detail the method used for region selection in the results as they are implemented for each particular analysis in the Results section. The following procedures describe the general strategies adopted.

First, when testing for seed-based confirmation of resolved networks, the estimated network boundaries and confidence maps of the Discovery sample were used to derive regional vertices to be tested in the Replication sample (e.g., see Fig. 3.16). Regions were chosen for (1) maximal spatial coverage of estimated networks, (2) avoiding network boundaries, and/or (3) their confidence in network assignments. We also defined new regions based on the correlation maps from the Discovery sample. For example, new regions might be chosen to be at or near the peaks of the correlation maps.

Second, for some analyses we utilized task-based fMRI to select regions. For example, visuotopic and functional characteristics revealed using fMRI can be used to estimate visual areas in the human (Hadjikhani et al. 1998; Sereno et al. 1995). The Caret software database provides estimated locations of multiple visual areas that were mapped into Caret PALS space using surface-based registration of an individual case in Hadjikhani et al (1998), although the foveal and peripheral extents of these areas are likely to be underestimated for technical reasons (Van Essen 2004). Landmark-based surface registration between FreeSurfer and Caret PALS allowed us to utilize these

fMRI-defined visuotopic regions for guiding our selection of regions in FreeSurfer surface space (e.g., V3A in Fig. 3.25). In addition, we also considered peak activation coordinates reported in fMRI literature (e.g., see Fig. 3.27). When the peak coordinates were reported in MNI space, we projected the coordinates to FreeSurfer surface space. The mapping between MNI152 volumetric space and FreeSurfer surface space is detailed in our companion study (Buckner et al. submitted). In cases where the peak activation coordinates were reported in the atlas space of Talairach and Tournoux (1988), the coordinates were first mapped to FSL MNI152 space (Lancaster et al. 2007) before being projected to FreeSurfer surface space.

Third, probabilistic histological maps in FreeSurfer surface space allowed for the selection of regions within histologically-defined areas (e.g., see Fig. 3.22). Postmortem human brains of fifteen subjects with no history of neurologic or psychiatric diseases were processed and analyzed (Amunts et al. 1999; Schleicher et al. 1999; Schormann and Zilles 1998). The histological sections were aligned to postmortem MR volume of the same brain using nonlinear warping (Schormann and Zilles 1998) to build an undistorted 3-dimensional histological volume. Cytoarchitectonic areas, including V1 (Amunts et al. 2000) and hOc5/MT+ (Malikovic et al. 2007) were segmented using observer-independent criteria (Schleicher et al. 1999). The MR volumes were segmented to separate white matter from other tissue classes, and the segmentation was used to generate topologically correct and geometrically accurate surface representations of the cerebral cortex using FreeSurfer (Fischl et al. 2008). The cortical surfaces of the fifteen subjects were registered to FreeSurfer surface space and the histological areas were

sampled onto the surface space. While there were fifteen subjects, each cytoarchitectonic area was only analyzed in at most ten subjects.

Prior work has demonstrated good across-subject alignment of lower order cortical areas in the surface coordinate system, with average misregistration errors as small as 2-3 mm for V1 (Fischl et al. 2008; Hinds et al. 2008; Yeo et al. 2010a), which is around the spatial resolution of the present fMRI data. For higher-order regions such as BA44, BA45 and hOc5/MT+, intersubject agreement is worse, with average misalignment errors in the order of 6-12 mm (Fischl et al. 2008; Yeo et al. 2010a; 2010b), but still an improvement from standard volumetric alignment (Amunts et al. 1999). In the case of histologically defined hOc5, considered to be putative MT+ (Malikovic et al. 2007), we were able to verify (not shown) that the probabilistic map of hOc5 in FreeSurfer surface space (Yeo et al. 2010b) was consistent with that of MT+ defined in Caret PALS space (Van Essen 2004) and peak MT+ coordinates reported in fMRI attention literature (Shulman et al. 1999). Certain anatomical landmarks were also useful in the selection of regional vertices. For example, the calcarine fissure was used as a guide to select regions in the lower and upper visual field representations as well as in the central and peripheral visual field representations within V1 (e.g., see Fig. 3.22).

Comparison of network boundaries with cytoarchitectonic areas

In addition to their utility for selecting regions, the probabilistic histological maps were useful in relating the estimated network boundaries to human cytoarchitectonic areas. Because the Statistical Parametric Mapping (SPM) Anatomy toolbox contained a more complete set of probabilistic histological maps of the same subjects in MNI Colin27

volumetric space (Eickhoff et al. 2005), we projected these probability maps to FreeSurfer surface space by establishing spatial correspondence between Colin27 and FreeSurfer surface space using the same procedure as that used for mapping between MNI152 volumetric space and FreeSurfer surface space (Buckner et al. 2011). Cytoarchitectonic areas common to both datasets were those of the primary motor cortex (areas 4a and 4p; Geyer et al. 1996), premotor cortex (area 6; Geyer 2004), primary somatosensory cortex (areas 3, 2 and 1; Geyer et al. 1999), early visual cortex (areas 17 and 18; Amunts et al. 2000), hOc5/MT+ (Malikovic et al. 2007) and BA44/45 (Amunts et al. 1999). Consistent with previous discussion about surface-based versus volume-based registration, we found Eickhoff's probabilistic maps in FreeSurfer space to be more diffuse than the maps obtained from the purely surface-based approach, implying poorer intersubject alignment. Consequently, for cytoarchitectonic areas common to both datasets, the surface-based probabilistic maps were used (Fischl et al. 2008; Yeo et al. 2010b) (e.g., see Fig. 3.22). We were also able to verify reasonable overlap (not shown) between the projected Eickhoff's maps and the purely surface-based probabilistic maps for areas common to both datasets, substantiating the validity of the mapping between the Colin27 space and FreeSurfer surface space.

Effect of resting condition on functional connectivity

For certain analyses, it was important to check that findings were not the result of overt eye movements that might shift edges and visual boundaries in and out of the central field. The core dataset (N = 1000) employed an eyes open rest condition because it is comparable to visual fixation in terms of signal strength (Van Dijk et al. 2010) but

can be acquired in studies that do not employ a setup for visual display. To examine the effects of the task employed during the resting-state, the effect of condition was analyzed for certain key analyses (e.g., for analyses that quantified the functional connectivity strengths among visual regions). As the results will show, the type of resting condition (EOR, ECR or FIX) is not a significant factor influencing our results (e.g., see Fig. 3.17).

Visuotopic fMRI data

The analyses of the visual cortex involved the visuotopic organization of the V1-V3 complex. The fMRI data were analyzed in the native subjects' volumetric space and the results sampled onto FreeSurfer surface space and averaged across subjects. The details of the analysis, which provided eccentricity estimates of the visual representation in the V1-V3 complex, are described elsewhere (Hinds et al. 2009). A 1mm smoothing kernel was applied to the averaged eccentricity estimate in FreeSurfer surface space. Because of the limited range of visual angle that could be stimulated in the MRI scanner, and because fixational eye movements that occur during visual stimulation prevent stable stimulation of the fovea, the eccentricity estimates did not cover the representation of the periphery or of the center of visual field within the V1-V3 complex (Hinds et al. 2009; Polimeni et al. 2005), but were sufficient for our analyses.

Distribution of parcellations and raw data

A primary result of this study is the parcellation of cortical networks and the estimation of boundaries of regions within the networks. The parcellations of parietal and prefrontal cortices, in particular, represent demarcations of complex topographical

regions that have been perplexing to understand in relation to task-based functional neuroimaging studies. We have uploaded the parcellations in Caret PALS surface space into the Surface Management System Database (SumsDB) for open use (Dickson et al. 2001) (sumsdb.wustl.edu:8081/sums/directory.do?id=8286317). The parcellations in FreeSurfer surface space are also available (http://www.freesurfer.net/fswiki/CorticalParcellation_Yeo2011). Movies of the region-based functional connectivity estimates can be downloaded from http://www.youtube.com/yeokrienen. The raw fMRI data from the 1000 subjects will be made openly available to researchers using the procedures established by the OASIS data releases (Marcus et al. 2007; 2010) and the 1000 Functional Connectomes Project (Biswal et al. 2010).

Results

Estimates of cerebral networks are reliable

The cerebral cortex was parcellated into multiple networks using clustering. The parcellations resulted in networks that involved primarily adjacent areas (e.g., visual cortex) and networks that involved areas widely distributed throughout the cortex (e.g., heteromodal association cortex). Figure 3.7 shows the 7-network estimates for the Discovery and Replication samples. A total of 97.4% of the vertices were assigned to the same networks across both datasets. Varying the particular choice of binarization threshold (ranging from 5% to 15%) and smoothing (ranging from no smoothing to 6mm FWHM) minimally affected the results (not shown). Figure 3.8 shows the confidence

(silhouette) value for each vertex with respect to its assigned network for the 7-network estimate. Regions close to the boundaries between networks were less confident in their assignment. Spatial variation within individual components of the estimated networks was also observed beyond the boundary regions. Often these low-confidence regions anticipated further fractionation of the networks into smaller subnetworks that emerged when larger numbers of networks were allowed (e.g., compare the lateral prefrontal extent of the orange network in Fig. 3.7 with its confidence map in Fig. 3.8, and then note subsequent fractionation of this region in Fig. 3.9). Figure 3.9 shows the 17-network estimates for the Discovery and Replication data samples, and Figure 3.10 shows the confidence map for the Discovery dataset. For the 17-network estimate, 97.0% of the vertices were assigned to the same networks across both datasets.

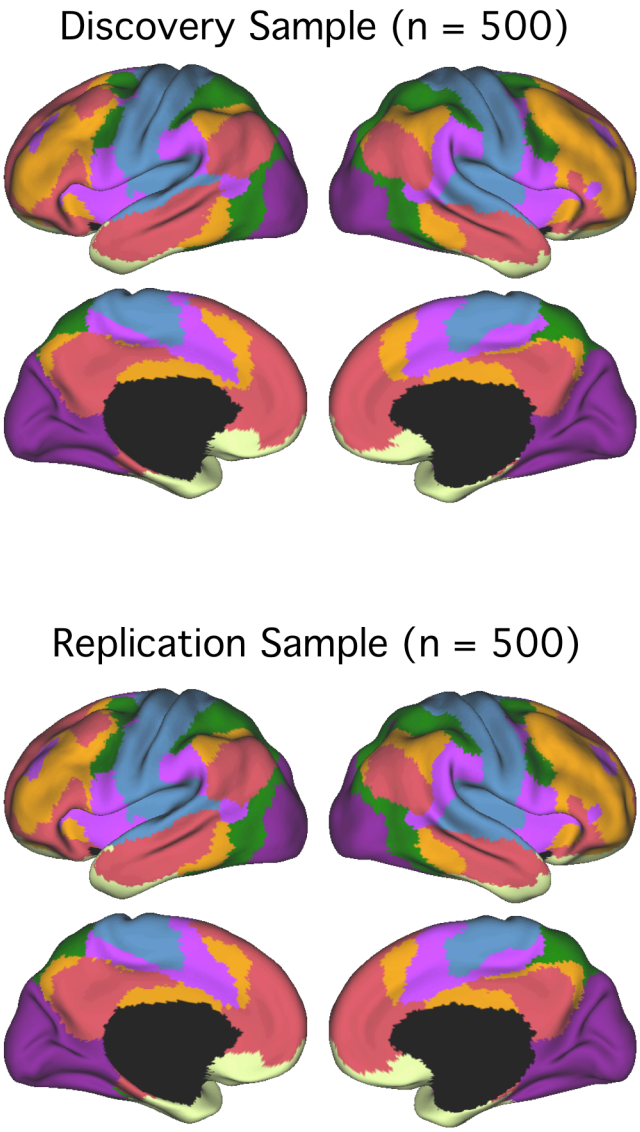

Figure 3.7 Discovery and Replication of a 7-network cortical parcellation. The 7-network estimates are highly consistent across the Discovery (n = 500) and Replication (n = 500) datasets. 97.4% of the vertices were assigned to the same network.

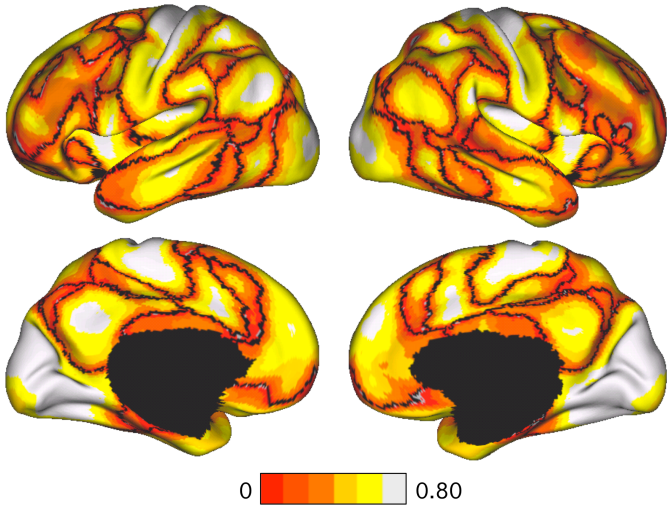

Figure 3.8 Confidence of 7-network estimate in Discovery dataset. Confidence (silhouette) value for each vertex with respect to its assigned network is shown for the Discovery dataset. Regions close to the boundaries between networks were less confident of their assignment, although we also observed structured spatial variation within individual components of the estimated networks, such as lateral prefrontal cortex, which foreshadows its division in the 17-network estimate (Fig. 3.10).

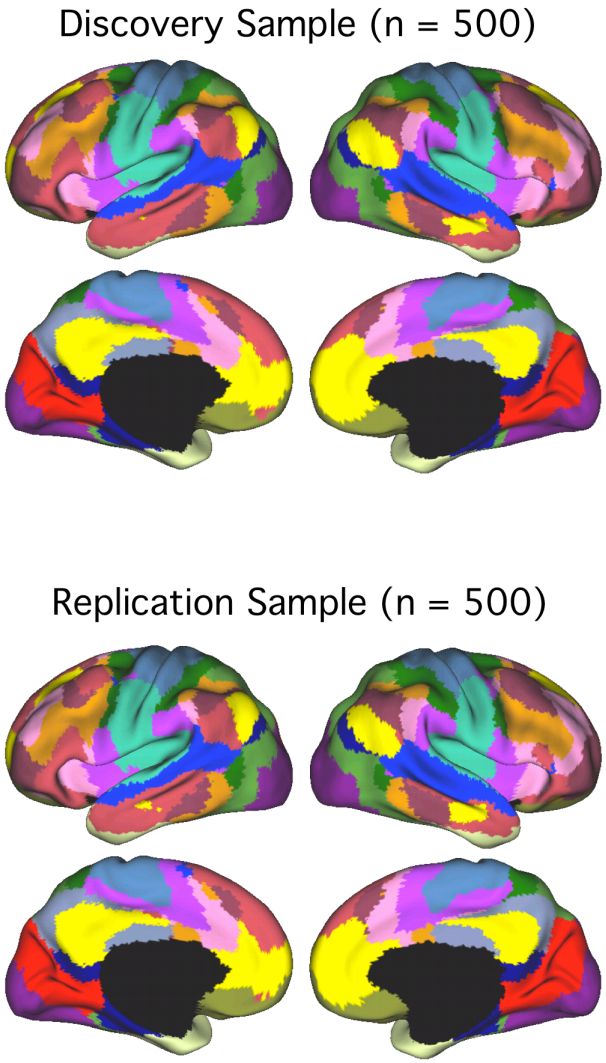

Figure 3.9. Discovery and Replication of a 17-network cortical parcellation. The 17-network estimates are highly consistent across the Discovery (n = 500) and Replication (n = 500) datasets. A total of 97.0% of the vertices were assigned to the same network.

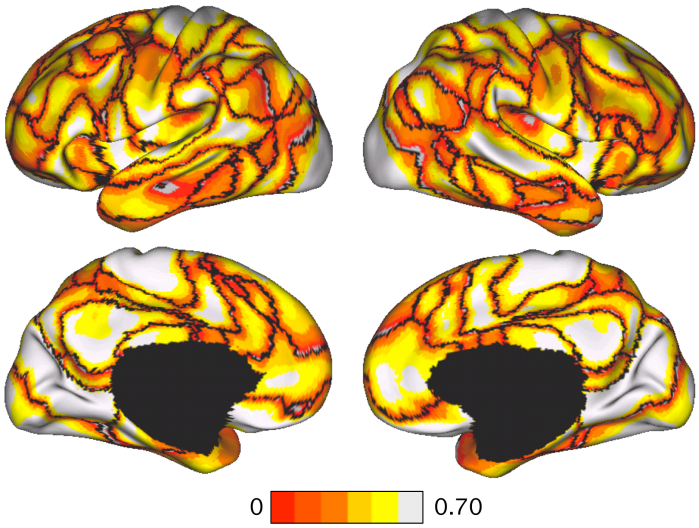

.

Figure 3.10. Confidence of 17-network estimate in Discovery dataset. Confidence (silhouette) value for each vertex with respect to its assigned network is shown for the Discovery dataset. Again, regions close to the boundaries between networks were less confident of their assignment, while structured spatial variation were observed within individual components of the estimated networks.

Estimates of cerebral networks from 1000 subjects

To provide the best estimates of the cerebral cortical networks, clustering was performed on the full sample of 1000 subjects. Figures 3.11 and 3.13 show the 7- and 17-network parcellation estimates. Several results are notable. A salient feature of the estimated networks is the separation of the early sensory and late motor cortices (blue and purple) from association cortex, consistent with the observation that early sensory and late motor regions exhibit local anatomical connectivity in primates (Felleman and Van Essen 1991; Jones et al. 1978; Markov et al. 2010) and preferential local functional coupling in humans (Sepulcre et al. 2010). Sensory and motor cortices, whose functional

connectivity networks were preferentially local, comprised only 35% of the cerebral mantle and were the exception in terms of network structure.

The majority of the human cerebral cortex is comprised of multiple, distinct networks of association areas. The association networks in the 7-network estimate converged and extended upon networks previously described in the resting-state literature, including those referred to as the dorsal and ventral attention (green and violet respectively; Fox et al. 2006), the frontoparietal control (orange; Dosenbach et al. 2007; Vincent et al. 2008) and the default (red; Buckner et al. 2008; Greicius et al. 2003) networks (Fig. 3.12). We also note that the 7-network parcellation of the parietal cortex is similar to those proposed using seed-based approaches (Vincent et al. 2008) and using the areal boundary detection method (Cohen et al. 2008; Nelson et al. 2010). The convergence of multiple different analysis approaches suggests that the parcellation is intrinsic to the resting-state data rather than an artifact of the algorithm used.

Generally, the 17-network estimate fractionated the 7-network estimate into smaller subnetworks. Some aspects of the fractionation, such as the emergence of a parahippocampal-retrosplenial-lateral parietal network, are anticipated by other studies using hierarchical-clustering techniques (e.g., Andrews-Hanna et al. 2010). Other aspects of the fractionation were unexpected, such as the emergence of subnetworks within the visual and motor cortices that did not respect areal boundaries but rather appear to align with topographic organization. In the following sections, we quantify and further explore the patterns of functional connectivity that give rise to these networks.

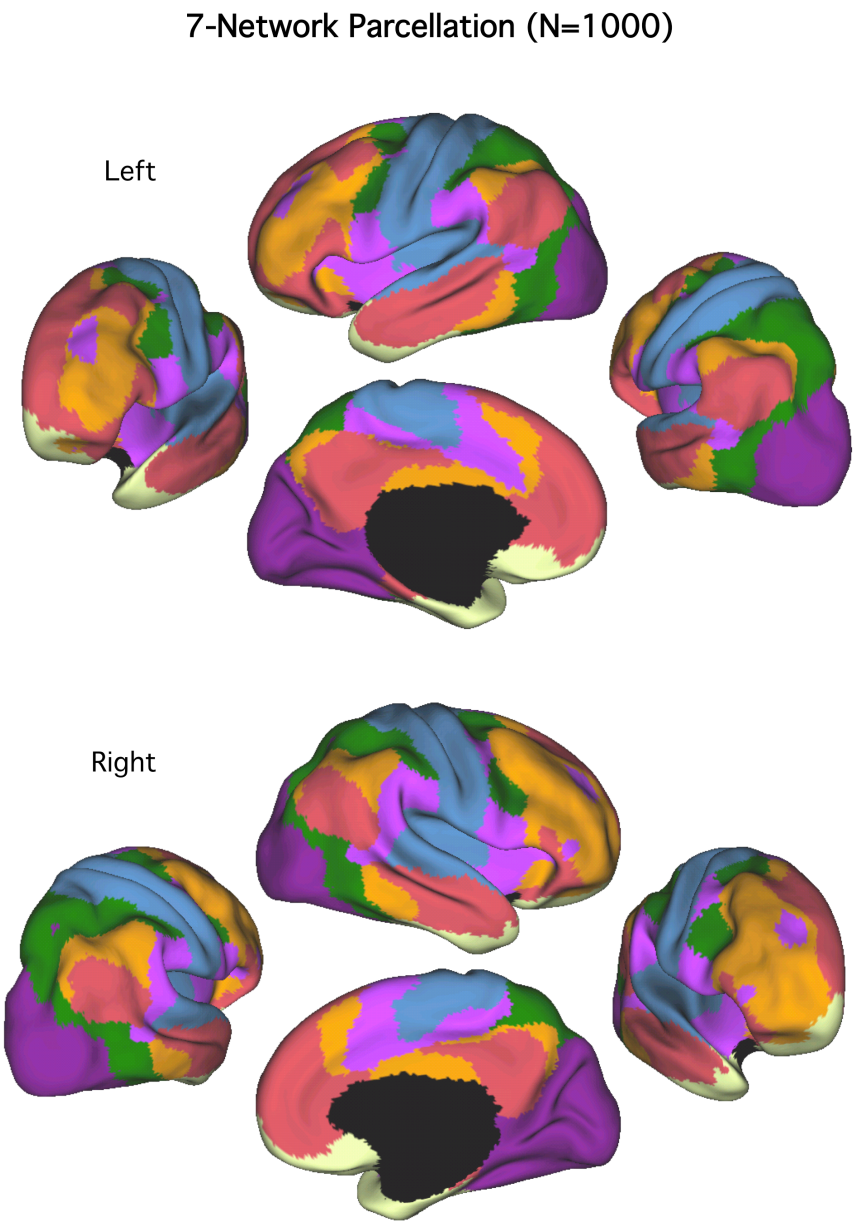

Figure 3.11. A coarse (7-network) parcellation of the human cerebral cortex based on 1000 subjects. To provide the best estimates of the 7 cortical networks, clustering was performed on the fMRI data of the full 1000 subjects. A salient feature is the separation of the early sensory and late motor cortices (blue and purple) from the association cortex. The association networks converged and extended upon networks previously described in the resting-state literature, including the dorsal attention, ventral attention, frontoparietal control and the default networks.

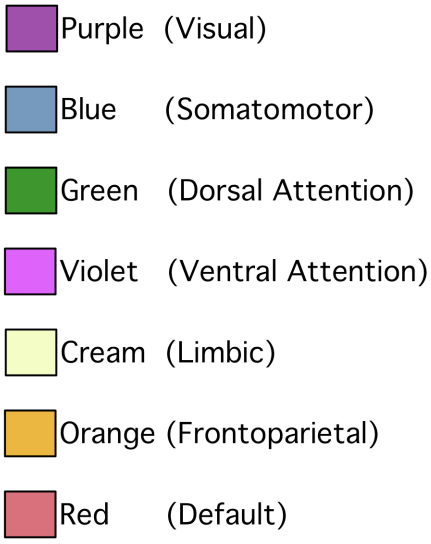

Figure 3.12. Table of colors assigned to networks in the 7-network estimate. Common names associated with each network in the neuroimaging literature are included in the brackets. This should not be taken to mean that our estimated networks correspond exactly to those in the literature or that the networks code solely for functions associated with their assigned name. For example, components of the green network are implicated in spatial attentional tasks (Corbetta and Shulman 2002) and so we refer to the green network as the dorsal attention system. However, from the macaque literature, components of the green network have also been described in relation to the hierarchical processing of sensory information (e.g., Felleman and Van Essen 1991) and recruited in tasks involving sensory-guided decisions (e.g., Andersen and Buneo 2002). As other examples of limitations of heuristic reference labels, the violet ventral attention network is likely an aggregate of (or closely adjacent to) multiple networks in the literature variably referred to as the salience (Seeley et al. 2007) and cingulo-opercular networks (Dosenbach et al. 2007), and the red default network can be fractionated (e.g., Andrews-Hanna et al. 2010). Many of these details are reflected in Figure 3.13.

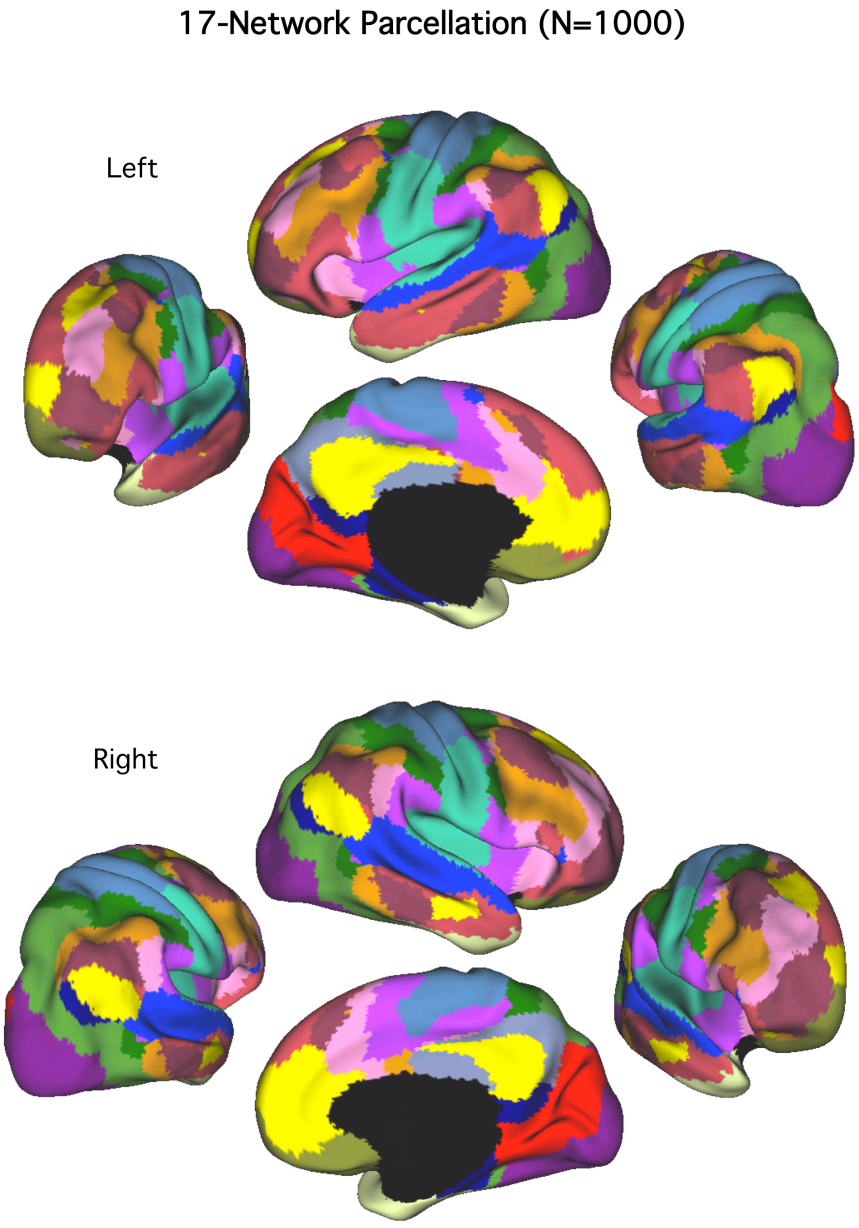

Figure 3.13. A fine-resolution (17-network) parcellation of the human cerebral cortex based on 1000 subjects. To provide the best estimates of the 17 cortical networks, clustering was performed on the fMRI data of the full 1000 subjects. The 17-network estimate fractionated the 7-network into smaller networks. Some aspects of the fractionations have been previously noted in other studies.

A cautionary note about potential artifacts

Before exploring the estimated networks in more detail, it is important to point out aspects of the data that are difficult to interpret because of potential fMRI signal blurring across gyri and signal loss associated with susceptibility (Ojemann et al. 1997). Figure 3.14A illustrates one example. Somatomotor, auditory and posterior insular cortices are correlated within a single network (also see Fig. 3.11). The ventral portion of somatomotor cortex is clustered with the auditory cortex in the 17-network parcellation (Fig. 3.13). While non-human primate tracing studies suggest auditory and somatomotor cortices are connected via multiple areas within the insular cortex (Disbrow et al. 2003; Mesulam and Mufson 1982), an equally likely explanation for the observed correlation is blurring of the BOLD signal across the Sylvian fissure (Fig. 3.14A). We could not find a way, in these data, to resolve whether the coupling was an artifact of limited resolution or a true, coupled network.

Figure 3.14B illustrates a second example of how fMRI signal blurring might affect the interpretation of the results. In this case, the primary somatosensory cortex (S1) and primary motor cortex (M1) are clustered within the same network (Fig. 3.11). While there is anatomical evidence of direct connectivity between S1 and M1 in the macaque (Jones et al. 1978; Pons and Kaas 1986), we are unable to resolve whether the coupling was an artifact of limited resolution due to the close proximity of M1 and S1 in volumetric space.

As an example of uncertainty occurring near regions of MR susceptibility, Figure 3.14C illustrates a cream-colored network of regions in the temporal pole and orbital frontal cortex (also see Fig. 3.11). While there is anatomical evidence from the primate

tracing literature supporting the existence of this network (Carmichael and Price 1995; Kondo et al. 2003; Moran et al. 1987), the spatial distortion and signal loss caused by MR susceptibility creates uncertainty in the location of the network boundaries.

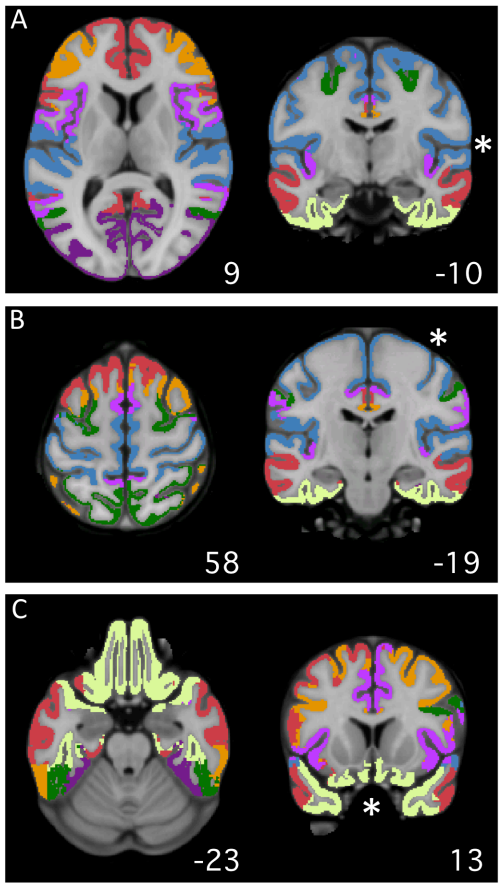

Figure 3.14. Uncertain observations due to limited data resolution and MR susceptibility. When interpreting the clustering results, potential artifacts and uncertainties must be considered. Because of the close proximity of the somatomotor and auditory cortices (A) and the close proximity of the pre- and post-central gyri (B), we are unable to resolve whether the clustering of the somatomotor and auditory cortices (A) and the clustering of the primary somatosensory and primary motor cortices (B) are due to the result of fMRI blurring across sulci or a true, coupled network of distributed areas as predicted by macaque tracing studies. (C) The orbital frontal-temporopolar network (cream color) consists of temporopolar and orbital frontal regions that are affected by MR susceptibility. Since MR susceptibility spatially distorts the MR signal and reduces SNR, there is uncertainty in the exact boundary of the orbital frontal-temporopolar network and the true extent of the network is probably underestimated.

Sensory and motor cortices exhibit topographically-specific functional connectivity

The sensory and motor cortices were clustered separately from the association cortex in the 7-network estimate (Fig. 3.11). This result by itself suggests that sensory and motor cortices distinguish themselves from distributed networks of association areas. Within the sensory and motor networks, there were a number of further observations. Of most interest, the 17-network parcellation fractionated the sensory and motor cortices into subnetworks (Fig. 3.13). Specifically, early visual regions formed two distinct subnetworks that did not respect areal boundaries. Somatomotor cortex was similarly fractionated along its lateral extent. Our hypothesis is that these fractionations reflect topographic organization – topographic representation of visual space in the visual regions and topographic representation of body space in the somatomotor regions.

Visual topography. The visual network in the 7-network estimate (Fig. 3.11) was fractionated into two separate subnetworks (purple and bright red) in the 17-network estimate (Fig. 3.13). The boundary between the two visual subnetworks cut perpendicularly across the calcarine fissure, suggesting the division of the early visual areas into central and peripheral components. To evaluate this possibility, Figure 3.15 overlays the eccentricity estimates of the Visuotopic dataset over the boundaries of the two separate visual subnetworks. The early visual areas were divided into two subnetworks along an isoeccentricity line of approximately 4^{o}. We refer to these two subnetworks as "central" and "peripheral", although an immediate question arises as to whether the division of lower visual areas into central and peripheral components extends to higher visual areas. The particular traveling wave paradigm used in the Visuotopic dataset was designed to estimate visual eccentricity within the V1-V3 complex and is

therefore unreliable outside the complex. To gain further clarification on visual areas outside the V1-V3 complex, we inspected the boundaries of the 17-network parcellation overlaid on the map of approximate human visual areas provided by Van Essen (2004). The boundary between the central and peripheral representations continues through the extrastriate visual areas consistent with the possibility that the division of lower visual areas into central and peripheral components generally applies to the extrastriate cortex with certain caveats that will be taken up in the Discussion.

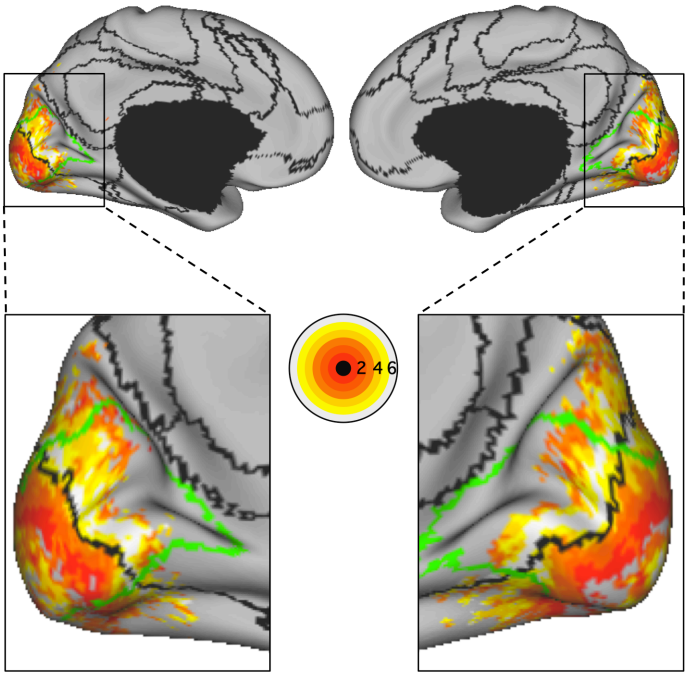

Figure 3.15. Eccentricity estimates quantify the division of the early visual cortex into central and peripheral systems. Eccentricity estimates in the early visual areas of 4 subjects were averaged and overlaid on the boundaries (in black) of the 17-network estimate. The boundary between areas 18 and 19 estimated from the Histological dataset is overlaid in green. The 17-network estimate divides the early visual areas along an isoeccentricity line of approximately 4^{o}. Note that the eccentricity estimates are not reliable outside the V1-V3 complex.

To assess the validity of the clustering analysis of visual cortex, six seed regions were selected from the Discovery sample (Table 3.1), and their fcMRI maps were computed using the Replication sample. The regions were selected to include V1 and V3 regions that fell within the central and peripheral representations. Using the calcarine fissure, histological V1 estimates (Amunts et al. 2000; Fischl et al. 2008) and the network boundaries as landmarks, two regions labeled $V1_c$ and $V1_p$ were selected to correspond to central and peripheral V1 respectively. Using the probabilistic histological maps of the SPM Anatomy toolbox (Eickhoff et al. 2005), two regions labeled $V3_{cv}$ and $V3_{pv}$ were selected at or near visual area V3v (Rottschy et al. 2007; Wilms et al. 2010) corresponding to the central and peripheral representations respectively. The two remaining regions were selected from the extrastriate regions of the central and peripheral visual subnetworks. In all cases, the confidence (silhouette) map of the 17-network estimate from the Discovery sample (Fig. 3.10) was used as a guide.

The fcMRI maps of the six seed regions confirm the network demarcations (Fig. 3.16). Compared with the other seed regions of the central visual system, $V1_c$ demonstrated weaker correlation to the extrastriate regions of the central visual system. This is reflected by the lower confidence of $V1_c$ in its network assignment as shown in Table 3.1. Consistent with this observation, as the number of networks in the clustering analysis was increased (not shown), the central V1 region separated from the extrastriate component of the central visual system.

Table 3.1: Locations of Visual Cortex Seed Regions. Notes: $V1_c$ and $V1_p$ seed regions are selected from the central and peripheral regions of V1. $V3_{cv}$ and $V3_{pv}$ seed regions are selected from the central and peripheral regions at or near V3v. ExC and ExP are selected from the purple-colored "central" and bright red-colored "peripheral" visual systems respectively. The confidence of the seeds in their network assignment is computed from the Replication dataset. Coordinates reflect the approximate center location based on the atlas space of the Montreal Neurological Institute (MNI).

Seed Region	Coordinates	Confidence
$V3_{pv}$ (Rottschy et al. 2007; Wilms et al. 2010)	-12, -67, -3	0.74
ExP	-3, -74, 23	0.81
$V1_p$ (Amunts et al. 2000; Fischl et al. 2008)	-16, -74, 7	0.78
$V3_{cv}$ (Rottschy et al. 2007; Wilms et al. 2010)	-23, -91, -15	0.67
ExC	-32, -89, -1	0.75
$V1_c$ (Amunts et al. 2000; Fischl et al. 2008)	-13, -100, -8	0.48

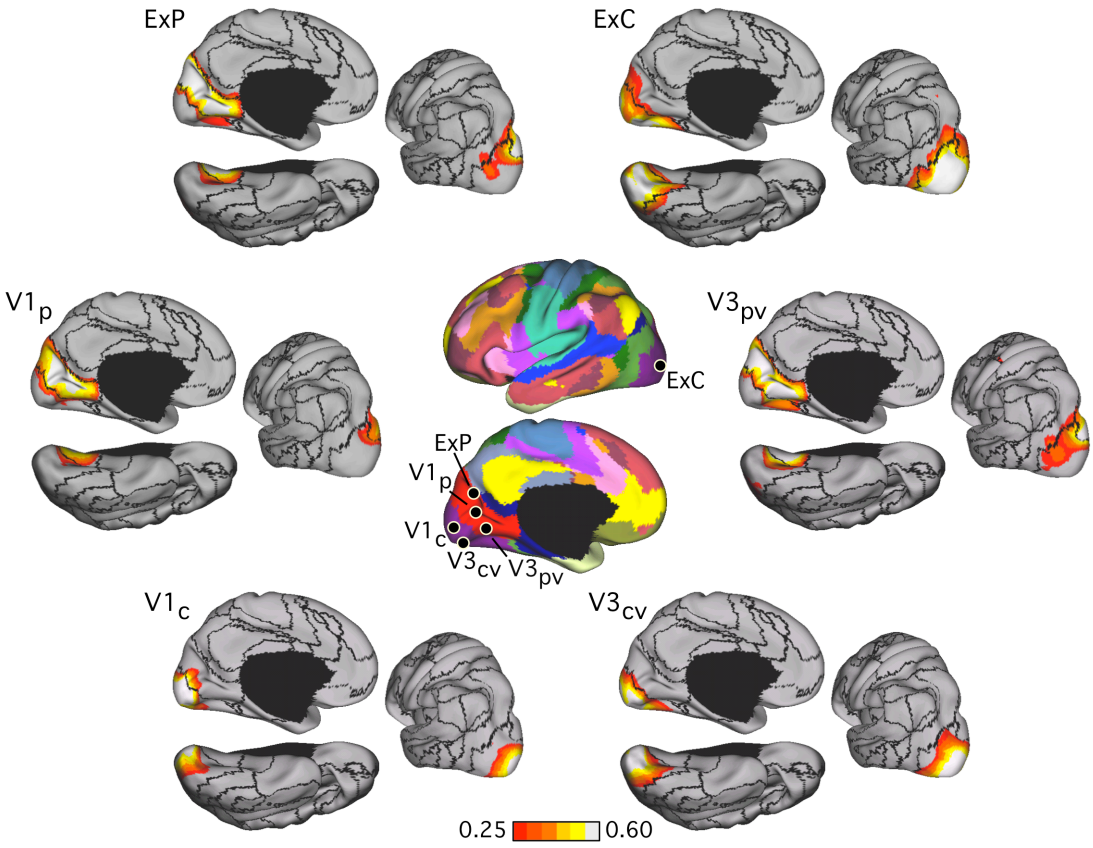

Figure 3.16. Evidence that the fractionation of the visual system reflects fcMRI topography within the v isual cortex. Six left hemisphere seed regions were picked from the Discovery dataset: $V1_c$ and $V1_p$ correspond to central and peripheral visual field representation within V1 respectively; $V3_{cv}$ and $V3_{pv}$ correspond to central and peripheral V3v respectively; ExC and ExP correspond to two seed regions within the extrastriate visual cortex in the estimated locations of the central and peripheral visual fields (purple and bright red in center panel). The six seed regions are illustrated in the center panel and their coordinate locations are reported in Table 3.1. Their left hemisphere fcMRI maps were computed using the Replication dataset and arranged around the center panel. Note that the central visual seed regions are selectively correlated with the central visual representation, while the peripheral visual seed regions are selectively correlated with the peripheral visual representation.

To quantify the dissociation between the central and peripheral representations within the visual subnetworks, Figure 3.17A shows polar plots of the correlation of $V1_p$ and $V1_c$ with five regions in the Replication sample. Since the Discovery and Replication samples consist of resting data collected under the eyes open rest condition, the patterns of functional connectivity were also quantified for the Task Effect dataset (Fig. 3.17B). The results revealed that the central and peripheral V1 seed regions displayed distinct patterns of functional connectivity that generalized across multiple data acquisition conditions including eyes closed rest and visual fixation.

.

Although there are differences in visual field properties, such as magnification factors and receptive field sizes, between the central and peripheral regions of the V1-V3 complex, these differences vary smoothly from central to peripheral vision within an area (Balasubramanian et al. 2002; Dow et al. 1981; Rovamo and Virsu 1979). To explore this further, functional connectivity was examined among seed regions spanning the eccentricity axes of V1 and V3v (Fig. 3.18). Results did not suggest a sharp transition in

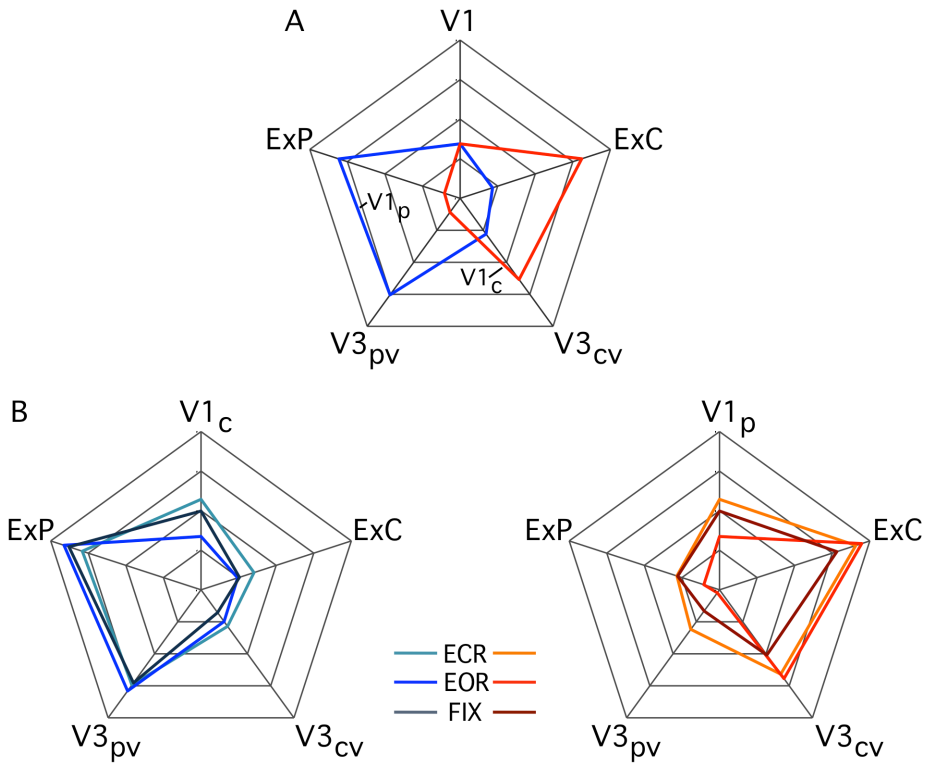

Figure 3.17. Quantification of fcMRI topography within the visual cortex and independence of the topography from task condition. (A) Quantification measures of functional connectivity strength are plotted in polar form for $V1_c$ (central V1) and $V1_p$ (peripheral V1) seed regions for the Replication dataset. Note that V1 refers to $V1_c$ for the $V1_p$ polar plot (blue) and $V1_p$ for the $V1_c$ polar plot (red). Coordinate locations for all six seed regions ($V1_c$, $V1_p$, $V3_{cv}$, $V3_{pv}$, ExC, ExP) are reported in Table 3.1. (B) Polar plots of (A) replicated with the Task Effects dataset (EOR = eyes open rest; ECR = eyes closed rest; FIX = fixation) to ensure that the results obtained using the EOR Replication dataset were not due to overt eye movements that might shift edges and visual boundaries in and out of the central field. Left figure shows $V1_p$ polar plot. Right figure shows $V1_c$ polar plot. The polar plots quantify the differential functional coupling of central and peripheral V1 with higher visual areas. The polar scales range from r = -0.1 (center) to r = 0.7 (outer boundary) in 0.2-step increments

functional connectivity between V1 and V3v seed regions moving from central to peripheral representations. The resulting division of the V1-V3 complex along the isoeccentricity line of 4° was therefore likely driven by the functional connectivity of visual regions outside the V1-V3 complex or may be an artifact of the small number of networks being mandated by the analyses.

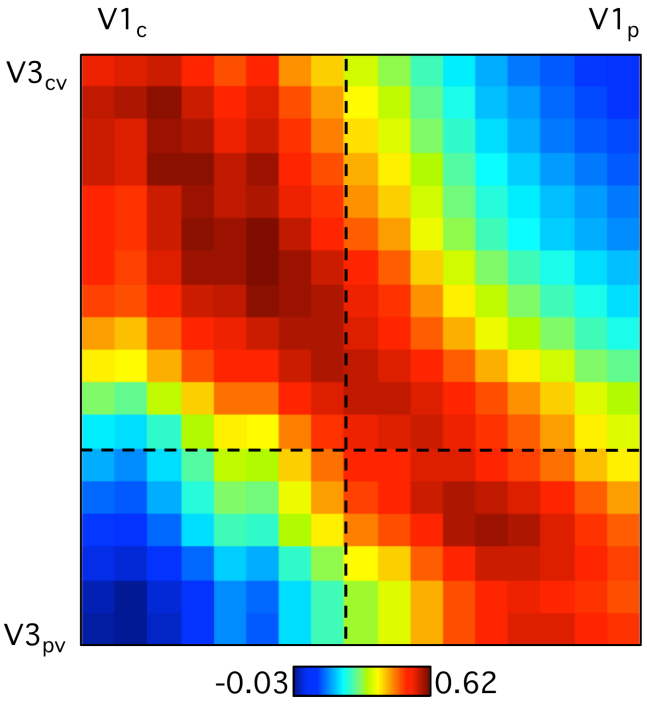

Figure 3.18. V1 and V3 functional correlations display a smooth transition from the central to peripheral representations. Correlation of two series of seed regions spanning the eccentricity axes of V1 and V3v is shown for the full 1000 subjects. V1 seed regions of low eccentricity are strongly correlated with V3 seed regions of low eccentricity. V1 seed regions of high eccentricity are strongly correlated with V3 seed regions of high eccentricity. There is a gradual transition in functional connectivity strength between the central to peripheral representations.

Somatomotor topography. The 7-network parcellation estimate clustered the somatomotor cortex into a single network (the blue network in Fig. 3.11). Figure 3.19 shows the boundaries of the 7-network estimate overlaid on the probabilistic histological maps of areas 6 (Geyer 2004), 2 (Grefkes et al. 2001) and 5L (Scheperjans et al. 2008a; 2008b). The histological estimates of areas 1, 3 and 4 (Geyer et al. 1996; 1999) are sandwiched between areas 2 and 6 and are not shown. Recent work (Amunts et al. 2010) has delineated three additional premotor areas anterior to the ventral half of area 6 shown in Figure 3.19; the ventral half of area 6 in Figure 3.19 is therefore an underestimation.

Based on these areal references, the somatomotor network likely includes MI (area 4) and caudal premotor area 6, SI (areas 3, 1 and 2) and most, if not all of early somatosensory area 5L. The somatomotor network also includes a small portion of the mid-cingulate sulcus and possibly area 5M (not shown; Scheperjans et al. 2008a; 2008b).

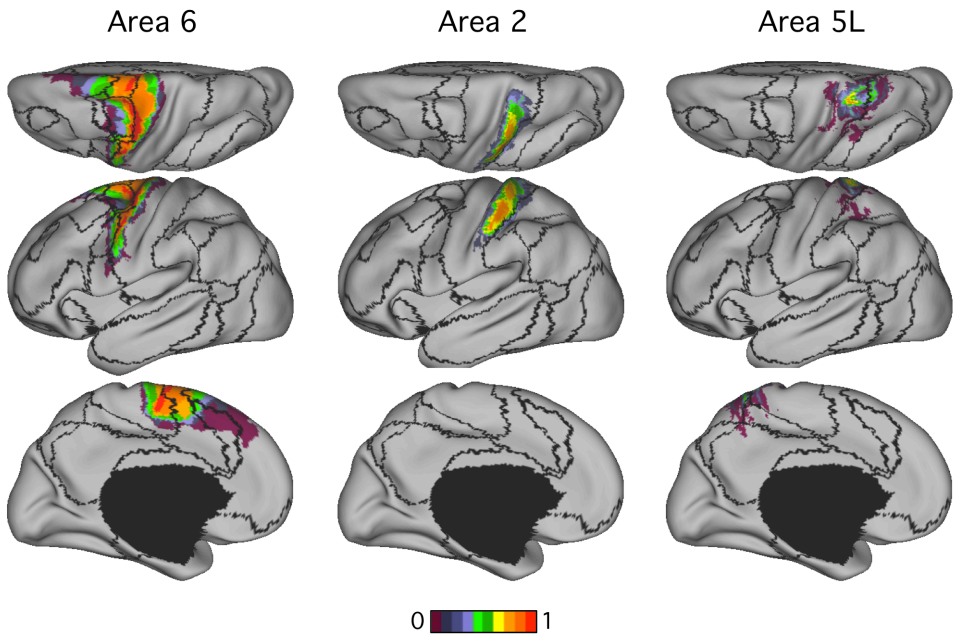

Figure 3.19. 7-network boundaries on probabilistic maps of areas 6, 2 and 5L. Boundaries of 7-network estimate based on the full 1000 subjects are overlaid on the surface-based probabilistic histological maps of areas 6, 2 and 5L. The somatomotor network includes most, if not all of areas 2 and 5L, but only caudal half of area 6.

The 17-network parcellation divided the somatomotor strip into dorsal and ventral subnetworks across the axis that represents body space (Fig. 3.13). To investigate this division, the parcellations were compared to activation maps of 24 subjects who were instructed to move their tongue, hand or foot in response to a visual cue (for a detailed explanation of this dataset, see Buckner et al. 2011). As shown in Figure 3.20A, the boundary between the dorsal and ventral somatomotor subnetworks was roughly

positioned between the hand and tongue representations. To quantify this observation, seed regions were selected from the left hemisphere hand, foot and tongue activation maps and verified to fall within the probabilistic histological map of area 4 (Fischl et al. 2008; Geyer et al. 1996). Figure 3.20B shows pairwise correlations computed among the hand, foot and tongue regions averaged over 1000 subjects (Hand coordinates: -41, -20, 62; Foot coordinates: -6, -26, 76; Tongue coordinates: -55, -4, 26). The hand-foot correlation was significantly higher than the hand-tongue correlation ($p < .001$) and foot-tongue correlation ($p < .001$). Thus, like the visual system, functional coupling forms networks within the somatomotor system that reflect topographic organization.

There were two further results that must be interpreted cautiously because of volumetric signal blurring. The 7- and 17-network parcellations of somatomotor cortex included both the precentral and postcentral representations of body space thus forming networks that spanned areas (M1 and S1). This observation is difficult to interpret because precentral and postcentral gyri abut each other in volumetric space (see Fig. 3.14B). Similarly, the ventral somatomotor network in the 17-network parcellation included parts of the insula and auditory cortex, perhaps reflecting a polysynaptic circuit of functional coupling linked to speech movements and hearing one's own voice. We do not interpret this observation because of their volumetric proximity (see Fig. 3.14A).

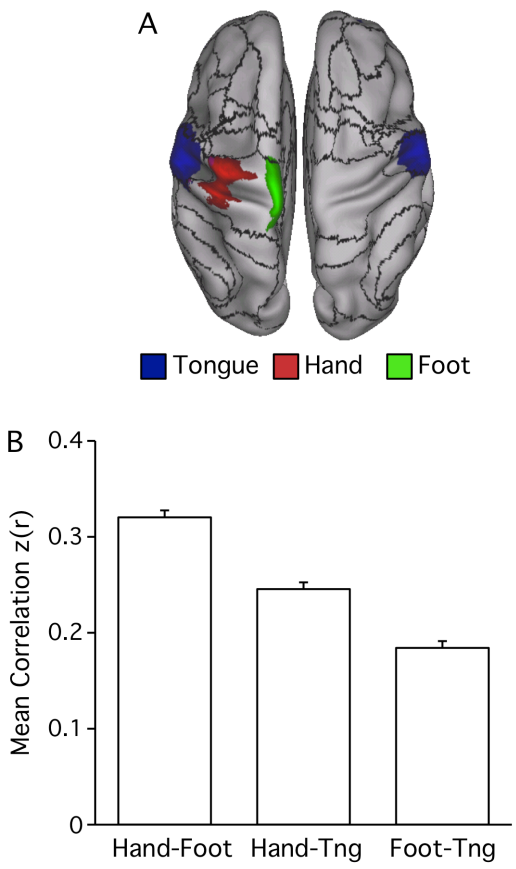

Figure 3.20. Evidence that the fractionation of the somatomotor cortex reflects fcMRI topography within the somatosensory and motor cortex. (A) Average fMRI activation maps of 24 subjects instructed to move their tongue (blue), right hand (red) or right foot (green) across separate conditions. Black lines correspond to boundaries of the 17-network estimate. The dorsoventral split of the somatomotor network occurs spatially between the tongue and hand activations. (B) Quantification of correlation strength between the left hemisphere tongue, hand and foot seed regions selected from the activation maps. Hand coordinates = -41, -20, 62; Foot coordinates = -6, -26, 76; Tongue coordinates: -55, -4, 26. Hand-foot correlation is significantly higher than hand-tongue correlation, which is in turn significantly higher than foot-tongue correlation.

Asymmetry of functional coupling varies across somatomotor topography

Analysis of asymmetries in functional coupling is beyond the scope of this paper. However, we observed an interesting variation in the asymmetry of functional coupling that reinforces the observation of functional differences along the somatomotor body representation. Specifically, pairwise correlations between homotopic pairs of hand, foot and tongue representations (Hand coordinates: ±41, -20, 62; Foot coordinates: ±6, -26, 76; Tongue coordinates: ±55, -4, 26) were measured between the hemispheres (Fig. 3.21A). The homotopic hand correlation was significantly weaker than that of the homotopic foot ($p < .001$) and tongue ($p < .001$) correlations. We are unable to rule out

the possibility that the higher correlation between homotopic tongue regions is an artifact of subjects moving their tongues during scanning.

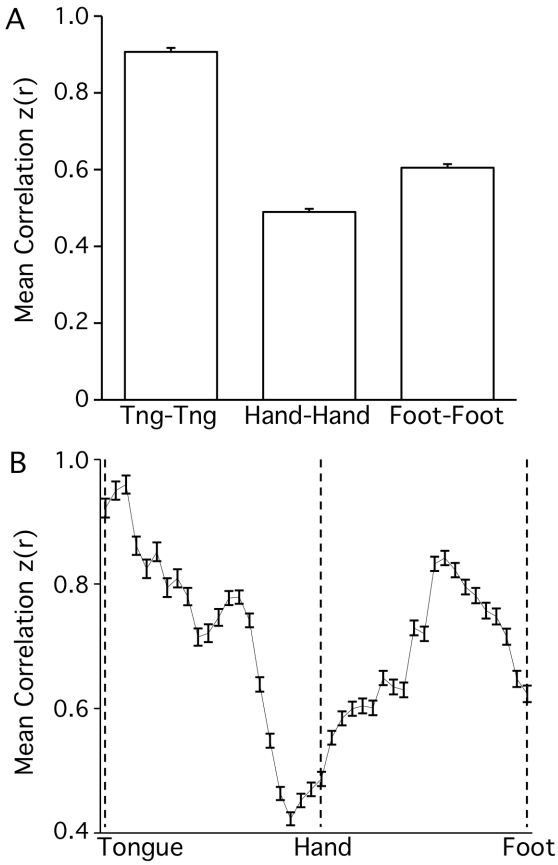

Figure 3.21. Evidence that the interhemispheric fcMRI of homotopic regions within the primary motor cortex is topographically organized. (A) Correlation strength of left hemisphere tongue, hand and foot seed regions with corresponding contralateral seed regions averaged over all 1000 subjects. Right hemisphere vertices were obtained by reflection across the midline. Hand coordinates = ±41, -20, 62; Foot coordinates = ±6, -26, 76; Tongue coordinates = ±55, -4, 26. The tongue representation has the strongest interhemispheric correlation, followed by the foot and then the hand. (B) Plot of interhemispheric correlation along the ventral (tongue) to dorsal (foot) extent of motor cortex. Maximal interhemispheric correlation is highest near the tongue representation and also peaks between the hand and foot representations, possibly corresponding to the trunk representation.

To explore the somatotopy of interhemispheric fcMRI beyond the hand, foot and tongue representations, we estimated the sequence of vertices lying in the shortest path connecting the left tongue region with the left hand region and those lying in the shortest path connecting the left hand region with the left foot region. For each left hemisphere motor vertex, we found the corresponding right hemisphere vertex that was maximally correlated with it in the Discovery sample. Figure 3.21B plots the correlation between the left hemisphere vertices, arranged ventral to dorsal, and the corresponding right

hemisphere vertices in the Replication data sample. Defining the maximally correlated right hemisphere vertices in the Discovery sample avoided bias in the correlation values and the issue of picking truly homotopic representations in either hemisphere. Consistent with Figure 3.21A, the maximal tongue correlation was higher than that of the foot, which was in turn higher than that of the hand. The region in between the hand and foot representations, possibly corresponding to the trunk representation, also displayed higher maximal interhemispheric correlation than those of the hand or foot representations.

The observed somatotopy of interhemispheric fcMRI is consistent with non-human primate studies that have shown that the representations of midline structures in S1 and M1, such as the face and trunk, have denser callosal connections than those of distal limbs, such as the hand and foot (Gould et al. 1986; Jones and Wise 1977; Killackey et al. 1983, Pandya and Vignolo 1971).

Hierarchical processing within a canonical sensory-motor pathway

Parcellation of the cerebral cortex into distinct networks will not capture information about interactions between regions that fall across separate networks. This is particularly problematic because the canonical system-level description of cortical processing involves interactions across hierarchical pathways of sensory and motor areas. The above analyses leave open the question of how the distinct networks interact as is expected for sensory-motor pathways.

To explore this question, we selected the canonical sensory-motor pathway that extends from primary visual cortex to the precentral motor regions (including the putative homologue of FEF) via the motion-sensitive MT+ complex and posterior parietal cortex

at or near putative human LIP. In the macaque literature, this pathway has been extensively studied in relation to sensory-guided decisions resulting in eye movements and associated processes linked to spatial attention (e.g., Andersen and Buneo 2002; Colby and Goldberg 1999; Gold and Shadlen 2007; Shadlen and Newsome 2001). In the human literature, this pathway has been studied both in relation to spatially-directed movements and also in relation to spatial attention, with components of the pathway sometimes referred to as the dorsal attention system or network (Corbetta and Shulman 2002). Most critically, the anatomic relations between the areas within the pathway have been extensively explored beginning with the seminal work of Maunsell and Van Essen (1983).

Early visual cortex. Analysis focused initially on the bottom of the sensory-motor pathway by investigating functional connectivity between V1 and putative human MT+[3]. For this analysis, two V1 regions were selected in dorsal ($V1_{cd}$) and ventral ($V1_{cv}$) central V1 corresponding to the lower and upper visual field representations. Two additional V1 regions were selected in dorsal ($V1_{pd}$) and ventral ($V1_{pv}$) peripheral V1 corresponding to the lower and upper visual field representations. Two MT+ seed regions ($MT+_d$, $MT+_v$) were selected following the dorsoventral extent of the surface-based probabilistic histological map of MT+ (Malikovic et al. 2007; Yeo et al. 2010b). The $MT+_d$ and $MT+_v$ seed regions likely correspond to peripheral and central visual field representations respectively (Huk et al. 2002; Maunsell and Van Essen 1987) and were analyzed to

[3] In humans, the MT+ complex is used to denote the putative human homologue of macaque area MT and neighboring visual areas that are sensitive to motion stimuli (DeYoe et al. 1996). Here we are able to constrain the location of MT+ using surface based histological maps of hOc5 which is thought to be the cytoarchitectonic correlate of the human MT+ complex (Malikovic et al. 2007; Yeo et al. 2010b).

illustrate differential connectivity within MT+. Because of the over-representation of the lower visual field within macaque MT (Maunsell and Van Essen 1987), the distinct MT+ seed regions might also represent the lower visual field, although human fMRI studies have so far failed to yield strong evidence of this representational bias within MT+ (Amano et al. 2009; Kolster et al. 2010; Tootell et al. 1995). In the following analyses, MT+ was either analyzed as two regions using the extreme seed regions ($MT+_d$ and $MT+_v$) or as a single region using the center seed region (MT+) for analyses that did not require the complexities of topographic distinctions. A single aMT+ (anterior MT+) region was chosen anterior to and outside the histological MT+[4]. The regions are shown in Figures 3.22A and 3.24; their coordinates are reported in Table 3.2.

[4] Multiple seed regions are used throughout the paper. The abbreviation of the names of these seed regions obeyed the following convention: the suffix following a region indicates relative spatial location *within* the region, while the prefix preceding a region indicates relative spatial location *outside* the region. Therefore, $MT+_d$ is a seed region *within* the dorsal aspect of the MT+ complex, while aMT+ is a seed region anterior to and *outside* the MT+ complex.

Table 3.2: Locations of Seed Regions Utilized in the Sensory-Motor Pathway Analysis. Notes: Four V1 seed regions were selected using the calcarine fissure, histological V1 estimates (Amunts et al. 2000; Fischl et al. 2008) and the 17-network boundary estimate in the Discovery dataset. $V1_{pd}$ and $V1_{pv}$ were from the dorsal and ventral parts of peripheral V1, likely representing the ventral and dorsal peripheral visual fields respectively. $V1_{cd}$ and $V1_{cv}$ were from the dorsal and ventral parts of central V1, likely representing the ventral and dorsal central visual fields respectively. $MT+_d$, MT+ and $MT+_v$ seed regions were selected from the dorsal, center and ventral parts of the histological map of the MT+ complex, so that $MT+_d$ and $MT+_v$ likely represented peripheral and central visual fields respectively. Based on the over-representation of the lower visual field within macaque MT (Maunsell and Van Essen 1987), it is possible that the three MT+ seed regions might also represent the lower visual field. aMT+ was selected to be anterior and outside the MT+ histological map. V3A and V4 were selected based on their high correlation with MT+ in the Discovery sample and named using the approximate map of human visual areas (Van Essen 2004) as reference. FEF and PrC_v were selected from the caudal frontal cortex, while IPS2, $IPS3_m$, SPL7A, SPL7P and IPS1 were at or near IPS. FEF, IPS2, SPL7A and SPL7P were derived from the meta-analysis of fMRI studies (see Table 3.4). The PrC_v region was selected based on its correlation with aMT+. $IPS3_m$ was chosen spatially between IPS2 and SPL7A. IPS1 was chosen on the lateral wall of rostral IPS. IPS2, $IPS3_m$, SPL7A, SPL7P and IPS1 were named using the probabilistic histological maps of the parietal cortex as reference (Choi et al. 2006; Scheperjans et al. 2008a; 2008b). Coordinates reflect the approximate center location based on the MNI atlas space.

Name	Coordinates
$MT+_d$	-44, -72, 8
MT+	-45, -72, 3
$MT+_v$	-45, -79, -1
aMT+	-51, -64, -2
$V1_{pd}$	-18, -70, 8
$V1_{pv}$	-8, -63, 6
$V1_{cd}$	-8, -95, 3
$V1_{cv}$	-8, -92, -5
V3A	-17, -92, 20
V4	-22, -65, -9
FEF	-26, -6, 48
PrC_v	-50, 6, 30
IPS2	-40, -37, 42
$IPS3_m$	-31, -48, 46
SPL7A	-28, -61, 60
SPL7P	-14, -68,64
IPS1	-46, -49, 51

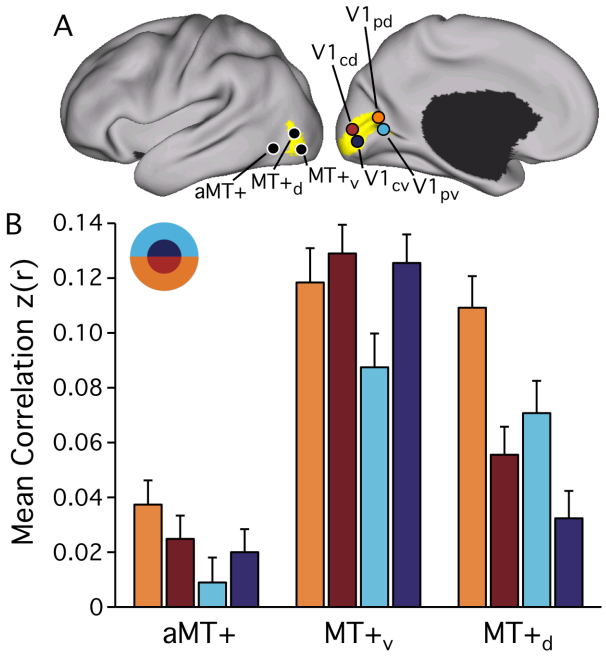

Figure 3.22. Functional connectivity between MT+ and V1 is topographically organized. (A) Two MT+ seed regions, $MT+_d$ and $MT+_v$, were selected in the dorsal and ventral portions of the histological MT+ estimate. aMT+ (anterior MT+) seed region was selected anterior to histological MT+. Four V1 seed regions were selected using the histological V1 estimate: $V1_{cd}$ and $V1_{cv}$ were selected in dorsal and ventral central V1; $V1_{pd}$ and $V1_{pd}$ were selected in dorsal and ventral peripheral V1. Coordinate locations of seed regions are reported in Table 3.3. (B) Correlation strength of aMT+ and MT+ seed regions with V1 in the Replication dataset. There are four observations to be noted: (1) V1-aMT+ correlation is weaker than V1-MT+ correlation, (2) MT+ correlation with the lower visual field is stronger than the upper visual field, (3) $MT+_d$ correlation with peripheral V1 is stronger than central V1 and (4) $MT+_v$ correlation with central V1 is stronger than peripheral V1.

Figure 3.22B quantifies the differential functional coupling of the four V1 regions with MT+ and aMT+ within the Replication sample. V1 showed strong functional coupling to MT+ and significantly weaker coupling to aMT+ ($p < .001$ for both $MT+_v$ and $MT+_d$). The dorsal and ventral MT+ regions also demonstrated differential functional coupling with the four V1 regions, confirmed by a 2x2x2 ANOVA including eccentricity

(central or peripheral), polar angle (upper or lower visual field), and MT+ region (dorsal or ventral). Both MT+ regions were more strongly coupled with the lower visual field V1 seed regions than the upper visual field V1 seed regions ($p < .001$). Furthermore, dorsal MT+ was more strongly coupled with peripheral V1 than central V1 ($p < .001$), while ventral MT+ was more strongly coupled with central V1 than peripheral V1 ($p < .05$). These results suggest the topographic pathways between V1 and the MT+ complex are largely consistent with the visual field representations of the two areas.

Since V1 is a relatively large structure compared with MT+, to ensure the results were robust to the particular choice of the V1 seed regions, Figure 3.23 shows fcMRI maps of the aMT+, $MT+_d$ and $MT+_v$ regions computed using the Replication dataset. By all accounts, V1 is functionally coupled to MT+ while aMT+ shows minimal coupling, leading to their separation into distinct networks in the cortical parcellation.

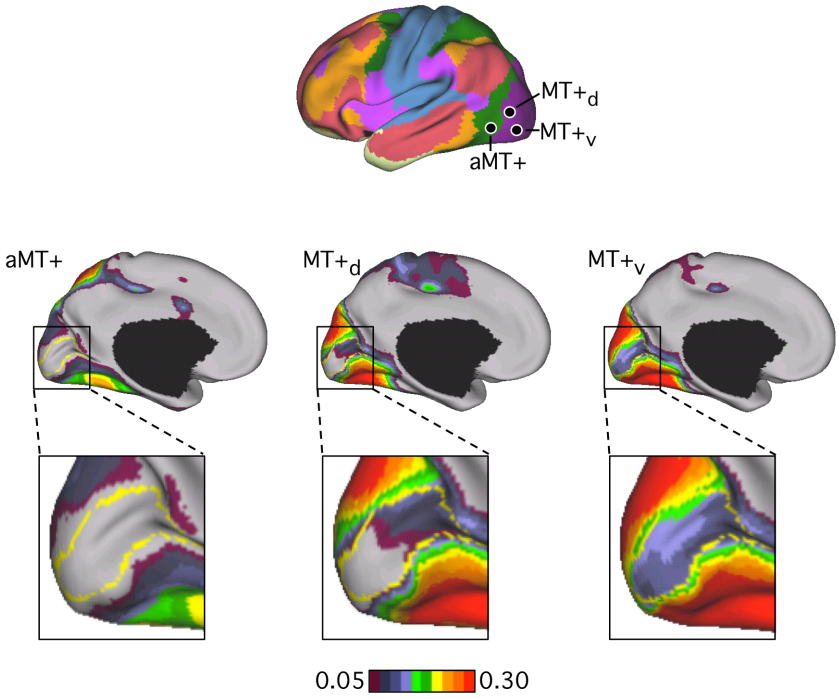

Figure 3.23. Functional connectivity maps of MT+ reveal topographic organization. Functional connectivity maps of aMT+, $MT+_v$ and $MT+_d$ are computed using the Replication dataset and shown with views focusing on V1. V1 showed little or no correlation to aMT+, but strong correlations with both MT+ seeds. In both MT+ fcMRI maps, there is stronger correlation with dorsal V1 (lower visual field) than ventral V1 (upper visual field). There is also increasing correlation with central V1 as we proceed from $MT+_d$ to $MT+_v$. Yellow line denotes areal boundary of V1.

Visual association and parietal association cortices. Moving up the sensory-motor pathway, the functional connectivity of MT+ and aMT+ with parietal and frontal cortices was next examined. Figure 3.24 shows the fcMRI maps of MT+ and aMT+ seed regions computed using the Replication sample with views focusing on the parietal and lateral frontal cortices. In the parietal lobe, both MT+ and aMT+ demonstrated correlation with the SPL and IPS, but little or no correlation with the inferior parietal lobe

(IPL). In the frontal cortex, correlations were mostly limited to the precentral sulcus and gyrus. Compared with the MT+ seed region, the aMT+ seed region demonstrated stronger correlation with the parietal and frontal cortices. The MT+ and aMT+ seed regions were also maximally correlated with different parts of the parietal and frontal cortices, suggesting differential influence on nearby regions of sensory-association cortex.

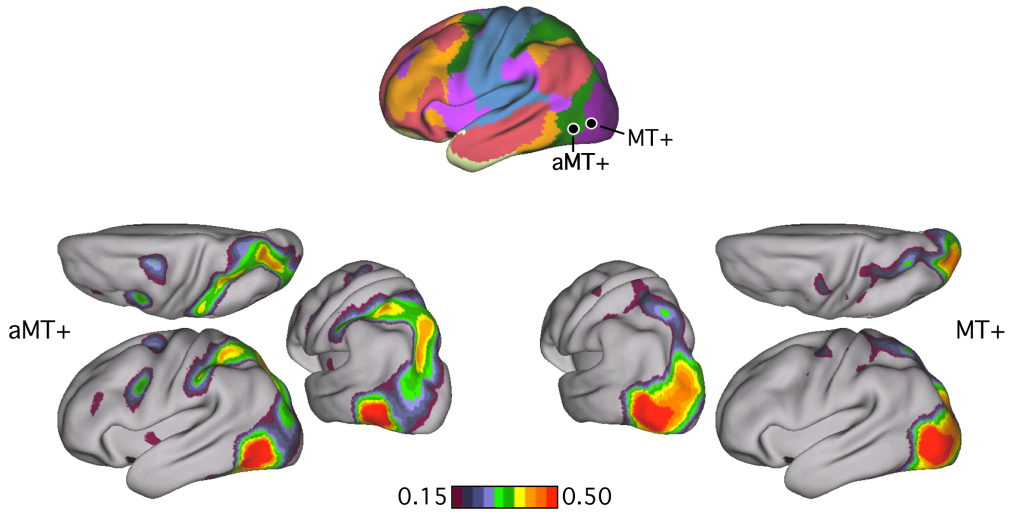

Figure 3.24. aMT+ and MT+ demonstrate differential functional connectivity with parietal and frontal cortices. Functional connectivity maps of aMT+ and MT+ seed regions computed using the Replication dataset. Coordinate locations of the regions are reported in Table 3.2. MT+ and aMT+ are more strongly correlated with SPL and IPS than with IPL. Correlation with frontal cortex is mostly limited to precentral sulcus and gyrus. aMT+ demonstrates stronger overall correlation with parietal and frontal cortices, compared with MT+. MT+ and aMT+ are maximally correlated with different parts of parietal and frontal cortices.

To quantify the pattern of differential functional coupling, we computed the correlation of the MT+ and aMT+ seed regions with four visual, four parietal and two frontal cortical regions (Fig. 3.25A). Two of the visual cortex regions, $V1_{cd}$ and $V1_{pd}$,

were previously used in the V1-MT+ connectivity analysis. V3A and V4 were selected based on their high correlation with MT+ in the Discovery sample and named using the approximate map of human visual areas (Van Essen 2004) as reference. The four parietal regions were chosen at or near the IPS. Three of the parietal regions (IPS2, SPL7A, SPL7P) were selected based on a meta-analysis of fMRI literature of tasks that reportedly activate the human homologues of macaque areas AIP (anterior intraparietal), LIP (lateral intraparietal) and PIP (posterior intraparietal) respectively. The final parietal region, $IPS3_m$, was selected using the Discovery sample to be physically between IPS2 and SPL7A. The parietal regions were labeled based on their proximity to the probabilistic histological maps. In particular, IPS2 is at or near area hIP2 at the anterior most part of IPS (Choi et al. 2006), while SPL7A and SPL7P are at or near areas 7A and 7P of the SPL (Scheperjans et al. 2008a; 2008b). Finally, $IPS3_m$ is on the medial wall of IPS at or near area hIP3 (Scheperjans et al. 2008a; 2008b). The dorsal frontal region, putatively FEF, was selected based on the meta-analysis of fMRI literature of saccade tasks. The ventral frontal region PrC_v (precentral ventral) was selected based on its high correlation with aMT+ in the Discovery sample. The locations of the visual, parietal and frontal regions are reported in Table 3.2. Table 3.3 summarizes the set of fMRI studies used to derive the coordinates of IPS2, SPL7A, SPL7P and FEF.

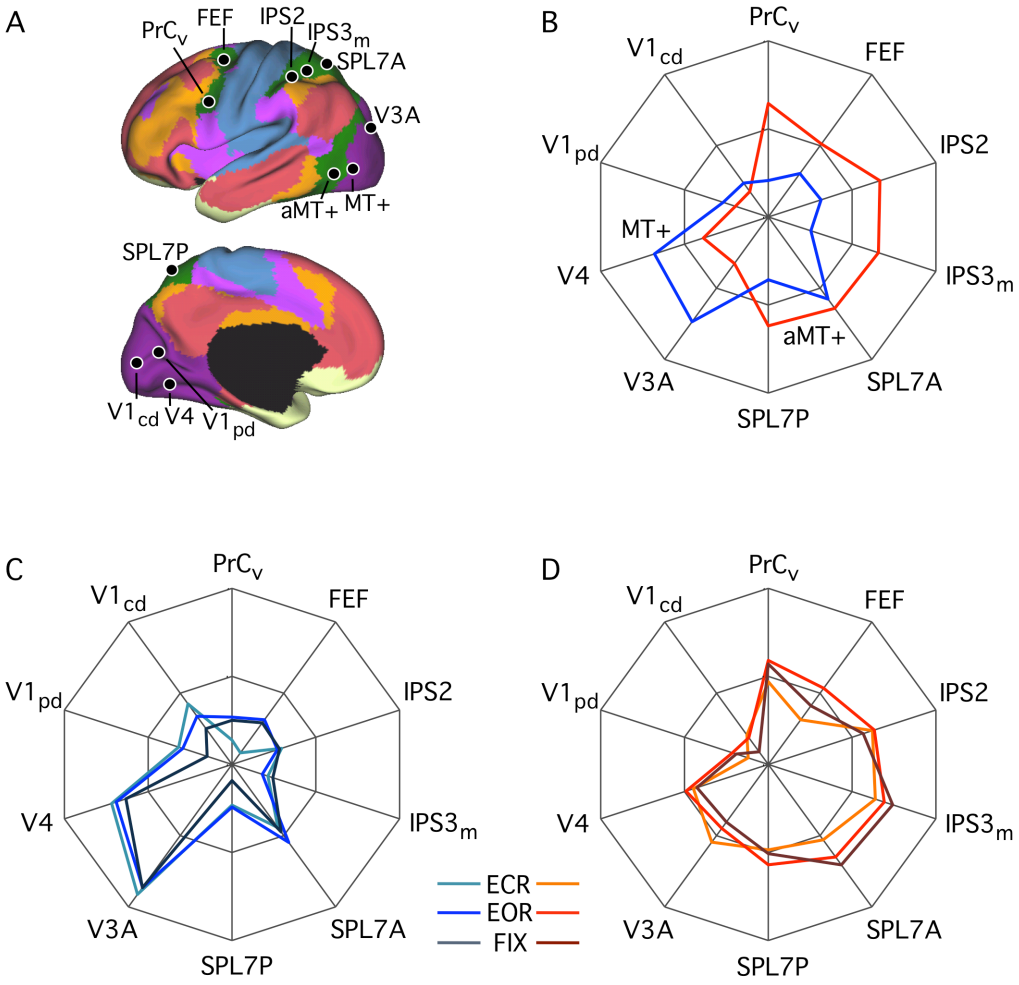

Figure 3.25. aMT+ and MT+ functional connectivity patterns generalize across task conditions. (A) Four visual, four parietal and two frontal seed regions were used to quantify the functional coupling of aMT+ and MT+ to distributed cortical regions. Coordinate locations of the seed regions are reported in Table 3.3 and were chosen either using the Discovery dataset or meta-analysis of fMRI studies (Table 3.4). (B) Polar plots of MT+ (blue) and aMT+ (red) connectivity with the visual, parietal and frontal seed regions are computed using the Replication dataset. MT+ is more strongly correlated with visual cortex as compared with parietal and frontal cortices. The converse is true for aMT+. (C, D) Polar plots of MT+ (blue) and aMT+ (red) connectivity replicated in the Task Effects dataset demonstrate that the functional coupling differences generalize across multiple data acquisition conditions. The polar scales range from r = -0.1 (center) to r = 0.6 (outer boundary) in 0.35-step increments.

Table 3.3: Summary of fMRI Meta-analysis to Obtain Coordinates for IPS2, SPL7A, SPL7P and FEF. Notes: For papers that only report right hemisphere coordinates, left hemisphere coordinates were obtained by reflection across the midline. Coordinates reflect the approximate center location based on the MNI atlas. For IPS2, tasks generally involved perception of 3D objects. Studies reporting responses at or near SPL7A used saccadic eye movement tasks. Studies reporting responses at or near SPL7P involved tasks requiring surface/orientation discrimination. FEF coordinates come from studies of saccadic eye movements.

Name	Coordinates	Putative Macaque Homology	Literature
IPS2	-40, -37, 42	AIP (anterior intraparietal)	Binkofski et al. 1999; Binkofski et al. 1998; Culham et al. 2003; Grefkes et al. 2002; Jäncke et al. 2001; Shikata et al. 2001; Shikata et al. 2003
SPL7A	-28, -61, 60	LIP (lateral intraparietal)	Hagler et al. 2007; Heide et al. 2001; Koyama et al. 2004; Luna et al. 1998; Medendorp et al. 2003; Sereno et al. 2001 (as reported in Table 1 of Hagler et al. 2007); Shulman et al. 2003
SPL7P	-14, -68, 64	PIP (posterior intraparietal)	Faillenot et al. 2001; Shikata et al. 2001; Shikata et al. 2003; Taira et al. 2001
FEF	-26, -6, 48	FEF (frontal eye fields)	Connolly et al. 2000; Connolly et al. 2002; Corbetta et al. 1998; Heide et al. 2001; Koyama et al. 2004; Luna et al. 1998; Perry and Zeki 2000

Figure 3.25B shows the polar plots of the regional correlations using the Replication sample. To ensure that the results were not the result of overt eye movements, the polar plots were also replicated using the Task Effect dataset in Figures 3.25C and 3.25D. In all cases, MT+ had significantly stronger correlation with early visual cortex as compared with aMT+. In contrast, aMT+ had significantly stronger correlation with the parietal and frontal regions compared with MT+. MT+ and aMT+ are strongly coupled to one another ($r = 0.30$ in the Replication sample). Thus, consideration of functional coupling between these regions in detail suggests that early visual areas are coupled to regions at or near MT+, which are in turn directly (or indirectly through intermediate regions, such as aMT+) coupled to parietal and frontal regions associated with sensory-motor integration. The differential coupling of MT+ and aMT+ resulted in their inclusion into distinct cortical networks.

Frontoparietal interactions. We next considered the differential functional coupling of FEF and PrC_v with the parietal cortex. Figure 3.26 shows the fcMRI maps of FEF and PrC_v computed using the Replication sample. While both FEF and PrC_v demonstrated strong correlation with the SPL and IPS, differences in correlation patterns also emerged. Specifically, PrC_v was strongly correlated with more ventral portions of rostral SPL and IPS, while FEF was strongly correlated with caudal SPL and IPS. To quantify this phenomenon, we computed the correlation of FEF and PrC_v with five parietal regions at or near SPL and IPS. Four of the parietal regions (IPS2, $IPS3_m$, SPL7A, SPL7P) were the same as those used in the previous analysis. Using the Discovery sample, a fifth parietal region was selected on the lateral wall of rostral IPS, within what is often termed the frontoparietal control network (orange; Fig. 3.11). Since the region was located at or near the histological map of hIP1 (Choi et al. 2006) projected to FreeSurfer space, we labeled the seed IPS1. The regions are displayed in Figure 3.27A and their coordinates reported in Table 3.2.

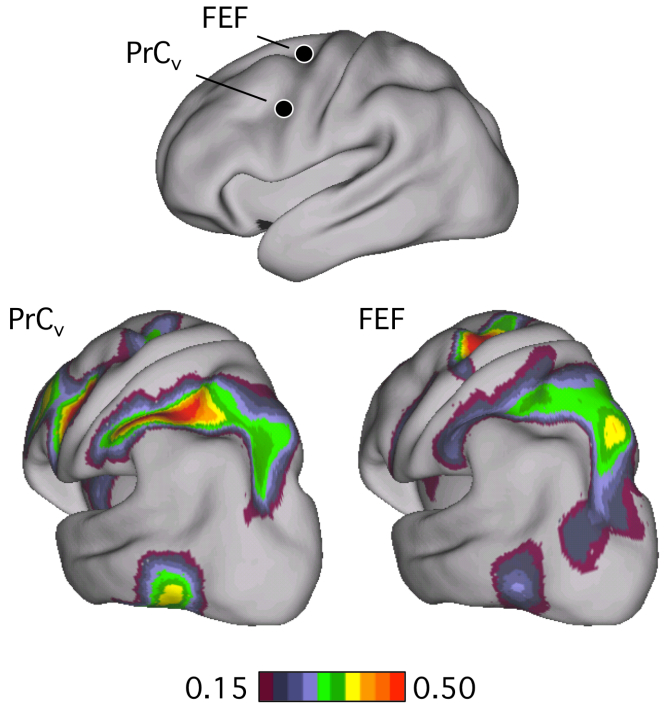

Figure 3.26. Differential connectivity of dorsal and ventral caudal frontal cortex with SPL and IPS. Functional connectivity maps of FEF and PrC_v are computed using the Replication dataset and shown with view focusing on parietal cortex. Both FEF and PrC_v demonstrate strong correlation with SPL and IPS. PrC_v is more strongly correlated with ventral portions of rostral SPL and IPS, while FEF is more strongly correlated with caudal SPL and IPS.

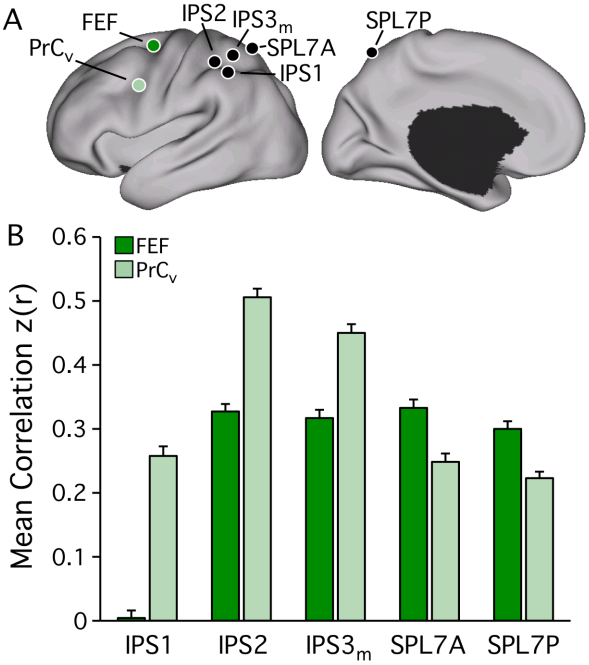

Figure 3.27. Evidence for segregated pathways linking caudal frontal cortex with SPL and IPS. (A) Five parietal seed regions were selected along the rostrocaudal extent of SPL and IPS. Two frontal seed regions, FEF and PrC_v, were selected in dorsal and ventral precentral sulcus. All seed regions were selected using the Discovery dataset or meta-analysis of fMRI studies (Table 3.4). The coordinate locations are reported in Table 3.3. (B) Functional connectivity of FEF and PrC_v with the five parietal seed regions, arranged in rostral (lateral) to caudal (medial) order, from the Replication dataset. Rostrolateral IPS seed regions (IPS1, IPS2, $IPS3_m$) were more strongly correlated with PrC_v than FEF, while the mediocaudal SPL seed regions (SPL7A, SPL7P) were more strongly correlated with FEF than PrC_v.

Figure 3.27B shows the correlation of FEF and PrC_v with the five parietal regions computed in the Replication sample, arranged in rostral (lateral) to caudal (medial) order. The rostrolateral IPS regions (IPS1, IPS2, $IPS3_m$) were more strongly correlated with PrC_v than FEF, while the caudomedial SPL regions (SPL7A, SPL7P) were more strongly correlated with FEF than PrC_v. A 2x6 ANOVA including frontal regions (FEF, PrC_v) and parietal regions (IPS1, IPS2, $IPS3_m$, SPL7A, SPL7P) found a significant interaction ($p < .001$). In particular, FEF was more strongly correlated with the three IPS seeds (all $p <$

.001) while PrC_v was more strongly correlated with SPL7A and SPL7P (both $p < .001$). These results reveal differential coupling between distinct parietal and frontal regions, likely reflecting multiple pathways involved in sensory-motor integration (Kurata 1991; Rizzolatti et al. 1998; Tanné-Gariépy et al. 2002).

Hierarchical analysis. Assuming a visual hierarchy similar to that proposed by Maunsell and Van Essen (1983) exists in human cerebral cortex, V1 is expected to be near the bottom of the hierarchy and FEF to be near the top (also see Felleman and Van Essen 1991; Ungerleider and Desimone 1986). While there are uncertainties as to the exact homologies of our MT+ and aMT+ seed regions, they are likely to be in the middle of the hierarchy with aMT+ higher than MT+. In our analysis, we found that V1 and MT+, which are close together in the hierarchy, have stronger correlation than V1 and aMT+, which are farther apart in the hierarchy (Figs. 3.22 and 3.25). We also found that aMT+ and FEF, which are closer in the hierarchy, have stronger correlation than MT+ and FEF, which are farther apart in the hierarchy (Figs. 3.24 and 3.25).

These results suggest that correlation between regions in the visual hierarchy may provide some insight into the organization of the pathways. To explore this hypothesis, we examined the arrangement of six seed regions ($V1_{pd}$, V3A, MT+, aMT+, SPL7A, FEF) discussed earlier based on the assumption that stronger correlations are consistent with closer positioning in the processing hierarchy. By examining alternative arrangements of regions, the analysis was able to investigate which particular arrangement was most consistent with the functional connectivity pattern. Figure 3.28 illustrates this approach. Figure 3.29 shows the two best hierarchical arrangements of the six regions when seeking a five-level hierarchy using the Replication sample. In both

cases, the relative ordering of the regions within the functional hierarchy agrees well with the previously proposed and refined models of macaque visual hierarchy (Felleman and Van Essen 1991; Maunsell and Van Essen 1983; Ungerleider and Desimone 1986). By contrast, alternative arrangements of the visual areas lead to large proportions of violated constraints (Figs. 3.29D and 3.29E).

Control analyses using the Discovery set shows that the fcMRI strengths of all pairs of the six seed regions are inversely correlated ($r = -0.78$, $p < .001$) with respect to the hierarchical distance between the regions in the hierarchy as defined by Felleman and Van Essen (1991). By contrast, the fcMRI strengths of all pairs of the six seed regions are not correlated ($p = 0.23$) with respect to the physical distance between the seed regions. These results suggest that spatial proximity does not explain these correlations; rather, the pattern of correlations reflects relative positions of regions within the hierarchy.

These findings converge on two main results. First, there are functional interactions between networks but the interactions are selective. V1 shows minimal coupling with association regions within parietal cortex but it does couple with MT+. The between-network interactions also do not typically violate the network organizations revealed earlier by the clustering approaches: regions show stronger functional coupling to other regions within their network as contrast to regions outside their network. Second, when examined together, the pattern of correlations between regions in different networks is consistent with a hierarchical organization by which sensory information could influence regions associated with motor control (Fig. 3.29).

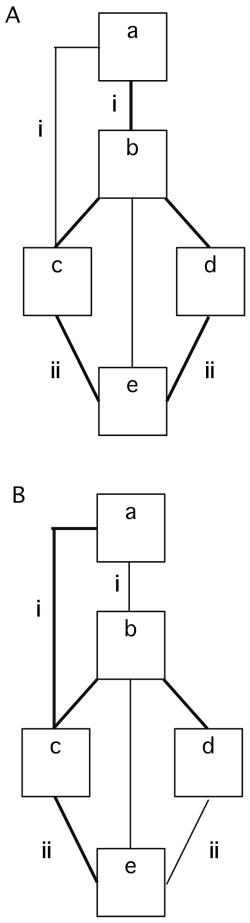

Figure 3.28. Examples of satisfied and violated constraints in estimating the functional hierarchy of cortical regions based on fcMRI. A functional hierarchy is estimated based on the assumption that regions closer in a hierarchy have stronger correlation. (A) Five cortical regions are arranged in a four-level hierarchy whose functional connectivity strengths satisfy both hierarchical and lateral constraints. (B) Identical arrangement of five cortical regions in a four-level hierarchy with different functional connectivity strengths that violate both hierarchical and lateral constraints. Thick lines correspond to strong correlations. Thin lines correspond to weak correlations. (i) Regions "a" and "c" are farther apart that regions "a" and "b". In example (A), correlation of regions "a" and "c" is weaker than correlation of regions "a" and "b", so a hierarchical constraint is satisfied. In example (B), correlation of regions "a" and "c" is stronger than correlation of regions "a" and "b", so a hierarchical constraint is violated. (ii) Regions "c" and "d" are on the same hierarchical level. In example (A), correlation of regions "c" and "e" is approximately the same as the correlation of regions "d" and "e", so a lateral constraint is satisfied. In example (B), correlation of regions "c" and "e" is stronger than the correlation of regions "d" and "e", so a lateral constraint is violated. In the context of hierarchy estimation in this paper, we consider two correlations within 0.2 of each other to be approximately the same when assessing lateral constraints.

Given the pairwise correlations of a set of seed regions and a *known* number of levels in the hierarchy, we can seek the best hierarchical arrangement of the seed regions with the following local optimization procedure: (1) randomly arrange the seed regions into a hierarchy, (2) consider swapping a pair of seed regions or shifting a single seed region to a different hierarchical level without changing the number of levels in the hierarchy such that the proportion of violated constraints is maximally decreased, (3) terminate when no further improvement in the proportion of violated constraints can be achieved and (4) repeat the preceding steps 20 times picking the solution with the least proportion of violated constraints. The best solution obtained using this optimization procedure is (in practice) the same as a brute-force search over all possible hierarchical arrangements of the seed regions. We note that we are generally unable to infer the number of levels in the functional hierarchy, since the number of possible constraints can be drastically different for hierarchies with different number of levels, and so the proportion of violated or satisfied constraints is not comparable across hierarchies with different levels. In practice however, the solution space is robust; for example, the best solution for a 5-level hierarchy typically differs from the best solution for a 4-level hierarchy by the collapsing of regions from two adjacent levels into one level. Uncovering the true hierarchical structure in the macaque visual hierarchy based on anatomical connectivity has also proved to be problematic (Hilgetag et al. 1996).

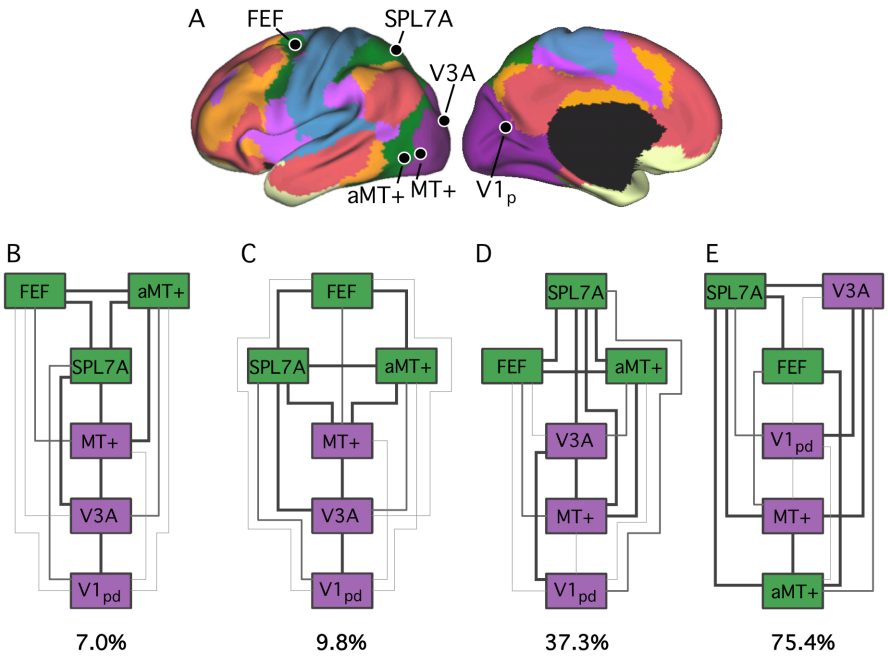

Figure 3.29. Functional connectivity estimates of the hierarchical organization of a canonical sensory-motor pathway. (A) Six seed regions are arranged into a five-level functional hierarchy using the Replication dataset. (B, C) Two best hierarchical arrangements of the seed regions as measured by the proportion of violated hierarchical and lateral constraints. A violation occurred when the ordering placed more strongly correlated regions farther apart in the hierarchy than more weakly correlated regions (see Fig. 3.28). (D, E) Two poor hierarchical arrangements of the seed regions as measured by the proportion of violated hierarchical and lateral constraints. Relative ordering of the seed regions (A, B) within the functional hierarchy agrees well with the proposed macaque visual hierarchy (see text).

Parietal and prefrontal association cortices possess multiple regions with distinct connectivity profiles

The analyses above describe separate sensory and motor networks, and address the question of how sensory and motor networks might interact through intermediate areas such as aMT+. However, these networks make up only a minority of the human cerebral cortex. Networks of widely distributed regions comprise the majority of the human cerebral cortex as illustrated by the violet, orange, and red networks in the 7-

network solution (Fig. 3.11). The network complexity expands when the 17-network parcellation is considered (Fig. 3.13). These association networks will be the remaining focus of the results. First, we examined the topography of parietal and frontal association cortices to quantitatively illustrate that multiple neighboring regions possess markedly different functional connectivity fingerprints. Next we explored the relations between distributed regions to demonstrate that the association cortex is comprised of multiple, interdigitated association networks.

Parietal association cortex. The basic approach employed to characterize the connectivity properties of parietal cortex was to extend the strategy applied in Figure 3.25 to construct polar plots that quantify coupling with multiple, distributed cortical regions. Following the work of Passingham et al. (2002), we refer to these plots as "functional connectivity fingerprints" with the idea that the graphical representation will facilitate the visualization of similarities in connectivity properties between regions as well as any differences that make them unique. The plots are quantitative in that eccentricity displays the strength of functional coupling between each seed region and a single target region.

For this analysis, multiple regions within parietal cortex were selected to cover the IPL and immediately adjacent portions of the SPL. Regions were further selected to survey distinct networks as revealed by the clustering maps. Some of the regions were used previously in the sensory-motor pathway analysis (IPS2, SPL7A). Other regions (PF, PGa, $IPS3_l$, PGp_d and PGp_v) were selected using the Discovery dataset and then labeled according to the probabilistic histological maps. In particular, the PF and PGa seed regions were at or near human inferior parietal areas PF and PGa, respectively (Caspers et al. 2006; 2008), while the $IPS3_l$ seed region was on the lateral lip of the IPS

at or near human hIPS3 (Scheperjans et al. 2008a; 2008b). PGp_d and PGp_v corresponded to the dorsal and ventral aspects of area PGp in the IPL (Caspers et al. 2006; 2008). One additional seed region at or near the temporoparietal junction (TPJ) was selected based on the peak coordinates reported in a human fMRI study of mental state inference (Saxe and Powell 2006), which accords well with the predicted mean peak in a recent meta-analysis on the same topic (Van Overwalle and Baetens 2009).

Twenty-two cortical target regions were distributed over the lateral and medial aspects of the cerebral cortex such that multiple regions covered each association network. Four of the cortical regions (aMT+, MT+, FEF and PrC_v) were used previously in the sensory-motor pathway analysis. Many labels for the frontal seed regions reflect gross anatomical landmarks as atlas-based human histological references were not available; subscripts denote relative positions. It is worth noting that target region 6vr+ was selected to be anterior to the map of premotor area 6 (Geyer 2003) and labeled to reflect a new delineation of the ventral precentral sulcus (Amunts et al. 2010). Target region PFC_V fell within the histological map of BA45 (Amunts et al. 1999). The coordinates of the parietal seed regions and cortical target regions are reported in Table 3.4.

Table 3.4: Locations of Seed Regions Used for Analysis of Connectivity Fingerprints (Figs. 3.30 and 3.31). Notes: Where possible, seed regions were carried forward from previous analyses (i.e., IPS2, SPL7A, FEF, PrC_v, aMT+ and MT+; see Tables 3.2 & 3.3). Seed regions PF and PGa were at or near human inferior parietal area PF and PGa, respectively (Caspers et al. 2006; 2008). The $IPS3_l$ seed region was selected to be on the lateral lip of the IPS at or near human hIPS3, while the 5Ci seed region corresponded to the human posterior cingulate sulcal region 5Ci (Scheperjans et al. 2008a; 2008b). PG_{pd} and PG_{pv} corresponded to the dorsal and ventral aspects of area PGp in the inferior parietal lobule (Caspers et al. 2006; 2008). The TPJ seed region was selected based on the peak coordinates reported in a human fMRI study of mental state inference (Saxe and Powell 2006) which accords well with the predicted mean peak in a recent meta-analysis on the same topic (Van Overwalle and Baetens 2009). Seed region 6vr+ was selected to be anterior to the map of premotor area 6 (Geyer 2003) and labeled to reflect a new cytoarchitectonic delineation within the ventral precentral region (Amunts et al. 2010). Seed region PFC_v fell within the histological map of BA45 (Amunts et al. 1999; Fischl et al. 2008). The remaining seed regions were selected to provide comprehensive coverage of the lateral and medial aspects of the cortical surface and such that each association network was represented by multiple targets. Labels for the remaining seed regions were determined according to gross anatomical landmarks and given subscripts to denote relative positions: Cing = cingulate sulcus; pCun = precuneus; ITG = inferior temporal gyrus; PCC = posterior cingulate cortex; PFC = prefrontal cortex; PHC = parahippocampal cortex; RSP = retrosplenial cortex; STS = superior temporal sulcus. Subscripts a = anterior; p = posterior, l = lateral, m = medial, d = dorsal and v = ventral. Coordinates reflect the approximate center location based on the MNI atlas.

Parietal Cortex	**Coordinates**
PGa	-52, -50, 49
IPS2	-40, -37, 42
SPL7A	-28, -61, 60
$IPS3_l$	-35, -56, 42
PGp_d	-49, -63, 45
PGp_v	-49, -69, 28
TPJ	-51, -57, 27
PF	-60, -37, 38
5Ci	-16 -32 39
PCC	-3, -49, 25
pCun	-10, -57, 35
Frontal Cortex	
PFC_{la}	-41, 55, 4
PFC_l	-38,33,16
PFC_{da}	-31,39,30
PFC_{lp}	-45, 29, 32
PFC_{dp}	-44,15,48
PrC_v	-50, 6, 30

Table 3.4. Locations of Seed Regions Used for Analysis of Connectivity Fingerprints (Continued)	
Parietal Cortex	**Coordinates**
FEF	-26, -6, 48
PFC_v	-55,24,13
6vr+	-55, 6, 11
PFC_m	-7, 46, -2
PFC_{dm}	-4, 49, 32
PFC_{mp}	-5, 22, 47
$Cing_a$	-10, 13, 40
$Cing_m$	-5, 2, 29
Occipital/Temporal Cortex	
STS_a	-49, 5, -26
STS	-55, -10 -16
STS_p	-49, -34, -4
ITG	-59, -53, -14
aMT+	-51,-64,-2
MT+	-45, -72, 3
Limbic Cortex	
PHC	-25, -31, -20
RSP	-7, -50, 7

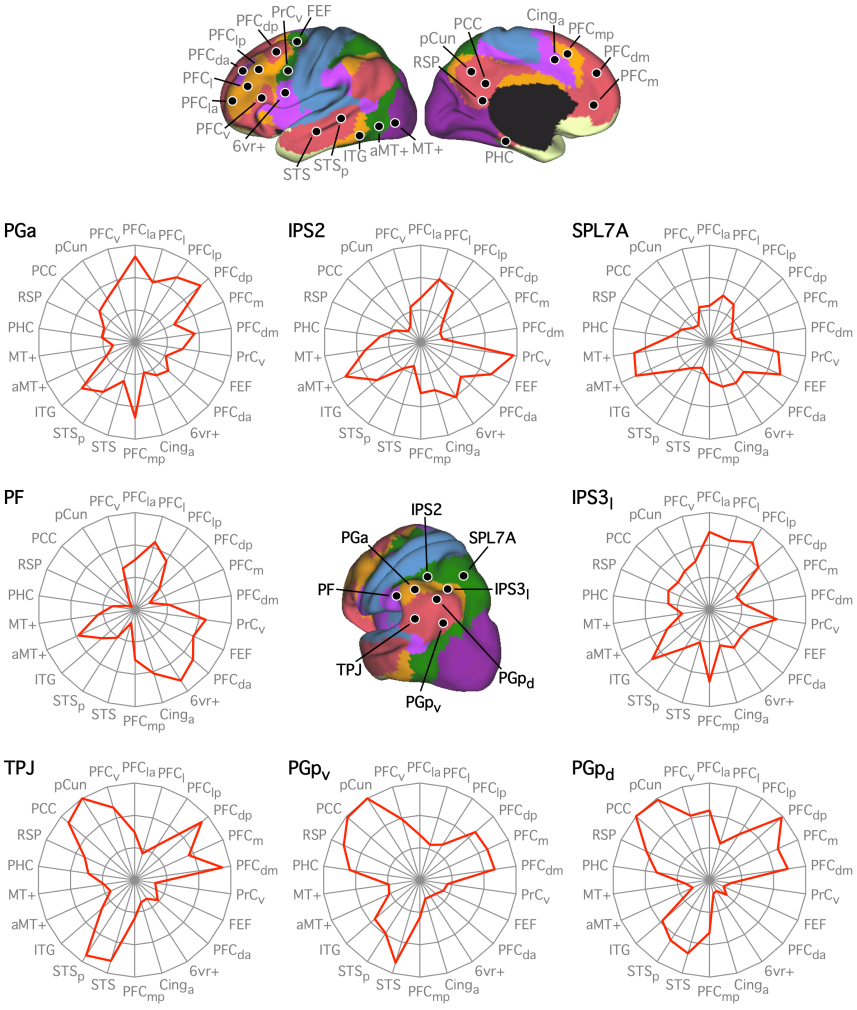

Figure 3.30. Adjacent parietal regions exhibit distinct functional connectivity fingerprints. Correlations of eight parietal seed regions (center panel) with 22 cortical target regions (top panel) from the Replication dataset and displayed as polar plots. Colors represent the 7-network segmentation (from Fig. 3.11). The coordinate locations are reported in Table 3.4. Parietal seed regions that belong to the same network (e.g., TPJ, PGp$_v$ and PGp$_d$) have generally similar functional connectivity fingerprints that are distinct from other parietal seed regions. Close inspection of the polar plots reveals distinct connectivity fingerprints even for parietal regions within the same network, some of which anticipate the further fractionation of the parietal cortex in the 17-network estimate (Fig. 3.13). Note that the cortical targets from Cinga to pCun on the left side of the polar plots are the same as that of the frontal polar plots (Fig. 3.31) to allow for comparison across the two sets of polar plots. The remaining cortical targets are different across the two sets of polar plots but are arranged so that cortical targets at the same location in the polar plots belong to the same network in the 7-network estimate. The polar scales range from r = -0.4 (center) to r = 0.5 (outer boundary) in 0.3-step increments.

The results are illustrated in Figure 3.30. Parietal association cortex is comprised of multiple regions that can show similarities but often display markedly different functional connectivity fingerprints. Visual inspection of the plots allows appreciation of the resemblance of correlation patterns for parietal seed regions that cause them to fall within common networks. For example, the PGp_d, PGp_v, and TPJ seed regions all fall within the default network as defined in the extant neuroimaging literature. Their connectivity fingerprints are largely defined by their correlations with other association and limbic regions, and near complete absence of correlations with visual regions including MT+ and aMT+. This general fingerprint pattern can be directly contrasted with parietal regions such as those represented by IPS2 and SPL7A that are associated with distributed cortical regions linked to sensory and motor function (e.g., strong correlations with MT+ and aMT+). These distinct parietal regions (IPS2 and SPL7A) are likely at or near the putative human homologue to macaque AIP and LIP and fall within the functional network that has been discussed as the dorsal attention network in the human literature and described in detail above in Figures 3.22 to 3.29.

There are also subtle differences across regions that fall within the same broad networks. For example, while parietal seed regions TPJ, PGp_v and PGp_d are strongly correlated with posterior cingulate cortex (PCC) and the precuneus (pCun), PGp_v has comparatively stronger correlation to retrosplenial cortex (RSP) and parahippocampal complex (PHC). In contrast, TPJ has the strongest correlation with posterior superior temporal sulcus (STS_p) and lower correlation with RSP and PHC. PGp_d has the strongest correlation with medial prefrontal cortex (PFC_m). These differential correlations account

for the fractionation of the posterior IPL into three components in the 17-network estimate (Fig. 3.13) and may be important to the functional properties of the region.

Frontal association cortex. Analysis of frontal association cortex applied the same approach as for parietal association cortex. The 8 frontal seed regions selected for analysis were among the cortical targets in the parietal plots discussed previously. The 22 cortical target regions selected for analysis were distributed throughout the cortex and selected so that multiple target regions covered each association network. Eleven regions were carried forward from the previous analysis of the parietal cortex (e.g., IPS2, SPL7A, FEF, PrC_v, aMT+ and MT+) and these were arranged in the same spatial locations in the polar plots (Cinga clockwise to pCun). The remaining 11 cortical target regions were unique to analysis of frontal cortex but are arranged in the plots so that cortical target regions at the same location in the polar plots belong to the same network in the 7-network estimate. The arrangement of the cortical target regions therefore facilitates the comparison of polar plots across the parietal and frontal figures. The coordinates of the frontal seed regions and cortical target regions are reported in Table 3.4.

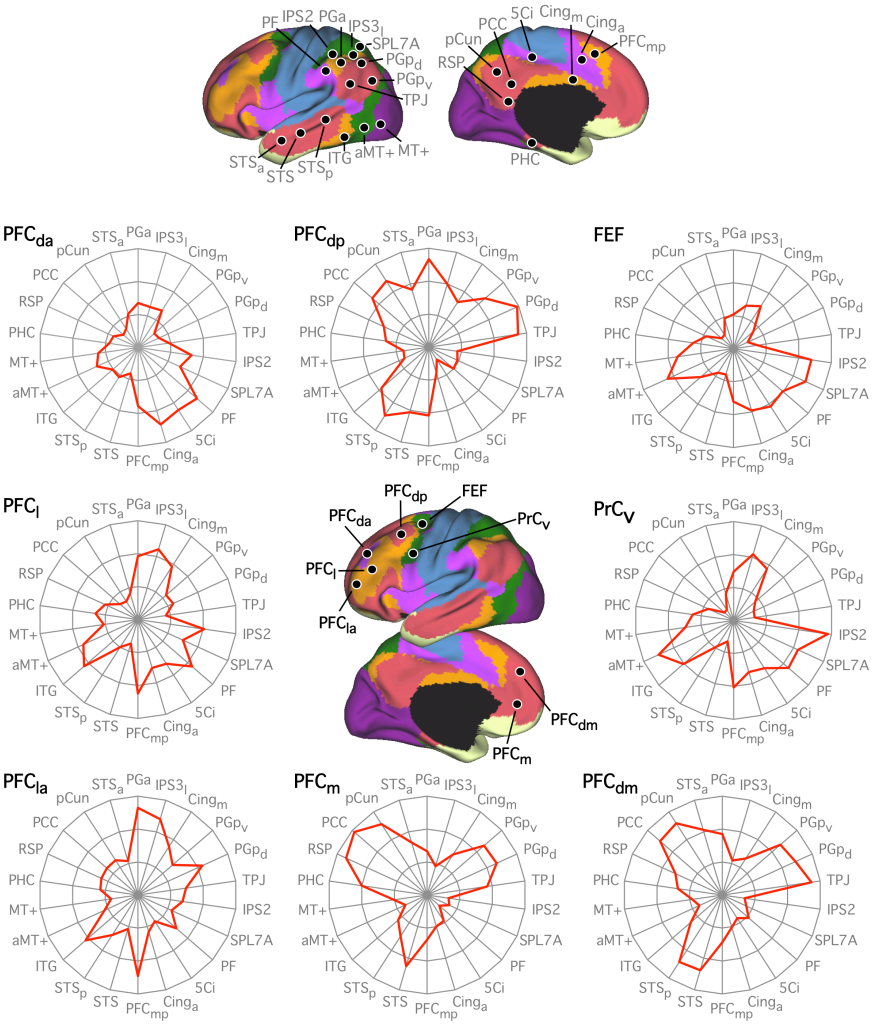

Figure 3.31. Adjacent frontal regions exhibit distinct functional connectivity fingerprints. The format and plotting are the same as Figure 3.30 with regions tailored for exploration of frontal cortex. The coordinate locations are reported in Table 3.4. The polar scales range from r = -0.4 (center) to r = 0.5 (outer boundary) in 0.3-step increments.

Figure 3.31 shows the polar plots of correlations for the 8 frontal seed regions with the 22 target regions in parietal, temporal, frontal and cingulate cortices. Many of the same properties observed for parietal association cortex were again apparent. Figure 3.31 demonstrates that frontal seed regions in the same network generally share similar

functional connectivity fingerprints that are distinct from those of neighboring seed regions belonging to a different network. A simple posterior-to-anterior hierarchy is not present as might be expected from some models of frontal hierarchy based on anatomical connectivity (e.g., Petrides 2005). Rather, regions with similar functional connectivity fingerprints appeared at posterior and anterior locations as evidenced by PFC_{da}, which is considerably rostral to most of its partner regions, and PFC_{dp} which is considerably caudal to its partner regions.

The arrangement of the cortical target regions also allows a key feature of connectivity to be appreciated when frontal Figure 3.31 is directly compared to parietal Figure 3.30: parietal and frontal seed regions from the same network, for instance PG_{pd} and PFC_{m}, have similar functional connectivity fingerprints. These similarities suggest that association cortex is made of parallel interdigitated networks of regions consistent with suggestions based on double-labeling analyses of monkey association cortex (Goldman-Rakic 1988; Selemon and Goldman-Rakic 1988). In our final analysis, we explored this possibility directly by comparing functional connectivity maps for multiple seed regions distributed across each association network.

Association cortex is comprised of multiple, interdigitated large-scale networks

The parcellations derived from clustering suggest that there are multiple, large-scale networks interdigitated throughout association cortex. Thus, components of the green, violet, orange and red networks in the 7-network estimates are spatially adjacent in the parietal, temporal and frontal cortices (Fig. 3.11). A similar organization is observed in the 17-network estimate (Fig. 3.13). However, such an impression could be an artifact

of the winner-take-all implementation of clustering that assigned each cortical vertex to a single network. The complex functional connectivity fingerprints demonstrated that regions within the same networks showed similar functional connectivity fingerprints even when distributed across the cortex, consistent with their inclusion in common networks, but also revealed differences between regions that suggest subtler organizational properties. In our final analysis, we sought to explore patterns of functional connectivity using an exclusively seed-based approach in a comprehensive manner to contrast connectivity patterns for multiple regions embedded within the same networks.

For this analysis, six left hemisphere seed regions from each of the four major association networks were analyzed beginning with the canonical sensory-motor network (known as the dorsal attention network in human neuroimaging literature). The ventral attention, frontoparietal control and default networks were subsequently explored. These four networks were identified in the 7-network estimate based on the Discovery dataset. Where possible we used the same seed regions as used by the other analyses in this paper. For this reason, the selected regions were not always the most confident in terms of network assignment as assessed by their silhouette plots or other means. Table 5 reports the coordinates of the seed regions.

The left hemisphere fcMRI maps of the seed regions were computed using the Replication dataset and illustrated in Figures 3.32 to 3.35. Each seed region is functionally coupled *primarily* to regions within the same network, thus largely confirming the 7-network estimate and the existence of multiple, large-scale distributed networks in human association cortex. The network patterns were even reproduced when

target regions were isolated in relation to adjacent cortical regions (e.g., Fig. 3.33A). Thus, this verifies that the networks identified via clustering capture the predominant functional coupling patterns within association cortex. Note that this result is not obligated – the maps derived from the analysis of seed regions are not constrained to respect the borders of the networks defined by clustering. Furthermore, while the broad patterns confirmed the boundaries of the networks as expected, several exceptions were also observed.

Table 3.5: Locations of Seed Regions Used for Analysis of Parallel Networks in Association Cortex. Notes: The confidence of the seed regions in their network assignment is computed from the Replication dataset. Coordinates reflect the approximate center location based on the MNI atlas.

Name	Coordinates	Confidence
Dorsal Attention A	-22, -8, 54	0.54
Dorsal Attention B	-34, -38, 44	0.53
Dorsal Attention C	-18, -69, 51	0.46
Dorsal Attention D	-51, -64, -2	0.55
Dorsal Attention E	-8, -63, 57	0.32
Dorsal Attention F	-49, 3, 34	0.49
Ventral Attention A	-31, 39, 30	0.49
Ventral Attention B	-54, -36, 27	0.63
Ventral Attention C	-60, -59, 11	0.27
Ventral Attention D	-5, 15, 32	0.65
Ventral Attention E	-8, -24, 39	0.57
Ventral Attention F	-31, 11, 8	0.67
Control A	-40, 50, 7	0.52
Control B	-43, -50, 46	0.51
Control C	-57, -54, -9	0.25
Control D	-5, 22, 47	0.43
Control E	-6, 4, 29	0.27
Control F	-4, -76, 45	0.25
Default A	-27, 23, 48	0.46
Default B	-41, -60, 29	0.63
Default C	-64, -20, -9	0.61
Default D	-7, 49, 18	0.60
Default E	-25, -32, -18	0.22
Default F	-7, -52, 26	0.61

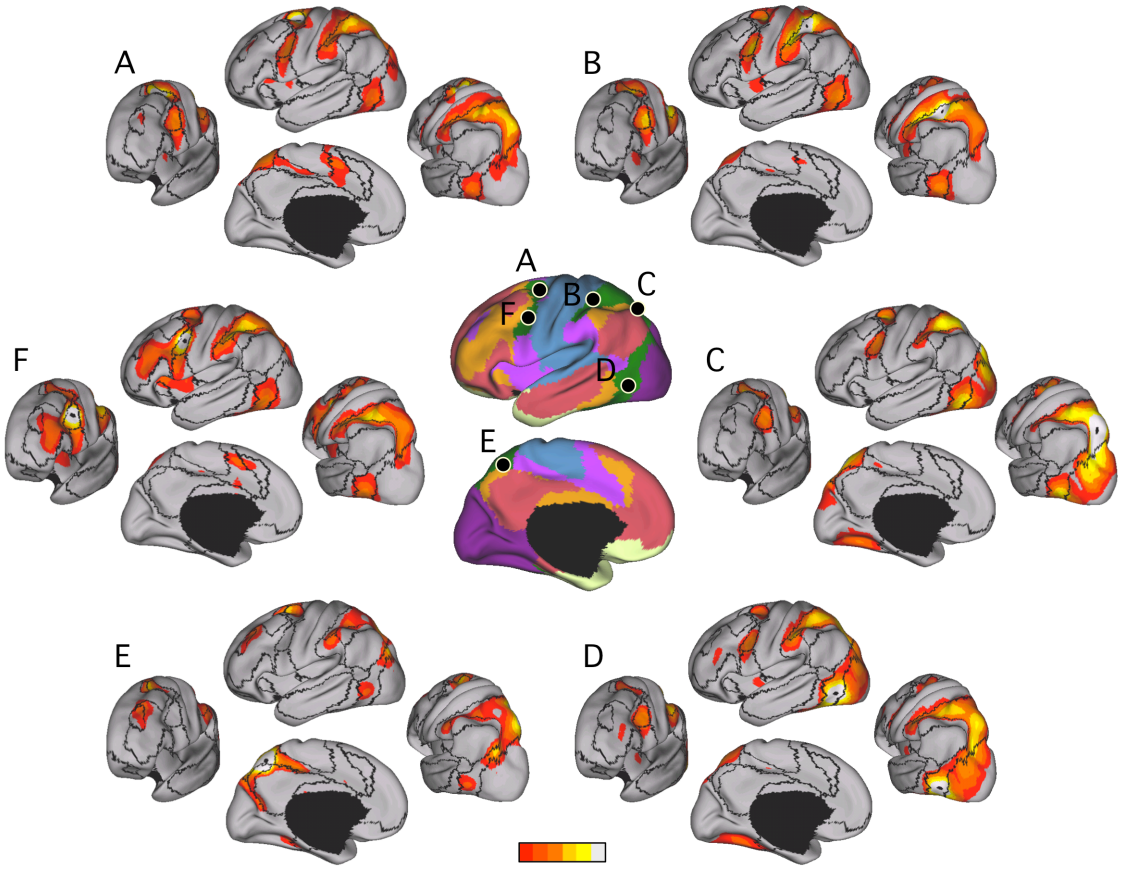

Figure 3.32. Functional connectivity for regions within the canonical distributed cortical network. This network is often called the dorsal attention network. The five seed regions are displayed in the center overlaid on top of the 7-network parcellation from Figure 3.11. The coordinate locations are reported in Table 3.5. Each panel displays the functional connectivity map for one of the six seed regions for the Replication dataset overlaid on a surface that shows the 7-network boundaries (in light black lines) as reference. Each seed region displays functional coupling with all of the regions of the distributed network. However, there are important differences between regions. In particular the regions near aMT+ (panel D) and SPL7A (panel C) show strong functional coupling with earlier visual areas. The region at or near the putative homologue of FEF (panel A) shows minimal functional coupling with earlier visual areas but does show strong coupling with midline motor regions (see midline section of panel A). The color scale (bottom) shows the plotted correlation range for the maps.

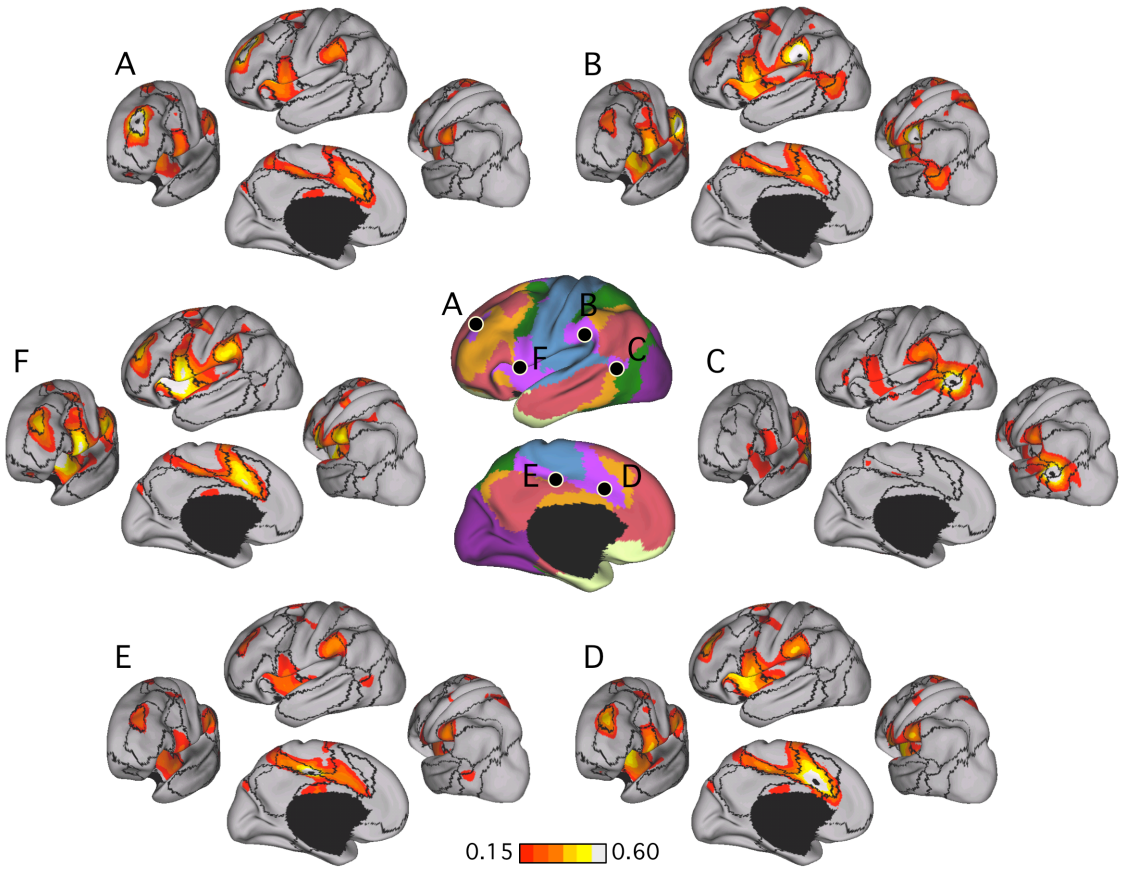

Figure 3.33. Functional connectivity for distributed regions within a second large-scale association network. This network is often called the ventral attention network. The format and plotting are the same as Figure 3.32 and coordinate locations are reported in Table 3.5. Each seed region is functionally coupled mostly with regions within the same network revealing that each component of the network recapitulates the others. There is a general absence of crosstalk between networks except for local correlation around the seed regions.

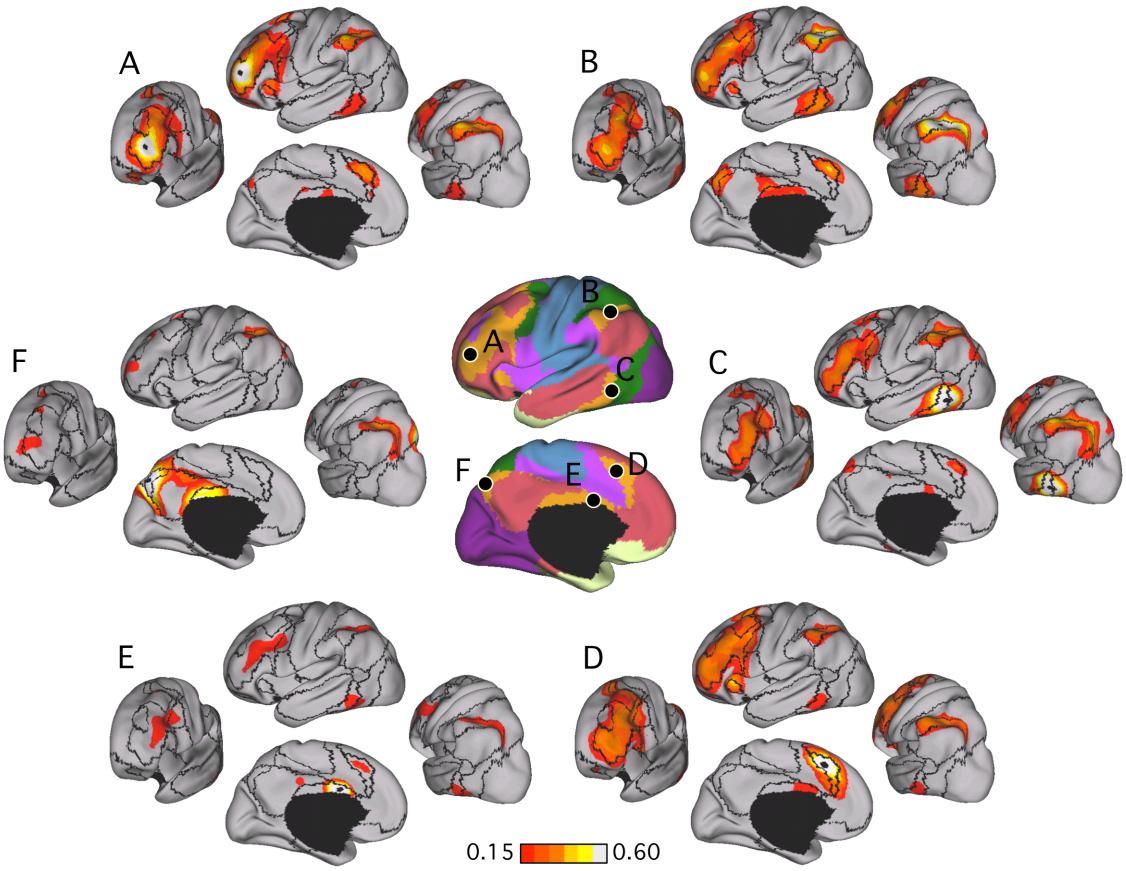

Figure 3.34. Functional connectivity for distributed regions within a third large-scale association network. This network is often called the frontoparietal control network. The format and plotting are the same as Figure 3.32 and coordinate locations are reported in Table 3.5. In addition to a general absence of crosstalk between networks this network also shows no functional coupling to sensory and motor regions. Rather its topography reveals a distributed network that is interdigitated with the networks illustrated in Figures 3.33 and 3.35.

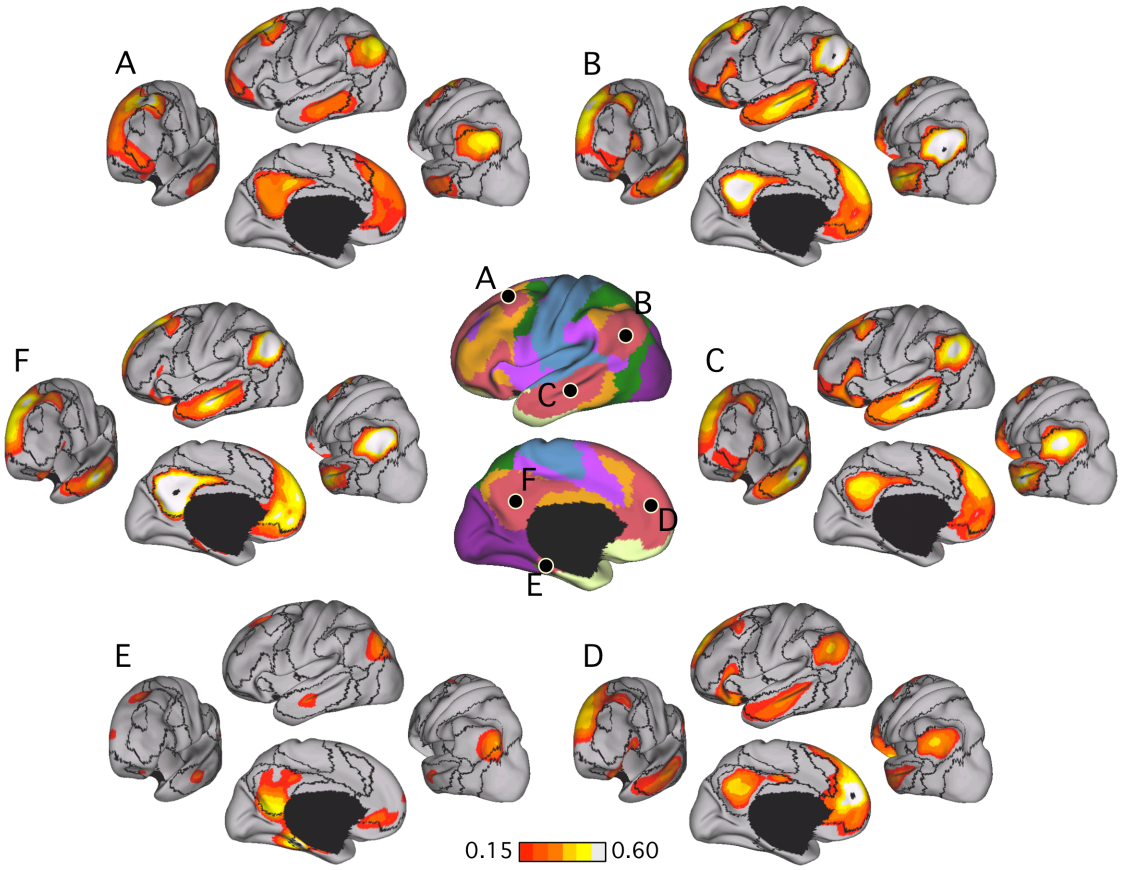

Figure 3.35. Functional connectivity for distributed regions within a fourth large-scale association network. This network makes up the prominent components of the network often called the default network. The format and plotting are the same as Figure 3.32 and coordinate locations are reported in Table 3.5. Each seed region is functionally coupled mostly with regions within the same network again revealing that each component of the network recapitulates components the remaining network, with some exceptions. For example, the seed region in the parahippocampal cortex (panel E) shows functional connectivity with the retrosplenial cortex, ventral medial prefrontal cortex, and a specific region with the caudal IPL. These patterns of functional connectivity lead to the fractionation into subnetworks as illustrated in Figure 3.13. The fractionation of this particular network is largely to subdivide the broader network rather than to display functional coupling with regions in distinct networks.

Close inspection of the maps (Figs. 3.32 to 3.35) reveals evidence for crosstalk among the networks, consistent with the earlier analyses of the canonical sensory-motor pathway. For example, Figure 3.32C/D suggests interaction between the dorsal attention network and regions within the visual system, possibly related to the previously described hierarchical flow of information within the sensory-motor pathway (Fig. 3.29). In contrast, Figure 3.32F suggests functional coupling between the dorsal attention and the frontal components of the frontoparietal control and ventral attention systems.

A further observation is that the fcMRI maps of seed regions chosen from the same network anticipate fractionation of the networks in ways also suggested by the analysis of connectivity fingerprints. For example, the PHC seed region is strongly coupled with the RSP, but not with the full extent of the posterior cingulate (Fig. 3.35E). It is also strongly coupled to the IPL but not the anterior IPL. This suggests that the 7-network estimate is likely insufficient to capture the full complexity of the functional couplings across different brain regions. As predicted by the fcMRI map of the PHC seed, the 17-network estimate differentiates the posterior IPL, RSP and the posterior PHC into an IPL-RSP-PHC system (dark blue in Fig. 3.13) distinct from the other regions of the default network.

These collective results thus illustrate patterns of connectivity that are largely captured by a relatively small number of interdigitated, large-scale networks but also reveal more detailed properties that suggest crosstalk and fractionation within the major networks.

Discussion

The present results suggest association cortex comprises the majority of the human cerebral mantle and is made up of multiple, interdigitated association networks. The properties of association networks were found to be quite different from that of sensory and motor cortices. Sensory and motor areas are embedded within cerebral networks that are organized in a topographic fashion forming preferentially local networks – meaning that adjacent areas tend to show strong functional coupling with one another. Hierarchical relations progress from early visual areas to premotor areas. By contrast, multiple association networks involve areas distributed throughout the cortex, always including discrete regions within prefrontal, parietal, temporal and midline cortices. These distributed association networks are interdigitated in a manner that yields complex zones, particularly in parietal and prefrontal association cortices. Within these zones, nearby regions possess markedly different connectivity patterns that can be explained by their being embedded within distinct association networks. In the following sections we explore the details of these patterns and discuss what the connectivity patterns suggest about how the human cerebral cortex may have expanded during evolution.

The cerebral cortex comprises multiple, distinct functionally coupled networks

A primary result of our analyses is the cerebral maps depicted in Figures 3.11 and 3.13. Figure 3.11 displays a coarse parcellation of the cerebral cortex into 7 functionally coupled networks, and Figure 3.13 displays a finer parcellation into 17 networks. These maps represent our current best estimate of the organization of the human cerebral cortex

based on fcMRI. The large number of contributing subjects (N = 1000) and surface-based alignment procedures helped to detect topographical details with considerable confidence. However, these maps are still limited in resolution owing to between-subject averaging and the acquisition resolution of the data, and will presumably be improved in the future. At their present resolution, they have been surprisingly informative for providing insights into cerebral organization and, as will be illustrated by our companion paper, they also provide a basis to explore the organization of subcortical structures (Buckner et al. 2011).

Two broad properties are immediately apparent when examining the maps, which will be the focus of discussion. First, sensorimotor and visual cortices form their own networks in the coarse parcellation that are fractionated into subnetworks in the finer parcellation. The fractionations do not follow simple divisions such as between somatosensory and motor areas along the central sulcus, or between early (e.g., V1) and late (e.g., V3) retinotopic visual areas in the occipital cortex. We will discuss hypotheses about what these fractionations might represent in upcoming sections. Second, association cortex comprises multiple, interdigitated networks that are distributed throughout cortex. Multiple aspects of these networks, in particular the properties of the coarse networks displayed in Figure 3.11, have previously been described using seed-based (e.g., Biswal et al. 1995; Greicius et al. 2003; Fox et al. 2006; Vincent et al. 2006) and independent component analysis (e.g., Beckmann et al. 2005; Damoiseaux et al. 2006; De Luca et al. 2006) approaches. Many aspects of the organization, especially within the higher resolution parcellation (Fig. 3.13), are novel. We will discuss the details of the organization of association cortex in upcoming sections with particular focus on

zones of parietal and prefrontal cortices that represent nexuses of convergence among multiple, distinct networks.

Visual cortex displays local, topographically organized functional coupling

Early visual areas were strongly functionally coupled to one another and only minimally correlated to regions outside of visual cortex. Examining the coupling properties more closely revealed evidence for an intrinsic gradient within the early visual cortex that likely corresponds to the transition from the central to peripheral visual field representations (Figs. 3.15 to 3.17). The division is not absolute (Fig. 3.18) but appears as an abrupt division into central and peripheral networks when assignments into distinct networks are forced, providing a convenient way to map the topographical organization across visual areas. Inspection of the boundaries of the functionally coupled networks on visual areas suggests that the division of lower visual areas into central and peripheral components might extend to higher visual areas. The ventral boundary of the central and peripheral visual systems continued outside the V1-V3 complex and divided V4v in two. Since the eccentricity representation of the V1-V3 complex is continuous through V4v (Brewer et al. 2005; Hadjikhani et al. 1998), it is likely that V4v was also divided into central and peripheral components. Anterior to V4v, at least two hemifield maps have been found, all of which have a distinctly large foveal representation and respond strongly to central visual stimuli throughout their extent (Brewer et al. 2005; Wandell et al. 2005), and are therefore consistent with the inclusion of these regions within the central visual system (but see Hadjikhani et al. 1998).

However, there were inconsistencies as might be expected because of limited resolution and the inherent complexity of the visual cortex (see Wandell et al. 2007 for a review). Multiple hemifield maps have been found in the extrastriate cortex lateral to the V1-V3 complex (DeYoe et al. 1996; Larsson and Heeger 2006; Tootell and Hadjikhani 2001), such as regions that are part of the object-selective lateral occipital complex (LOC; Malach et al. 1995) and motion-selective area MT+ (Huk et al. 2002; Malikovic et al. 2007; Tootell and Taylor 1995). The inclusion of these entire visual regions within the "central" visual system suggests a violation of the central-peripheral division in these areas, although we note that the ventral visual stream (of which human LOC is a part) is dominated by signals from the fovea in the macaque monkey (Baizer et al. 1991). The dorsal boundary of the central and peripheral visual networks continued outside the V1-V3 complex and cut through the hemifield maps dorsal and lateral to V3v, possibly including V3A, V3B and V7 (Larsson and Heeger 2006; Swisher et al. 2007; Tootell et al. 1998). Because these regions have separate foveal representation from the V1-V3 complex (Wandell et al. 2007) and because of the complex trajectory of the boundary through these regions, we were unable to judge whether the central-peripheral division applied to these regions.

The central-peripheral functional coupling of the human visual system is consistent with many aspects of known anatomy. Anatomical studies in non-human primates have shown that the topography of connections between visual areas generally respects the visual field representation (Cragg 1969; Maunsell and Van Essen 1983; Van Essen and Zeki 1978; Zeki 1969). For example, a region of V1 that responds strongly to a particular eccentricity and polar angle will project to the region of V2 that responds

strongly to the same eccentricity and polar angle, presumably because of feedforward input (Van Essen and Zeki 1978). Because of the larger receptive field size of neurons in V2, the degenerated target area tends to be larger than that of the source lesion. Our result of higher functional connectivity strength between V1c and V3c (as well as between V1p and V3p) than between V1c and V1p may reflect the topography of anatomical connections within the visual system.

If anatomical connectivity respects visuotopic representation and functional connectivity is *constrained* by anatomical connectivity, a question then arises as to why the clustering analysis divided the visual areas (especially the lower visual areas) into central and peripheral regions rather than into upper and lower visual fields? A split along the eccentricity axis is supported by proposals that higher visual areas are organized according to central versus peripheral field bias (Baizer et al. 1991; Grill-Spector and Malach 2004; Levy et al. 2001), although such an organization has also been disputed (Wandell et al. 2005; 2007). A more mundane and likely reason is that eccentricity representation runs in parallel across multiple visual areas in contrast with angular representation that alternates in visual field sign across multiple visual areas (see Fig. 1 in Larsson and Heeger 2006; Sereno et al. 1995). Because this study utilized smoothing and intersubject averaging to boost SNR, any topography in functional connectivity that respects the high spatial frequency of angular representation is likely to be washed out. The resulting limitation in spatial resolution might also explain why visual regions dominated by foveal signals are grouped entirely within the central visual system even though they possess quarterfield or hemifield representations spanning both central and peripheral vision.

Together these observations suggest that functional connectivity of the visual cortex followed the topographic organization of these areas up to a point. Certain observations, such as the lack of functional connectivity topography reflecting angular visual representation, could not be reconciled with prior anatomical observations. These differences may reflect the limitations of our approach, true differences between fcMRI and anatomical connectivity or novel connectivity findings that have yet to be revealed in anatomical studies. We will discuss these limitations and ambiguities later.

Somatomotor cortex displays topographical organization

Estimates of functional connectivity networks grouped multiple somatosensory and motor areas into a single functionally coupled network for the low-resolution estimate of cortical organization (Fig. 3.11) and into a dorsal-ventral division for the high-resolution estimate (Fig. 3.13)[5]. Like visual cortex, the somatomotor network was characterized by its strong functional coupling to nearby areas but absence of functional coupling to distributed regions across the cortex (barring regions across the insular cortex). Even when regional analyses were explored that did not constrain the topography to form separate networks, no evidence was found for functional coupling to distributed cortical regions. Figure 3.19 shows that the motor component of the somatomotor network included MI (area 4) and caudal premotor area 6, while the somatosensory component included SI and most, if not all of early somatosensory area 5L. The somatomotor network also included a small portion of the mid-cingulate sulcus and

[5] Auditory cortex was also functionally coupled to the ventral somatomotor network. However, as illustrated in Figure 3.14, this may be an artifact of signal bleeding across the insula in volumetric space. For this reason, while the finding may reflect a meaningful functional interaction, we do not discuss it further in the present paper.

possibly part of area 5M. Within the somatomotor cortex of non-human primates, areas 1 to 6 are densely, but not fully, connected (see meta-analysis in Felleman and Van Essen 1991) by association fibers that enter the white matter and re-enter the cortex (Jones et al. 1978).

The non-human primate premotor area 6 has been subdivided into rostral and caudal areas that may provide further insight into the functional connectivity patterns (Barbas and Pandya 1987; Matelli et al. 1985; 1991; Zilles et al. 1995). The caudal premotor areas are densely and topographically connected to M1, but not to the prefrontal cortex. In contrast, the rostral premotor areas are connected to prefrontal cortex but not M1 (Barbas and Pandya 1987; Luppino et al. 1993; Matelli et al. 1986). The caudal premotor areas are also more densely connected to each other than the adjacent rostral premotor areas. While there are competing hypotheses over the exact homology between primate and human premotor areas (Geyer 2004; Petrides 2005; Rizzolatti et al. 1998), converging studies have suggested a rostrocaudal subdivision of human premotor cortex (see chapter 4.4 of Geyer 2004 for a review), which might reflect the absorption of caudal human area 6 into the somatomotor network as revealed by functional coupling. Despite evidence that the early somatosensory and late motor fields are densely integrated, we must be cautious of the possibility of fMRI signal blurring across the central sulcus, which may cause an overestimation of functional coupling between the parallel strips of SI, MI and premotor area 6.

Of most interest, the analysis also revealed a dorsoventral division of the somatomotor strip, which was confirmed by targeted regional analyses (Fig. 3.20). In non-human primates, the connections between the different somatosensory-motor areas

are generally topographic, so that for example, the hand region of area 2 receives projections from the hand region of areas 3 and 1 (Pons and Kaas 1986). In addition, the somatomotor association fibers have been reported to terminate in mediolaterally oriented strips (see for example Fig. 4 in Jones et al. 1978; Jones and Wise 1977), although others have raised questions concerning the strip-like nature of callosal connections (Gould et al. 1986; Killackey et al. 1983). Our observations of fcMRI correlations within the human somatomotor cortex, whose anteroposterior extents were shorter than their mediolateral extents, were therefore consistent with the observations of ipsilateral strip-like anatomical connections. One possibility is that the dorsoventral boundary revealed by our clustering analysis might correspond to the boundary of the face and body representations.

Evidence for a prototype distributed cortical pathway

The results discussed above reveal interesting organizational properties of local networks of areas within sensorimotor and visual cortices. In considering the organization of the cerebral cortex, an immediate question arises as to how information in the sensory systems might propagate to influence motor representations? Functional connectivity is limited in its ability to provide insight into this question, but some aspects of the results are informative and consistent with anatomical and physiological studies of sensory-motor pathways.

The canonical sensory-motor pathway that has been studied in the monkey is the pathway that includes retinotopic visual cortex, the MT+ complex, parietal area LIP, and the FEF (e.g., Andersen et al. 1990; Colby and Goldberg 1999; Gold and Shadlen 2007; Shadlen and Newsome 2001). The basic idea is that incoming visual information

propagates from early visual areas to MT+, which provides constraints on decision processes that arise from interactions with LIP and FEF. FEF, in turn, interacts with motor regions to generate motor signals. Hierarchical anatomic connections support such a pathway (Felleman and Van Essen 2001; Maunsell and Van Essen 1983). The question here is whether the human functional connectivity results also reveal evidence for such a pathway and, if so, what properties emerge?

Of particular interest are the quantitative results presented in Figures 3.22 to 3.27 that reveal interactions between distinct networks. While primary visual cortex is largely absent functional coupling to association or premotor cortices, it is topographically coupled to MT+ (Fig. 3.22), which is in turn strongly coupled to aMT+ as well as modestly coupled to parietal regions including SPL7A (Figs. 3.24 and 3.25). aMT+ is functionally coupled to PrC_v and FEF (Fig. 3.25) completing the pathway. While the organization of the human MT+ complex is still unresolved, human MT+ is thought to include the human homologues of macaque MT, MST and FST (Amano et al. 2009; Huk et al. 2002; Kolster et al. 2010). Based on its location, aMT+ might correspond to macaque MST/FST (Maunsell and Van Essen 1983; Ungerleider and Desimone 1986) or TEO/PIT (Felleman and Van Essen 1991; von Bonin and Bailey 1947). Our observation that aMT+ is less correlated with V1 than MT+ (Figs. 3.22 and 3.23) is therefore consistent with multiple studies showing that macaque TEO/PIT or MST/FST is less densely connected with V1 compared with MT (Distler et al. 1993; Felleman and Van Essen 1991; Markov et al. 2010). Although there are uncertainties to using functional connectivity to infer hierarchical arrangements among areas, if one uses the simple assumption that the more strongly two areas are functionally coupled together, the closer

they are to one another in a processing hierarchy, a sensory-motor processing hierarchy emerges that is consistent with the extant literature (Figs. 3.28 and 3.29).

Analysis of interactions among networks illustrates a number of further points. Most critically, the hierarchy across networks reveals how a distributed network might serve as a bridge between sensory and motor networks that themselves possess preferentially local interactions (resulting in their parcellation into their own networks in Figs. 3.11 and 3.13). One speculation is that the distributed cortical network illustrated as the green network in Figure 3.11 -- and known within the neuroimaging literature as the dorsal attention system -- is the prototype distributed cortical network. It possesses multiple properties that are common to all association networks. Specifically, its component regions are distributed throughout temporal, parietal, and frontal cortices and show strong functional couplings between all pairs of regions (Fig. 3.32). We speculate that this network is a prototype because it is more strongly functionally coupled to extrastriate sensory regions and premotor regions than the remaining association networks that will be discussed later and also because it is well represented in the macaque. The presence of similar networks in humans and macaques suggests that they are homologous, and thus were present in the last common ancestor, which lived about 25-30 million years ago (Pilbeam and Young 2004). As will be discussed in the next section, the remaining distributed association networks, which in the human represent the majority of association cortex, display the same general organization but appear to have lost direct functional coupling to sensory and motor regions, at least insofar as measured by intrinsic functional connectivity.

Another important feature of this hierarchy is apparent when one considers finer details of the functional coupling patterns. Within the broad hierarchy, there is evidence for specialization indicative of parallel hierarchical arrangements. This is perhaps best illustrated by the differential functional coupling of premotor regions FEF and PrC_v with the multiple regions localized around the superior parietal lobule (Figs. 3.26 and 3.27). Anatomical tracing work in the macaque has suggested two segregated sensory-motor pathways from parietal cortex to dorsal and ventral aspects of frontal cortex, including premotor cortex (Kurata 1991; Rizzolatti et al. 1998; Tanné-Gariépy et al. 2002) and the frontal eye fields (Petrides and Pandya 2006; Stanton et al. 1995). These frontoparietal connections have a dorsomedial to ventrolateral axis: dorsal portions of caudal frontal cortex are preferentially connected to medial and dorsal parts of parietal cortex including the superior parietal lobule and medial parietal cortex, while caudal ventral frontal cortex preferentially communicates with lateral and ventral aspects of parietal cortex and largely lacks connections with dorsal and medial parietal areas. Our demonstration that PrC_v was strongly correlated with more ventral portions of rostral SPL and IPS, while FEF was strongly correlated with caudal SPL and IPS (Figs. 3.26 and 3.27) is consistent with descriptions of frontoparietal sensory-motor circuits in the macaque. Thus, evidence for specialization of subpathways is present in this canonical sensory-motor pathway. Taking the speculation that this canonical pathway represents the prototype distributed association network, it is tempting to wonder whether the interdigitated association networks that comprise the remaining human association cortex are evolutionary expansions of this basic prototype with multiple, interdigitated pathways that have become nearly completely differentiated.

Association cortices are nexuses of regions with distinct connectivity fingerprints.

Association cortex, in particular parietal cortex near the inferior parietal lobule, has been challenging to characterize. Human association cortex shows disproportionate expansion in relation both to macaque and great apes (Preuss 2004; Van Essen and Dierker 2007; Hill et al. 2010). In a few instances, it is an open question as to whether homologies should be expected (Orban et al. 2006). For example, in his seminal work in 1909, Korbinian Brodmann noted that the human inferior parietal lobule included two cytoarchitectonic areas that are absent in the monkey (areas 39 and 40). The possibility that these association areas are vastly expanded in hominid evolution, or are even novel areas altogether, figured prominently in the classic description of disconnection syndromes by Geschwind (1965). For these reasons anatomic connectivity in the monkey cannot uniformly be presumed to apply to the human. Adding further complication, nearby regions of association cortex are often active across quite distinct forms of tasks suggesting functional diversity (e.g., Culham and Kanwisher 2001). As extreme examples of functional diversity, parietal regions near the superior parietal lobule, including those discussed in the preceding section, respond during sensory-motor decision tasks (Corbetta and Shulman 2002). Regions near the temporoparietal junction respond during social tasks that require participants to infer what others are thinking (Saxe 2006; Van Overwalle and Baetens 2009), and regions within the caudal portion of the inferior parietal lobule respond during episodic remembering (Cabeza et al. 2008; Vilberg and Rugg 2008; Wagner et al. 2005).

Our results demonstrate that parietal association cortex includes multiple nearby regions that possess markedly different connectivity profiles that parallel similar distinctions in prefrontal cortex. The results in parietal cortex are anticipated by both anatomic studies in the monkey and prior studies using human functional connectivity. Specifically, the caudal portion of macaque 7a, labeled Opt by Pandya and colleagues (Pandya and Seltzer 1982), has connections to the parahippocampal cortex, retrosplenial cortex, and posterior cingulate (Seltzer and Pandya 1994; Andersen et al. 1990; Suzuki et al. 1994; Lavenex et al. 2002). Nearby areas, such as LIP, are preferentially connected to visual association cortex and premotor areas leading Andersen et al. (1990) to note that "area 7a appears to be very different from other visual areas in the inferior parietal lobule in that it is the only area that connects to some of the highest centers of the brain." Examination of functional connectivity of parietal association cortex in the human has also revealed notable diversity. Vincent et al. (2006) illustrated that neighboring parietal regions are functionally coupled to distinct sensory-motor and limbic circuits. In later studies, parietal association cortex was found to possess between three (Vincent et al. 2008) and four (Nelson et al. 2010) distinct zones distinguished by their functional connectivity profiles (see also Sestieri et al. 2011).

Differential functional coupling across parietal and prefrontal regions are displayed in Figures 3.30 and 3.31. Drawing from Passingham and colleagues (2002), we refer to these regional connectivity profiles as 'fingerprints' because they illustrate the connectivity patterns across regions that make them distinct. In examining the many fingerprints, several principles emerge that provide insight into cortical organization. First, nearby regions can show abrupt transitions in their connectivity fingerprints. The

transitions from SPL7A to $IPS3_l$ and from $IPS3_l$ to PGp_d are such examples. SPL7A, which may be at or near the human homologue to macaque LIP, is functionally coupled to extrastriate (MT+ and aMT+) and premotor (FEF and PrC_v) regions. $IPS3_l$ shows a fundamentally distinct connectivity fingerprint with coupling to prefrontal regions that are within dorsolateral prefrontal cortex (PFC_l and PFC_{lp}) and amodal posterior temporal association regions (ITG). $IPS3_l$ is absent coupling to sensory or motor regions. PGp_d is distinguished by prominent functional coupling to limbic regions including posterior cingulate (PCC), retrosplenial cortex (RSP), and the medial temporal lobe (PHC). This tripartite division separates the major parietal zones that form the dorsal attention, frontoparietal control, and default networks discussed extensively in the human neuroimaging literature (green, orange, and red networks in Fig. 3.11).

Second, within these broad divisions there are further distinctions that demarcate more subtle regional differences. Across these regions, most connectivity properties are shared but there are also key differences, forming 'connectional families' of regions (see Passingham et al. 2002 for discussion). These differences within connectional families lead to the finer parcellation observed in Figure 3.13 and are likely of functional importance. For example, the TPJ and PGp_v possess similar connectivity fingerprints, and both fall within the broader network that is globally called the default network. However, the TPJ is preferentially coupled to medial prefrontal regions (PFC_{dm}), the posterior cingulate cortex (PCC) and precuneus (pCun), and the superior temporal sulcus (STS and STS_p). While PGp_v possesses a broadly similar fingerprint, it is also prominently coupled to regions associated with the medial temporal lobe memory system (RSP and PHC). This is of particular interest because both of these parietal association regions have been

proposed to be involved with higher mental functions linked to internal mentation and social cognition (see Buckner et al. 2008 for review), but functional distinctions have also been noted (e.g., Rosenbaum et al. 2007).

The final organization principle that emerges is that association regions belonging to the same connectional families can always be found widely distributed across the cortical mantle. Contrasting the fingerprints of regions within prefrontal cortex (Fig. 3.31) with those falling within parietal cortex (Fig. 3.30) illustrates this last principle. PFC_{dm} and TPJ are prime examples. These regions possess nearly the same functional connectivity fingerprints that differ from nearby regions within their own lobes. This accounts for why these distributed regions form such tightly coupled functional connectivity networks and suggests that association cortex might be best conceptualized as a series of interdigitated, distributed networks.

Association cortex is comprised of multiple, interdigitated large-scale circuits

The majority of the human cerebral cortex is made up of multiple large-scale networks that include functionally coupled regions distributed across the brain. Such organization is apparent in prior studies (e.g., Beckmann et al. 2005; Damoiseaux et al. 2006; De Luca et al. 2006; Fox et al. 2006; Greicius et al. 2003; 2004; Vincent et al. 2008) and is evident in all of the analyses presented here. By analyzing the complete topography of the cortical surface, we were further able to illustrate that the multiple, distributed networks are interdigitated with one another forming complex convergence zones in parietal and prefrontal association cortices (Figs. 3.32 to 3.35). What do these patterns suggest about the organization of the cerebral cortex?

At the broadest level, these observations emphasize the need to adopt network approaches when exploring cerebral function. By network approach, we refer to the idea that the relevant functional unit may be the interconnected network itself, as suggested by Mesulam (1981; 1986) and Goldman-Rakic (1988). Mesulam (1981) proposed a network approach as an alternative to centrist approaches to localization, in which complex functions relied on specific cortical areas exclusively devoted to that function. While recognizing that functional specializations exist among areas of the same network, the network framework emphasizes that functions arise as emergent properties of these reciprocally connected systems of brain areas (see Fig. 4 of Mesulam 1981; 1990). In other words, distributed systems of areas, spanning different cortical lobes and subcortical structures, form functional units via their dense interconnections. This is a quite different organization than is evident in sensory cortex, which is characterized by dense connectivity among local areas. The two frameworks are not entirely different because all areas are presumably embedded within systems of interacting brain areas; however, the focus in many theories is on processing specialization within areas and processing hierarchies among neighboring areas. The present analyses suggest that functional unit of interest may be the distributed network itself.

Goldman-Rakic (1988) offered three specific anatomic observations that provide evidence for distributed cerebral networks. First, prefrontal and parietal areas that are directly connected to one another also tend to have convergent projections to additional temporal and limbic areas (see Fig. 3 of Goldman-Rakic 1988). Second, interconnected association areas are tied together by common thalamic connections. And third, arguing against a typical hierarchical model of cortical organization, interconnected association

areas tend not to have laminar projection patterns with clear feedforward and feedback relations (also see Felleman and Van Essen 1991). We suspect that the distributed networks that comprise the majority of human association cortex are networks of this type – highly interconnected, without strong hierarchical relations among areas, and integrated into a common functional unit of some form. This does not mean that areas within prefrontal and parietal cortices are making the same contributions to the network, but the emphasis does shift to asking how the separate networks make distinct functional contributions rather than asking how different areas within prefrontal or parietal cortices may be locally differentiated. That is, association cortex is characterized by multiple modules (Bullmore and Sporns 2009) that are each comprised of nodes distributed widely across the cortex.

Of further interest, the distributed cerebral networks converge on regions of association cortex that are late to develop in terms of myelination (see Fig. 3 of Catani and ffytche 2005) and cortical surface area (Hill et al. 2010), and are expanded in the human brain relative to the modern macaque brain (Van Essen and Dieker 2007). For these reasons, it is likely that distributed association networks have been under strong selective pressure to expand in recent hominid evolution. The network parcellations presented in Figures 3.11 and 3.13 provide a current best estimate of the organization of the interdigitated networks that comprise human association cortex.

Caveats and limitations

Measuring functional connectivity is not the same as directly measuring anatomical connectivity. Functional connectivity is *constrained* by anatomic connectivity

(e.g., Johnston et al. 2008; Honey et al. 2009) but those constraints are not restricted to monosynaptic connectivity. For example, functional coupling is present between the two hemispheres for striate cortex in the macaque (Vincent et al. 2007) while interhemispheric connections are absent except at the border of V1 (Van Essen and Zeki 1978). The pervasiveness of functional coupling is both a weakness and strength of the technique as it allows one to map large-scale polysynaptic circuits, but leaves ambiguities and uncertainties, which will require follow-up by other methods such as diffusion imaging techniques and detailed examination of homologies to non-human primates. Cerebrocerebellar circuits are a place that perhaps best illustrates that functional connectivity is constrained by anatomy but is more pervasive than monosynaptic connectivity. Cerebrocerebellar circuits – which are exclusively polysynaptic (Evarts and Thach 1969; Kemp and Powell 1971; Strick 1985) – demonstrate functional coupling that tracks the contralateral organization of anatomic projections and is topographically specific as described in our companion paper (Buckner et al. 2011). Thus, functional connectivity is informative but should not be considered a direct measure of anatomic connectivity. Functional connectivity also appears sensitive to other factors, including recent experience and the state of the subject during scanning (Fox and Raichle 2007; Moeller et al. 2009; Buckner 2010). An assumption made in the present paper is that the dominant contribution to the measured correlations reflect stable properties of cortical architecture – an assumption we believe is warranted but nonetheless needs to be made explicit as boundary conditions and violations of this assumption may emerge.

A further limitation of the present work is resolution. Even at the relatively finer resolution of the 17-network estimate, discrete components of a given network likely

span multiple cytoarchitecturally distinct cortical areas. The association networks described in this paper are at a coarser resolution than the networks inferred by Goldman-Rakic (1988) and others in the macaque. Our limited data resolution, as a result of voxel size, smoothing and intersubject averaging including potential errors in surface-based alignment, may miss important features of the cortical topography and the results should be interpreted accordingly. Future, high resolution studies of individuals may provide better estimates of cortical topography.

A final limitation is our use of clustering to parcellate the cerebral cortex. The assumption made by the clustering approach is that each vertex belongs to a single network. Our seed-based analyses (Figs. 3.32-3.35) suggest that this is a reasonable beginning point for analysis even though crosstalk exists between networks. However, there are specific places where the parcellation results might be particularly sensitive to inaccuracies, including the characterization of cortical regions that serve as putative hubs of communication between networks (Buckner et al. 2009; Hagmann et al. 2008; Mesulam 1998). We also note that the 17-network estimate does not cleanly fractionate individual networks within the 7-network estimate, implying that cortical networks are not spatially organized in a strictly hierarchical fashion[6], like that suggested in the toy example (Fig. 3.5). Our efforts to enforce strict subdivisions of coarser networks by using hierarchical clustering (not shown) failed to provide stable results across the Discovery and Replication datasets. Recent advances in graph theoretic clustering approaches are promising in providing the possibility for regions to belong to multiple networks or communities (e,g., Ahn et al. 2010).

---

[6] Here "hierarchy" refers to the spatial organization of the networks rather than the concept of "hierarchical processing pathways".

Conclusions

Different regions of the cerebral cortex display distinct characteristics. Functional connectivity of retinotopic visual areas display dense local functional coupling that is organized across areas in a fashion that respects functional topography. Association cortex is comprised of multiple, interdigitated large-scale networks that, while exhibiting crosstalk, possess predominantly parallel organization. The map of these cerebral networks is provided as a reference for future functional characterization and confirmation by complementary approaches that can directly visualize anatomic connectivity.

References

Ahn Y-Y, Bagrow JP, Lehmann S. Link communities reveal multiscale complexity in networks. *Nature* 466: 761-764, 2010.

Amano K, Wandell BA, Dumoulin SO. Visual field maps, population receptive field sizes, and visual field coverage in the human MT+ complex. *J Neurophysiol* 102: 2704-2718, 2009.

Amunts K, Lenzen M, Friederici AD, Schleicher A, Morosan P, Palomero-Gallagher N, Zilles K. Broca's region: Novel organizational principles and multiple receptor mapping. *PLoS Biol* 8: e1000489, 2010.

Amunts K, Malikovic A, Mohlberg H, Schormann T, Zilles K. Brodmann's areas 17 and 18 brought into stereotaxic space - Where and how variable? *Neuroimage* 11: 66-84, 2000.

Amunts K, Schleicher A, Bürgel U, Mohlberg H, Uylings HBM, Zilles K. Broca's region revisited: Cytoarchitecture and intersubject variability. *J Comp Neurol* 412: 319-341, 1999.

Andersen RA, Buneo CA. Intentional maps in posterior parietal cortex. *Annu Rev Neurosci* 25: 189-220, 2002.

Andersen RA, Asanuma C, Essick G, Siegel RM. Corticocortical connections of anatomically and physiologically defined subdivisions within the inferior parietal lobule. *J Comp Neurol* 296: 65-113, 1990.

Andrews-Hanna JR, Reidler JS, Sepulcre J, Poulin R, Buckner RL. Functional-anatomic fractionation of the brain's default network. *Neuron* 65: 550-562, 2010.

Baizer JS, Ungerleider LG, Desimone R. Organization of visual inputs to the inferior temporal and posterior parietal cortex in macaques. *J Neurosci* 11: 168-190, 1991.

Balasubramanian M, Polimeni J, Schwartz EL. The V1-V2-V3 complex: Quasiconformal dipole maps in primate striate and extra-striate cortex. *Neural Networks* 15: 1157-1163, 2002.

Barbas H, Pandya D. Architecture and frontal cortical connections of the premotor cortex (area 6) in the rhesus monkey. *J Comp Neurol* 256: 211-228, 1987.

Basser PJ, Mattiello J, LeBihan D. Estimation of the effective self-diffusion tensor from the NMR spin echo. *J Magn Reson B* 103: 247-254, 1994.

Beckmann CF, DeLuca M, Devlin JT, Smith SM. Investigations into resting-state connectivity using independent component analysis. *Philos Trans R Soc Lond B Biol Sci* 360: 1001-1013, 2005.

Beckmann CF, Smith SM. Probabilistic independent component analysis for functional magnetic resonance imaging. *IEEE Trans Med Imaging* 23: 137-152, 2004.

Bellec P, Rosa-Neto P, Lyttelton OC, Benali H, Evans AC. Multi-level bootstrap analysis of stable clusters in resting-state fMRI. *Neuroimage* 51: 1126-1139, 2010.

Ben-Hur A, Elisseeff A, Guyon I. A stability based method for discovering structure in clustered data. *Pacific Symposium on Biocomputing:* 6-17, 2002.

Binkofski F, Buccino G, Posse S, Seitz RJ, Rizzolatti G, Freund H-J. A fronto-parietal circuit for object manipulation in man: Evidence from an fMRI-study. *Eur J Neurosci* 11: 3276-3286, 1999.

Binkofski F, Dohle C, Posse S, Stephan KM, Hefter H, Seitz RJ, Freund H-J. Human anterior intraparietal area subserves prehension: a combined lesion and functional MRI activation study. *Neurology* 50: 1253-1259, 1998.

Biswal B, Yetkin FZ, Haughton VM, Hyde JS. Functional connectivity in the motor cortex of resting human brain using echo-planar MRI. *Magn Reson Med* 34: 537-541, 1995.

Biswal BB, Mennes M, Zuo X-N, Gohel S, Kelly C, Smith SM, Beckmann CF, Adelstein JS, Buckner RL, Colcombe S, Dogonowski A-M, Ernst M, Fair D, Hampson M, Hoptman MJ, Hyde JS, Kiviniemi VJ, Kötter R, Li S-J, Lin C-P, Lowe MJ, Mackay C, Madden DJ, Madsen KH, Margulies DS, Mayberg HS, McMahon K, Monk CS, Mostofsky SH, Nagel BJ, Pekar JJ, Peltier SJ, Petersen SE, Riedl V, Rombouts SARB, Rypma B, Schlaggar BL, Schmidt S, Seidler RD, Siegle GJ, Sorg C, Teng G-J, Veijola J, Villringer A, Walter M, Wang L, Weng X-C, Whitfield-Gabrieli S, Williamson P, Windischberger C, Zang Y-F, Zhang H-Y, Castellanos FX, Milham MP. Toward discovery science of human brain function. *Proc Natl Acad Sci USA* 107: 4734-4739, 2010.

Blinkov SM, Glezer II. *The Human Brain in Figures and Tables.* New York: Basic Books 1968.

Brewer AA, Liu J, Wade AR, Wandell BA. Visual field maps and stimulus selectivity in human ventral occipital cortex. *Nat Neurosci* 8: 1102-1109, 2005.

Brodmann K. *Localization in the Cerebral Cortex.* Translated by Garey LJ. New York: Springer 1909/2006.

Buckner RL. Human functional connectivity: New tools, unresolved questions. *Proc Natl Acad Sci USA* 107: 10769-10770, 2010.

Buckner RL, Andrews-Hanna JR, Schacter DL. The brain's default network: Anatomy, function, and relevance to disease. *Ann N Y Acad Sci* 1124: 1-38, 2008.

Buckner RL, Krienen FM, Castellanos A, Diaz JC, Yeo BTT. The organization of the human cerebellum estimated by functional connectivity. *J Neurophysiol*, 106: 2322-2345, 2011.

Buckner RL, Sepulcre J, Talukdar T, Krienen FM, Liu H, Hedden T, Andrews-Hanna JR, Sperling RA, Johnson KA. Cortical hubs revealed by intrinsic functional connectivity: Mapping, assessment of stability, and relation to Alzheimer's disease. *J Neurosci* 29: 1860-1873, 2009.

Bullmore E, Sporns O. Complex brain networks: Graph theoretical analysis of structural and functional systems. *Nat Rev Neurosci* 10:186-198, 2009.

Cabeza R, Ciaramelli E, Olson IR, Moscovitch M. The parietal cortex and episodic memory: An attentional account. *Nat Rev Neurosci* 9: 613-625, 2008.

Carmichael ST, Price JL. Limbic connections of the orbital and medial prefrontal cortex in macaque monkeys. *J Comp Neurol* 363: 615-641, 1995.

Caspers S, Eickhoff SB, Geyer S, Scheperjans F, Mohlberg H, Zilles K, Amunts K. The human inferior parietal lobule in stereotaxic space. *Brain Struct Funct* 212: 481-495, 2008.

Caspers S, Geyer S, Schleicher A, Mohlberg H, Amunts K, Zilles K. The human inferior parietal cortex: Cytoarchitectonic parcellation and interindividual variability. *Neuroimage* 33: 430-448, 2006.

Catani M, ffytche DH. The rises and falls of disconnection syndromes. *Brain* 128:2224-2239, 2005.

Cavada C, Goldman-Rakic PS. Posterior parietal cortex in rhesus monkey: II. Evidence for segregated corticocortical networks linking sensory and limbic areas with the frontal lobe. *J Comp Neurol* 287: 422-445, 1989a.

Cavada C, Goldman-Rakic PS. Posterior parietal cortex in rhesus monkey: I. Parcellation of areas based on distinctive limbic and sensory corticocortical connections. *J Comp Neurol* 287: 393-421, 1989b.

Choi H-J, Zilles K, Mohlberg H, Schleicher A, Fink GR, Armstrong E, Amunts K. Cytoarchitectonic identification and probabilistic mapping of two distinct areas within the anterior ventral bank of the human intraparietal sulcus. *J Comp Neurol* 495: 53-69, 2006.

Cohen AL, Fair DA, Dosenbach NUF, Miezin FM, Dierker D, Van Essen DC, Schlaggar BL, Petersen SE. Defining functional areas in individual human brains using resting functional connectivity MRI. *Neuroimage* 41: 45-57, 2008.

Colby CL, Goldberg ME. Space and attention in parietal cortex. *Annu Rev Neurosci* 22:319-349, 1999.

Connolly JD, Goodale MA, Desouza JF, Menon RS, Vilis T. A comparison of frontoparietal fMRI activation during anti-saccades and anti-pointing. *J Neurophysiol* 84: 1645-1655, 2000.

Connolly JD, Goodale MA, Menon RS, Munoz DP. Human fMRI evidence for the neural correlates of preparatory set. *Nat Neurosci* 5: 1345-1352, 2002.

Corbetta M, Akbudak E, Conturo TE, Snyder AZ, Ollinger JM, Drury HA, Linenweber MR, Petersen SE, Raichle ME, Van Essen DC, Shulman GL. A common network of functional areas for attention and eye movements. *Neuron* 21: 761-773, 1998.

Corbetta M, Shulman GL. Control of goal-directed and stimulus-driven attention in the brain. *Nat Rev Neurosci* 3: 201-215, 2002.

Cragg BG. The topography of the afferent projections in the circumstriate visual cortex of the monkey studied by the Nauta method. *Vision Res* 9: 733-747, 1969.

Culham JC, Danckert SL, DeSouza JFX, Gati JS, Menon RS, Goodale MA. Visually guided grasping produces fMRI activation in dorsal but not ventral stream brain areas. *Exp Brain Res* 153: 180-189, 2003.

Culham JC, Kanwisher NG. Neuroimaging of cognitive functions in human parietal cortex. *Curr Opin Neurobiol* 11: 157-163, 2001.

Dale AM, Fischl B, Sereno MI. Cortical surface-based analysis - I. Segmentation and surface reconstruction. *Neuroimage* 9: 179-194, 1999.

Damoiseaux JS, Rombouts SARB, Barkhof F, Scheltens P, Stam CJ, Smith SM, Beckmann CF. Consistent resting-state networks across healthy subjects. *Proc Natl Acad Sci USA* 103: 13848-13853, 2006.

De Luca M, Beckmann CF, De Stefano N, Matthews PM, Smith SM. fMRI resting state networks define distinct modes of long-distance interactions in the human brain. *Neuroimage* 29: 1359-1367, 2006.

DeYoe EA, Carman GJ, Bandettini P, Glickman S, Wieser J, Cox R, Miller D, Neitz J. Mapping striate and extrastriate visual areas in human cerebral cortex. *Proc Natl Acad Sci USA* 93: 2382-2386, 1996.

Dickson J, Drury H, Van Essen DC. 'The surface management system' (SuMS) database: A surface-based database to aid cortical surface reconstruction, visualization and analysis. *Philos Trans R Soc Lond B Biol Sci* 356: 1277-1292, 2001.

Disbrow E, Litinas E, Recanzone GH, Padberg J, Krubitzer L. Cortical connections of the second somatosensory area and the parietal ventral area in macaque monkeys. *J Comp Neurol* 462: 382-399, 2003.

Distler C, Boussaoud D, Desimone R, Ungerleider LG. Cortical connections of inferior temporal area TEO in macaque monkeys. *J Comp Neurol* 334: 125-150, 1993.

Dosenbach NUF, Fair DA, Miezin FM, Cohen AL, Wenger KK, Dosenbach RAT, Fox MD, Snyder AZ, Vincent JL, Raichle ME, Schlaggar BL, Petersen SE. Distinct brain networks for adaptive and stable task control in humans. *Proc Natl Acad Sci USA* 104: 11073-11078, 2007.

Dow BM, Snyder AZ, Vautin RG, Bauer R. Magnification factor and receptive field size in foveal striate cortex of the monkey. *Exp Brain Res* 44: 213-228, 1981.

Eickhoff SB, Stephan KE, Mohlberg H, Grefkes C, Fink GR, Amunts K, Zilles K. A new SPM toolbox for combining probabilistic cytoarchitectonic maps and functional imaging data. *Neuroimage* 25: 1325-1335, 2005.

Engel SA, Glover GH, Wandell BA. Retinotopic organization in human visual cortex and the spatial precision of functional MRI. *Cereb Cortex* 7: 181-192, 1997.

Engel SA, Rumelhart DE, Wandell BA, Lee AT, Glover GH, Chichilnisky EJ, Shadlen MN. fMRI of human visual cortex. *Nature* 369: 525, 1994.

Evarts EV, Thach WT. Motor mechanisms of the CNS: Cerebrocerebellar interrelations. *Ann Rev Physiol* 31:451-498, 1969.

Faillenot I, Sunaert S, Van Hecke P, Orban GA. Orientation discrimination of objects and gratings compared: An fMRI study. *Eur J Neurosci* 13: 585-596, 2001.

Felleman DJ, Van Essen DC. Distributed hierarchical processing in the primate cerebral cortex. *Cereb Cortex* 1: 1-47, 1991.

Fischl B, Liu A, Dale AM. Automated manifold surgery: Constructing geometrically accurate and topologically correct models of the human cerebral cortex. *IEEE Trans Med Imaging* 20: 70-80, 2001.

Fischl B, Rajendran N, Busa E, Augustinack J, Hinds O, Yeo BTT, Mohlberg H, Amunts K, Zilles K. Cortical folding patterns and predicting cytoarchitecture. *Cereb Cortex* 18: 1973-1980, 2008.

Fischl B, Sereno MI, Dale AM. Cortical surface-based analysis - II: Inflation, flattening, and a surface-based coordinate system. *Neuroimage* 9: 195-207, 1999a.

Fischl B, Sereno MI, Tootell RBH, Dale AM. High-resolution intersubject averaging and a coordinate system for the cortical surface. *Hum Brain Mapp* 8: 272-284, 1999b.

Fox MD, Snyder AZ, Vincent JL, Corbetta M, Van Essen DC, Raichle ME. The human brain is intrinsically organized into dynamic, anticorrelated functional networks. *Proc Natl Acad Sci USA* 102: 9673-9678, 2005.

Fox MD, Corbetta M, Snyder A, Vincent J, Raichle ME. Spontaneous neuronal activity distinguishes human dorsal and ventral attention systems. *Proc Natl Acad Sci USA* 103: 10046, 2006.

Fox MD, Raichle ME. Spontaneous fluctuations in brain activity observed with functional magnetic resonance imaging. *Nat Rev Neurosci* 8: 700-711, 2007.

Frahm HD, Stephan H, Baron G. Comparison of brain structure volumes in Insectivora and Primates: V. Area striata (AS). *J. Hirnforsch* 25:537-577, 1984.

Friedman DP. Laminar patterns of termination of cortico-cortical afferents in the somatosensory system. *Brain Res* 273: 147-151, 1983.

Friston KJ. Functional and effective connectivity in neuroimaging: A synthesis. *Hum Brain Mapp* 2: 56-78, 1994.

Geschwind N. Disconnexion syndromes in animals and man. I. *Brain* 88:237-294, 1965.

Geyer S. The microstructural border between the motor and the cognitive domain in the human cerebral cortex. *Adv Anat Embryol Cell Biol* 174: 1-89, 2004.

Geyer S, Ledberg A, Schleicher A, Kinomura S, Schormann T, Bürgel U, Klingberg T, Larsson J, Zilles K, Roland PE. Two different areas within the primary motor cortex of man. *Nature* 382: 805-807, 1996.

Geyer S, Schleicher A, Zilles K. Areas 3a, 3b, and 1 of human primary somatosensory cortex 1. Microstructural organization and interindividual variability. *Neuroimage* 10: 63-83, 1999.

Gold JI, Shadlen MN. The neural basis of decision making. *Annu Rev Neurosci* 30: 535-574, 2007.

Goldman-Rakic PS. Topography of cognition: Parallel distributed networks in primate association cortex. *Annu Rev Neurosci* 11: 137-156, 1988.

Golland P, Golland Y, Malach R. Detection of spatial activation patterns as unsupervised segmentation of fMRI data. In *Proc. MICCAI: Medical Image Computing and Computer Assisted Intervention, LNCS 5241:745-753*, 2007.

Gould HJ, Cusick CG, Pons TP, Kaas JH. The relationship of corpus callosum connections to electrical stimulation maps of motor, supplementary motor, and the frontal eye fields in owl monkeys. *J Comp Neurol* 247: 297-325, 1986.

Grefkes C, Geyer S, Schormann T, Roland P, Zilles K. Human somatosensory area 2: Observer-independent cytoarchitectonic mapping, interindividual variability, and population map. *Neuroimage* 14: 617-631, 2001.

Grefkes C, Weiss PH, Zilles K, Fink GR. Crossmodal processing of object features in human anterior intraparietal cortex: An fMRI study implies equivalencies between humans and monkeys. *Neuron* 35: 173-184, 2002.

Greicius MD, Krasnow B, Reiss AL, Menon V. Functional connectivity in the resting brain: A network analysis of the default mode hypothesis. *Proc Natl Acad Sci USA* 100: 253-258, 2003.

Greicius MD, Srivastava G, Reiss AL, Menon V. Default-mode network activity distinguishes Alzheimer's disease from healthy aging: Evidence from functional MRI. *Proc Natl Acad Sci USA* 101: 4637-4642, 2004.

Greve DN, Fischl B. Accurate and robust brain image alignment using boundary-based registration. *Neuroimage* 48: 63-72, 2009.

Grill-Spector K, Malach R. The human visual cortex. *Annu Rev Neurosci* 27: 649-677, 2004.

Hadjikhani N, Liu A, Dale A, Cavanagh P, Tootell RBH. Retinotopy and color sensitivity in human visual cortical area V8. *Nat Neurosci* 1: 235-241, 1998.

Hagler DJ, Riecke L, Sereno MI. Parietal and superior frontal visuospatial maps activated by pointing and saccades. *Neuroimage* 35: 1562-1577, 2007.

Hagmann P, Cammoun L, Gigandet X, Meuli R, Honey CJ, Wedeen VJ, Sporns O. Mapping the structural core of human cerebral cortex. *PLoS Biol* 6: e159, 2008.

Heide W, Binkofski F, Seitz RJ, Posse S, Nitschke MF, Freund H-J, Kömpf D. Activation of frontoparietal cortices during memorized triple-step sequences of saccadic eye movements: An fMRI study. *Eur J Neurosci* 13: 1177-1189, 2001.

Hilgetag C, O'Neill M, Young M. Indeterminate organization of the visual system. *Science* 271:776-777, 1996.

Hill J, Inder T, Neil J, Dierker D, Harwell J, Van Essen D. Similar patterns of cortical expansion during human development and evolution. *Proc Natl Acad Sci USA* 107: 13135-13140, 2010.

Hinds O, Polimeni JR, Rajendran N, Balasubramanian M, Amunts K, Zilles K, Schwartz EL, Fischl B, Triantafyllou C. Locating the functional and anatomical boundaries of human primary visual cortex. *Neuroimage* 46: 915-922, 2009.

Hinds OP, Rajendran N, Polimeni JP, Augustinack JC, Wiggins G, Wald LL, Diana Rosas HD, Potthast A, Schwartz EL, Fischl B. Accurate prediction of V1 location from cortical folds in a surface coordinate system. *Neuroimage* 39: 1585-1599, 2008.

Honey CJ, Sporns O, Cammoun L, Gigandet X, Thiran JP, Meuli R, Hagmann P. Predicting human resting-state functional connectivity from structural connectivity. *Proc Natl Acad Sci USA* 106: 2035-2040, 2009.

Hubel DH, Wiesel TN. Receptive fields, binocular interaction and functional architecture in the cat's visual cortex. *J Physiol* 160: 106-154, 1962.

Huk AC, Dougherty RF, Heeger DJ. Retinotopy and functional subdivision of human areas MT and MST. *J Neurosci* 22: 7195-7205, 2002.

Iwamura Y. Hierarchical somatosensory processing. *Curr Opin Neurobiol* 8: 522-528, 1998.

James W. *Principles of Psychology, Vol 1*. New York: Holt 1890.

Jenkinson M, Bannister P, Brady M, Smith S. Improved optimization for the robust and accurate linear registration and motion correction of brain images. *Neuroimage* 17: 825-841, 2002.

Johansen-Berg H, Behrens TEJ, Robson MD, Drobnjak I, Rushworth MFS, Brady JM, Smith SM, Higham DJ, Matthews PM. Changes in connectivity profiles define functionally distinct regions in human medial frontal cortex. *Proc Natl Acad Sci USA* 101: 13335-13340, 2004.

Johnston JM, Vaishnavi SN, Smyth MD, Zhang D, He BJ, Zempel JM, Shimony JS, Snyder AZ, Raichle ME. Loss of resting interhemispheric functional connectivity after complete section of the corpus callosum. *J Neurosci* 28: 6453-6458, 2008.

Jones EG, Coulter JD, Hendry SHC. Intracortical connectivity of architectonic fields in the somatic sensory, motor and parietal cortex of monkeys. *J Comp Neurol* 181: 291-347, 1978.

Jones EG, Powell TPS. An anatomical study of converging sensory pathways within the cerebral cortex of the monkey. *Brain* 93: 793-820, 1970.

Jones EG, Wise SP. Size, laminar and columnar distribution of efferent cells in the sensory-motor cortex of monkeys. *J Comp Neurol* 175: 391-438, 1977.

Kaas JH. The organization of neocortex in mammals: Implications for theories of brain function. *Annu Rev Psychol* 38: 129-151, 1987.

Kemp JM, Powell TPS. The connexions of the striatum and globus pallidus: Synthesis and speculation. *Phil Trans R Soc Lond B* 262:441-457, 1971.

Killackey HP, Gould HJ, Cusick CG, Pons TP, Kaas JH. The relation of corpus callosum connections to architectonic fields and body surface maps in sensorimotor cortex of new and old world monkeys. *J Comp Neurol* 219: 384-419, 1983.

Kolster H, Peeters R, Orban GA. The retinotopic organization of the human middle temporal area MT/V5 and its cortical neighbors. *J Neurosci* 30: 9801-9820, 2010.

Kondo H, Saleem KS, Price JL. Differential connections of the temporal pole with the orbital and medial prefrontal networks in macaque monkeys. *J Comp Neurol* 465: 499-523, 2003.

Koyama M, Hasegawa I, Osada T, Adachi Y, Nakahara K, Miyashita Y. Functional magnetic resonance imaging of macaque monkeys performing visually guided saccade tasks: Comparison of cortical eye fields with humans. *Neuron* 41: 795-807, 2004.

Kurata K. Corticocortical inputs to the dorsal and ventral aspects of the premotor cortex of macaque monkeys. *Neurosci Res* 12: 263-280, 1991.

Kwong KK, Belliveau JW, Chesler DA, Goldberg IE, Weisskoff RM, Poncelet BP, Kennedy DN, Hoppel BE, Cohen MS, Turner R, Cheng H-M, Brady T, Rosen BR. Dynamic magnetic resonance imaging of human brain activity during primary sensory stimulation. *Proc Natl Acad Sci USA* 89: 5675-5679, 1992.

Lancaster JL, Tordesillas-Gutierrez D, Martinez M, Salinas F, Evans A, Zilles K, Mazziotta JC, Fox PT. Bias between MNI and Talairach coordinates analyzed using the ICBM-152 brain template. *Hum Brain Mapp* 28: 1194-1205, 2007.

Larsson J, Heeger DJ. Two retinotopic visual areas in human lateral occipital cortex. *J Neurosci* 26: 13128-13142, 2006.

Lange T, Roth V, Braun M, Buhmann JM. Stability-based validation of clustering solutions. *Neural Comput* 16: 1299-1323, 2004.

Lashkari D, Vul E, Kanwisher N, Golland P. Discovering structure in the space of fMRI selectivity profiles. *Neuroimage* 50: 1085-1098, 2010.

Lavenex P, Suzuki WA, Amaral DG. Perirhinal and parahippocampal cortices of the macaque monkey: Projections to the neocortex. *J Comp Neurol* 447: 394-420, 2002.

Levy I, Hasson U, Avidan G, Hendler T, Malach R. Center-periphery organization of human object areas. *Nat Neurosci* 4: 533-539, 2001.

Logothetis NK. What we can do and what we cannot do with fMRI. *Nature* 453: 869-878, 2008.

Luna B, Thulborn KR, Strojwas MH, McCurtain BJ, Berman RA, Genovese CR, Sweeney JA. Dorsal cortical regions subserving visually guided saccades in humans: an fMRI study. *Cereb Cortex* 8: 40-47, 1998.

Luppino G, Matelli M, Camarda R, Rizzolatti G. Corticocortical connections of area F3 (SMA-proper) and area F6 (pre-SMA) in the macaque monkey. *J Comp Neurol* 338: 114-140, 1993.

Malach R, Reppas JB, Benson RR, Kwong KK, Jiang H, Kennedy WA, Ledden PJ, Brady TJ, Rosen BR, Tootell RBH. Object-related activity revealed by functional magnetic resonance imaging in human occipital cortex. *Proc Natl Acad Sci USA* 92: 8135-8139, 1995.

Malikovic A, Amunts K, Schleicher A, Mohlberg H, Eickhoff SB, Wilms M, Palomero-Gallagher N, Armstrong E, Zilles K. Cytoarchitectonic analysis of the human extrastriate cortex in the region of V5/MT+: A probabilistic, stereotaxic map of area hOc5. *Cereb Cortex* 17: 562-574, 2007.

Marcus DS, Fotenos AF, Csernansky JG, Morris JC, Buckner RL. Open access series of imaging studies: Longitudinal MRI data in nondemented and demented older adults. *J Cogn Neurosci* 22: 2677-2684, 2010.

Marcus DS, Wang TH, Parker J, Csernansky JG, Morris JC, Buckner RL. Open access series of imaging studies (OASIS): Cross-sectional MRI data in young, middle aged, nondemented, and demented older adults. *J Cogn Neurosci* 19: 1498-1507, 2007.

Markov NT, Misery P, Falchier A, Lamy C, Vezoli J, Quilodran R, Gariel MA, Giroud P, Ercsey-Ravasz M, Pilaz LJ, Huissoud C, Barone P, Dehay C, Toroczkai Z, Van Essen DC, Kennedy H, Knoblauch K. Weight consistency specifies regularities of macaque cortical networks. *Cereb Cortex* 2010.

Matelli M, Camarda R, Glickstein M, Rizzolatti G. Afferent and efferent projections of the inferior area 6 in the macaque monkey. *J Comp Neurol* 251: 281-298, 1986.

Matelli M, Luppino G, Rizzolatti G. Architecture of superior and mesial area 6 and the adjacent cingulate cortex in the macaque monkey. *J Comp Neurol* 311: 445-462, 1991.

Matelli M, Luppino G, Rizzolatti G. Patterns of cytochrome oxidase activity in the frontal agranular cortex of the macaque monkey. *Behav Brain Res* 18: 125-136, 1985.

Maunsell JHR, Van Essen DC. The connections of the middle temporal visual area (MT) and their relationship to a cortical hierarchy in the macaque monkey. *J Neurosci* 3: 2563, 1983.

Maunsell JHR, Van Essen DC. Topographic organization of the middle temporal visual area in the macaque monkey: Representational biases and the relationship to callosal connections and myeloarchitectonic boundaries. *J Comp Neurol* 266: 535-555, 1987.

Medendorp WP, Goltz HC, Vilis T, Crawford JD. Gaze-centered updating of visual space in human parietal cortex. *J Neurosci* 23: 6209-6214, 2003.

Mesulam MM. A cortical network for directed attention and unilateral neglect. *Ann Neurol* 10: 309-325, 1981.

Mesulam MM. Frontal cortex and behavior. *Ann Neurol* 19: 320-325, 1986.

Mesulam MM. Large-scale neurocognitive networks and distributed processing for attention, language, and memory. *Ann Neurol* 28: 597-613, 1990.

Mesulam MM. From sensation to cognition. *Brain* 121 (6): 1013-1052, 1998.

Mesulam MM, Mufson EJ. Insula of the old world monkey. III: Efferent cortical output and comments on function. *J Comp Neurol* 212: 38-52, 1982.

Moeller S, Nallasamy N, Tsao DY, Freiwald WA. Functional connectivity of the macaque brain across stimulus and arousal states. *J Neurosci* 29: 5897-5909, 2009.

Moran MA, Mufson EJ, Mesulam MM. Neural inputs into the temporopolar cortex of the rhesus monkey. *J Comp Neurol* 256: 88-103, 1987.

Nelson SM, Cohen AL, Power JD, Wig GS, Miezin FM, Wheeler ME, Velanova K, Donaldson DI, Phillips JS, Schlaggar BL, Petersen SE. A parcellation scheme for human left lateral parietal cortex. *Neuron* 67: 156-170, 2010.

Ogawa S, Tank DW, Menon R, Ellermann JM, Kim SG, Merkle H, Ugurbil K. Intrinsic signal changes accompanying sensory stimulation: Functional brain mapping with magnetic resonance imaging. *Proc Natl Acad Sci USA* 89: 5951-5955, 1992.

Ojemann JG, Akbudak E, Snyder AZ, McKinstry RC, Raichle ME, Conturo TE. Anatomic localization and quantitative analysis of gradient refocused echo-planar fMRI susceptibility artifacts. *NeuroImage* 6: 156-167, 1997.

Orban GA, Van Essen D, Vanduffel W. Comparative mapping of higher visual areas in monkeys and humans. *Trends in Cogn Sci* 8: 315-324, 2004.

Orban GA, Claeys K, Nelissen K, Smans R, Sunaert S, Todd JT, Wardak C, Durand J-B, Vanduffel W. Mapping the parietal cortex of human and non-human primates. *Neuropsychologia* 44: 2647-2667, 2006.

Pandya DN, Kuypers HG. Cortico-cortical connections in the rhesus monkey. *Brain Res* 13: 13-36, 1969.

Pandya DN, Seltzer B. Intrinsic connections and architectonics of posterior parietal cortex in the rhesus monkey. *J Comp Neurol* 204: 196-210, 1982.

Pandya DN, Vignolo LA. Intra- and interhemispheric projections of the precentral, premotor and arcuate areas in the rhesus monkey. *Brain Res* 26: 217-233, 1971.

Passingham RE, Stephan KE, Kötter R. The anatomical basis of functional localization in the cortex. *Nat Rev Neurosci* 3: 606-616, 2002.

Perry RJ, Zeki S. The neurology of saccades and covert shifts in spatial attention: An event-related fMRI study. *Brain* 123: 2273-2288, 2000.

Petrides M. Lateral prefrontal cortex: Architectonic and functional organization. *Philos Trans R Soc Lond B Biol Sci* 360: 781-795, 2005.

Petrides M, Pandya DN. Efferent association pathways originating in the caudal prefrontal cortex in the macaque monkey. *J Comp Neurol* 498: 227-251, 2006.

Pilbeam D, Young N. Hominoid evolution: Synthesizing disparate data. *Comptes Rendus Palevol* 3:305-321, 2004.

Preuss T. What is it like to be a human? In: *The Cognitive Neurosciences, Third Edition,* edited by Gazzaniga MS. Cambridge, MA: MIT Press, 2004, p. 5-22.

Polimeni JR, Fischl B, Greve DN, Wald LL. Laminar analysis of 7T BOLD using an imposed spatial activation pattern in human V1. *Neuroimage* 52: 1334-1346, 2010.

Polimeni JR, Hinds OP, Balasubramanian M, van der Kouwe AJW, Wald L,L Dale AM, Fischl B, Schwartz EL. The human V1–V2–V3 visuotopic map complex measured via fMRI at 3 and 7 Tesla. *Abstr Soc Neurosci,* 2005.

Pons TP, Kaas JH. Corticocortical connections of area 2 of somatosensory cortex in macaque monkeys: A correlative anatomical and electrophysiological study. *J Comp Neurol* 248: 313-335, 1986.

Posner MI, Petersen SE, Fox PT, Raichle ME. Localization of cognitive operations in the human brain. *Science* 240: 1627-1631, 1988.

Power JD, Fair DA, Schlaggar BL, Petersen SE. The development of human functional brain networks. *Neuron* 67: 735-748, 2010.

Raichle ME. Circulatory and metabolic correlates of brain function in normal humans. In: *Handbook of Physiology. The Nervous System V*. Bethesda MD: Am. Physiol. Soc., 1987, p. 643–674.

Rajkowska G, Goldman-Rakic PS. Cytoarchitectonic definition of prefrontal areas in the normal human cortex: II. Variability in locations of areas 9 and 46 and relationship to the Talairach Coordinate System. *Cereb Cortex* 5: 323-337, 1995.

Rizzolatti G, Luppino G, Matelli M. The organization of the cortical motor system: New concepts. *Electroencephalogr Clin Neurophysiol* 106: 283-296, 1998.

Rockland KS, Pandya DN. Laminar origins and terminations of cortical connections of the occipital lobe in the rhesus monkey. *Brain Res* 179: 3-20, 1979.

Rosenbaum RS, Stuss DT, Levine B, Tulving E. Theory of mind is independent of episodic memory. *Science* 318: 1257, 2007.

Rottschy C, Eickhoff SB, Schleicher A, Mohlberg H, Kujovic M, Zilles K, Amunts K. Ventral visual cortex in humans: Cytoarchitectonic mapping of two extrastriate areas. *Hum Brain Mapp* 28: 1045-1059, 2007.

Rousseeuw PJ. Silhouettes: A graphical aid to the interpretation and validation of cluster analysis. *J Comput Appl Math* 20: 1987.

Rovamo J, Virsu V. An estimation and application of the human cortical magnification factor. *Exp Brain Res* 37:495-510, 1979.

Saleem KS, Kondo H, Price JL. Complementary circuits connecting the orbital and medial prefrontal networks with the temporal, insular, and opercular cortex in the macaque monkey. *J Comp Neurol* 506: 659-693, 2008.

Saxe R. Uniquely human social cognition. *Curr Opin Neurobiol* 16: 235-239, 2006.

Saxe R, Powell LJ. It's the thought that counts: Specific brain regions for one component of theory of mind. *Psychol Sci* 17: 692-699, 2006.

Scheperjans F, Eickhoff SB, Hömke L, Mohlberg H, Hermann K, Amunts K, Zilles K. Probabilistic maps, morphometry, and variability of cytoarchitectonic areas in the human superior parietal cortex. *Cereb Cortex* 18: 2141-2157, 2008a.

Scheperjans F, Hermann K, Eickhoff SB, Amunts K, Schleicher A, Zilles K. Observer-independent cytoarchitectonic mapping of the human superior parietal cortex. *Cereb Cortex* 18: 846-867, 2008b.

Schleicher A, Amunts K, Geyer S, Morosan P, Zilles K. Observer-independent method for microstructural parcellation of cerebral cortex: A quantitative approach to cytoarchitectonics. *Neuroimage* 9: 165-177, 1999.

Schormann T, Zilles K. Three-dimensional linear and nonlinear transformations: An integration of light microscopical and MRI data. *Hum Brain Mapp* 6: 339-347, 1998.

Ségonne F, Dale AM, Busa E, Glessner M, Salat D, Hahn HK, Fischl B. A hybrid approach to the skull stripping problem in MRI. *Neuroimage* 22: 1060-1075, 2004.

Ségonne F, Pacheco J, Fischl B. Geometrically accurate topology-correction of cortical surfaces using nonseparating loops. *IEEE Trans Med Imaging* 26: 518-529, 2007.

Seeley WW, Menon V, Schatzberg AF, Keller J, Glover GH, Kenna H, Reiss AL, Greicius MD. Dissociable intrinsic connectivity networks for salience processing and executive control. *J Neurosci* 27: 2349-2356, 2007.

Selemon LD, Goldman-Rakic PS. Common cortical and subcortical targets of the dorsolateral prefrontal and posterior parietal cortices in the rhesus monkey: Evidence for a distributed neural network subserving spatially guided behavior. *J Neurosci* 8: 4049-4068, 1988.

Seltzer B, Pandya DN. Parietal, temporal, and occipital projections to cortex of the superior temporal sulcus in the rhesus monkey: A retrograde tracer study. *J Comp Neurol* 343: 445-463, 1994.

Seltzer B, Pandya DN. Further observations on parieto-temporal connections in the rhesus monkey. *Exp Brain Res* 55:301-312, 1984.

Sepulcre J, Liu H, Talukdar T, Martincorena I, Yeo BTT, Buckner RL. The organization of local and distant functional connectivity in the human brain. *PLoS Comput Biol* 6: e1000808, 2010.

Sereno MI, Dale AM, Reppas JB, Kwong KK, Belliveau JW, Brady TJ, Rosen BR, Tootell RBH. Borders of multiple visual areas in humans revealed by functional magnetic resonance imaging. *Science* 268: 889-893, 1995.

Sereno MI, Pitzalis S, Martinez A. Mapping of contralateral space in retinotopic coordinates by a parietal cortical area in humans. *Science* 294: 1350-1354, 2001.

Sestieri C, Corbetta M, Romani GL, Shulman GL. Episodic memory retrieval, parietal cortex, and the default mode network: Functional and topographic analyses. *J Neurosci* 31: 4407-4420, 2011.

Shadlen MN, Newsome WT. Neural basis of a perceptual decision in the parietal cortex (area LIP) of the rhesus monkey. *J Neurophysiol* 86: 1916-1936, 2001.

Shikata E, Hamzei F, Glauche V, Knab R, Dettmers C, Weiller C, Büchel C. Surface orientation discrimination activates caudal and anterior intraparietal sulcus in humans: an event-related fMRI study. *J Neurophysiol* 85: 1309-1314, 2001.

Shikata E, Hamzei F, Glauche V, Koch M, Weiller C, Binkofski F, Büchel C. Functional properties and interaction of the anterior and posterior intraparietal areas in humans. *Eur J Neurosci* 17: 1105-1110, 2003.

Shulman GL, McAvoy MP, Cowan MC, Astafiev SV, Tansy AP, d'Avossa G, Corbetta M. Quantitative analysis of attention and detection signals during visual search. *J Neurophysiol* 90: 3384-3397, 2003.

Shulman GL, Ollinger JM, Akbudak E, Conturo TE, Snyder AZ, Petersen SE, Corbetta M. Areas involved in encoding and applying directional expectations to moving objects. *J Neurosci* 19: 9480-9496, 1999.

Smith SM, Fox PT, Miller KL, Glahn DC, Fox PM, Mackay CE, Filippini N, Watkins KE, Toro R, Laird AR, Beckmann CF. Correspondence of the brain's functional architecture during activation and rest. *Proc Natl Acad Sci USA* 106: 13040-13045, 2009.

Smith SM, Jenkinson M, Woolrich MW, Beckmann CF, Behrens TEJ, Johansen-Berg H, Bannister PR, De Luca M, Drobnjak I, Flitney D, Niazy RK, Saunders

J, Vickers J, Zhang Y, De Stefano N, Brady JM, Matthews PM. Advances in functional and structural MR image analysis and implementation as FSL. *Neuroimage* 23: S208-S219, 2004.

Stanton GB, Bruce CJ, Goldberg ME. Topography of projections to posterior cortical areas from the macaque frontal eye fields. *J Comp Neurol* 353: 291-305, 1995.

Strick PL. How do the basal ganglia and cerebellum gain access to the cortical motor areas? *Behav Brain Res* 18:107-123, 1985.

Suzuki WA, Amaral DG. Perirhinal and parahippocampal cortices of the macaque monkey: Cortical afferents. *J Comp Neurol* 350: 497-533, 1994.

Swisher JD, Halko MA, Merabet LB, McMains SA, Somers DC. Visual topography of human intraparietal sulcus. *J Neurosci* 27: 5326-5337, 2007.

Taira M, Nose I, Inoue K, Tsutsui K. Cortical areas related to attention to 3D surface structures based on shading: an fMRI study. *Neuroimage* 14: 959-966, 2001.

Talairach J, Tournoux P. *Co-planar Stereotaxic Atlas of the Human Brain: 3-Dimensional Proportional System: An Approach to Cerebral Imaging*. New York: Thieme Medical Publishers 1988.

Tanné-Gariépy J, Rouiller EM, Boussaoud D. Parietal inputs to dorsal versus ventral premotor areas in the macaque monkey: Evidence for largely segregated visuomotor pathways. *Exp Brain Res* 145: 91-103, 2002.

Thirion B, Pinel P, Meriaux S, Roche A, Dehaene S, Poline J-B. Analysis of a large fMRI cohort: Statistical and methodological issues for group analyses. *Neuroimage* 35: 105-120, 2007.

Tootell RBH, Hadjikhani N. Where is 'dorsal V4' in human visual cortex? Retinotopic, topographic and functional evidence. *Cereb Cortex* 11: 298-311, 2001.

Tootell RBH, Hadjikhani N, Hall EK, Marrett S, Vanduffel W, Vaughan JT, Dale AM. The retinotopy of visual spatial attention. *Neuron* 21: 1409-1422, 1998.

Tootell RBH, Reppas JB, Kwong KK, Malach R, Born RT, Brady TJ, Rosen BR, Belliveau JW. Functional analysis of human MT and related visual cortical areas using magnetic resonance imaging. *J Neurosci* 15: 3215-3230, 1995.

Tootell RBH, Taylor JB. Anatomical evidence for MT and additional cortical visual areas in humans. *Cereb Cortex* 5: 39-55, 1995.

Ungerleider LG, Desimone R. Cortical connections of visual area MT in the macaque. *J Comp Neurol* 248: 190-222, 1986.

van der Kouwe AJW, Benner T, Fischl B, Schmitt F, Salat DH, Harder M, Sorensen AG, Dale AM. On-line automatic slice positioning for brain MR imaging. *Neuroimage* 27: 222-230, 2005.

van der Kouwe AJW, Benner T, Salat DH, Fischl B. Brain morphometry with multiecho MPRAGE. *Neuroimage* 40: 559-569, 2008.

Van Dijk KRA, Hedden T, Venkataraman A, Evans KC, Lazar SW, Buckner RL. Intrinsic functional connectivity as a tool for human connectomics: Theory, properties, and optimization. *J Neurophysiol* 103: 297-321, 2010.

Van Essen DC. Organization of visual areas in macaque and human cerebral cortex. In: *The Visual Neurosciences,* edited by L. Chalupa and J.S. Werner. Cambridge, MA: MIT Press, 2004, p. 507-521, 2004.

Van Essen DC. A population-average, landmark-and surface-based (PALS) atlas of human cerebral cortex. *Neuroimage* 28: 635-662, 2005.

Van Essen DC, Anderson CH, Felleman DJ. Information processing in the primate visual system: An integrated systems perspective. *Science* 255: 419-423, 1992.

Van Essen DC, Dierker DL. Surface-based and probabilistic atlases of primate cerebral cortex. *Neuron* 56: 209-225, 2007.

Van Essen DC, Zeki SM. The topographic organization of rhesus monkey prestriate cortex. *J Physiol* 277: 193-226, 1978.

Vilberg KL, Rugg MD. Memory retrieval and the parietal cortex: A review of evidence from a dual-process perspective. *Neuropsychologia* 46:1787-1799, 2008.

Vincent JL, Patel GH, Fox MD, Snyder AZ, Baker JT, Van Essen DC, Zempel JM, Snyder LH, Corbetta M, Raichle ME. Intrinsic functional architecture in the anaesthetized monkey brain. *Nature* 447:83-86, 2007.

Vincent JL, Kahn I, Snyder AZ, Raichle ME, Buckner RL. Evidence for a frontoparietal control system revealed by intrinsic functional connectivity. *J Neurophysiol* 100: 3328-3342, 2008.

Vincent JL, Snyder AZ, Fox MD, Shannon BJ, Andrews JR, Raichle ME, Buckner RL. Coherent spontaneous activity identifies a hippocampal-parietal memory network. *J Neurophysiol* 96: 3517-3531, 2006.

Van Overwalle F, Baetens K. Understanding others' actions and goals by mirror and mentalizing systems: A meta-analysis. *Neuroimage* 48: 564-584, 2009.

von Bonin G, Bailey P. *The Neocortex of Macaca Mulatta*. Urbana: University of Illinois Press 1947.

Wagner AD, Shannon BJ, Kahn I, Buckner RL. Parietal lobe contributions to episodic memory retrieval. *Trends Cogn Sci* 9: 445-453, 2005.

Wandell BA, Brewer AA, Dougherty RF. Visual field map clusters in human cortex. *Philos Trans R Soc Lond B Biol Sci* 360: 693-707, 2005.

Wandell BA, Dumoulin SO, Brewer AA. Visual field maps in human cortex. *Neuron* 56: 366-383, 2007.

Wessinger CM, VanMeter J, Tian B, Van Lare J, Pekar J, Rauschecker JP. Hierarchical organization of the human auditory cortex revealed by functional magnetic resonance imaging. *J Cogn Neurosci* 13: 1-7, 2001.

Wilms M, Eickhoff SB, Hömke L, Rottschy C, Kujovic M, Amunts K, Fink GR. Comparison of functional and cytoarchitectonic maps of human visual areas V1, V2, V3d, V3v, and V4(v). *Neuroimage* 49: 1171-1179, 2010.

Yeo BTT, Sabuncu MR, Vercauteren T, Ayache N, Fischl B, Golland P. Spherical demons: Fast diffeomorphic landmark-free surface registration. *IEEE Trans Med Imaging* 29: 650-668, 2010a.

Yeo BTT, Sabuncu MR, Vercauteren T, Holt DJ, Amunts K, Zilles K, Golland P, Fischl B. Learning task-optimal registration cost functions for localizing cytoarchitecture and function in the cerebral cortex. *IEEE Trans Med Imaging* 29: 1424-1441, 2010b.

Zeki SM. Representation of central visual fields in prestriate cortex of monkey. *Brain Res* 14: 271-291, 1969.

Zilles K, Schlaug G, Matelli M, Luppino G, Schleicher A, Qü M, Dabringhaus A, Seitz R, Roland PE. Mapping of human and macaque sensorimotor areas by

integrating architectonic, transmitter receptor, MRI and PET data. *J Anat* 187: 515-537, 1995.

Concluding Remarks

Human brain expansion has not been proportional (Hill et al. 2010). For example, primary visual cortex (area 17) and motor cortex are both about the same size in humans and modern chimps (Blinkov & Glezer 1968; Frahm et al. 1984), yet our absolute brain size is about three times as large. From endocasts of preserved skulls, it seems the reduction in proportional size of primary visual cortex probably occurred early in the hominin lineage (Kaas 2006). Moreover, while larger brains generally have more subdivisions (Kaas 2008), it is not clear whether cortical fields that are late to evolve and develop are constrained by the same processes that anchor the early and highly conserved basic sensory areas (Rosa 2002; Rosa & Tweedale 2005).

Because the human brain is not likely simply a scaled up prototypical primate brain, neuroscience has long awaited techniques for exploring long-range connections in human brains directly (Crick & Jones 1993). The latter half of the 20th century saw rapid progress in neuroanatomical mapping in the brains of laboratory animals. Anatomical tract tracing methods such as silver impregnation, pioneered by Walle Nauta and others (Nauta & Ryan 1952), made it possible to map connections from the site of a lesion by slowly and painstakingly following the trace of degenerating axons in the histological tissue. In the 1970s, a neuroanatomical revolution occurred with the development of tracers that were taken up by axonal anterograde or retrograde transport and enabled visualization of neuronal pathways (Mesulam 1976; a good review of early techniques is found in Kristensson 1978). However, anatomic tracing techniques have historically had limited utility in post-mortem human brains (Buckhalter, Bernardo & Charles 1993).

Detailed studies of the somatosensory and visual systems in cats and non-human primates were particularly influential for early models of the functional architecture of the neocortex (Mountcastle 1957; Hubel & Wiesel 1962; 1977). Serial, hierarchical processing stages as the basis for the sensory faculties were proposed well before circuit tracing methods were available (e.g. Walton & Paul 1901). Van Essen's work with John Maunsell (Maunsell & Van Essen 1983) and his later, exhaustive meta-analysis (Felleman & Van Essen 1991) produced iconic diagrams of the visuomotor hierarchy for information flow in the monkey brain. These "wiring diagrams" are still considered the most comprehensive description of the visuomotor pathway in primates.

Consequently, principles for brain organization derived from studying sensory systems have influenced ideas about the rest of the brain. For instance, some assumed the expanded portions of human cortex inherits the features of the early, evolutionarily conserved sensory processing areas, such as a modular organization with well-defined borders (Kaas 1987). Functionally, the concept of a hierarchy has moved beyond perceptual processing to other domains, leading to functional descriptions of "action" and "cognitive" hierarchies with corresponding physical realities in the frontal lobes (Fuster 1993; Koechlin et al. 2003; Badre & D'Esposito 2007).

Goldman-Rakic (1988), Mesulam (1990) and others challenged the assumption that hierarchical processing best characterized the organization of association cortex. In the classic view, the apex of sensorimotor hierarchies was often reserved for prefrontal cortex (Nauta 1971; Fuster 1993; but see Brutkowski 1965 for an earlier critique of this

view).[7] Goldman-Rakic's double-labeling experiments (e.g. Cavada & Goldman-Rakic 1989a, 1989b) showed that the traditional definition for hierarchical organization was violated by the lateral interconnections between regions that spanned frontal, cingulate, temporal and parietal association cortex. The notion of convergence and reciprocal connections in areas beyond primary sensory cortices was articulated earlier (e.g. Jones & Powell 1970), but Goldman-Rakic's experiments showed the precise laminar co-localization of projections from different association areas onto a common target in a manner that violated the definition of a hierarchy. She further emphasized the parallel nature of circuits that interdigitate neighboring regions of association cortex (Goldman-Rakic 1988). The organization of networks in the orbital and medial prefrontal cortices of non-human primates is consistent with the view that association cortex consists of complexes of distinct networks whose cortical constituents do not have an obviously hierarchical organization (Barbas et al. 1999; Öngür & Price 2000). In their seminal paper, Felleman & Van Essen mention Goldman-Rakic's work as an important caveat to their estimate of the visuomotor hierarchy, since a large proportion of connections in the upper levels of their diagram are inconsistent with the purely hierarchical framework (Felleman & Van Essen 1991).

The work presented in this dissertation seeks to assess these different organizational concepts in the human brain at the macroscopic level. The primary question we address is: do connectivity patterns in the expanded portions of human neocortex and cerebellum exhibit an organization reminiscent of early sensory-motor circuits (local, hierarchical), or rather of distributed networks of the form articulated by

[7] This is an ironic recasting, given prefrontal cortex was historically considered the "silent" portion due to its inexcitability by electrical stimulation (e.g. Ferrier 1874).

Mesulam (1990) and Goldman-Rakic (1988)? Using non-invasive imaging and capitalizing on large data samples, we were able to interrogate stable features of organization that both confirm and extend our understanding of human brain organization. Some of these principles motivate us to revisit common assumptions of organization, such as the view that the prefrontal cortex and its associated white matter volume has unique status as a region of marked expansion and change in humans (Semendeferi et al. 2002; Schoenemann, Sheehan & Glotzer 2005), the view that the cerebellum is predominately connected to regions involved in motor control functions (Evarts & Thach 1969), and the view that brain expansion is associated with an increase in the number of modules (areas) similar in form to early sensory areas, i.e. they are rigidly specified and have clear and distinct borders (Kaas 1987). As I will discuss, each of these views have largely been extended to the human brain on theoretical grounds owing to the lack of techniques for assessing them in humans directly. Though indirect and suffering from poor resolution, neuroimaging methods have the potential to begin to address these questions.

New advances for making large, intact sections of tissue optically and chemically transparent appear to be on the horizon for human systems neuroscience (e.g. Chung et al. 2013). There is at this moment a great deal of excitement in the neuroscience community surrounding large-scale projects and consortiums that seek to comprehensively map connections between every cell in the brains of laboratory animals (e.g. micro-connectomics, Lichtman, Livet & Sanes 2008), or between macroscopic portions of gray matter in the human brain (e.g. the Human Connectome Project, Van Essen & Ugurbil 2012). However, even with new techniques the connectivity of the

human brain is by any measure dauntingly complex. Principles of connectivity derived from nonhuman primates provide important insights, both in the details and in the broad pattern of connections and organizational properties described at the macroscopic level.

Advancements in *in vivo* imaging methods, such as diffusion imaging and functional connectivity MRI, have allowed us to begin to make inferences about connectivity (Johansen-Berg & Rushworth 2009; Behrens & Sporns 2012), as well as disruptions to connectivity (Buckholtz & Meyer-Lindenberg 2012), in human brains directly. In what follows I will discuss the contribution the studies described in this dissertation have made in mapping the macroscopic topography of functional connectivity in the human cerebral cortex and cerebellum. I will also discuss the empirical work we have done to understand the limitations of fcMRI. These limitations likely preclude its ability to identify boundaries between functional areas, but the general properties of network organization appear consistent across different applications, lending some confidence in the emerging picture of what is unique about human brain organization. I will then discuss other general conclusions from this body of work.

Cerebro-Cerebellar Circuits

In Paper I (Krienen & Buckner, 2009), we examined the strength of correlations between regions in frontal cortex and the cerebellum. In line with expectations from polysynaptic tract tracing results obtained in non-human primates (Middleton & Strick 2001), we saw that the anterior hemispheres as well as lobule VIIIB of the human cerebellum was preferentially coupled to regions in somatomotor cortex. Conversely, we found that the posterior portions (Crus I and II) of the cerebellum are more correlated to

lateral and medial prefrontal cortex. This was also expected from the work of Strick and colleagues, who demonstrated that these portions of the posterior hemispheres of the cerebellum of non-human primates participate in closed, polysynaptic circuits with lateral prefrontal cortex (Kelley & Strick 2003). By choosing different seed regions in prefrontal cortex, we saw that there were at least 3 interdigitated and only partially overlapping patterns of correlation in the cerebellum. These patterns were first detected in a dataset of 40 subjects and then replicated in a second sample of 40 subjects. We could also see evidence for the same patterns at the individual subject level.

More recently we have refined and expanded our mapping of human cerebro-cerebellar circuits (Buckner et al. 2011). We replicated the primary result described in Paper I, showing that the posterior lobules of the human cerebellum participate in functional networks that span portions of cerebral association cortex. Application of a clustering algorithm to group together portions of the cerebellum that share similar connectivity fingerprints to the cerebral cortex further revealed a complex interdigitation of networks across the cerebellar cortex. These analyses also revealed an intriguing patterning across the anterior-posterior axis of the cerebellum. Specifically, these results showed that the cerebellar regions linked to association cortex as well as somatomotor cortex form separate anterior and posterior representations that appear as mirror images in the sagittal or coronal planes (Buckner et al. 2011). There was also some indication that a third map might exist in the most posterior portions of the cerebellum (lobule X). In general, the extent of the cerebellum that participated in a network was predicted by the proportional size of the network in the cerebral cortex. Measured in this way, fully

more than half of the human cerebellum appears to participate in network involving association cortex.

Interestingly, the lateral hemispheres of the cerebellum appear to have undergone significant expansion in recent hominid evolution. Although fcMRI likely does not have the ability to delimit precise areal boundaries nor distinguish direct from indirect connections, the roughly homotopic relationship between representations in the cerebrum and the cerebellum in humans recalls the coordinated scaling of the cerebro-cerebellar complex across the primate radiation (Whiting & Barton 2003). These demonstrations are particularly interesting as they point to coordinated scaling between subcortical structures and the neocortex, structures that originally evolved over phylogenetically different timescales (Striedter 2005).

What remains unclear is the extent to which this coordination is due to hard-wired developmental programs, to population matching, or to experience-dependent refinement of connectivity (Striedter 2005). It is intriguing that the cerebellum develops in the anterior-posterior direction, with the lateral hemispheres appearing latest (Sillitoe & Joyner 2007). Cerebellar Purkinje cells and most interneurons also share a common germline with the cortical precursor cells originating in the ventricular zone (VZ) (Altman & Bayer 1997). Afferent connections from the cerebrum by way of the pontine nucleus target the anterior or posterior lobules with a chronometrically sequential topography along the anterior-posterior axis (Sillitoe & Joyner 2007). This developmental pattern is broadly consistent with the developmental sequence that occurs in cortex, in which the primary sensory and motor areas emerges before association cortex. However, it is not yet clear whether the cerebro-cerebellar connectivity patterns

generally achieve their orderly formation in temporal succession, whether the connectivity of the dual representation of each network would be achieved simultaneously, and the extent to which these networks are genetically or experientially determined.

Relation of Functional Connectivity to Anatomic Connectivity

To appreciate the topography of connectivity patterns, we have found it particularly informative to animate whole-brain connectivity maps of a small seed region as it is moved smoothly across the cortical surface (see www.youtube.com/yeokrienen and www.youtube.com/bucknerkrienen for examples of corticocortical and cerebrocerebellar connectivity movies). Abrupt transitions in the connectivity patterns of neighboring regions occur fairly often. The exact locations of these transitions are also reasonably stable across small samples of participants, if using the same analysis stream and data collected from the same behavioral state. These coupling transitions have been proposed to mark 'functional boundaries' between putative areas in the human brain at the level of individual subjects (Cohen et al. 2008). Though we do not hold this view, it is striking how abrupt some of the coupling transitions are. Similarly, it can be striking how uniform or gradual are the transitions in other regions of the neocortex.

Connectivity-based parcellations of the human brain based on resting state functional connectivity or on structural connectivity have proliferated in recent years (Cohen et al. 2008, Nelson et al. 2010; Yeo et al. 2011; Power et al. 2011; Mars et al. 2011). Broadly, parcellations are a means of reducing the whole brain voxel-to-voxel (or vertex-to-vertex) connectivity matrix into "networks" or "clusters" of regions that may be

physically far apart but nonetheless share similarities in their connectivity fingerprints (Passingham et al. 2002). Parcellations and other ways of reducing and organizing coupling patterns have made vast datasets tractable, but have also allowed us to appreciate the general consistency of solutions across laboratories, data samples, and methods.

In Paper II we examined two factors that can influence functional connectivity patterns and the resultant parcellations of fcMRI data. The first factor deals with technical aspects of fcMRI analysis. Specifically, choices made in the analysis and weighting criteria for defining functional networks or identifying coupling transitions can influence the exact locations of borders between adjacent regions. The second factor concerns the transient contributions to the fcMRI signal from the behavioral state of the participants. Since fcMRI is not fully determined by anatomical connectivity patterns, some portion of the variance in coupling patterns is due to the particular behavioral state of the participant.

We found that task-derived fcMRI borders better conform to the pattern of responses derived from the task, compared to borders derived from resting data. This is important because it has been claimed that resting state networks correspond well with task-induced activations across a broad range of cognitive domains (Smith et al. 2009; Nelson et al. 2010; but see Mennes et al. 2012). However, while the number of resting state fMRI studies appears to be increasing exponentially (Snyder & Raichle 2012), functional connectivity parcellations are rarely performed in other types of task data. The predominance of studies that use passive rest data may reinforce the (implicit or explicit) assumption that passive rest states are the most appropriate states for fcMRI analyses.

This has been bolstered by observations that resting-state patterns conform well to task activation patterns across a wide range of behavioral tasks (e.g. Smith et al. 2009). However, we found that task-derived fcMRI patterns are equally good at predicting task coactivation patterns obtained from the Brainmap database (Thomas Yeo, unpublished observations).

Going beyond technical and experimental considerations, a final reason not to expect fcMRI patterns to recapitulate areal boundaries is that anatomic connections themselves do not necessarily align uniformly with cytoarchitectural divisions. It is well known that some areas are distinguished by heterogeneous connections to other regions. For example, connections in early visual cortex link together regions that share similar visual field representation (Maunsell & Van Essen 1983). The fcMRI signal measured across V1-V3 is a graded pattern that preferentially links central (foveal) representations together, as distinct from peripheral visual field representations, across the V1-V3 complex (Yeo et al. 2011).

An additional complexity is that gradients may be a true feature of cortical connectivity. While the traditional definition of a brain area is often taken to mean that there are clear demarcations between areas, sharp connectivity-based borders may not always exist. While the borders of primary sensory and motor areas are determined by strong evolutionary and developmental constraints (Rakic 1988), and can therefore be identified clearly (Kaas 1987), brain areas that are later to evolve and develop may not be subject to the same rigorous molecular specification. For this reason, some argue that the demarcations between cortical areas, particularly those that subdivide association cortex,

may be better described as transitional gradients rather than clear, unequivocal borders (Rosa & Tweedale 2005; Barbas 2007).

This important point was not lost to many of the early comparative cytoarchitectonists. The idea that the phylogenetic age of cortex might be related to its cytoarchitectonic stability can be found even in early works of comparative anatomy (e.g. Campbell 1904). Though contemporary reproductions of the maps of Brodmann (1909) and von Bonin and Bailey (1961) are often redrawn in a manner that depicts sharp delineations between areas, the original works emphasize suspected gradual transitions between neocortical fields as well as uncertainties in the locations of certain areal boundaries. With this in mind we should not expect fcMRI to produce hard boundaries that accurately reflect areal organization (Buckner, Krienen & Yeo 2013), particularly in regions of the brain that have undergone disproportionate expansion in hominins (Hill et al. 2010).

Though fcMRI does not recover areal boundaries, it has shown its potential to reveal other important principles of organization. One example is the confirmation that the cerebellum participates in non-motor networks (Habas et al. 2009; Krienen & Buckner 2009; Buckner et al. 2011). Another is the characterization of circuits involving the cerebral cortex and the striatum, which reveals both the expected motor circuits as well as an orderly sequence of coupling to association regions (Choi et al. 2012). Investigating the circuit properties has also revealed new insights into how information propagates within networks. For example, association cortex exhibits relatively higher distant (as compared to local) connectivity (Sepulcre et al. 2009), consistent with the non-human primate anatomy (Selemon & Goldman-Rakic 1998), as well as more recent

modeling of white matter imaging in humans (Hagmann et al. 2008). Graph theoretic techniques applied to fcMRI data have also yielded proposals for how information might be propagated or integrated across networks (He et al. 2009; Sepulcre et al. 2012).

As a final illustration of how fcMRI has advanced understanding of brain organization, several studies have investigated functional connectivity in anesthetized macaques. Broadly, these find parallels for a number of the networks that have been characterized in humans (Vincent et al. 2007; Margulies et al. 2009; Hutchison et al. 2011; 2012). For example, a recent paper by Hutchison et al (2012) shows that fcMRI of distinct clusters in the cingulate cortex reveals distinct fingerprints of connectivity that are broadly consistent both with the human imaging literature (e.g. Beckmann et al. 2009) and the anatomical tracing literature.

Motivated by the view that characterization of cerebral cortex is incomplete without converging evidence that includes connectivity information, Paper III of this dissertation analyzed resting-state fcMRI data from 1000 subjects with two primary objectives. First, we sought to provide parcellations that are a current best estimate of the organization of human cortical networks as measured by functional connectivity MRI. Second, we took advantage of the power of a large data sample to quantitatively measure functional connectivity strength among many regions. We explored the patterns of corticocortical functional coupling that give rise to these networks, guided by the non-human primate anatomy when available.

The results revealed that parcellations of 7 and 17 networks were stable clustering solutions. We began by exploring the general properties of these parcellations. Networks in visual and motor cortices are comprised of regions whose functional coupling is

mainly restricted to local neighborhoods. Using knowledge of the hierarchical organization of connections from primary visual cortex up to premotor and parietal association areas in the monkey, we were able to show that connectivity strength predicts hierarchical distance within this canonical visuomotor circuit with human fcMRI data. In contrast, association cortex was found to consist of large, interdigitated networks that span frontal, parietal, temporal and cingulate cortices. Here, connectivity strengths and patterns are largely consistent across the distributed regions of a given network such that no clear hierarchy between them emerges (Figures 3.32-35).

Summary, Caveats and Future Directions

Several important points are worth revisiting from Paper II regarding the parcellations of resting-state data that were presented in Paper III. First, though the topography of functional connectivity networks is remarkably stable across large (Figures 3.8-9) and small (Figure 2.1) data samples, we expect the details of the topography to change if different clustering approaches are applied, different task states are measured, or different populations are sampled. Though we have made these parcellations publicly available for the community to use, we caution against interpreting them as the 'ground truth' of functional networks in the cerebral cortex. At the very least, if applying these parcellations to other data, we expect the alignment to be most appropriate for datasets of passive rest in healthy young adults.

Second, fcMRI is constrained by anatomy but is not fully determined by it. This places important limits on how the observed "connectivity" maps should be interpreted.

For example, fcMRI networks change as a function of analysis technique used (Paper II), as well as the current or past behavioral state of participants (McIntosh et al. 2003; Hampson et al. 2004; Rissman et al. 2004; Hampson et al. 2006; Summerfield et al. 2006; Albert et al. 2009; Lewis et al. 2009; Hasson et al. 2009; Pyka et al. 2009; Sepulcre et al. 2010; Stevens et al. 2009; Tambini et al. 2010; Shirer et al. 2011; Vahdat et al. 2011; Mennes et al. 2012; Norman-Haignere et al. 2012).

There is also a growing appreciation of the non-stationarity of the fcMRI signal over time. The typical fcMRI analysis measures average correlation of time series over the course of minutes. A growing body of literature points to the existence of shorter 'micro-state' patterns that transiently emerge and dissolve on the order of seconds (Chang & Glover 2010; Kiviniemi et al. 2011; Allen et al. 2012; reviewed in Hutchison et al. 2013). For example, Kiviniemi et al (2011) and Allen et al (2012) show that the Default Network transiently couples to other regions or networks at shorter timescales, and that there is some regularity in the progression of these brief states. In some cases this non-stationarity may be attributable to the change in behavioral state, including the participants vigilance and drowsiness over the course of the scan. It will be interesting to see whether at least some of this non-stationarity has a non-conscious/experiential basis.

Another important caveat to our parcellations (Paper III) is that while the vast majority of connectivity studies are performed on passive rest states, our current perspective is that passive rest is an 'active' task just like any other task. Therefore some portion of the coupling patterns measured during rest states are influenced by active cognitive operations. Others have advanced the argument that passive rest states are unique biological states (Deco & Corbetta 2011). We do not hold this view. Though

behavior is typically not measured during passive rest, mental operations clearly persist during passive states. Introspective thought-probes can even reveal the distribution of categories of mental content that participants typically experience during these states (Andrews-Hanna et al. 2010). The argument that rest is special would have to make an exception for regions that typically *increase* their BOLD response during passive states, such as those belonging to the Default Network. Our preliminary observations suggest little reason to believe that passive rest states stand out as exemplary states for measuring functional connectivity patterns. However, it is not yet clear what the full dynamic range of connectivity patterns actually is. While the details change, broad properties of organization seem to remain stable across task states. These include the interdigitation of networks in the cerebrum as well as the cerebellum (Paper II).

In general, it is still not clear how to interpret the strength of temporal correlations, or rather, relative differences in the strength of correlations. For example, the correlation strength between a seed region in somatomotor cortex and its peak correlation in the cerebellum is generally lower than if the seed region is moved to medial prefrontal cortex and its corresponding peak in the cerebellum is found. It is unclear what mediates the difference in connectivity strength. The distance is the same in these two cases (both in terms of approximate physical distance as well as the number of synapses that separate the cortical seeds from their cerebellar counterparts), and the microstructure of the cerebellum is quite uniform. Possible candidate factors include differences in signal-to-noise, in intersubject variability in alignment or in locations of underlying cortical fields, in the size of the respective networks or regions, among other possibilities. This example shows that though the field has made compelling discoveries and advances

using functional connectivity, a great deal remains to be explored about the basic properties of the source and relevance of the signals measured by fcMRI.

Occasionally, methods not only advance knowledge of a system, but also fundamentally constrain the way the system is conceptualized. For instance, conceiving the single neuron as the relevant functional unit of the nervous system may stem from a historical dependence on single-electrode recordings (Alivisatos et al. 2012; Logothetis, 2012). Though fMRI provides whole-brain images, traditional localization and subtraction methods may ironically reinforce the assumption that isolated 'areas' (fMRI blobs) are the meaningful unit of functional processing (Smith 2012). All brain areas are presumably embedded within systems of interacting brain areas or subunits within areas. The work presented in this dissertation supports the view that the functional unit of interest might rather be the distributed network itself. At the same time, the limitations and ambiguities inherent to the methods I have used are readily acknowledged.

Concluding References

Alivisatos AP, Chun M, Church GM, Greenspan RJ, Roukes ML, Yuste R. The Brain Activity Map project and the challenge of functional connectomics. *Neuron* 74: 970-974, 2012.

Allen E, Damaraju E, Plis SM, Erhardt E, Eichele T, Calhoun VD. Tracking whole-brain connectivity dynamics in the resting state. *Cereb Cortex* doi: 10.1093/cercor/bhs352, 2012.

Altman J, Bayer SA. Development of the Cerebellar System in Relation to its Evolution, Structure, and Functions. New York: CRC Press. 783 pp, 1997.

Amunts K, Schleicher A, Burgel U, Mohlberg H, Uylings HB, Zilles, K. Broca's region revisited: cytoarchitecture and intersubject variability. *J Comp Neurol* 412: 319–341, 1999.

Amunts K, Schleicher A, Zilles K. Cytoarchitecture of the cerebral cortex – more than localization. *Neuroimage* 37: 1061-1065, 2007.

Andrews-Hanna JR, Reidler JS, Sepulcre J, Poulin R, Buckner RL. Functional-anatomic fractionation of the brain's default network. *Neuron* 65: 550-562, 2010.

Badre D, D'Esposito M. Functional magnetic resonance imaging evidence for a hierarchical organization of the prefrontal cortex. *J Cogn Neurosci* 19: 2082-2089, 2007.

Barbas H, Ghashghaei H, Dombrowski SM, Rempel-Clower NL. Medial prefrontal cortices are unified by common connections with superior temporal cortices and distinguished by input from memory-related areas in the rhesus monkey. *J Comp Neurol* 410: 343-367, 1999.

Barbas H. Specialized elements of orbitofrontal cortex in primates. *Ann NY Acad Sci* 1121: 10-32, 2007.

Blinkov SM, Glezer II. *The Human Brain in Figures and Tables.* New York: Basic Books 1968.

Behrens TEJ, Sporns O. Human connectomics. *Curr Opin Neurobiol* 22: 144-153, 2012.

Brodmann K. Localization in the cerebral cortex. L. J. Garey, Trans. (London: Imperial College Press), 1909/1999.

Brutkowski S. Functions of prefrontal cortex in animals. *Physiol Rev* 45: 721-746, 1965.

Buckner RL, Krienen FM, Castellanos A, Diaz JC, Yeo BTT. The organization of the human cerebellum estimated by functional connectivity. *J Neurophysiol* 106: 2322-2345, 2011.

Buckner RL, Krienen FM, Yeo BTT. Opportunities and Limitations of Intrinsic Functional Connectivity MRI. *Nat. Neurosci,* in press.

Burkhalter A. Bernardo KL, Charles V. Development of local circuits in human visual cortex. *J Neurosci* 13: 1916-1931, 1993.

Buckholtz JW, Meyer-Lindenberg A. Psychopathology and the human connectome: toward a transdiagnostic model of risk for mental illness. *Neuron* 74: 990-1004.

Campbell AW. Further histological studies on the localization of cerebral function – the brains of *Felis, Canis*, and *Sus* compared with that of *Homo*. *Proc R Soc Lond* 72: 390-392, 1904.

Cavada C, Goldman-Rakic PS. Posterior parietal cortex in rhesus monkey: I. Parcellation of areas based on distinctive limbic and sensory corticocortical connections. *J Comp Neurol* 287: 393-421, 1989a.

Cavada C, Goldman-Rakic PS. Posterior parietal cortex in rhesus monkey: II. Evidence for segregated corticocortical networks linking sensory and limbic areas with the frontal lobe. *J Comp Neurol* 287: 422-445, 1989b.

Chang C, Glover GH. Time-frequency dynamics of resting-state brain connectivity measured with fMRI. *Neuroimage* 50: 81–98, 2010.

Choi EY, Yeo BTT, Buckner RL. The organization of the human striatum estimated by intrinsic functional connectivity. *J Neurophysiol* 108: 2242-2263, 2012.

Chung K, Wallace J, Kim S-Y**, Kalyanasundaram S, Andalman AS, et al.** Structural and molecular interrogation of intact biological systems. *Nature* 497: 332-337, 2013.

Cohen AL, Fair DA, Dosenbach NUF, Miezin FM, Dierker D, Van Essen DC, Schlaggar BL, Petersen SE. Defining functional areas in individual human brains using resting functional connectivity MRI. *Neuroimage* 41: 45-57, 2008.

Crick F, Jones E. Backwardness of human neuroanatomy. *Nature* 361: 109-110, 1993.

Deco G, Corbetta M. The dynamical balance of the brain at rest. *The Neuroscientist* 17: 107-123, 2011.

Devlin JT, Poldrack RA. In praise of tedious anatomy. *Neuroimage* 37: 1033-1041, 2007.

Evarts EV, Thach WT. Motor mechanisms of the CNS: cerebrocerebellar interrlations. *Ann Rev Physiol* 31: 451-498, 1969.

Felleman DJ, Van Essen DC. Distributed hierarchical processing in the primate cerebral cortex. *Cereb Cortex* 1: 1-47, 1991.

Ferrier D. Experiments on the brain of monkeys – No. I. *Proc R Soc Lond B Biol Sci* 23: 409-430, 1874.

Finlay BL, Darlington RB. Linked regularities in the development and evolution of mammalian brains. *Science* 268: 1578-1584, 1995.

Frahm HD, Stephan H, Baron G. Comparison of brain structure volumes in Insectivora and Primates: V. Area striata (AS). *J. Hirnforsch* 25:537-577, 1984.

Fuster JM. Frontal lobes. *Curr Opin Neurobiol* 3: 160-165, 1993.

Goldman-Rakic PS. Topography of cognition: Parallel distributed networks in primate association cortex. *Annu Rev Neurosci* 11: 137-156, 1988.

Geyer S, Schleicher A, Zilles K. Areas 3a, 3b, and 1 of human primary somatosensory cortex. *Neuroimage* 10: 63–83, 1999.

Hill J, Inder T, Neil J, Dierker D, Harwell J, Van Essen D. Similar patterns of cortical expansion during human development and evolution. *Proc Natl Acad Sci USA* 107: 13135-13140, 2010.

Hubel DH, Wiesel TN. Receptive fields, binocular interaction and functional architecture in the cat's visual cortex. *J Physiol* 160: 106-154, 1962.

Hubel DH, Wiesel TN. Ferrier lecture: functional architecture of macaque monkey visual cortex. *Proc R Soc Lond B Biol Sci* 198: 1-59, 1977.

Hutchison RM, Leung LS, Mirsattari SM, Gati JS, Menon RS, Everling S. Resting-state networks in the macaque at 7 T. *Neuroimage* 56: 1546-1555, 2011.

Hutchison RM, Womelsdorf T, Gati JS, Leung LS, Menon RS, Everling S. Resting-state connectivity identifies distinct functional networks in macaque cingulate cortex. *Cereb Cortex* 22: 1294-1308, 2012.

Jefferson G. Notes on cortical localization. *J Canad Med Assn* 6: 30-38, 1916.

Johansen-Berg H, Rushworth MFS. Using diffusion imaging to study human connectional anatomy. *Annu Rev Neurosci* 32: 75-94, 2009.

Jones EG, Powell TPS. An anatomical study of converging sensory pathways within the cerebral cortex of the monkey. *Brain* 93: 793-820, 1970.

Kaas JH. The organization of neocortex in mammals: Implications for theories of brain function. *Annu Rev Psychol* 38: 129-151, 1987.

Kaas JH. Evolution of the neocortex. *Curr Biol* 16: R910-R914, 2006.

Kass JH. The evolution of complex sensory and motor systems of the human brain. *Behav Res Bull* 75: 384-390, 2008.

Kiviniemi V, Vire T, Remes J, Abouelseoud A, Starck T, Tervonen O, Nikkinen J. A sliding time-window ICA reveals spatial varia- bility of the default mode network in time. *Brain Connectivity* 1: 339–347, 2011.

Koechlin E, Ody C, Kouneiher F. The architecture of cognitive control in the human prefrontal cortex. *Science* 302: 1181-1185, 2003.

Kristensson K. Retrograde transport of macromolecules in axons. *Ann Rev Pharmacol Toxicol* 18: 97-110, 1978.

Lichtman JW, Livet J, Sanes JR. A technicolour approach to the connectome. *Nature Rev Neurosci* 9: 417–422, 2008.

Logothetis NK. Intracortical recordings and fMRI: an attempt to study operational modules and networks simultaneously. *Neuroimage* 62: 962-969, 2012.

Lu H, Zuo Y, Gu H, Waltz JA, Scholl CA, et al. Synchronized delta oscillations correlate with the resting-state functional MRI signal. *Proc Natl Acad Sci USA* 104: 18265–18269, 2007.

Margulies DS, Kelly AM, Uddin LQ, Biswal BB, Castellanos FX, Milham MP. Mapping the functional connectivity of anterior cingulate cortex. *Neuroimage* 37: 579-588, 2007.

Mars RB, Jbabdi S, Sallet J, O'Reilly JX, Croxson PL, et al. Diffusion-weighted imaging tractography-based parcellation of the human parietal cortex and comparison with human and macaque resting-state functional connectivity. *J Neurosci* 31: 4087-4100, 2011.

Maunsell JHR, Van Essen DC. The connections of the middle temporal visual area (MT) and their relationship to a cortical hierarchy in the macaque monkey. *J Neurosci* 3: 2563, 1983.

Mesulam MM. The blue reaction product in horseradish peroxidase neurohistochemistry: incubation paramters and visibility. *J Histochem Cytochem* 24: 1273-1280, 1976.

Mesulam MM. Large-scale neurocognitive networks and distributed processing for attention, language, and memory. *Ann Neurol* 28: 597-613, 1990.

Middleton FA, Strick PL. Cerebellar projections to the prefrontal cortex of the primate. *J Neurosci* 21: 700-712, 2001.

Mountcastle VB. Modality and topographic properties of single neurons of cat's somatic sensory cortex. *J Neurophysiol* 20: 408-434, 1957.

Nauta WJ, Ryan LF. Selective silver impregnation of degenerating axons in the central nervous system. *Stain Technol* 27: 175-179, 1952.

Nauta WJ. The problem of the frontal lobe: a reinterpretation. *J Psychiat Res* 8: 167-187, 1971.

Nelson SM, Cohen AL, Power JD, Wig GS, Miezin FM, Wheeler ME, Velanova K, Donaldson DI, Phillips JS, Schlaggar BL, Petersen SE. A parcellation scheme for human left lateral parietal cortex. *Neuron* 67: 156-170, 2010.

Nir Y, Mukamel R, Dinstein I, Privman E, Harel M et al. Interhemispheric correlations of slow spontaneous neuronal fluctuations revealed in human sensory cortex. *Nature Neurosci* 11: 1100-1108, 2008.

Ongur D, Price JL. The organization of networks within the orbital and medial prefrontal cortex of rats, monkeys and humans. *Cereb Cortex* 10: 206-219, 2000.

Passingham RE, Stephan KE, Kötter R. The anatomical basis of functional localization in the cortex. *Nat Rev Neurosci* 3: 606-616, 2002.

Power JD, Cohen AL, Nelson SM, Wig GS, Barnes KA, Church JA, Vogel AC, Laumann TO, Miezin FN, Schlaggar BL, Petersen SE. Functional network organization of the human brain. *Neuron* 72: 665-678, 2011.

Preuss TM, Caceres M, Oldham MC, Geschwind DH. Human brain evolution: insights from microarrays. *Nat Genetics* 5: 850-860, 2004.

Rakic P. Specification of cerebral cortical areas. *Science* 241: 170-176, 1988.

Rosa MGP. Visual maps in the adult primate cerebral cortex: some implications for brain development and evolution. *Braz J Med Biol Res* 35: 1485-1498, 2002.

Rosa MGP, Tweedale R. Brain maps, great and small: lessons from comparative studies of primate visual cortex organization. *Phil Trans R Soc B* 360: 665-691, 2005.

Sanides F. Comparative architectonics of the neocortex in mammals and their evolutionary interpretation. *Ann NY Acad Sci* 167: 404-423, 1969.

Semendeferi K, Lu A, Schenker N, Damasio H. Humans and great apes share a large frontal cortex. *Nat Neurosci* 5: 272-276, 2002.

Schoenemann PT, Sheehan MJ, Glotzer LD. Prefrontal white matter volume is disproportionately larger in humans than in other primates. *Nat Neurosci* 8: 242-252, 2005.

Smith SM. The future of FMRI connectivity. *Neuroimage* 62: 1257-1266, 2012.

Sillitoe RV, Joyner AL. Morphology, molecular codes, and circuitry produce the three-dimensional complexity of the cerebellum. *Ann Rev Cell Dev Biol* 23: 549-577, 2007.

Streidter GF. Principles of brain evolution. Sunderland, MA: Sinauer Associates, 2005.

Synder AZ, Raichle ME. A brief history of the resting state: the Washington University perspective. *Neuroimage* 62: 902-910, 2012.

Toga AW, Thompson PM, Mori S, Amunts K, Zilles K. Towards multimodal atlases of the human brain. *Nat Rev Neuro* 7: 952-966, 2006.

Ugolini GG. Rabies virus as a transneuronal tracer of neuronal connections. *Adv Vir Res* 79: 165-201, 2011.

Van Essen DC, Dierker DL. Surface-based and probabilistic atlases of primate cerebral cortex. *Neuron* 56: 209-225, 2007.

Van Essen DC, Ugurbil K. The future of the human connectome. *Neuroimage* 62: 1299-1310, 2012.

von Bonin G, Bailey P. The neocortex of Macaca mulatta. Urbana, IL: University of Illinois Press, 1947.

Walton GL, Paul WE. Contribution to the study of the cortical sensory areas. *Brain* 430-452, 1901.

Whiting BA, Barton RA. Evolution of the cortico-cerebellar complex in primates: anatomical connections predict patterns of correlated evolution. *J Hum Evol* 44: 3-10, 2003.

Yeo BTT, Krienen FM, Sepulcre J, Sabuncu MR, Lashkari D, Hollinshead M, Roffman JL, Smoller JW, Zollei L, Polimeni J, Fischl B, Liu H, Buckner RL. The organization of human cerebral cortex estimated by intrinsic functional connectivity. *J Neurophysiol* 106: 1125-1165, 2011.

Vincent JL, Patel GH, Fox MD, Snyder AZ, Baker JT, van Essen DC, Zempel JM, Snyder LH, Corbetta M, Raichle ME. Intrinsic functional architecture in the anaesthetized monkey brain. *Nature* 447: 83-86, 2007.

Segregated Fronto-Cerebellar Circuits Revealed by Intrinsic Functional Connectivity

Supplementary Materials

Assessing the significance of fronto-cerebellar correlations.

The correlation maps illustrating fronto-cerebellar connectivity all employed a somewhat arbitrary threshold ($r(z) > 0.1$). In order to formally assess how robust these results are, we conducted random effects analyses on the un-thresholded maps. First, we performed two t-tests, one each for the left and right MOT- and DLPFC- correlated maps in order to test the finding that left neocortical seeds are preferentially correlated with right cerebellar regions (and vice versa). Supplementary Figure S1.1 below displays the seed regions (top row) and results (bottom two rows) of the MOT t-test (A) and DLPFC t-test (B) thresholded at $p<0.001$, corrected for multiple comparisons across the whole brain. The left (red) seed for both MOT and DLPFC maps results in significantly higher correlations with the right cerebellar hemisphere. Conversely, the right (blue) seed produces significantly higher correlations in the left cerebellar hemisphere. Notably, the topography of the effects is qualitatively very similar to the subtraction maps shown in Figure 1.1 in the text.

Figure 1.3 in the text shows the result of subtracting a correlation map generated from one frontal site with the correlation map generated from another. The purpose of this analysis was to assess the topography of different fronto-cerebellar connections. For instance, subtracting the DLPFC-correlated map from the MOT-correlated map resulted in a map which clearly dissociated the MOT correlations in lobule V from the DLPFC

correlations in Crus I/II. Here again, however, threshold for the correlation coefficient is difficult to interpret. Accordingly, our second random effects analysis computed the significance of these subtraction maps. The correlation maps submitted to this analysis were, as in the original analysis, averages of left and right seeds. T-tests were performed on four pairs of the averaged maps (MOT-DLPFC, DLPFC-MPFC, MPFC-APFC, APFC-MOT), as shown in Supplementary Figure S1.2. The first two columns represent the placement of the frontal seeds, while the final column shows a representative slice of the cerebellum t-score map. The results are color-coded such that warm colors on the statistical map were significantly more correlated with the seeds in the first column, while blue colors were more correlated with seeds in the second column. Here again the results are thresholded at $p<0.001$, corrected for multiple comparisons.

Overall cerebellar topography is insensitive to the exact placement of frontal seeds.

We preformed an additional control analysis in order to determine whether the pattern of results that emerged from this study was sensitive to the choice of the particular seed coordinates in frontal cortex. To this end, we displaced each of our frontal seeds at least 8mm from their original locations and recomputed the correlation maps for each. This enabled us to assess whether slight variations of the seed regions would have an appreciable effect on the topography of cerebellar correlations.

The results are displayed in Supplementary Figure S1.3. Panel (A) shows the four pairs of new seeds in the MOT, DLPFC, MPFC and APFC regions. Each new seed location was generated by moving the old seed at least 8mm away from the original coordinate (coordinates of original seeds in Table 1.2 in the text) while remaining within

in the same approximate frontal region as the original. Panel (B) displays representative slices of the resulting cerebellar correlations. Comparing these maps to the original maps in Figure 1.8 reveals that the displacement appeared to have a negligible effect on the overall topography of the results.

Estimated cytoarchitectonic targets of cerebellar projections.

Seeding lobule V and Crus I in the cerebellum produced distinct patterns of neocortical correlations. Figure 1.2A in the text displays the two networks projected onto the PALS inflated neocortical surface (Van Essen, 2005). We identified the peak coordinates of both neocortical networks and list them below in Supplementary Table S1.1 along with their estimated areal boundaries. These areal boundaries should be considered approximate and are primarily useful as heuristic landmarks. Note that in addition to the correlations with DLPFC, other PFC zones such as anterior PFC including part of pars opercularis also contain peak correlations with this cerebellar region. Lobule V contains peak correlations at or near bilateral premotor and primary motor cortices.

Supplementary Table S1.1. Peak Correlations in Frontal Cortex.

Seed Region	BA	Description	x	y	z	z(r)
Crus I (CBM_{DLPFC})						
	46	Dorsolateral PFC	-42	50	0	0.3
	10	Anterior PFC	34	62	2	0.29
	9	Dorsolateral PFC	48	16	42	0.28
	44	pars opercularis	50	26	54	0.28
	44	pars opercularis	-50	20	38	0.27
	9	Dorsolateral PFC	40	12	54	0.27
	46	Dorsolateral PFC	42	50	-8	0.24
Lobule V ($CBM_{MOT)}$						
	6	Premotor cortex	30	-14	75	0.22
	6	Premotor cortex	-36	-12	68	0.2
	4	Primary Motor Cortex	-40	-16	64	0.18
	4	Primary Motor Cortex	38	-20	64	0.17

Note: Atlas coordinates (x,y,z) represent the Montreal Neurological Institute (MNI) coordinate system (Evans et al., 1993) based on the MNI152/ACBM-152 target. CBM = seed region placed in cerebellar cortex, MOT = motor cortex, DLPFC = dorsolateral prefrontal cortex, BA = approximate Brodmann's area.

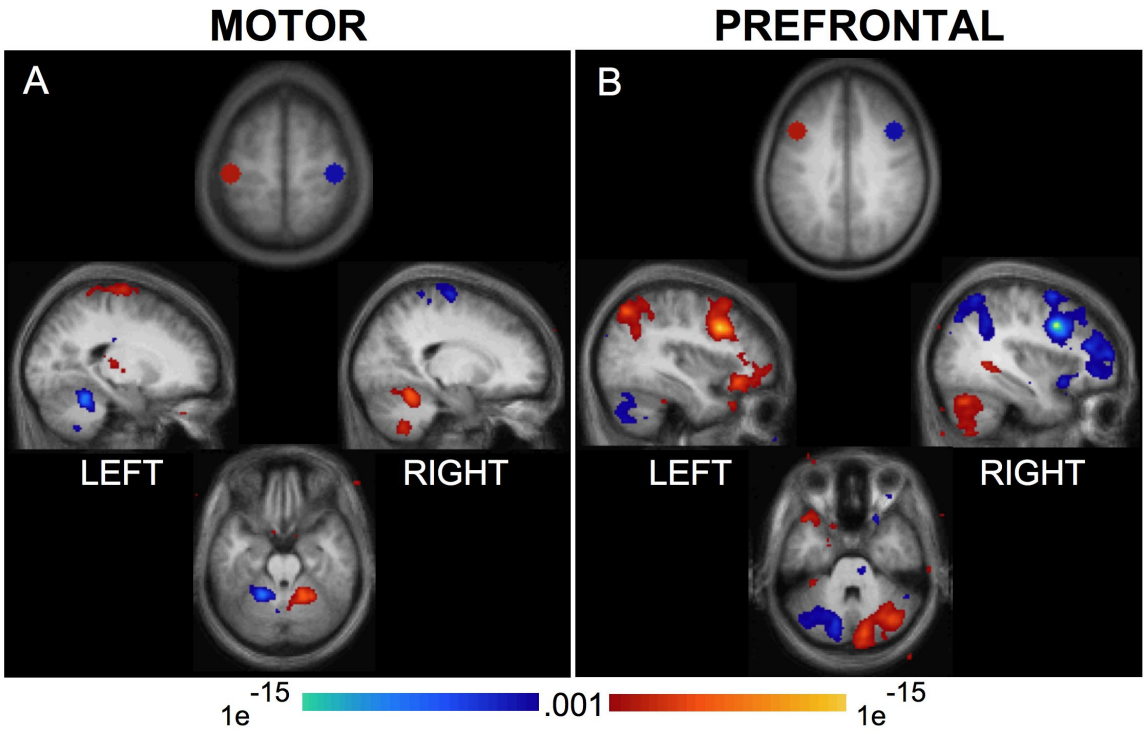

Supplementary Figure S1.1. Statistical significance of cerebro-cerebellar fcMRI.

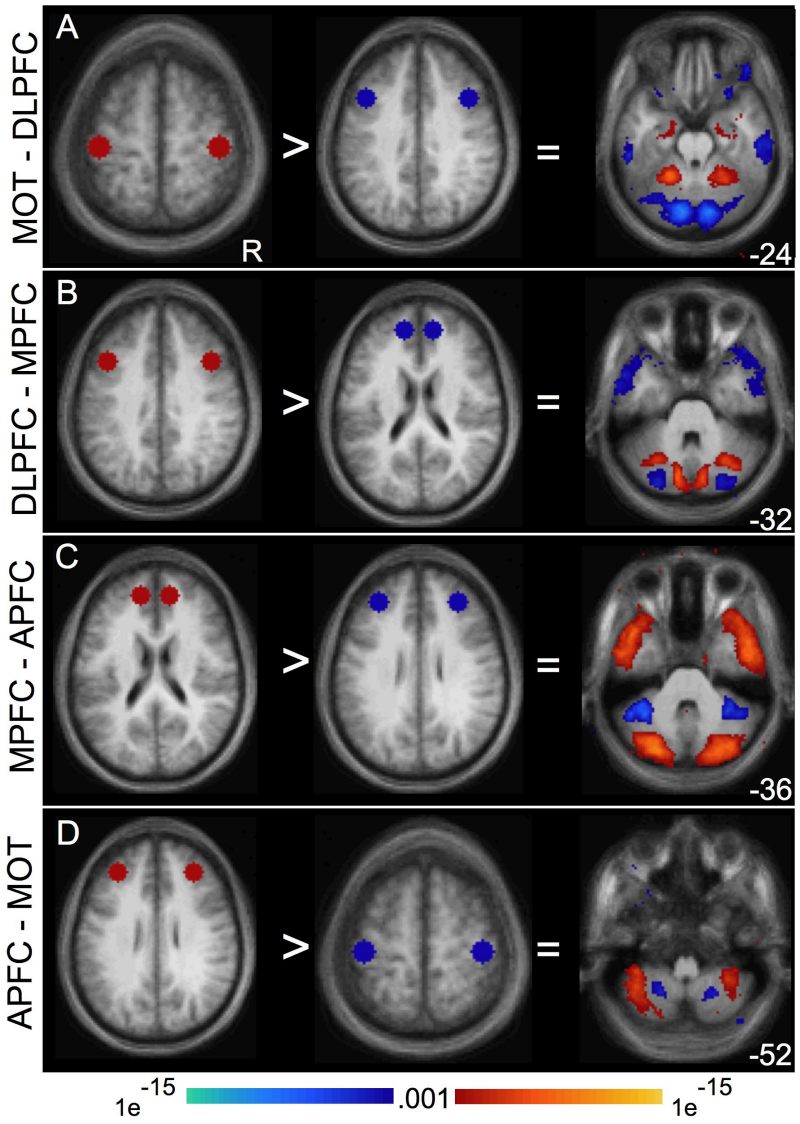

Supplementary Figure S1.2. Statistical significance of pairwise frontal seed comparisons.

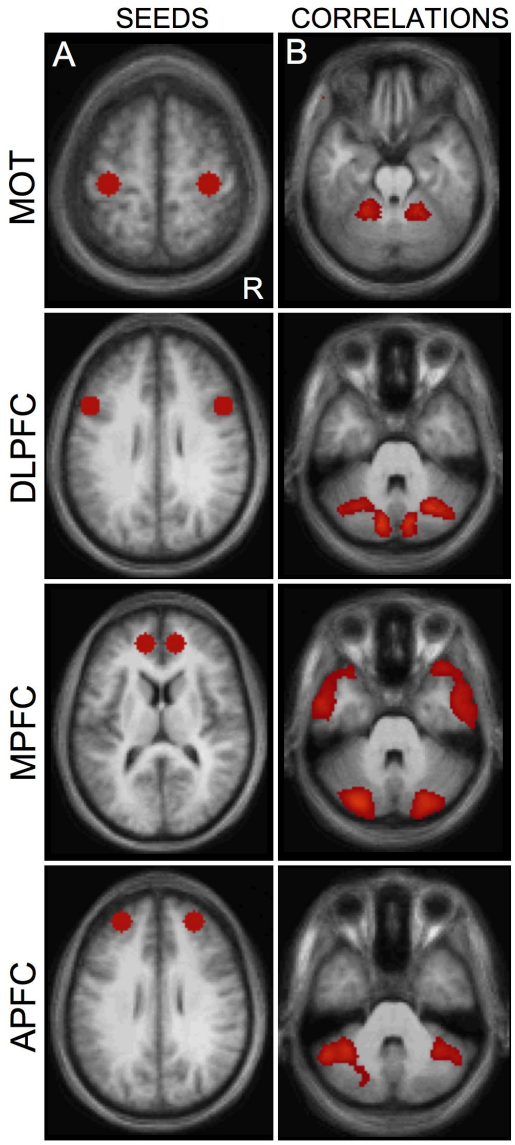

Supplementary Figure S1.3. Patterns in cerebellum are robust to local displacement of seeds in frontal cortex.

Boundaries on Functional Connectivity Boundaries: Theory and Practice

Supplementary Materials

In the toy example (Supplementary Figure S2.1), two (spatially) close dots represent two cortical regions (possibly spatially far apart) that have similar time courses (e.g., high correlation or similar functional connectivity profiles). There is clear structure in the data such that clustering the dots produces reasonable solutions for both 2 and 3 networks (Supplementary Figure S2.1B). As can be seen however, the boundary between the red and blue network shifts depending on whether a 2-network or 3-network solution is sought. In particular, the dot identified by the arrow was assigned to the red network in the 2-network solution, but to the blue network in the 3-network solution. This happens because in the 2-network case, the group of blue dots in the upper right corner of the canvas renders the blue network (on average) to be less similar to the dot compared with the red network. When seeking a 3-network solution, however, we see that the dot's connectivity profile is now more similar to the blue cluster than to the red cluster because of the break-up of the original blue network into the green and blue sub-networks, and therefore the dot is reassigned to blue. As a result, the network boundaries will shift in the 3-network case relative to the 2-network case.

The encroachment of the IPL-RSP-PHC network boundary into the Dorsal Attention Network (Figure 2.2 in the text) is likely a consequence of this kind of phenomenon. Specifically, the regions in question assigned to the Dorsal Attention Network in the 7-network solution in truth have a more similar connectivity profile with the IPL-RSP-PHC subnetwork of the Default Network, which leads to the reassignment of those regions and subsequent shift of the Dorsal Attention border in the 17-network solution. This intrusion into the Dorsal Attention Network is particularly inconsonant since the IPL-RSC-PHC network is typically regarded as a component of the Default Network (Vincent et al. 2006; Andrews-Hanna et al. 2010; Yeo et al. 2011), and the Default and Dorsal Attention Networks are often negatively correlated (Fox et al. 2005). Consequently, there exist cortical regions assigned to the Dorsal Attention Network in the

7-network solution that become assigned to a component of the Default Network in the 17-network solution.

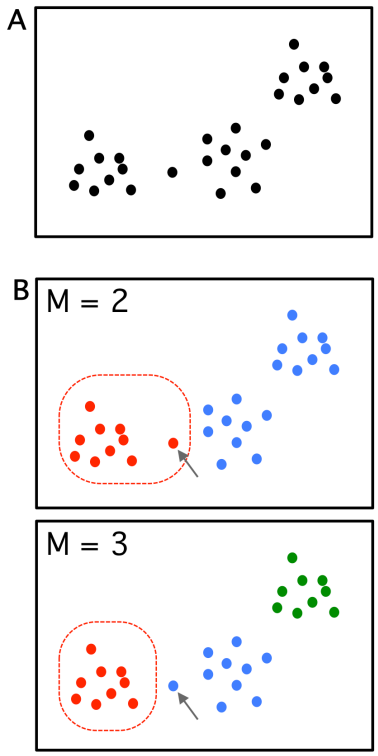

Supplementary Figure S2.1, related to Figure 2.2. Toy example illustrating border shifts resulting from changing analysis criteria. (A) A hypothetical arrangement of dots is shown on a 2-dimensional canvas. Dots positioned close together represent cortical regions (possibly spatially far apart) that have similar time courses (e.g., high correlation or similar functional connectivity profiles). Clustering is achieved by coloring the dots that share similarities. (B) Example solutions for M = 2 and M = 3 clusters are shown. These each depict reasonable solutions given the underlying structure in the data. However, the boundary between the red and blue network shifts depending on whether a 2-network or 3-network solution is sought because one dot (gray arrow) adopts a different network affiliation for these cases. This happens because in the M = 2 case, this dot is on average more similar to the red dots than it is to the blue dots. In the M = 3 case, however, the further division of the blue cluster into blue and green subnetworks changes the profile of the blue cluster such that the dot is now more similar to blue than to red. This has the consequence of shifting the red border in the 3-network case relative to the 2-network case.